

Structural Modeling and Characterization of Steel Fiber Reinforced Concrete Beams under Bending Shear

By

Timothy Nyomboi

Structural Systems Engineering (System Science)
Graduate School of Science and Technology



Structural Modeling and Characterization of Steel Fiber Reinforced Concrete Beams under Bending Shear

Timothy Nyomboi

Structural Systems Engineering (System Science)
Graduate School of Science and Technology
Nagasaki University
Japan

A PhD dissertation

Submitted in partial fulfillment for the award of Doctor of philosophy in Engineering (Structural Engineering), Graduate school of Science and Technology, Nagasaki University, Japan.

Supervisors

Prof. Dr. Eng. Hiroshi MATSUDA

Prof. Dr. Eng. (assoc.) Morita CHIHIRO

All rights reserved. No reproduction, copy or transmission of this publication in part or full may be made without written permission from the Author or Nagasaki University Japan.

©TN January 2010.1



©Nagasaki University, Japan

Dedication

To my loving wife and children

This piece of work is a testimony of your immense patience, love and prayers; you were always in my heart, for nothing can replace a loving family.

TN2010.2

ABSTRACT

As the need for the adoption of improved structural materials emerge, so does the need for experimental, analysis and design methods that can account for the technical benefit inherent in these materials. In the case of structural application of SFRC in shear strengthening, the methods should be able to provide realistic and accurate assessment of the shear strength, stiffness and ductility characteristics. Literature survey informs a limited understating and lack of transparency in existing information on steel fiber reinforced concrete (SFRC) as a structural material, particularly in shear strengthening. Moreover, there is no universally accepted design guideline for structural applications of SFRC which limits further, its wider application such as in shear strengthening. In this research, strength and deformation behavior in steel fiber reinforced concrete (SFRC) beams, under bending-shear, is investigated by analytical and experimental methods. For clarity on the shear strength merit offered by steel fibers, the experimentation process also employed a comparative fiber and stirrup reinforced beam evaluations. In practice, steel fibres are discretely and randomly constituted in the concrete volume of a structural member. They bridge cracks and transfer stress, thereby enhancing the post cracking strength which indeed is responsible for improvement in structural capacity such as shear strength and deformation. It is therefore imperative to investigate and clarify these influencing factors in detail. However, limitations of conventional measurements techniques and the difficulty associated with measurement of strain fields as well as visualisation and identification of the cracking behaviour hinders the full potential of evaluating and quantifying the performance of SFRC as structural material. To overcome this difficulty, optical full-field electronic speckle pattern interferometry (ESPI) and digital image correlation method (DICM) measurement techniques have been applied in this research to supplement conventional measurement methods in the experimentation process. Design requires predictive methods for gauging the performance of structural elements without the need of a practical test at the design stage. Currently there is no information on shear strength-deformation evolution prediction model for SFRC beams. This research proposes a unified theoretical model capable of predicting the shear load deflection and shear stress-strain response to failure in SFRC beams. Parametric analysis was undertaken to gauge the performance of the model and the variables that influence shear capacity of SFRC beams. FEM simulation of SFRC beams under bending shear was also undertaken with application of an experimentally derived material model for the SFRC. Results from the experimental investigations and the FEM analysis were further applied to validate the proposed theoretical model. By applying these techniques as discussed above, structural characteristics of SFRC beams under bending shear are clarified, quantified and a practical design case for shear strengthening using steel fibers in which the proposed Equivalent Shear Design Method (ESDM) for SFRC beams is applied is illustrated.

| Content | Page |
|---|-------------|
| Abstract..... | i |
| Table of content..... | ii |
| Summary (in English)..... | v |
| Summary (in Japanese)..... | viii |
| Acknowledgement..... | x |
| | |
| 1 Introduction | |
| 1.1 Introduction | 1 |
| 1.2 Research problem and significance | 2 |
| 1.3 Objectives | 3 |
| | |
| 2. Applications of SFRC and shear capacity of RC beams with and without steel fibers | |
| 2.1 Introduction..... | 4 |
| 2.2 Applications of SFRC..... | 4 |
| 2.2.1 Current application in RC structures..... | 4 |
| 2.2.2 Potential applications..... | 5 |
| 2.2.3 Characteristics of steel fibers as applied in concrete..... | 6 |
| 2.3 Assessment of shear capacity in RC beams..... | 7 |
| 2.3.1 RC beams with and without stirrup reinforcement..... | 7 |
| 2.3.2 RC beams reinforced with steel fibers..... | 10 |
| 2.3.3 Experimental and Numerical investigations on steel fiber RC beams..... | 15 |
| 2.4 Concluding remarks..... | 17 |
| | |
| 3. Experimental and analytical research methodology | |
| 3.1 Introductions..... | 19 |
| 3.2 Experimental methods..... | 19 |
| 3.2.1 Bending shear tests..... | 19 |
| 3.2.2 Compression and split tests..... | 20 |
| 3.2.3 Conventional measurements methods..... | 21 |
| 3.2.4 Non contact full field optical methods..... | 21 |
| 3.2.5 Schedule and specimen design..... | 25 |
| 3.2.6 Specimen manufacture and curing..... | 27 |
| 3.3 Analytical methods applied..... | 30 |
| 3.4 Concluding remarks..... | 30 |
| | |
| 4. Development of a new theoretical shear evolution response model for SFRC beams | |
| 4.1 Introduction..... | 31 |
| 4.2 Derivation of expressions for the forces acting to resist the shear force..... | 32 |
| 4.2.1 Model concept details..... | 32 |
| 4.2.2 Concrete compressive and tensile forces..... | 34 |
| 4.2.3 Shearing forces..... | 35 |
| 4.2.4 Fiber forces..... | 35 |
| 4.2.5 Dowel force..... | 39 |

| | |
|--|----|
| 4.2.6 Re bar tensile force..... | 42 |
| 4.3 Equilibrium analysis and the shear capacity predictive equations..... | 43 |
| 4.3.1 Equilibrium of forces..... | 44 |
| 4.3.2 Shear strength prediction..... | 44 |
| 4.3.3 Shear strain prediction..... | 48 |
| 4.3.4 Deflection prediction..... | 49 |
| 4.4 Parametric analysis and prediction response..... | 50 |
| 4.4.1 Structural and material parameters..... | 50 |
| 4.4.2 Influence of fiber variation..... | 52 |
| 4.4.3 Influence of shear span to depth ratio variation..... | 55 |
| 4.5 Concluding remarks..... | 55 |
| | |
| 5. Properties of steel fiber reinforced normal concrete | |
| 5.1 Introductions..... | 56 |
| 5.2 Materials..... | 57 |
| 5.2.1 Fiber Concrete..... | 57 |
| 5.2.2 Reinforcements..... | 57 |
| 5.3 Tests procedure..... | 57 |
| 5.4 Effect of steel fibers on rheology of fresh concrete..... | 59 |
| 5.5 Hardened SFRC material properties..... | 59 |
| 5.5.1 Average material properties..... | 59 |
| 5.5.2 Compressive strength..... | 60 |
| 5.5.3 Tension strength and deformation..... | 60 |
| 5.5.4 Shear deformation and strength..... | 62 |
| 5.6 Concluding remarks..... | 64 |
| | |
| 6. Shear strength and deformation characteristic in steel fiber RC beam | |
| 6.1 Introduction..... | 65 |
| 6.2 Deformation observation and measurement by ESPI method..... | 65 |
| 6.3 Observation of cracking and ductility development in SFRC beams..... | 66 |
| 6.3.1 Specimen and test procedure..... | 66 |
| 6.3.2 Physical failure and load defection response..... | 67 |
| 6.3.3 Visualization of cracking development..... | 69 |
| 6.3.4 Ductility and crack strain characteristics..... | 73 |
| 6.4 Strength and deformation comparisons with stirrup RC beam..... | 73 |
| 6.4.1 Specimens and test procedure..... | 73 |
| 6.4.2 Comparative failure modes and ultimate load capacity..... | 74 |
| 6.4.3 Comparative full-field deformation characteristic..... | 77 |
| 6.3.5 Comparative shear stress deformation characteristics..... | 79 |
| 6.5 Concluding remarks..... | 83 |
| | |
| 7. FEM simulation of SFRC beams under bending shear and verification | |
| 7.1 Introduction..... | 85 |
| 7.2 Basic theoretical principles and analysis procedure..... | 85 |
| 7.2.1 Plane stress element and constitutive formulation..... | 85 |

| | |
|--|------------|
| 7.2.2 Constitutive laws..... | 87 |
| 7.2.3 Summary of FE analysis method..... | 88 |
| 7.2.4 Implementation procedure..... | 89 |
| 7.3 FE structural and material models for SFRC beams..... | 90 |
| 7.3.1 Structural model..... | 90 |
| 7.3.2 Material models..... | 90 |
| 7.4 FEM analysis results and verifications..... | 92 |
| 7.4.1 FEM shear load deflection response..... | 92 |
| 7.4.2 Cracking pattern..... | 93 |
| 7.4.3 FEM and experimental synchronized load deflection response..... | 96 |
| 7.4.4 FEM and Test ultimate strength comparisons..... | 98 |
| 7.4.5 Stress strain distributions..... | 99 |
| 7.5 Concluding remarks..... | 101 |
| | |
| 8. Theoretical model verification and design application | |
| 8.1 Introduction..... | 102 |
| 8.2 Model prediction comparisons with experimental results..... | 102 |
| 8.2.1 Synchronized load deformation response..... | 102 |
| 8.2.2 Ultimate strength comparison with experimental result found in the literature..... | 106 |
| 8.3 Model prediction comparisons with FEM results..... | 110 |
| 8.4 Shear design application and performance evaluation..... | 112 |
| 8.4.1 Proposed Equivalent Shear Design method (ESDM)..... | 112 |
| 8.4.2 Typical design case for shear in SFRC beams by ESDM..... | 114 |
| 8.4.3 Performance evaluation of the beams designed by ESDM..... | 116 |
| 8.5 Concluding remarks..... | 121 |
| | |
| 9. Overall discussions, Conclusion and Recommendations | |
| 9.1 Overall discussion..... | 121 |
| 9.2 Conclusions..... | 123 |
| 9.3 Recommendation for future work..... | 125 |
| | |
| References..... | 126 |
| | |
| Appendix | |
| (I) Notations..... | 131 |
| (II) List of figures..... | 133 |
| (III) List of Tables..... | 135 |
| (IV) Equivalent shear design method procedure..... | 136 |
| (V) Mix design..... | 139 |
| (VI) CADINP Program..... | 143 |
| (VII) List of research output publications | 145 |

SUMMARY

Structural Modeling and Characterization of Steel Fiber Reinforced Concrete beams under Bending Shear

Literature survey shows that there is limited understating and lack of transparency in existing information on steel fiber reinforced concrete (SFRC) as a structural material. Moreover, use in shear strengthening is limited by a universally accepted design guideline for shear applications. In this research, shear strength and deformation behavior in SFRC beams under bending-shear is investigated by analytical and experimental methods. Practically, steel fibers are discretely and randomly constituted in the concrete volume of a structural member. They bridge cracks and transfer stresses, therefore post cracking strength is enhanced. For an in-depth understanding of the influence of the fibers it is imperative to investigate and clarify these influencing factors.

Limitations of conventional measurements techniques and the difficulties associated with measurement of strain fields as well as visualization and identification of the cracking behavior hinders the full potential of evaluating and quantifying the performance of SFRC as structural material. This research applied optical full-field measurement techniques, i.e. electronic speckle pattern interferometry (ESPI) and digital image correlation method (DICM), in addition to the conventional measurement methods in the experimentation process. Tension and compression tests results were used in the determination of SFRC material properties which were necessary in the theoretical research.

Through full-field optical measurements, visualization of cracking and evolution of strain characteristics in SFRC short beams clearly show that steel fibers improve strain ductility and cracking propagation in RC beams. Moreover, shear strength in SFRC beams is shown to be higher than that of non fibrous beams. A further comparative evaluation between steel fiber and stirrup RC beams showed that steel fiber RC beams have strength capacity close to that of stirrup beams.

In the analytical part of this research, theoretical derivations and numerical simulations of SFRC beams under bending-shear is undertaken. A new theoretical model, which makes it possible to predict shear load-deflection and shear stress-strain evolution response in SFRC beams to complete failure, is proposed. Unlike the few existing SFRC shear strength models, which are predominantly empirical and ultimate based, the proposed model is evolution based and could account for the shear response behavior to complete failure. It has been derived first theoretically and then verified with results from the experimental research. Further, ultimate shear strength predictions from the model are made and compared with experimental data from other research results in the literature. A parametric study is conducted to evaluate the response of the model to variation of fiber content and shear span to depth ratio on the shear capacity of SFRC beams.

Noting that both theoretical and empirical models are fundamental facets that are necessary in the analysis and design of engineering structures, a design method herein referred as “Equivalent Shear Design Method (ESDM)” is further proposed based on the developed theoretical model and existing conventional design methods for shear design in beams. The entire research is presented and discussed in the nine chapters. Schematic flow, description and association of the chapters are

shown in Fig.1.1 while the specific summary of the contents of each chapter are as follows:

Chapter 1: A brief background information on reinforced concrete as a structural material and the applicability of steel fibers in strengthening concrete for structural use are discussed. This is followed by a discussion on the research significance and finally the main objectives of the research are outlined.

Chapter 2: This chapter reviews the literature and discusses the contents relevant to the current research theme. The review is based on the current and potential application of SFRC in structures, characteristics of steel fibers as used in concrete and assessment of previous studies on shear capacity in SFRC beams.

Chapter 3: The relevant research methodologies are discussed in this chapter, with a view of introducing the methods adopted. Testing and measurement methods are discussed at length and an outline of the analytical approach adopted is further discussed in brief.

Chapter 4: The development of a new theoretical model for prediction of shear capacity evolution in SFRC beams is presented. Preliminarily, the validity of the model is theoretically evaluated and the results discussed.

Chapter 5: This chapter presents the material characteristics of SFRC as a material for structural use. SFRC material characteristics both in fresh and hardened state are presented and discussed. The material properties obtained in this chapter were applied in the verifications of the theoretical research work conducted.

Chapter 6: In this chapter, failure and ductility characteristics as well as visualization of cracking development by optical full-field ESPI methods are presented and discussed. In addition, the shear strengthening merit of steel fibers in comparison with an ordinarily RC beam with an equivalent amount of stirrups is evaluated and the validity of fiber content (as shear reinforcement) determination formula proposed in this research is checked.

Chapter 7: This chapter presents and discusses the FE analysis of SFRC beams under bending-shear. Finite element analysis by SOFISTIK FEM Code is shown to fairly simulate the strength and deformation behavior in SFRC beams.

Chapter 8: The derived theoretical model presented in chapter 4, is verified with the experimental and numerical results. Further, a design method making use of the derived model is proposed whereby a load bearing structure is used to illustrate the design procedure.

Chapter 9: This chapter discusses the overall conclusion of the entire research. The main findings are summarized and recommendations for further research are outlined.

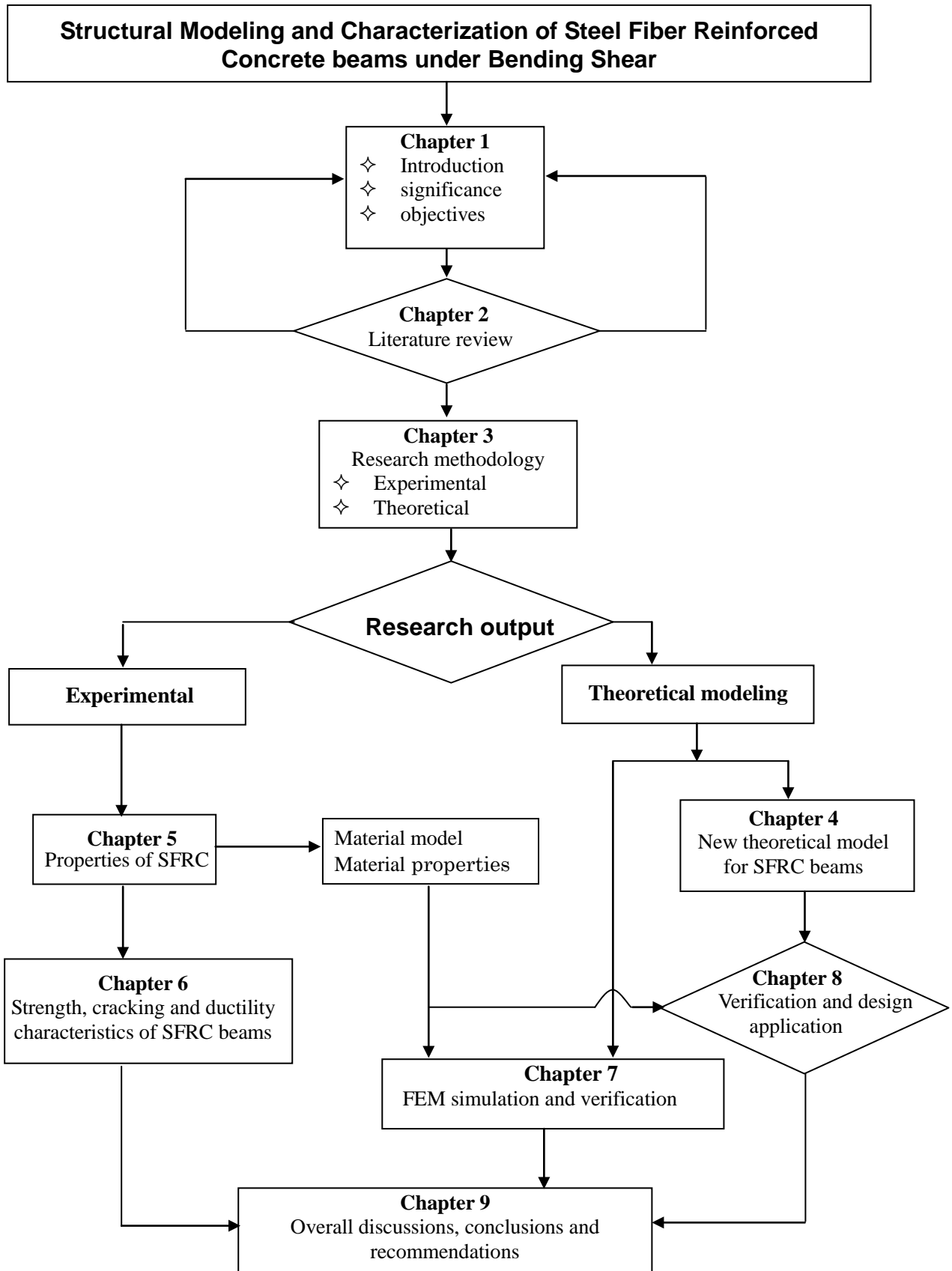


Fig.1.1 Schematic summary of the dissertation chapters and content

SUMMARY IN JAPANESE

鋼繊維補強鉄筋コンクリート梁のせん断挙動のモデル化とその特性 に関する研究

(Structural Modeling and Characterization of Steel Fiber Reinforced Concrete beams under Bending Shear)

鋼繊維補強コンクリートは、コンクリートマトリックス中に鋼繊維を分散混合することにより、コンクリート系材料に特有の低引張強度と脆性的破壊特性を改善することを目的として開発された複合材料の一種である。通常の鉄筋コンクリート（以後、RC と略記）のコンクリート中に鋼繊維を混入することにより曲げ耐力やじん性が向上する。しかしながら、鋼繊維補強 RC はりの破壊パターンがせん断による場合には、せん断耐力やその変形能に関しては、定量的な破壊メカニズムの解明は未だ十分には行われていない。そのため鋼繊維補強 RC を構造物に適用するための設計指針も限定的にしか存在せず、鋼繊維補強 RC 構造が広く普及しない一因となっている。本研究では、鋼繊維補強 RC はりのせん断耐力と変形挙動を定量的に明らかにすることを目的として、実験的及び解析的方法により検討したものである。

既往の研究によれば、鋼繊維によりひび割れ面で応力が伝達されるために、コンクリートの引張破壊特性が改善され、鋼繊維補強 RC 部材の斜め引張破壊荷重が増加する傾向や変形性能が改善されることが報告されている。したがって、鋼繊維補強 RC はりのせん断耐力と変形挙動を究明するためには、鉄筋のダウエル効果、コンクリートのせん断強度、骨材のかみ合わせ作用などの影響因子とともに、鋼繊維の補強効果を明らかにすることが不可欠となる。そのためには、ひび割れ発生位置におけるひずみの計測が重要となってくる。しかし、ひび割れ位置を正確に予測することは困難であり、また、ひずみゲージによる計測ではひび割れ発生・進展と同様にひずみ場の計測においても限界があり、鋼繊維補強 RC はりの鋼繊維の補強効果を定量的に評価することは困難であった。本研究では、光学的計測法である電子スペックルパターン干渉法（ESPI）及びデジタル画像相関法（DICM）を用いて実験を実施した。

短スパン鋼繊維補強 RC はりの実験より、ひび割れとひずみの発生・進展過程を全視野計測により可視化することができ、鋼繊維が RC はりの変形能の向上とひび割れ幅の低減効果に寄与することを明確に示すことができた。また、スパン長 1.6m 試験体による実験より、鋼繊維補強 RC はりの破壊耐力は鋼繊維を混入しない RC はりに比べ増大すること、さらに、鋼繊維補強 RC はりとせん断補強鉄筋を有する RC はりにおいては、両者はほぼ同等の破壊耐力と変形能を有することが確認された。

一方、解析的な面からは、曲げせん断荷重を受ける鋼繊維補強 RC はりの理論解析モデルを誘導した。経験に基づいたせん断耐力モデルと違い、本理論解析モデルは、力のつりあいによる理論展開がベースとなっており、破壊に至るまでのせん断挙動を説明できる。本

理論解析モデルの有効性を検討するために、前記の実験結果と比較し、よく一致することを確認した。なお、最大せん断耐力に関しては、既往の論文の研究結果でも大きなばらつきがあるが、それらとの比較において約 70%の精度で相関があることを確認した。さらに、鋼繊維混入量やせん断スパン有効高さ比 (a/d) の影響を明らかにするために、パラメトリック解析を実施するとともに、はりのせん断設計法として、理論解析モデルと従来の設計モデルを基に「等価せん断設計法(ESDM)」を提案した。

本論文は全 9 章で構成されている。それぞれの章の内容は以下に示す通りである。

第 1 章では、鋼繊維補強鉄筋コンクリートはりの研究の背景、意義、目的および構成について述べた。

第 2 章では、SFRC の適用可能性、コンクリート中の鋼繊維の特性、および SFRC 梁のせん断耐力に関する最近の研究に関する文献調査結果を述べた。

第 3 章では、本研究で採用した研究方法について概説するとともに、実験方法に関する詳細な説明を述べた。

第 4 章では、SFRC 梁のせん断耐力を予測するための新しい理論モデルについて詳述し、理論モデルの有効性について検討した。

第 5 章では、鋼繊維混入コンクリートの硬化前のコンクリートの材料特性を示すとともに、硬化後のコンクリートの力学的特性について述べた。これは解析的研究において重要な役割を果たすものである。

第 6 章では、短スパン SFRC はりの載荷試験を実施し、電子スペckルパターン干 (ESPI) 計測によるひび割れの発生・進展の可視化と破壊・変形特性について述べた。さらに、等価なせん断補強筋量を有する梁と比較し鋼繊維の補強効果を明らかにするとともに、本研究で用いた鋼繊維のせん断補強量の有効性を確認した。

第 7 章では、曲げせん断を受ける SFRC 梁の有限要素解析について述べた。SOFISTIK FEM Code による有限要素解析結果は、SFRC 梁の耐力と変形挙動をよく一致していることを示した。

第 7 章では、SFRC 梁のせん断耐力を予測する新しい理論解析モデルについて説明し、の SFRC 梁への適用性を検討した。

第 8 章では、第 4 章で導いた理論解析モデルと実験および数値解析による結果と比較検討した。さらに導出したモデルを用いて設計法を作成した。

第 9 章では、本研究のまとめと今後の展望について述べた。

ACKNOWLEDGEMENT

The author gratefully acknowledges the financial support received from the Japan Government Ministry of Education and Grant-in-Aid for Scientific Research (B19360205 and B21360217) of Japan Society for the Promotion of Science (JSPS). The success of this research was realized because of the timely advice, support and encouragement that was received from my principal supervisor Prof. Hiroshi MATSUDA who exhibited a great deal of expertise in the guidance of the research through to its completion of the writing of this dissertation. My second supervisor, Prof Chihiro MORITA who also in one way or another contributed to the success of the research is appreciated. Assistance provided by Mr. Yamashita and Mrs. Watanabe was invaluable and is acknowledged. Special gratitude goes to the Japanese students who were willing to lend a hand and endure the hard labor of fiber concrete manufacture, casting among other things for their invaluable hard work and support. Department of Systems Science (Structural Systems Engineering), Graduate School of Science and Technology, Nagasaki University and the International student center are acknowledged for the enrollment opportunity granted and the guidance offered during my stay and study at Nagasaki University, Japan. The Japanese language course offered to me by the international student center was instrumental in my day to day life in Japan and the training is highly appreciated. Dearly acknowledged are my loving wife Nodiah and daughters Nicole and Joy for their patience, support and understanding for being away from them for a long time, while pursuing my PhD studies in Japan.

© T. Nyomboi,

Chapter 1

Introduction

1.1 Background

For many years concrete has been used as a preferred structural material in many structures including buildings, bridges, pavements, sewer and storm pipes, liquid holding tanks and other structural systems. It is recognized that the great advantages of concrete are in its compressive strength and ability to be molded. Although concrete offered these advantages, it still presented the problem that its tensile strength is very small compared to its compressive strength. Methods to overcome structural weaknesses inherent in brittle materials such as concrete and clay have been adopted since ancient times. In the early times, the Roman architects overcame this problem by using concrete in the form of arches. Others such as the Pharaohs (Holy Bible, exodus chapter 5 verses 6 to 7), used straw fiber to reinforce clay bricks to strengthen in tension and shear. However, the first widely and commercially used manufactured composite incorporating fiber in mortar in the modern times was asbestos, which was developed in about 1900 with the invention of the Hatschek process [1]. Now fibers of various kinds are used to reinforce a number of different materials concrete and mortar included [1].

Advances in modern technology allowed engineers to add steel reinforcements in form of longitudinal re-bars to the concrete to overcome the tensile weakness inherent in concrete. However, with one problem solved another is created, for example, congested areas such as the dense presence of stirrups in beams or re-bars in slabs, become a source of difficulty in concrete placement and compaction. Moreover, cracking in the hardened concrete structure reduces stiffness and expose the main reinforcements to the corrosive agents that percolate into the RC structure through cracks. Some of the advances made to address these problems include (a) development of better concrete with good rheological properties (e.g. self compacting Concrete) (b) development of fibre reinforced composites, the most common being steel fibres reinforced concrete (SFRC), carbon fibres reinforced polymer (CFRP) sheets and re-bars. CFRP have been found to offer high strength properties, excellent durability, corrosion resistance and high strength-to-weight ratio, however, it is brittle and when used as reinforcement in concrete, sudden failure of CFRP can lead to brittle structural failures. It is mainly applied in civil engineering in retrofitting to strengthen and or repair an existing structure. On the other hand steel fiber reinforced concrete (SFRC) is attractive in reinforced concrete structures because; (a) steel fibres are effective in improving post cracking tensile strength in concrete, crack control and toughness thereby providing enhanced durability and structural performance, (b) provides a more ductile failure in otherwise brittle concrete, (c) It is a ready to use materials since it is mixed together with the concrete. However, despite these advantages, its application in concrete structures is

still limited because at present there are no universally accepted design guidelines [2]. Currently SFRC is applied in pre cast panels, tunnel linings, factory floor slabs, dams, bridge decks and pavements [3], [4], [5] for crack control, ductility and fatigue strengthening. Previous use of high steel fibre content significantly affected the workability of conventional concrete, however with the advent of flow-able concrete (self compacting concrete), this problem is no longer an issue and thus the potential of using SFRC in a wide range of structural applications is possible, provided design guidelines are developed to encompass the new applications.

Shear strengthening in concrete beams is one such particular potential application of SFRC. Numerous research studies in the area of shear strength have been done on conventionally reinforced concrete beams [6]. However, studies done on steel fiber reinforced concrete (SFRC) beams, apply conventional measurement methods in which experiments are conducted with realization of limited information. Existing predictive models for SFRC have all been developed empirically and some cases methods applied in conventionally reinforced (use of stirrups) beams are applied. In the case of conventional reinforcement in shear (use of stirrups), the empirical equations developed do not predict accurately the test results [6]. In regard to application of similar models in SFRC beams, it is obvious that this will only serve to increase the inaccuracy. Perhaps it is for this reason that until now there seem to be no conclusive design guideline for SFRC in shear strengthening. Dupont and Vandawalle [2]; Brandt [7], have pointed out that potential application of SFRC is hindered by lack of accepted design guidelines and limited understanding of SFRC material. Existing information on SFRC do not show much transparency, and there is need for more fundamental research to obtain a basic understanding of the SFRC [2].

1.2 Research problem and significance

A survey of the literature indicates the lack of information on full field deformation behavior of steel fibre reinforced concrete (SFRC) beams under bending shear in which the influence of the steel fibers on the shear strength and deformation capacity is characterized and quantified. Although full field deformation characteristics concurrent with strength are fundamental in understanding the structural performance of any SFRC member, they are seldom investigated. Steel fibers are discrete and randomly distributed in the concrete; they tend to be at a much closer spacing than the conventional reinforcements (stirrups or re-bars). This characteristic is expected to have more impact on the strain, cracking and ductility behavior throughout the concrete volume which in turn directly influences the load carrying capacity of any SFRC member. Significant interest is in the shear capacity and prediction of the response when steel fibbers are applied in RC beams. From literature it is found that a number of empirical methods have been proposed to predict shear capacity in SFRC beams. However, these existing empirical analytical models are ultimate based and they do not predict the shear capacity of SFRC beams in a unified manner [8]. Moreover, a purely theoretical model that accounts in a unified manner the actual contribution of the parameters involved in shear resistive

mechanism do not exist. It is well known that in SFRC, activation of steel fiber resistive mechanism begins when concrete starts to cracks (concrete yielding); an evolution based model is thus more suitable in tracking the shear response of SFRC through yielding to failure. Indeed, Dupont and Vandewalle [2] have point out the there is lack of transparency in the existing empirical relations.

Further, it has been noted that few attempts have been made in the past to numerically simulate the response of steel fiber reinforced elements [9]. Feheling [9] attributes this to the lack of suitable constitutive material models for SFRC composite. The developing of material models for SFRC is relatively a very complex task because of the different geometric scales involved in the initiation and propagation of damage leading to failure [9]. This research therefore shall also make an attempt to numerically simulate the shear response of SFRC beams by adopting simpler material models that can be obtained using standard experimental tests.

1.3 Research objectives

To address the short comings identified as discussed in section 1.2 above, this research set out specific targets that were deemed necessary. These targets formed the objectives of the research which were to:

- (a) Develop a new unified theoretical model for the prediction of shear strength-deformation evolution behavior to complete failure in SFRC beams without stirrups.
- (b) Characterize strength and deformation behavior in SFRC beams, with application of optical full field measurement techniques in deformation measurements.
- (c) Numerically simulate and characterize shear strength and deformation behavior in SFRC beams by applying an experimentally derived material model.
- (d) Verify the proposed new theoretical model with experimental and numerical results.
- (e) Propose a design method for shear strengthening of RC beams using steel fibers.

Chapter 2

Application of SFRC and shear capacity of RC beams with and without steel fibers (Literature review).

2.1 Introduction

SFRC has continued to attract a lot of research interests and the scope of research on SFRC is wide. It ranges from classical experimental investigations and modeling to sophisticated micro mechanical modeling applied to gain insight into fracture process of SFRC for development of constitutive material models needed in design and analysis applications. The basic target of the current research is on both analytical and experimental SFRC shear capacity and its applicability. To account for what has already been done, recommendations and or its short comings, a review of the literature on existing conventional shear capacity in RC beams without and with stirrup and steel fibers are discussed in this chapter. Particular attention is given to previous studies on steel fiber reinforced RC beams.

2.2 Applications of SFRC

2.2.1 Current application in RC structures

Conventionally, concrete reinforcements have been in the form of continuous reinforcing bars, normally placed in the concrete member at the appropriate locations to withstand the imposed loads. However, with the advent of steel fibers, their use has been in discontinuous form (discrete) distributed randomly throughout the concrete. In this form, they have been found to be effective in crack propagation control. Although there are other forms of fiber material applicable in concrete reinforcements, steel fibers have been considered as the optimal fibre material for concrete on the basis of compatibility, availability, cost and durability.

Currently, steel fiber reinforced concrete (SFRC) is applied in pre-cast panels, tunnel linings, short-crete slope stabilization, factory floor slabs, dams, bridge decks and pavements [3],[4],[5],[10][11],[12], (Fig.2.1). An in-depth assessment of these applications have been discussed in details in the ACI committee 544 report [12] generally the target technical advantage in the utilization of SFRC in these structures is mainly to control cracks, improve ductility and resistance to impact, abrasion or fatigue loads. It is argued that because of the good energy absorption and impact characteristics, SFRC can function well in providing ductility in beam column assembly [13], crack control in slabs, beams as well as pre-cast elements [14]. Despite the current use of steel fibers on concrete structures, wider application in reinforced concrete is still limited due to the lack of generally accepted design guidelines [2]. Lack of a universally accepted approach in the calculation of the

strength, verifications and standards for SFRC is one of the major obstacles in application of SFRC in design [7]. This fact is exemplified by the design code of the German Concrete Association (Deutsche Beton Verein, DBV) which recommends ignoring the additional shear capacity due to the fiber reinforcement [15].



(b) Industrial floor slabs



(a) Concrete bridge decks and piers



(c) Tunnel linings and slope stabilization



(d) RC dams

Fig. 2.1 various types of structures in which steel fibers are applied

2.2.2 Potential structural applications

One of the most promising uses of steel fibers is in the shear strengthening in structural members such as in beams and slab subjected to shear loading. Partial supplement of the conventional stirrup reinforcement is particularly attractive in areas where there is possibility of congestion of these stirrups [16] particularly in frame structures (Fig. 2.2b). Alternative use can also be in load bearing structures (Fig. 2.2a) where shear loading may not be as much as in the case of frame structures (Fig.

2.2b) of significant size and spans. In the former, steel fibers can be used as minimum shear reinforcements in tie and lintel beams. It is recognized that in load bearing structures, other than the foundation, the structural components are often the walls and the tie beams (monolithic with the slabs) as shown in Fig2.1. Others include use in thin sections where conventional shear reinforcements may not be admissible. Reports published in the past two and half decades have considered the possibility of utilizing steel fibers as shear reinforcements in structural elements [17]. Khuntia et al [8] and Greenough et al [16] emphasizes the additional merits as; significant reduction in construction time and costs especially in times of high labor shortages, since conventional stirrups are labor intensive, (for input to bend and fix in place). However, information of practical application of this structural and economic merit is un-available implying that it is yet to be realized.



(a) Use in beams on load bearing structures

(b) Supplement in frames assemblages

Fig.2.2 Load bearing and frame structures

2.2.3 Characteristics of steel fibers as applied in concrete

Steel fibers are made from prime hard-drawn steel wire to ensure high tensile strength and they come in many shapes and size each with different performance levels [11]. The surface geometry structure of the fiber is often deformed to improve bonding with concrete matrix. The performance of the fibers depends on both the content or dosage (kg/m^3) and the fiber parameters (tensile strengths, length, diameter and anchorage). A key factor for the quality of the fiber is the relationship between the length and the diameter of the fibers commonly defined as the aspect ratio. Higher aspect ratio (l_f/d_f) yield better performance in the hardened concrete, however, increased impedance to the flow (rheology) in fresh concrete will occur, hence pausing difficulties during casting [16, 18]. It is thus recommended to use water reducing agents or plasticizers to improve workability without increasing the water content. However, even with the use of admixture, it has been established that only certain amount of the fiber quaintly can be mixed with the concrete because of the workability and handling problems, as confirmed in this research.

Based on their own work and that of other seven researches, Altum et al [18] came to the conclusion

that the optimum steel fiber dosage for reinforcement in beams should be within 1-2.5% by absolute volume. A steel fiber (SF) dosage smaller than 1% becomes ineffective and dosages beyond 2.5% become also ineffective mainly due to the physical difficulties resulting in the lack of a homogeneous distribution of the fibers within the concrete causing an appreciable drop in the compressive strength as compared to the plain concrete of the same class. Presently, a tangible guide for the best SF dosage for SFRC beams does not exist, and a comprehensive economic study for usage of steel fibers in the concrete of RC beams is not available [18]. Although cracking in concrete is generally a common phenomenon particularly when it regards to intrinsic cracks such as shrinkage, drying and plastic cracks, the possibility of limiting the opening of these cracks with use of steel fibers has been established and applied [19].

2.3 Assessment of shear capacity in RC beams

Researchers have acknowledged that shear phenomenon is a complex and difficult property to predict [8, 20, and 21]. According Khuntia et al [8], even more rational analyses such as the modified compression field theory (MCFT) contains important semi-empirical expressions, such as expressions for stress strain relationship of cracked concrete in tension and aggregate interlocking shear. It is for this reason that in most cases simplified models which are mostly empirically developed are applied in analysis and design of most conventionally reinforced RC beams.

2.3.1 RC beams with and without stirrup reinforcements

(a) Resistive mechanism

Shear failure in RC beams essentially occurs when the shear resistive mechanism of the beam diminishes or is weaker and can not withstand further the applied load. The two failure mechanism considered to occur comprise the arch action in the case for deep beams and beam action in slender beams. The dominance of any of the two mechanisms is governed by the structural material and aspects related to shear span to depth ratio. The mechanism in beams without shear reinforcements is conventionally considered to constitute contributions from the concrete compressive and shear strength, aggregate interlocking action and dowel action of the main bending reinforcements. In the case with conventional shear reinforcements, the resistive action in addition to concrete strength and dowel action comprise the resistance offered by the stirrup reinforcements. Figs 2.3 and 2.4 illustrate the idealization of the resistive mechanisms in RC beam without and with stirrup reinforcements [22]. In theory the relationship that govern the failure type (beam action, arch action or a combination of both) in a RC beam with the dowel action ignored is generally given by

$$V = \frac{dM}{dx} = \frac{d(T_s jd)}{dx} = jd \frac{dT_s}{dx} + T_s \frac{d(jd)}{dx} \quad (2.1)$$

Whereby in the case of beam action the shear force is given by

$$V_B = \frac{dM}{dx} = jd \frac{dT_s}{dx} \quad (2.2)$$

While in the case of arch action the shear force is given by

$$V_A = \frac{dM}{dx} = T_s \frac{d(jd)}{dx} = C \frac{d(jd)}{dx} \quad (2.3)$$

Where M is the moment, jd is the lever arm (location of the compression resultant C), T is the tension chord, C is the compression chord and dx is the shear span.

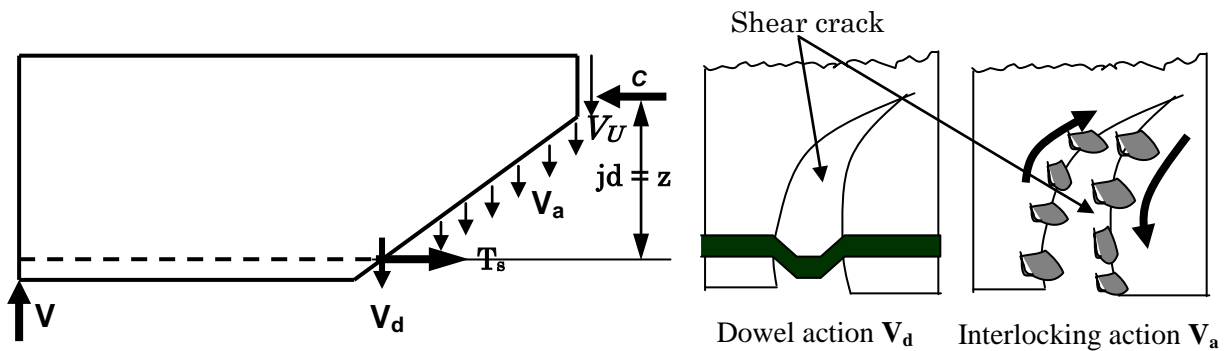


Fig. 2.3 Shear resistive mechanism in RC beam without shear reinforcement

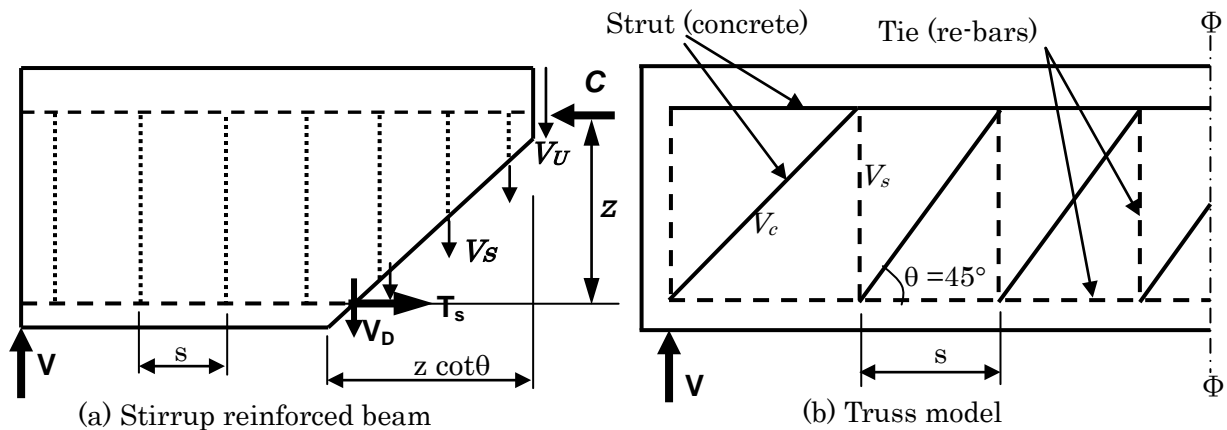


Fig. 2.4 Shear resistive mechanism in stirrup RC beam and the truss model

In Figs 2.3 and 2.4, V , V_D , and V_a are the shear force, dowel action, interlocking action of the rebars and interlocking action of the concrete along the shear crack, while V_U or V_c , C and z are the concrete shear strength, compressive strength and lever arm, respectively.

The interaction of these forces is often complex and difficult to predict, however simplified methods have been developed and applied in conjunction with empirical relations in the analysis and design of conventionally reinforced RC beams. The truss analogy as illustrated in Fig.2.4b is the most widely acknowledged method. The truss model is applied to simplify the complex shear resistive mechanism in RC beams. As shown in Fig.2.4b the truss model conceptual frame work, is idealized such that the forces in the beam are considered as a system comprising the tie forces acting on the reinforcements

(shear and bottom chord rebars) and the strut system mainly comprising the concrete in compression as well as the rebars in the compression. The truss model considers a constant inclination angle of 45° for the inclined concrete strut, while the vertical tensile strut is aligned to coincide with the stirrup reinforcements. This simplified mechanism allows for static analysis of the forces based on equilibrium of the applied load and the resistive strut and ties forces. Based on the forces shown in Fig 2.3, it is commonly implied theoretically that the shear capacity in RC beams with and without shear reinforcements is given by the summation of the individual contribution of the reinforcements and the concrete [22]. This is simply given by

$$V = V_U + V_a + V_d \quad (\text{Without stirrup reinforcement}) \quad (2.4)$$

$$V = V_U + V_s + V_a + V_d \quad (\text{Beam with conventional shear reinforcements}) \quad (2.5)$$

Application of the strut model simplifies the number of the dependents in the above equations and the prediction of shear capacity conventionally involves the use of the strut model and empirical relations defined for the unknowns parameters such as the concrete and dowel action contribution. In most cases the dowel action is seldom considered to influence much the shear capacity.

(b) Shear strength capacity predictive models

The simplified prediction capacity for beams conventionally reinforced in shear is generally given by

$$V = V_c + V_s \quad (\text{With shear reinforcements}) \quad (2.6)$$

Where concrete contribution is a function of the concrete compressive strength, aggregate interlocking strength and the main reinforcement ratio i.e. $V_c = f(V_u, V_a, \rho_s)$.

From the strut model shear strength contribution of the stirrup reinforcements is given by

$$\begin{aligned} V_s &= A_w f_{wy} n \\ &= A_w f_{wy} \frac{z \cot \theta}{s} \\ &= A_w f_{wy} \frac{z}{s} \end{aligned} \quad (2.7)$$

Contribution from the other parameters (concrete etc) are often obtained empirically and summed with that contributed by the stirrups reinforcements as given by Eq.2.6. There are a number of these relations for the prediction of shear capacity in the literature; however, given below are those from Japanese guide [22], American Concrete Institute [23] and Euro code (EC) [24]. According to Japanese standards [22], shear capacity in conventionally reinforced beam can be predicted by the following relation

$$V = 0.20 f_c'^{1/3} \rho_w^{1/3} d^{-1/4} \left(0.75 + \frac{1.4}{a/d} \right) b_w d + A_w f_{wy} \frac{z}{s} \quad (2.8)$$

Where, ρ_w is the rebar ratio, a is the shear span, b_w is beam width, d is the beam depth, A_w is the area of the stirrup reinforcements, f_{wy} is the stirrup yield strength, z is the lever arm, s is the stirrup spacing and n is the number of stirrups.

The American concrete institute (ACI 318-99) [23] relation for shear strength determinations is given by

$$V_c = k_{a/d} \left(0.158 \sqrt{f_c'} + 17 \rho \frac{V_u d}{M_u} \right) b d \leq 0.5 f_c' b d \quad \text{or} \quad 0.167 \sqrt{f_c'} b d \quad (\text{concrete contribution}) \quad (2.9)$$

$$V_s = \rho_v \left(\frac{1 + l_n/d}{12} \right) f_{vy} b d + \rho_{vh} \left(\frac{11 - l_n/d}{12} \right) f_{vy} b d \quad \text{for} \quad l_n/d < 5 \quad (\text{stirrup contribution}) \quad (2.10)$$

$$\text{or} \quad V_s = \rho_v f_{vy} b d \quad \text{for} \quad l_n/d < 5 \quad (\text{stirrup contribution}) \quad (2.11)$$

Where M_u is the flexural moment at the critical section, V_u is the shear force at the critical section and $k_{a/d} = 3.5 - 2.5 M_u / (V_u d) \leq 2.5$ and l_n is the clear span measured between supports.

For the Euro code (CEN) [24], shear strength capacity in conventionally reinforced RC beams is given by

$$V_c = \tau_{rd} k \beta (1.2 + 40 \rho) b d \quad \text{and} \quad V_s = 0.9 \rho_v f_{vy} b d \quad (2.12)$$

Where $k = 1.6 - d \geq 1$ (d in meters) $\beta = 1$ $a/d \geq 2.5$ and $\beta = 2.5d/a \leq 5$ for $a/d < 2.5$

$$\rho = \min[A_s / (b d), 0.02] \quad \tau_{rd} = 0.25 f_{ctk0.05} / \gamma_c \quad \gamma_c = 1.5; f_{ctk0.05} = 0.7 f_{ctm} \quad \text{and} \quad f_{ctm} = 0.3 f_c'^{2/3}$$

(f_c' in MPa)

2.3.2 RC beams reinforced with steel fibers

(a) Resistive mechanism

The resistive mechanism in Steel fiber RC beam is similar to conventional RC beams, only with the addition of the steel fiber contribution. The fibers bridge the cracks and transfer the stress across a crack as shown in Fig.2.5. However, unlike conventionally reinforced RC beams as previously discussed, a method of predicting the shear capacity in steel fiber RC beams has not been conclusive. And in effect there exists no method for prediction of the entire shear capacity evolution processes in any of the RC beams, i.e conventional and steel fiber RC beam. From Fig 2.5 above and following the summation analogy discussed in section 2.3.1 of the contributing forces to the overall shear resistance, the relevant shear capacity will be theoretically given by

$$V = V_U + V_a + V_d + V_f \quad (2.13)$$

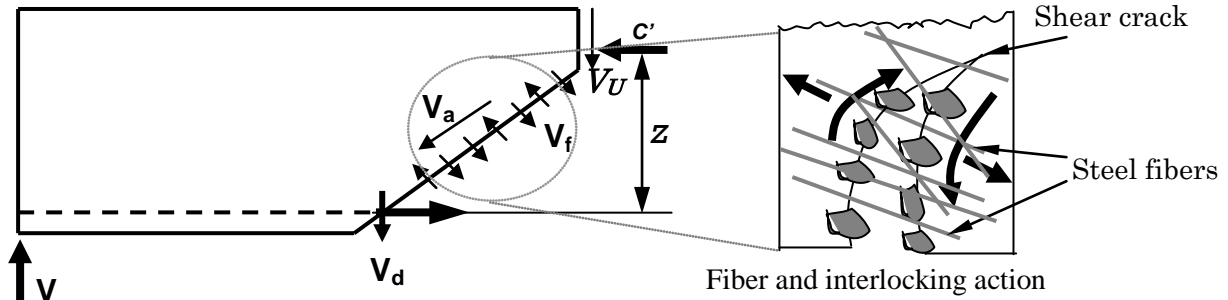


Fig. 2.5 Shear resistive mechanism in steel fiber RC beam

(b) Existing shear capacity prediction models for steel fiber RC beam

In the past two decades, a lot has been done on the computation of the ultimate shear capacity in SFRC and some empirical ultimate based relation have been proposed [6, 8, 25-34]. These empirical relations are mainly for estimation of the shear strength at failure.

The relations which are related directly to shear in SFRC are therefore summarized and discussed in detail in this section. Sharma [28] based on his own work and those of Batson, Jenkins and Spatney, proposed a simple empirical relation Eq.(2.14) for ultimate shear strength prediction in SFRC beams

$$v_u = k f_i (a/d)^{0.25} \quad (\text{MPa}) \quad (2.14)$$

Where v_u is the average shear stress at shear failure, $k = 2/3$, a/d is the shear span depth ratio, f_i is the split cylinder tensile strength of concrete if known or $f_i = 0.79(f_c)^{0.5}$ (MPa), incase the tensile strength is unknown and f_c is the concrete cylinder compressive strength. Although the equation is simple and has been recommended by ACI committee 544 [12], it does not account for all the factors that are known to affect the shear strength such as aggregate interlocking shear strength dowel action of the main reinforcement. Moreover, the relation does not directly account for the fiber content and by applying compressive strength to obtain the tensile strength for SFRC inaccurate results are obtained since it has been established recently that steel fibers has minimal influence on the compressive strength [3, 8, 26]. This fact is confirmed in the reported results [28] where by the correlation between the experimental and predicted shear strength results obtained based on (Eq.2.14) shows that for higher fiber content (1.5%) the ratio is between 1.22 and 1.22 compared to the results obtained for lower fiber content (less than 1%).

Narayanan and Darwish [32] proposed an improved empirical ultimate shear strength relation Eq.(2.15) for SFRC beams in which factors such as fiber content was accounted based on his own experimental work and that of four other researchers.

$$v_u = e \left[0.24 f_{spfc} + 80 \rho \frac{d}{a} \right] + v_b \quad (\text{Mpa}) \quad (2.15)$$

Where v_u is the average shear stress at shear failure, e is the arch action factor which is equal to 1.0 for $a/d > 2.8$ and $2.8a/d$ for $a/d \leq 2.8$, while $f_{spfc} = f_{cuf}/(20-\sqrt{F})+0.7+1.0\sqrt{F}$ (in MPa) is the computed split cylinder strength of fiber concrete, $F=(L_f/D_f)V_f d_f$ is the fiber factor, ρ is the flexural reinforcement ratio whereby L_f is the fiber length, D_f is the fiber diameter, V_f is the volume fractions and d_f is the bond factor (0.5 for round fibers and 0.75 for crimped fibers), f_{cuf} is the cube strength of fiber concrete, $v_b = 0.41\tau F$ and τ is the average fiber matrix interfacial bond stress, taken as 4.15MPa. In the derivation of the fiber contribution v_b , Narayanan and Darwish considered the contribution of the fibers along an ideal shear crack inclined at 45 degrees with the assumption that fiber failure is by pull out. This model has considered a number of parameters ignored in Eq. (2.11) with exception of the aggregate interlocking shear capacity. However, methods used to arrive at the dowel parameters are unclear. For example no indication of how the parameter e and factors; 0.24, 80, were obtained. Moreover, the non dimensional factor e is similar to that proposed by Zsutty [33] which is for beams without fibers and which in itself is arbitrary derived.

Equations (2.16), (2.17) and (2.18) are the empirical ultimate shear strength equations proposed by Ashour et al [31] for High strength fiber reinforced concrete (HSFRC) beams. These equations (Eqs. 2.16, 2.17 and 2.18) were obtained based on their own test results and modification of Zsutty's [33], Narayanan et al [32], ACI committee 318 buildings code and Swamy et al [35] equations.

$$v_u = \left(2.11\sqrt[3]{f'_c + 7F}\right) \left(\rho \frac{d}{a}\right)^{0.333} \quad (\text{MPa}) \quad \text{for } a/d \geq 2.5 \quad (2.16)$$

$$v_u = \left[Eq.3\right] \frac{2.5}{a/d} + v_b \left(2.5 - \frac{a}{d}\right) \quad (\text{MPa}) \quad \text{for } a/d \leq 2.5 \quad (2.17)$$

$$v_u = \left(0.7\sqrt{f'_c + 7F}\right) \frac{d}{a} + 17.2\rho \frac{d}{a} \quad (\text{MPa}) \quad (2.18)$$

In the above equations the terms are same as those described in Eqs (2.15) and (2.16). Equation (2.17) and (2.18) includes the same parameters that were incorporated in Eq.(2.15) and the constants in Eqs (2.14) and (2.15) were determined by regression analysis of the test results. According to the authors [31] these equations predicted well their experimental results on HSDRC beams. However, based on analysis on 139 tests, Kwak et al [25] established that Ashour's equations were less accurate than those of Narayanan (Eq.2.15). According to him the difference is as result of different sets of data and by including test results for beams with flexural reinforcement ratio of 0.37% or a/d of 6.0 to calibrate the equations.

The expression proposed by Imam et al Eq.(2.19) [34] is based on the modification of Bazant and Sun shear strength equation for conventional concrete beams which in addition accounts for the size effect. Bazant and Sun model [36] was developed based on fracture mechanics to account for the influence of the aggregates and stirrups in shear capacity. In fact Iman et al's modification of Bazant

and sun model is by substituting the reinforcement ratio ρ with a factored parameter $\omega = \rho(1+4F)$ and by adjusting the constants

$$v_u = 0.6\psi\sqrt[3]{\omega} \left[(f'_c)^{0.44} + 275\sqrt{\frac{\omega}{(a/d)^5}} \right] \text{ (MPa)} \quad (2.19)$$

Where $\psi = \text{Size effect} = \frac{1 + \sqrt{(5.08/d_a)}}{\sqrt{1 + d/(25d_a)}}$, ω is the reinforcement factor given by $(1+4F)$, F is the fiber factor $(L_f/D_f)V_f/d_f$ and d_f is bond factor equal to 0.5 for smooth fibres, 0.9 for deformed fibers and 1.0 for hooked fibres. In the evaluation by kwak et al [25], it is shown that the model was less accurate than that of Narayanan and Darwish (Eq.2.15).

Kwak et al developed a simplified model by combining zsutty's equations to arrive at a slightly modified shear strength equation than that of Narayanan and Darwish (Eq.2.15) as given in Eq.2.20.

$$v_u = 3.7ef_{spfc}^{2/3} \left(\rho \frac{d}{a} \right)^{1/3} + 0.8v_b \text{ (Mpa)} \quad (2.20)$$

Where $v_b = 0.41\tau F$ as defined in Eq. (2.15), and e is the arch action factor which is equal to 1.0 for $a/d > 3.5$ and $3.5a/d$ for $a/d \leq 3.5$. Equation is similar to Narayanan and Darwish [32] only that it accounts for higher shear span to depth ratio. Kwak [25] further proposed a simpler equation for estimation of the cracking shear strength (Eq.2.21) whose results were in agreement with the tests results by Narayanan.

$$v_{cr} = 0.24(f_{spfc}^{2/3}) \left(\rho \frac{d}{a} \right)^{1/3} \text{ (MPa)} \quad (2.21)$$

Analytical and experimental comparisons of most of these existing empirical shear strength relations by Choi et al [27] further showed Eq. (2.20) proposed by Kwak yield accurate results.

By considering a summation of the shear transfer forces (Fig.2.6) and empirical relations from other sources, Khuntia et al [8] proposed an empirical ultimate model for normal and high strength fiber concrete (Eq.2.22). In the derivation, ACI empirical relation for normal concrete $V = 0.167(\sqrt{f'_c})b_w d$ which accounts for the total shear resistance from concrete ($v_c = v_{cc} + v_a + v_d$) in which the contribution from the compression zone (v_{cc}), aggregate interlocking (v_a) and dowel action (v_d) were simply added to the post cracking tensile strength term ($V_{fr} = 0.25F(\sqrt{f'_c})b_w d$) previously proposed by other researchers (see Khuntia et al [8])

$$v_u = (0.167 + 0.25F)\sqrt{f'_c}b_w d \text{ (N)} \quad (2.22)$$

Where, F is a fiber factor given as $(F = \beta V_f d_f/d_f)$, β is a factor (equals 1 for hooked fibers, 2/3 for plain or round fibers for normal concrete otherwise 3/4 in the case of light weight concrete), V_f is the fiber

content, l_f is the fiber length, d_f is fiber diameter, f_c is concrete compression, b_w is the beam width and d is the beam depth. Although this model considers most of the parameters that account for shear resistance in beams, the mode of derivation in which direct use of empirical relations is simply superimposed and summed up without the actual contributory analysis as depicted in Fig.2.6 resulted in the less accurate results whose comparative statistical analysis with the experimental test results from other ten researchers showed a an under prediction of the experimental results by as much as 40% (see ref [8]) with a 0.37 standard deviation.

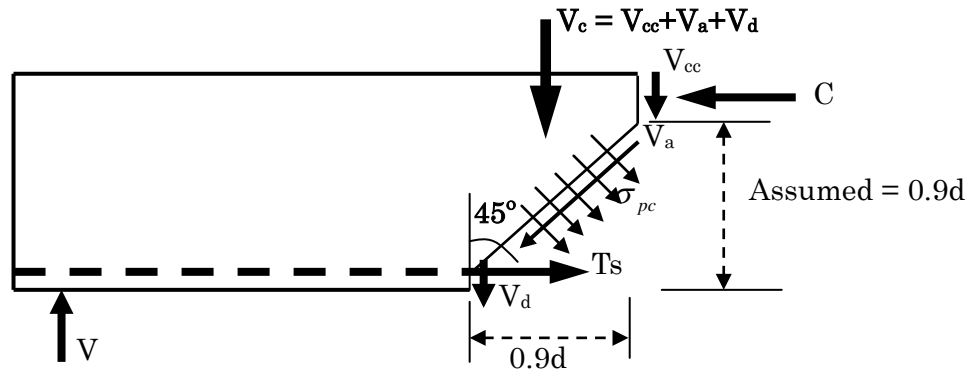


Fig.2.6 Strength contributions in SFRC beam [8]

The analysis by Kwak et al [25] clearly illustrated the fact that by applying same empirical equations previously derived (Narayanan) and those for beams without fibers (Zsutty's and ACI committee 318 equations), the shortcomings in these previous equations as earlier discussed are retained. In his analysis Kwak et al [25] established that the mean of the ratio of measured shear strength to calculated (from the analytical models) shear strength was 1.26 for the 139 tests considered and the coefficient of variation of this ratio was 37%. Even the experimental comparisons by Khuntia et al [8] were still not good either; in-fact the statistical accuracy was similar to that established by Kwak et al.

In an attempt to develop a purely theoretical model, Shitote [21] proposed an interesting model based on Compression field theory which was compared with the experimental results from [38]. The results showed fair agreement with overall behavior, however a large error in the initial phases is observed. More over the solutions requires initial guess of some parameters with use of variable relations and iterative solutions making it tedious to apply. The model ignored the contributions of the concrete tensile strength and dowel action of the re bars.

2.3.3 Experimental and Numerical investigations on Steel fiber RC beams

(a) Experimental investigation

Although shear behavior in SFRC beams has been investigated experimentally by a number of researchers [2-6, 8, 9, 15-18, 20-36, 35, 37, 38, 39], the information obtained in these studies is still considered limited [2, 7, 17]. Moreover, it has been noted that shear failure mechanism and its prediction is difficult to solve experimentally and analytically [40]. The assessment of shear capacity

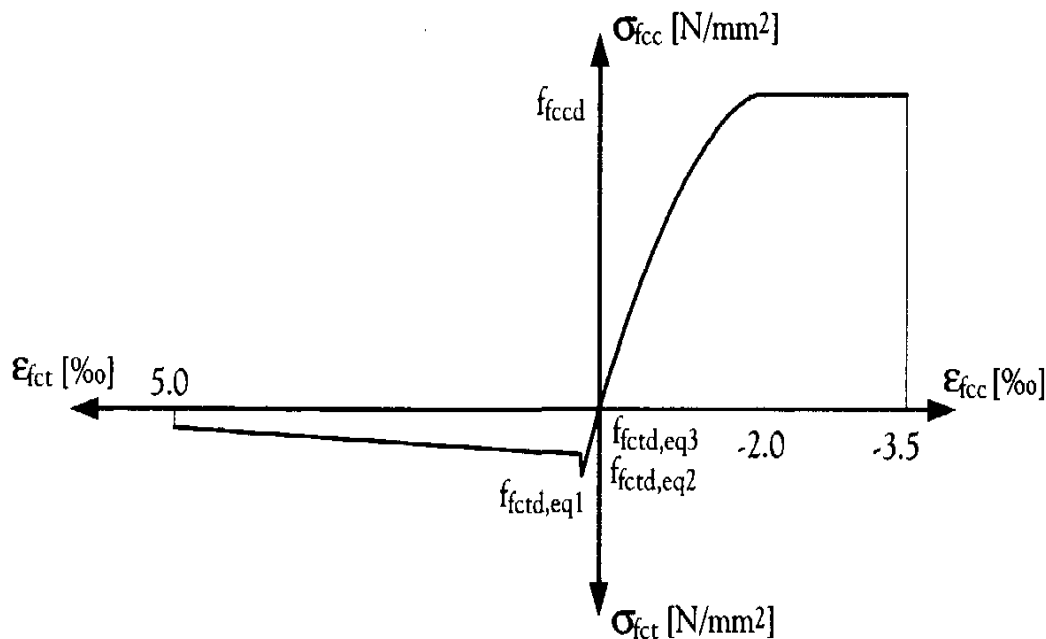
analysis models in section 2.3.2 indicates that all the relations were obtained on the basis of experimental investigations on steel fiber reinforced beams without stirrups. Moreover, it has been pointed out that a limited number of these researchers consider coupled investigations in which the performance of SFRC beams are evaluated against conventionally reinforced (with stirrups) beams in shear [17], [31]. Unfortunately, the few [17, 22, 27, 28, 30, 37] coupled investigations do introduce the shear reinforcement in the beams for purposes of comparisons with the fiber beams rather in an arbitrary way. There are no indications of how the amount of these stirrup reinforcements applied in the stirrup beams were obtained so that the comparisons made can be considered justifiable. In the use of the stirrups the reinforcing is such that either the beam is reinforced throughout with stirrups or only in the shear region. The questions that arise are: what was the criteria used in determination of the number of stirrups; why apply steel fibers throughout the beam and compare the test results with that of beam partially reinforced with arbitrary number of stirrups.

The test methods applied were mainly by three or four-point bending which can also be used an indirect shear test method while deformation measurement is by use linear variable displacement transducers (LVDT) and strain gauges. The use of strain gauges was found to be mainly limited to gauging the performance of the bar reinforcements. Although conventional experimental measurement techniques (use of strain gauges, LVDTs etc) have been applied successfully in RC beams, it is evident that certain fundamental aspects such as full field deformations (e.g. strain field) that would be more informing particularly in the case of SFRC beams as opposed to localized measurements (e.g. of strains), are never investigated. A survey of the experiments on SFRC beams [2-6, 9, 15-18, 20-27-36, 38, 39] confirms this shortcoming. The limitation of these conventional measurement methods hinders the full potential of quantifying and understanding SFRC as structural material and as applied in RC beams.

(b) Numerical investigations on

Few attempts have been made in the past to numerically simulate the response of steel fiber reinforced elements [9, 14]. According to Feheling [9]; lack of suitable constitutive material models for SFRC composite is considered as the contributing factor. Moreover, developing material models for SFRC is relatively a very complex task because of the different geometric scales involved in the initiation and propagation of damage leading to failure [9]. Despite this view, two generalized materials models have been proposed whose details including its disadvantages have been discussed in detail by Kooiman [19]. The German Concrete Society's (*Bemessungsgrundlagen für Stahlfaserbeton im Tunnelbau*) model for use in tunnel structures (Fig. 2.7) is the first attempt to generate a reliable design model for SFRC [19] and was developed based on experimental results derived from compression and four point bending tests on notched standard beams. The second is the stress strain relation (Fig 2.8) that given in the RILEM draft recommendations on test and design methods for SFRC (RILEM TC162-TDF). Although these models are applicable to SFRC, they are general and are intended as a guideline on

how to generate an idealized stress strain diagram for the use in design calculations. Indeed there exist commercial numerical codes (e.g DAINA, SOFISTIK MARC and ANSYS,) for which the simulation and analysis of almost any type of structure can be carried out. However, most of these analytical codes have been developed for the analysis design of structures making use of traditional engineering materials. However, with a user-defined or an ideal material model, it is possible to extend the analysis to structures making use of new or emerging materials such as SFRC. Although simple empirical relations may be applied in conventional analysis, only a method employing finite elements method is adequate for the study of the damage to structures for which the use of SFRC is advantageous [39].



- σ_{fcc} = compressive stress in fiber reinforced cementitious composite
- f_{fccd} = design compressive strength of SFRC
- σ_{fct} = compressive stress in fiber reinforced cementitious composite
- $f_{fctd,eq1,2,3}$ = Equivalent post cracking strength design values of SFRC
- ϵ_{fcc} = compressive strain in fiber reinforced cementitious composite
- ϵ_{fct} = Tensile strain in fiber reinforced cementitious composite

Fig. 2.7 Stress strain diagram according to DBV, Markblatt, 1992 [19]

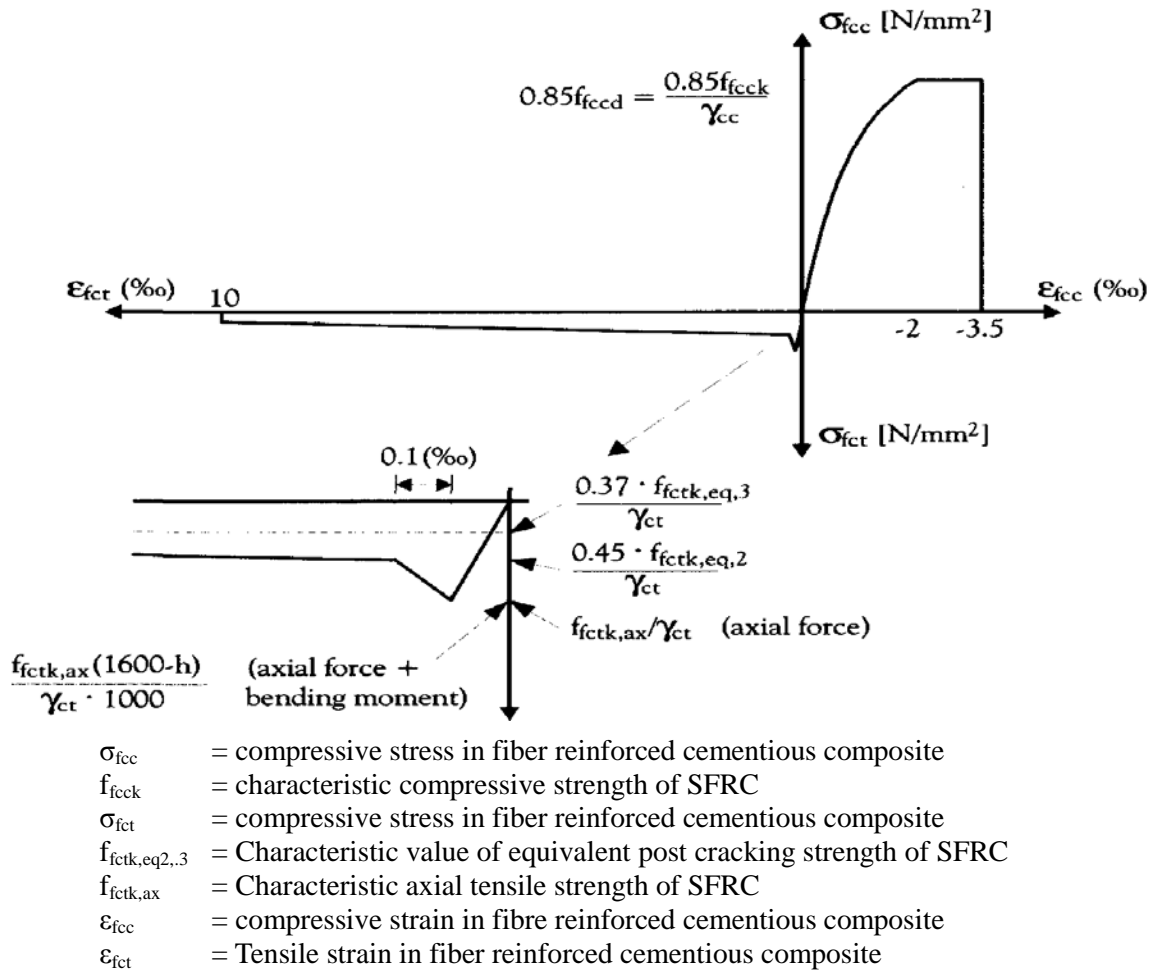


Fig. 2.8 Stress strain diagram according to RELIM TC 162-TFD, 2000 [19]

2.4 Concluding remarks

The review in this chapter informs the following: (a) ultimate shear strength has been the predominantly target in the analytical models identified, (b) the methods employed in developing these models are mainly empirical and in reality these empirical proposals can only yield results that are only valid if the input parameters fit the actual test parameters. This fact is supported by the detailed experimental and statistical evaluation by Kwak et al [25] and Choi [27] which revealed that apart from the models Narayanan and Darwish [32], most of the other empirical models do not accurately predict the shear strength capacity of SFRC beams, (c) contribution of the steel fibers to the shear strength is primarily estimated from compressive strength of SFRC; because of the characteristic material properties of steel fiber reinforced concrete (SFRC), a description of the shear phenomena is not realistic by using strength criteria like cube strength [14], moreover, unlike the shear capacity, the cube strength does not increase when steel fibers are added to the concrete [3, 18, and 25], in effect there is no much information on a rational method for the prediction of the actual contribution by the steel fibers, concrete and the dowel action of the main reinforcements, (d) in the comparative evaluations between fiber and stirrup reinforced beams, there was no method of obtaining the

equivalent amount of the fiber content and vice versa so as to justify the correlation of the results, (e) the only shear strength model that has so far been recommended for design considerations is that proposed by Sharma [28] which has been recommended by ACI committee 544 [12], (f) numerical investigations in SFRC structures are still lacking.

In view of these findings, the present research seeks to address the shortcoming by using theoretical, experimental and numerical methods that allow for the complete characterization of the shear response to failure. Some of the experimental drawbacks such as determination of the correct amount of stirrups and or fiber for comparison purposes as well as deformation measurements shall also be addressed.

Chapter 3

Experimental and theoretical research methodology

3.1 Introduction

This chapter describes the experimental and theoretical research methods that were considered and those that were applied in this research. A background description of the methods and reasons for adoption are discussed. Experimental method employed is given with specifics which include measurement techniques, materials and manufacture of specimens. The methods are presented and discussed in general without any reference to specific test results as these are presented and discussed in detail in the subsequent chapters.

3.2 Experimental methods

3.2.1 Bending-shear test

The most widely accepted standard testing method for flexural and shear investigations in beams is bending-shear test. This is because in practice most structures are subjected to bending and shear. Even though these laboratory tests may not replicate exactly the real situation as in the field, they offer a simple, cheap and practical means of evaluating structural systems for designs, monitoring and or performance. Bending-shear is often referred also as three-point bending or four-point bending testing depending on the loading set up status. To avoid any confusion in the usage of these terms, the latter and the former descriptions often imply test set up such that the shear spans or distance between the loading and supports points are equal so that there is symmetry about the mid span. Fig.3.1 illustrates the differences between the methods as applied in experimental research.

Four point bending is applied on standard unreformed beam in the determination of the material parameters such as modulus of rupture or flexural strength, while three point bending is often applied in notched and un-reinforced (in bending) standard beams for the study of crack opening behavior in concrete. Stress-crack width ($\sigma-w$) laws are purposely for development of material models for design applications [19] and often applied in numerical tools for numerical simulations. In the current research, use of notched beams in establishing a materials model for the numerical simulations was not considered as a choice. This was because of the following reasons: notched beams fully reinforced with steel fibers would be a waste given that the point of measurement would be localized at the notch area, moreover, sawing of the specimen would also be needed to create the notch; An option of localizing steel fibers during casting along the notch zone will not guarantee proper dispersions and orientation (random as in the real case); the choice of the numerical tool adopted in this research as

discussed in chapter 8 directly makes use of strain based models which can also be adopted from simple split tests, thus the use of crack based models was considered not necessary.

Depending on the purpose of the test one can adopted a form of test set up. In the current research both three and four point bending tests on reinforced un-notched beams were adopted. Principally, the two forms were adopted because the influence of shear span to depth ratio variation was needed not only in evaluating the response of the theoretical model but also in considering the effect of the fibers on the failure modes.

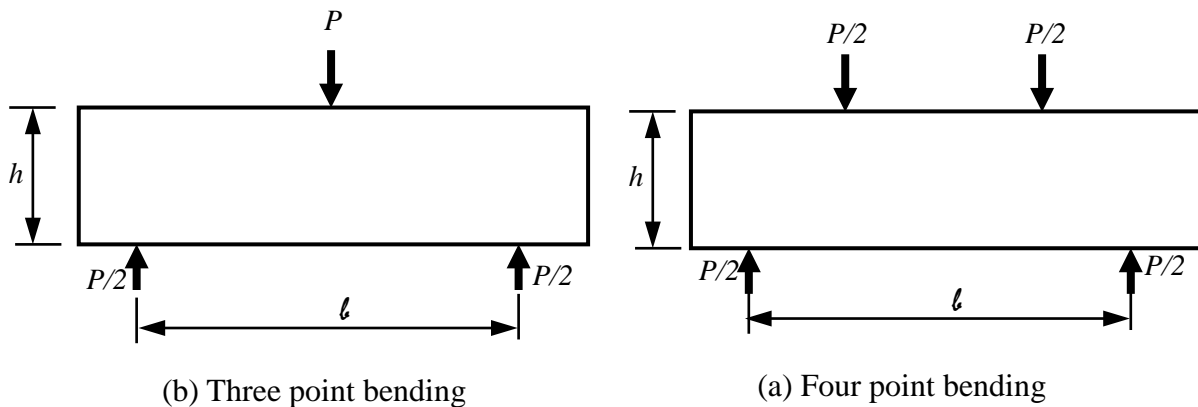


Fig.3.1 Forms of bending-shear tests

3.2.2 Compression and Split test

In practice evaluation of the mechanical behavior of a sample under conditions of tension and compression is performed to provide basic material property data that are critical for structural design and service performance assessment. For reliable investigations (analytical or experimental) in research, these materials parameters are not only necessary for control of the material applied on the test specimens under investigation but also are also a fundamental input data for modeling the structural behavior. In this research, compression and split tests have been applied not only to obtain the characteristic parameters for material control and structural modeling but also to study the deformation behavior of SFRC under direct splitting and compressive loads. Compressive strength is the maximum compressive stress a material is capable of withstanding without fracture. It is obtained by dividing the ultimate compressive load over the surface area applied which is often the cross sectional area of the test cylinders. Tensile strength is the maximum tensile stress a material can sustain without fracture. It is calculated by dividing the maximum load applied during the tensile test by the half the circumferential longitudinal cross sectional area of the sample. Other parameters obtained under these standard strength tests include, Poisson's ratio and modulus of elasticity which is the ratio of stress to strain, (i.e. the slope of the stress-strain curve below the proportional limit). Modulus of elasticity is considered as the measure of rigidity or stiffness of the material.

3.2.3 Conventional measurements methods

Data acquired from experimental research are often of two forms; deformation (displacements, strains and cracking pattern/widths) and load capacity. The standard techniques widely applied in obtaining these data are; using a data logger (connected with and or without a PC processor) for load monitoring and recording, linear variable displacement transducers (LVDT) and strain gauges (electronic/mechanical) for displacement and strain measurements respectively. Although crack widths can be measured by means of clip gauges/demec gauges (by measurement of the relative movement of studs bonded on the concrete's surface at a set distance apart across the crack), measurements and monitoring still poses difficulty particularly in experimental investigation of structural concrete. This is because of the difficulty in the identification of crack initiation and propagations locations as well as non existence of a proper measurement and monitoring methods which can be applied on a whole field scale without using notches at particular locations. It is for this reason that investigation on cracking behavior still makes use of the notched specimens to train the crack initiate from a specific point. This point offers possibility of monitoring the crack growth by means of demecs gauges/clip gauges and or LVDTs. In this research, non-conventional techniques which are relatively new particularly in the field of civil engineering sub discipline dealing with concrete structures have been applied. Non contact, optical full field techniques is one such method adopted.

3.2.4 Non contact full field optical measurement methods

A common occurrence in experimental mechanics is that when a sample is studied, e.g. in bending test, the sample is often simultaneously exposed to rigid body motions and small deformations. These deformations are often referred to as displacement fields. Conventional measurement techniques approximate these deformations based on measurements at a finite points using strain gauges or LVDTs for strains and displacements respectively. One of the objectives of this research is to also characterize the full field deformations of SFRC as a structural material. This objective is inspired by the opinion of the author that, deformations in SFRC are influenced by the random presence of steel fibers in the full volume of the parent concrete. Thus in addition to some of the conventional methods discussed in section 3.3.1, this research has adopted two optical measurement methods. These methods were used to characterize in detail the full field deformation including cracking behavior of SFRC as a structural material and as applied in RC beams. The details of these Optical methods are discussed further in the following subsections.

(a) Optical Electronic speckle pattern interferometry (ESPI)

ESPI is an optical measurement method that can be used to realize the dynamic and full field non-contact measurement and evaluation of the deformations. The technique is based on random speckle pattern (interferometry) generated by laser beamed over a surface (Fig.3.2a).The laser beam is

split into two illuminating beams. The beam reflected from the object surface (shown in yellow in Fig. 3.2a) and the reference surface (reference beam) then recombined after passing through a beam combiner. The reference beam is an expanded beam derived from the laser beam, and is added to the image of the object which is formed on the video camera. This result is an interference pattern called ‘speckle fringe pattern’ and is recorded digitally by the CCD sensor (Fig.3.2a) which is connected to an ESPI PC processor equipped with ESPI analysis program (ISTRA).

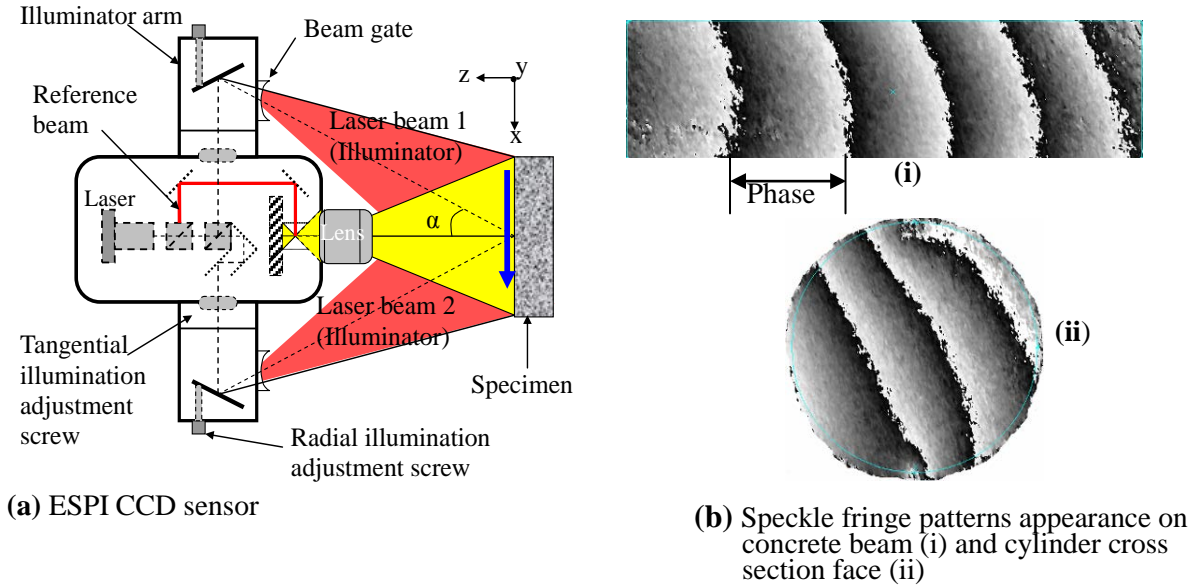


Fig.3.2 In plane ESPI measurement system

When the object is deforming, speckle interference occurs, the intensity differences between two consecutive speckle patterns ($I_2 - I_1$) result in fringes representing contours of displacement. These deformations are analytically determined based on the following correlation relations [41]

$$|I_2 - I_1| = 4a_1a_2 |\sin(\phi + \Delta\phi/2)| |\sin(\Delta\phi/2)| \quad (3.1)$$

Where ϕ is given by;

$$\phi(x, y) = \theta(x, y) + 2\pi k(x, y) \quad (3.2)$$

For an in plane case, the phase shift $\Delta\phi$ which relates to the object deformation is determined by [39, 40, 41]

$$\Delta\phi = \frac{4\pi u, v(x, y)}{\lambda} \sin \alpha \quad (3.3)$$

In the above equations, I_1 is the initial speckle intensity, I_2 is the subsequent speckle intensity, θ is the initial phase, a_1 and a_2 are amplitude factors, λ is the wavelength, α is the angle between illumination directions and the axis of observation (Fig.3.2a), u, v represents the in plane local

displacements in a given direction within the global geometry co-ordinates (x,y) and k is a frequency factor (see Fig 3.3). The entire procedure as described above is called phase shifting and is applied throughout the deformation process. Once the displacement fields are known, they are then used to estimate the strain fields by using strain displacement relations given by Eq.(3.4). Due to the complexity of the optical analytical methods and the volume of the data generated, the procedure requires the use of an ESPI software called ISTRA.

$$\varepsilon_x = \frac{\partial u}{\partial x}, \quad \varepsilon_y = \frac{\partial v}{\partial y}, \quad \gamma_{xy} = \frac{\partial u}{\partial y} + \frac{\partial v}{\partial x} \quad (3.4)$$

The advantage of the ESPI system is that it is sensitive to displacements on the order of between 0.05 to 1.1 microns depending on the object distance for an in plane case [44]

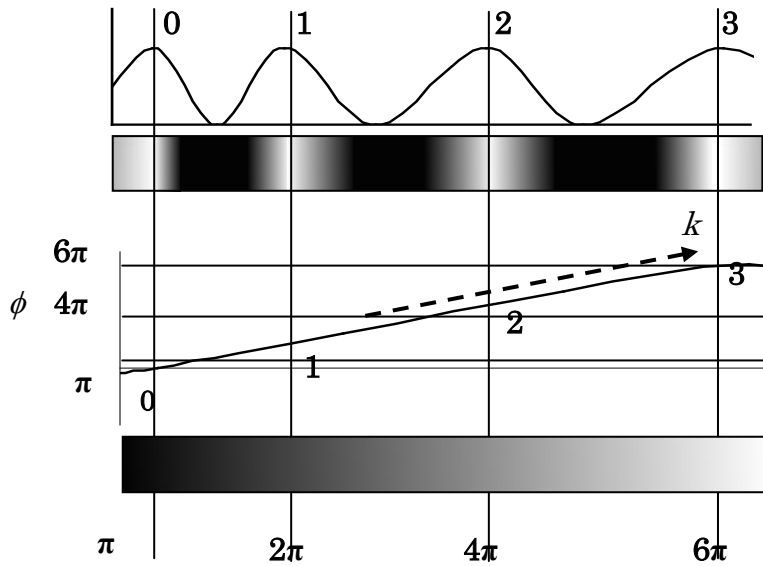


Fig 3.3 Phase distribution [41]

(b) Optical digital correlation Image methods (DCIM)

Like the ESPI method, digital image correlation is also a non-contact optical method for displacement and strain measurement. DCIM scheme generally comprise two digital cameras (1280×1024 pixels, 12bit) for taking the images, a PC equipped with processing algorithms programs (Vic-Snap or ARAMIS) for correlation analysis of the speckle images so as to obtain the for displacement and strain fields. Fig. 3.4 illustrates the schematic representation of DCIM.

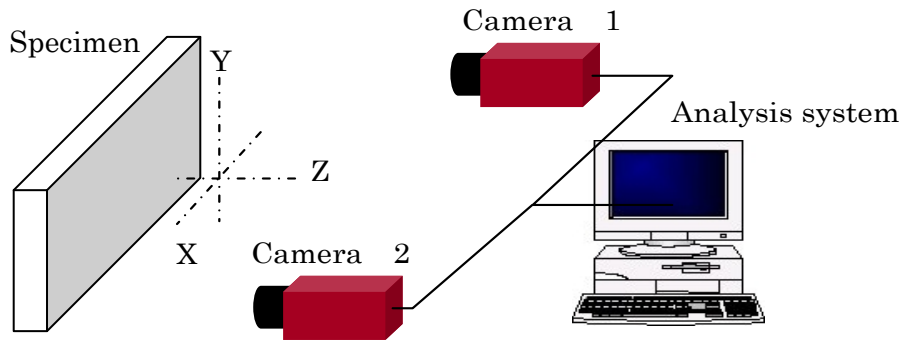


Fig.3.4 Schematic representation of DCIM equipment in front of a specimen

This method uses a cross-correlation function to compare images captured before and after deformation and obtain the whole field in-plane or out of plane displacements quantitatively with use of a processing algorithms. The method allows determination of displacements of selected points of the mesh on the surface of the deformed specimen by comparing successive images acquired during a test and cross-correlating the gray intensity patterns of the direct neighborhood of the points (or the reference areas). Unlike laser speckle techniques (ESPI), which require an optically rough, reflective surface and minimal vibration, the only requirement for surface condition is a visually ‘speckled’ surface. If not inherent to the material, this can be attained by application of a suitable random pattern such as with spray paints [45]. The basic principle applied in digital image correlation is that a set of neighboring points in an un-deformed state are assumed to remain as neighboring points after deformation. This would allow for auto correlation at each step. Fig.3.5 illustrates schematically this principle and the deformation process for a planar object [46].

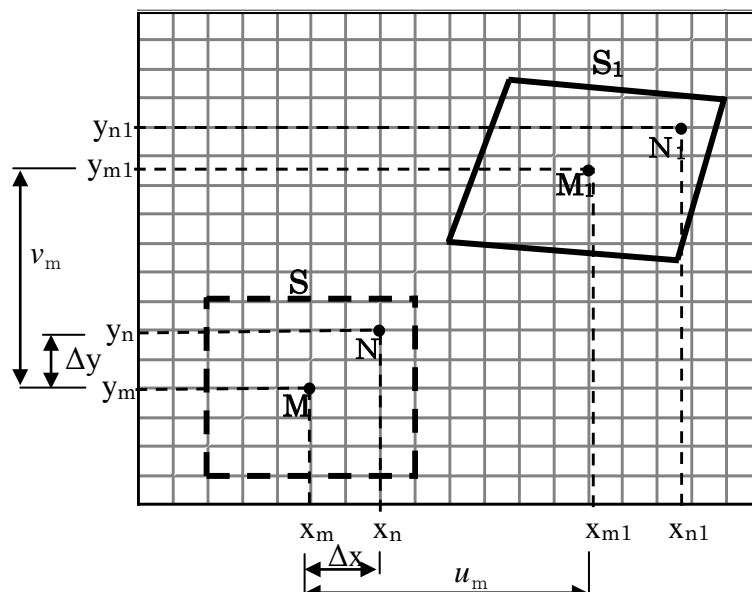


Fig.3.5 Idealized schematic deformation process [46]

The subset represented by quadrangle S (dash-line) is a reference (or un-deformed) sub-image and

quadrangle S_I (solid-line) is the corresponding deformed sub-image. In order to obtain in-plane displacements u_m and v_m of point M , sub-image S is matched with sub-image S_I using a correlation operation. For a sufficiently small subset S the coordinates of point M_I in S_I are approximated by first-order Taylor expansion as follows

$$x_{n1} = x_m + u_m + \left(1 + \frac{\partial u}{\partial x}\bigg|_M\right) \cdot \Delta x + \frac{\partial u}{\partial y}\bigg|_M \cdot \Delta y \quad (3.5)$$

$$y_{n1} = y_m + v_m + \left(1 + \frac{\partial v}{\partial x}\bigg|_M\right) \cdot \Delta x + \frac{\partial v}{\partial y}\bigg|_M \cdot \Delta y \quad (3.6)$$

By applying the above relations on correlation coefficient (Eq.3.7) and minimizing it, the displacement parameters are obtained. The minimization process makes use of non-linear optimization process, and iterations methods (e.g. Newton–Raphson) in the implementation of the image correlation process [45, 46].

$$C = \frac{\sum_{N \in S} [f(x_n, y_n) - f_d(x_{n1}, y_{n1})]^2}{\sum_{N \in S} [f(x_n, y_n)]^2} \quad (3.7)$$

In the above equations, $f(x,y)$ and $f_d(x,y)$ represent the gray value (speckle) distribution functions of the un-deformed and deformed image, respectively. The main objective of the correlation process is to find values of $u, v, \partial u / \partial x, \partial u / \partial y, \partial v / \partial x$ and $\partial v / \partial y$ for the subset under investigation, and then repeat it for all subsets in a given region so as to obtain the full field deformations. Once these full field displacement parameters are known, they are then used to estimate strain fields by using the standard following strain-displacement relation.

As mentioned earlier the entire analysis of the correlation process, determination and subsequent determination of the full field displacement and strains is carried out with the use computer software. Called Vic-snap and in similarity to ESPI, the data generated is often large and would require a data reduction process to narrow to the desired

3.2.5 Schedule and specimen design

The test methods discussed in section 3.2 were employed in the experimental programme of this research. The programme was divided in two categories: the first was manufacture and testing of cylinder and short SFRC beam specimens whose deformations were measured by conventional and optical methods. The geometrical dimensions of the beams considered at this stage were scaled down by a 1/5, 1/4 and 1/2 of a typical 2m × 0.4m × 0.2 m beam, respectively. The reason for this scaling down was because of the limitation of the available optical equipment particularly on the maximum area that can be accurately monitored and the need to monitor the full span deformation characteristics.

The second part of the experimental programme involved manufacture and testing of larger beams designed according to a proposed method for SFRC. Although deformations were measured also using optical DCIM method in addition to the conventional methods, in this case the target of deformation measurement was in the shear region.

In the first test programme, a total of twenty four short beams and twenty four cylinders were made whose distribution was as shown in Table 3.1.

Table 3.1 Specimens series matrix

| Test | series 1 | | | series 2 | Number of Cylinders Ø100×200mm | |
|-------------------------------------|---|-----|------|--|-----------------------------------|------------------------|
| a/d | 1 | 1.5 | 1.82 | 2.4 | | |
| Fiber/ stirrup content (%) | Number of short beams (400×100×100mm) | | | Number of large Beams (1800×230×150mm) | For compression test | For tensile test |
| 0 | 2 | 2 | 2 | 2 | 3,3 | 3,3 |
| 0.5 | 2 | 2 | 2 | - | 3 | 3 |
| 1.0 | 2 | 2 | 2 | 1 | 3 | 3 |
| 1.5 | 2 | 2 | 2 | 1 | 3 | 3 |
| Total | 24 | | | 4 | 15 | 15 |

Two beams were made in each category because of the need to have beams reinforced with steel fibers and stirrups for comparisons. The beams were variably reinforced with steel fibers ranging from 0 % to 1.5% fiber content. In the second part of the test programme, three large beams; two designed for shear in accordance with a proposed method for SFRC (appendix and Chapter 8 section 8.4) were made and tested. The test design of the larger beams was such that the shear span to depth ratio was between 2 and 2.5 which is a range within the critical ratio in which a diagonal tension shear or bending failure can occur according to classification of beams based on Kani's valley model [17]. In this group the deformation measurement in the shear region was measured using optical DCIM method. Stirrup reinforcements in the short beams were determined such that there was fiber–stirrup equivalency, however in the large beams stirrups were first obtained based on conventional method and equations then Eq. (.3.8) was applied to determine the equivalent amount of fiber content. This was carried out based a simple formula (Eq.3.8) which was derived based on the number of stirrups that would yield an equivalent amount of fibers volume in a beam of similar geometry.

$$N_s = \frac{v_f l_b A_b}{a_s l_s} \quad (3.8)$$

Where, N_s is the number of stirrups required, v_f is the equivalent fiber fraction, l_b is the beam length, A_b is cross sectional area of the beam, a_s and l_s are the stirrup cross-sectional area and lab-length, respectively. Fig.3.6 shows the main reinforcement grid applied on beams. The cylinder specimens were subject to compression and split tests in addition to evaluating the material strength, their deformation characteristics under these loads were examined by optical full field methods.



(a) Large beam stirrup-rebar's cage



(b) Large beams control and fiber rebar's



(c) Short beam stirrup-rebar's cage



(d) Short beam control and fiber beam rebar's

Fig 3.6 Beams Main reinforcement

3.2.6 Specimen manufacture and curing

The test specimens were manufactured from concrete made from ordinary Portland cement (OPC), crushed stone aggregates and sea sand whose gradation (see Appendix V) was in accordance with the Japan Society of Civil Engineer's (JSCE) guidelines [47]. End hooked steel fibers (Fig.3.7) with an aspect ratio of 48.4 and yield strength of 1000MPa was used in making SFRC. However, because steel fibers reduce the workability of the concrete, an admixture was used without increasing the amount water.

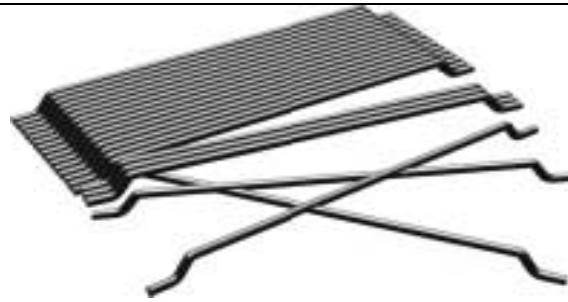


Fig.3.7 Collated end hooked steel fiber

The mix design was first established by carrying out trial mixes in which controlled water-cement ratio, admixture (air entraining; AE), fine to aggregate ratio were controlled until a suitable workable mixture with a constant water cement ratio of 0.47 and a fine to total aggregate ratio of slightly more than 40% was achieved. This design control was made to ensure that there was good optimum packing density of the aggregates, workable mix and retain the target strength. Table 3.2 shows the final mix proportions obtained which were used in the manufacture of all the specimens tested in this research.

Table 3.2 Mix design proportions

| Fiber Content (%) | Mix in Kg/m ³ | | | | |
|-------------------------|--------------------------|--------|--------|------|-----------|
| | Water | Cement | Gravel | Sand | admixture |
| 0.0 | 171 | 377 | 938 | 712 | 3 |
| 0.5 | 171 | 377 | 930 | 707 | 3 |
| 1.0 | 171 | 377 | 923 | 700 | 3 |
| 1.5 | 171 | 377 | 916 | 695 | 3 |

The mixing procedure followed in the steel fiber reinforced concrete (SFRC) can be summarized as follows;

- ✧ Course aggregates and fine aggregates were poured first into the mixer and spread gently
- ✧ The contents were mixed (in mixer) for about two minutes while ensuring that the in-sides of the mixer are free from clustered sand/aggregates
- ✧ Cement was then introduced gradually over the mixed aggregates and mixed until a uniform mix free from content segregation was achieved
- ✧ Water having been mixed prior with the admixture was then added and all the contents were then mixed for another three minutes.
- ✧ The steel fibers are added gradually on top of the freshly mixed concrete (Fig. 3.8a) and the contents are then mixed for about three minute.
- ✧ Finally the SFRC product (Fig.3.8b) is pour on the specimen moulds (Fig. 3.9)

Manufactured SFRC and plain concrete were cast in specific molds. During compaction vibration was applied shortly to evenly spread the mix and there after compaction was completed by side taping (see Fig.3.9b) of the mould to avoid segregation occurring. After leveling off excess concrete, the specimens were kept for 24 hours under dampen conditions before de-molding and curing for 28 days. In the specimens production, short beams were cast in standard steel moulds of 400×100×100mm (Fig 3.9b) while the larger beams were cast in tailor made timber mould of size 1800×230×150mm (Fig 3.9b). Cylinder specimens were cast using standard Ø100×200mm mould (Fig 3.9b). All the cylinders were cast concurrently with the beams. All short beams and cylinders were cured under complete emersion of water for 28days prior to testing, while the large beams were cured outside by covering with a continually dampened material for a similar period before testing.



(a) Addition of steel fibers



(b) SFRC product

Fig 3.8 SFRC manufacture and specimen casting



(a) Large beams



(b) Short beams and cylinders

Fig. 3.9 casting of specimens

3.3 Analytical methods applied

From the review in chapter 2, it was clear that ultimate shear strength has been the predominantly target in the empirical analytical models identified, moreover, numerical investigations in SFRC structures are still lacking. In the present research, two theoretical approaches have been adapted to

model and characterize strength and deformation behavior in SFRC beams under bending shear. These are;

- (a) Derivation of a purely theoretical shear strength and deformation evolution model based on shear failure mechanism of SFRC beams. The model derived is then verified experimentally from test results from this study and those found in the literature. The difference between the model proposed in this research and existing analytical models as discussed in chapter 2 is that the current model is an evolution based model which can also be adopted appropriately for both yield and ultimate shear strengths of SFRC beams. Secondly, the model is derived from first principles and then verified experimentally, numerically and by undertaking a parametric evaluation.
- (b) The second theoretical approach is a numerical simulation and verification with the experimental results from this study.

Details of the two theoretical methods as applied in this research are presented and discussed in detail in chapter 7 and 8.

3.4 Concluding remarks

The background of the research approach adopted has been discussed in this chapter. The experimental methods in particular have been given attention, because most of the experimental aspects discussed in this chapter have not been discussed in the subsequent chapters dedicated mainly to the specifics of the tests conducted and the results. However details pertaining to the theoretical derivations and numerical simulations and have been left out in this chapter. The details are related directly to the theoretical results and they are better understood when presented together these results.

Chapter 4

Development of a new theoretical shear evolution response model for SFRC beams

4.1 Introduction

Reinforced concrete structures are commonly designed to satisfy criteria of serviceability and safety against failure. Shear failure in reinforced concrete structural members is a major concern to civil and structural engineers, for it is known to be sudden and catastrophic. It occurs when the principal tensile stress limit in the shear region is exceeded. Conventionally, engineers reduce and control this problem in reinforced concrete structural systems through design by providing stirrup reinforcements. Use of steel fibers in reinforced concrete beams is expected to enhance post cracking strength, soften the shear brittle failure and prolong the deformation. However, in order to assess the margin of serviceability and safety against failure an accurate estimation of the yield and ultimate load is essential and the prediction of the load-deformation behavior throughout the range of elastic and inelastic response is desirable. Although within this framework the need for experimental research is necessary, it is only fundamental in the development stage of the theoretical model because the results of the model have to be evaluated by comparing with experiments on prototype models of structural sub-assemblages in this case beams. Ultimately a reliable theoretical model can reduce the number of required tests for the solution of a given problem, recognizing that tests are time-consuming and costly.

In similarity to shear capacity in conventional RC beams, the development of a purely theoretical shear model for the structural response in SFRC beams is difficult. This is corroborated by the fact that there exists no purely theoretical model for shear prediction whether an evolution or ultimate type. In the case of shear capacity in SFRC beams, the development can be complicated by a number of factors;(a) □SFRC is a composite material made up of concrete and steel materials with very different physical and mechanical behavior (b) concrete composite exhibits nonlinear behavior due to nonlinear material behavior and cracking, (c) reinforcing steel and concrete interact in a complex way. It is for these reasons that, prediction of shear phenomenon in SFRC beams is equally as complex as that of conventional RC Beams [8, 20, 21, and 40]. This complex shear phenomenon has led engineers in the past to rely heavily on empirical formulas for the design of concrete structures. From the literature survey in chapter two, it was evident that indeed there exists no unified theoretical expression to predict the complete shear strength evolution in which the ductility behavior, yield and ultimate strengths limits can be analytically characterized and quantified.

As presented in this chapter, an attempt is made to derive a theoretical expression which is capable

of predicting the shear deformation response evolution for steel fiber reinforced concrete beams with all the important parameters incorporated. The model proposed here differs from existing models in that it is derived first theoretically rather than from an empirical point of view, moreover it can be used to predict the shear load-deformation or shear stress-strain through elastic to inelastic range. This also allows for dimensioning of the model such that the yield and ultimate limits can be identified and quantified theoretically. The theoretical development and results are presented and discussed in this chapter whereas verification of the model against experimental and numerical results is discussed further in chapters 7 and 8 respectively

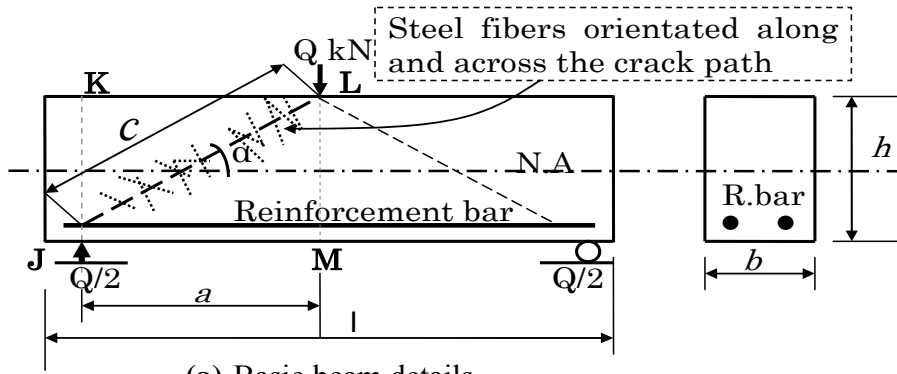
4.2 Derivation of expressions for the forces acting to resist the shear force

The knowledge of the shear response behavior of SFRC beams throughout out the elastic and in-elastic range and the ability to predict the same is paramount to the development of guidelines for design applications. The existence of a complex interaction of the various material and forces in the SFRC beam introduces difficulties. However, to overcome this problem, the derivation of the proposed model is made simple by making a number of assumptions and approximations in order to limit these complexities that would otherwise render the derivation of the same impossible. The development process entails determination of the internal resistive mechanism and equilibrium of forces. Solution of the equilibrium equations between the internal forces and the applied external load finally leads to a simplified predictive model. Deflections are determined and applied based on known theories [57, 58].

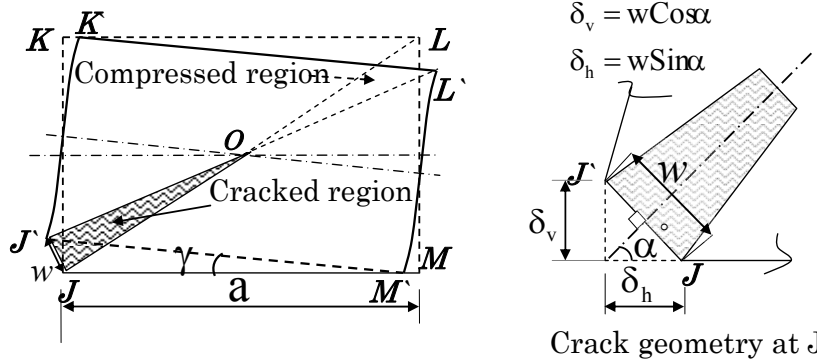
4.2.1 Model concept details

In SFRC beams without stirrups and under bending shear, interaction of the forces carried by the concrete, fibers and re-bars at a shear crack inclined at an angle (commonly at 45°) is often applied in determining the shear resistive mechanism [8, 37, 39, 59]. Similar approach is adopted in the present study; however, relations are derived based on the sheared geometry of a beam [58] and interactions of the resistive forces as shown in Fig.4.1 and Fig.4.2, respectively.

Using the forces and strain diagram illustrated in Fig.4.2, concrete and steel fibers contributions as well as the dowel action of the main reinforcements are considered. The response behavior is assumed interactively as illustrated in Fig.4.3. The stages indicated in Fig.4.3, are assumed to be roughly constituted in three parts; stage (I) is the range up to first concrete cracking in which the concrete contributes, stage (II) is the cracked stage in which fibers interact with the concrete such that, fiber-concrete bond behavior initiates stress transfers while aggregate interlocking (crack slip) offers additional shearing resistance and finally stage (III) whereby contribution from the dowel action of the re-bars occurs as the beam approaches its ultimate failure.



(a) Basic beam details



Crack geometry at J

(b) JKLM sheared profile and crack details at J

Fig 4.1 Conceptual model beam and shear deformation details

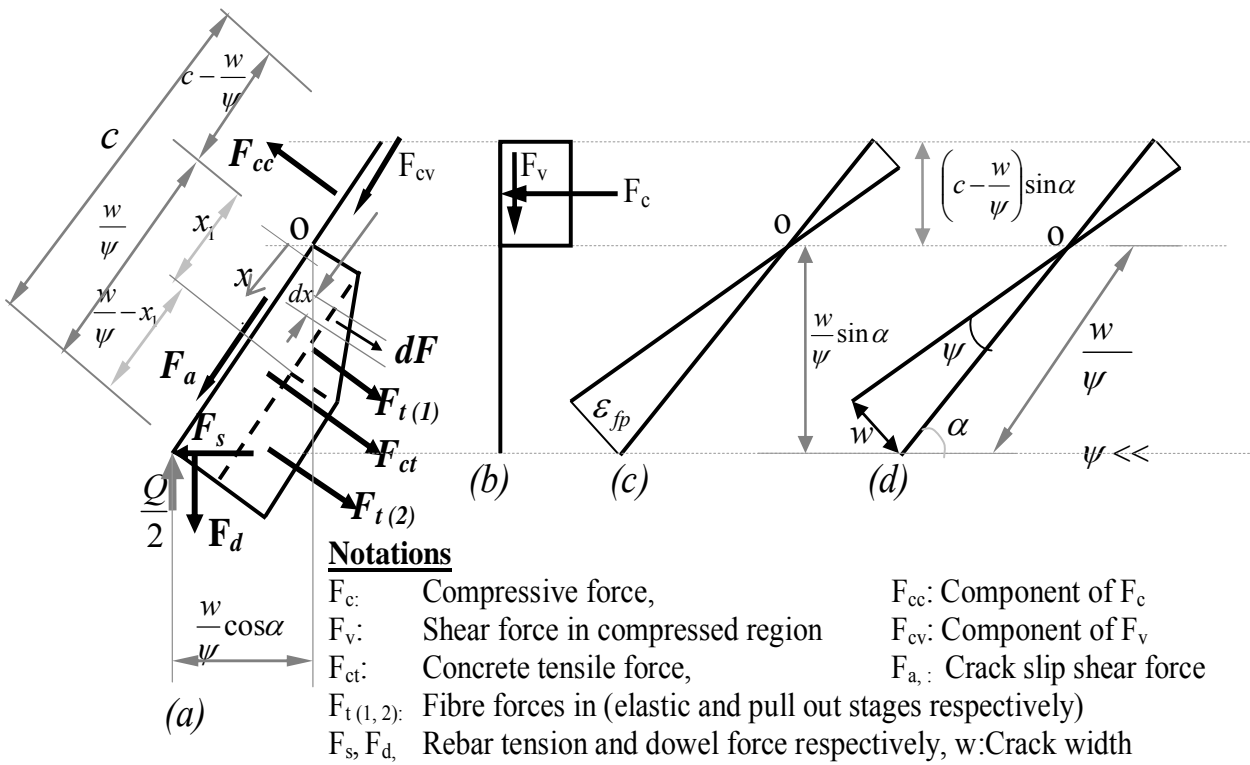


Fig 4.2 Tensile and compressive forces (a,b) strain (c) and crack opening d), diagrams

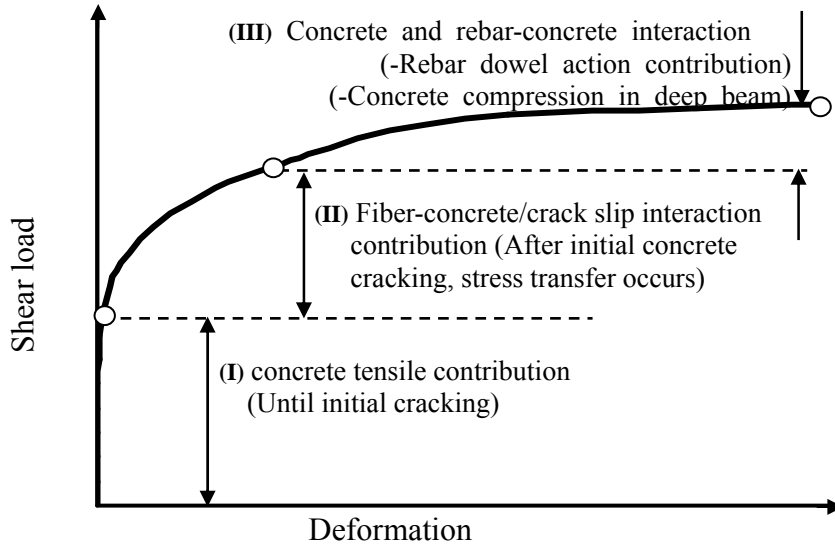


Fig.4.3 Idealized stages in the shear response behavior

In the derivation of the model the following principle assumptions were further made; (i) plane section remain plane (ii) shear crack occurs at 45° (iii) although concrete is brittle, it has some minimal tensile strength (iv) on yielding (concrete cracking), the fibers are assumed to elastically strain initially, de-bond and eventually pull out gradually from one side of the crack (v) dowel action of the flexural reinforcement bars contribute to the shear strength.

Due to symmetry, only half of the geometry shown in Fig.4.1a (i.e. portion *JKLM*) has been considered and its sheared profile analyzed. Based on Gere and Timonshenko's shear deformations in a beam [58], the cracked sheared profile of portion *JKLM* has been assumed to correspond to the profile shown in Fig.4.1b, while the stress, strain and crack opening diagrams along the crack path are assumed to be as shown in Figs 4.2.(a), (b), (c).

4.2.2 Concrete compressive force F_{cc} and Tensile force F_{ct}

In a beam under bending shear, tension and compression zones exist in which the compression zone is subjected to combined compressive and shear stresses [6]. As idealized in Fig.4.2a, it is assumed that the concrete possess some minimal tensile strength. After cracking the steel fibers transfer the tensile stresses across the shear crack. Considering the geometry of the model beam (Fig.4.1a) and the force/crack opening diagram (Fig.4.2), the expressions for the concrete compressive and tensile forces along the idealized crack path can be determined. Thus the resistive compressive and tensile forces from the concrete can be expressed by the following relation:

$$F_{cc} = \frac{F_c}{\sin \alpha} = \sigma_c b \left(c - \frac{w}{\psi} \right) \quad (4.1)$$

$$F_{ct} = \sigma_{ct} b \left(\frac{w}{\psi} \right) \quad (4.2)$$

4.2.3 Shearing forces (F_{cv} and F_a)

After carking, shearing the concrete in the compression region and crack slip over the cracked surfaces where the aggregates also interlock create yet another dimension of the overall shear resistive mechanism in a beam. The relation for these shearing forces (F_{cv} and F_a) in the compressed and cracked regions (Fig.4.2a) are established and considered under equilibrium analysis in section 4.3.1.

4.2.4 Fiber forces ($F_{t(1)}$ and $F_{t(2)}$)

In fiber reinforced concrete beam, after tensile cracking occurs, tensile stresses are transmitted across the crack and a resistive *mechanism* is developed [3]. The tensile stress transmitted is depended on; the effective number of fibers that bridge the crack orthogonally, bond strength and frictional forces. Practically, a complex interaction of these factors takes place. A simplified approach is adopted here. In order to determine the expression for the steel fiber tensile forces $F_{t(1)}$ and $F_{t(2)}$ (Fig.4.2a), expressions for the average normal fiber force and strain is first established.

(a) Average normal force per fiber and the fiber pull out strain

The derivations are made by considering an infinitesimal force dF acting over an equally infinitesimal distance dx as shown in Fig.4.2(a) and the orientation of the fibers across a shear crack as shown in Fig.4.4. In the derivation of the fiber forces, two regimes are considered as illustrated by the stress diagram in Fig.4.2 (a). The two regimes are;

- ✧ Elastic range (fibers elastically strain) $0 \leq x \leq x_1$
- ✧ Pull out range (fibers pulling out) $x_1 \leq x \leq \frac{w}{\psi}$

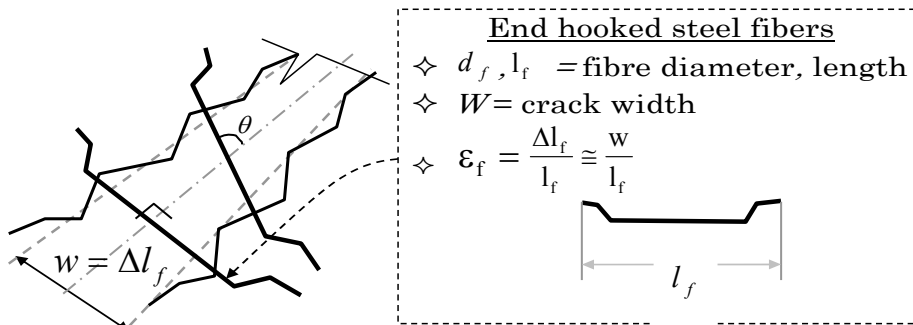


Fig.4.4 Fiber orientation across a shear crack and strain deduction

Elastic Range ($0 \leq x \leq x_1$)

According to micro crack mechanics investigations (Li et al [60]), when a crack tip approaches a fiber in the concrete, micro de-bonding of the order 200 μ m to 1000 μ m occurs and the fiber undergoes elastic stretching a phenomenon referred to as Cook-Gordon effect. As illustrated Fig.4.1a, this elastic behavior prior to full de-bonding of the fiber is considered in this study by deriving a relation for the force that accounts for it. The force per fiber crossing the crack at right angles in the elastic range can be expressed as

$$F_f = \sigma_f A_f = E_f A_f \varepsilon_f = E_f A_f \frac{w}{l_f} \quad (4.3)$$

Where σ_f , A_f , E_f and ε_f are the fiber stress, area elastic modulus and strain respectively. From Fig.4.2 (d), the crack width w at any distance x can be expressed as $w = x \tan \psi \cong x \psi$, where ψ is assumed to be small. Thus equation (4.3) becomes

$$F_f = E_f A_f \frac{w}{l_f} = E_f A_f \frac{x \psi}{l_f} \quad (\text{Where } l_f = \text{the fiber length}) \quad (4.4)$$

The fibers in practice are randomly distributed; each fiber crossing the shear crack can be oriented at an angle θ (Fig.4.4). Literature [61, 62, 63] reflects a common method of determining average fiber projection (orthogonal) factor $\zeta=2/\pi$. This factor according to Stroeven et al [61] yields the average number of effective fibers crossing a crack orthogonally in a plane and can be estimated by:

$$\zeta = \frac{\int_0^{\pi/2} \cos \theta d\theta}{\int_0^{\pi/2} d\theta} = \frac{2}{\pi} \quad (4.5)$$

Where θ is the fiber orientation angle across the line of crack (see Fig 4.4). Therefore, by applying Eq. (4.5) the average normal fiber force crossing a crack can be estimated by

$$F_{fN} = \zeta F_f \quad (4.6)$$

Substituting for the expression for force per fiber from Eq. (4.4) equation Eq. (4.6) yields the expression for the determination of the average force per fiber in the elastic range as

$$F_{fN}^e = \frac{2}{\pi} E_f A_f \frac{x \psi}{l_f} \quad (4.7)$$

Pull out range ($x_1 \leq x \leq w/\psi$)

Assuming that at this stage the fibers will gradually pull out, the average normal fiber force can be determined by applying a pull strain rather than an elastic strain on Eq. (4.3). The former is a kind out an equivalent effective strain, after cracking and it is arising-out of the interactive fiber concrete

reaction during the pull out process. Thus prior to establishing the fiber pull out force, the relationship that defines this pull out strain is first established.

Fiber pull-out strain (ϵ_{fp})

The fiber pull out strain is a function of the bond stress τ_b and the fiber aspect ratio A_f . To derive an expression for the pull out strain, an arbitrarily fiber pull out mechanism as shown in Fig.4.5 below is considered.

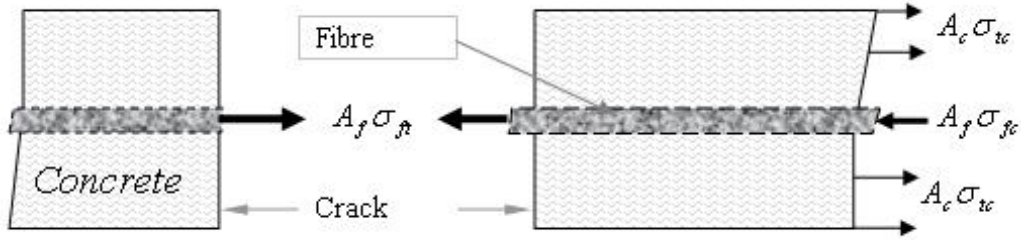


Fig. 4.5 Fiber pull-out equilibrium mechanism

The equilibrium of force between the concrete matrix and a fiber crossing a crack under a pull out forces will be given by

$$A_f \sigma_{ft} = A_c \sigma_{ct} - A_f \sigma_{fc} \quad (4.8)$$

Where A_f and A_c are the fiber and concrete areas respectively while σ_{ft} and σ_{ct} are the fiber and concrete stresses respectively. Assuming that the effect of the fiber compression force (σ_{fc} , A_f) is negligible, then

$$A_f \sigma_{ft} = A_c \sigma_{ct} \quad (4.9)$$

For compatibility, the equilibrium of forces at the fiber-concrete interface can be expressed as

$$A_c \sigma_{ct} = \tau_b \pi d_f l_f \quad (4.10)$$

Where τ_b is the bond strength, A_f and E_f are the fiber aspect ratio and elastic modulus of the fiber, respectively. The condition for the fiber to pull out is that the force in the fiber should exceed the interfacial shear force. This can be expressed by combining Eqs (4.9) and (4.10) as

$$A_f \sigma_{ft} \geq A_c \sigma_{ct} \geq \tau_b \pi d_f l_f, \text{ therefore } A_f E_f \epsilon_{fp} \geq \tau_b \pi d_f l_f \quad (4.11)$$

$$\epsilon_{fp} = \frac{\tau_b \pi d_f l_f}{A_f E_f} \quad (4.12)$$

As fiber pull out tests were not conducted in this research, a commonly applied value of the net fiber pull out length is established from literature [62, 64 and 65] as equal to $l_f / 4$. Thus Eq.(4.12) can be re-written to give the relation for fiber pull out strain as

$$\varepsilon_{fp} = \frac{\tau_b A_r}{E_f} \quad (4.13)$$

Where $A_r=l/d_f$ is the fiber aspect ratio. Applying the above established fiber pull out strain relation in Eq.(4.3) and subsequently Eq. (4.6), the average normal fiber force (per fiber) in the pull out range can be estimated by

$$F_{fN}^p = \frac{2}{\pi} E_f A_f \varepsilon_{fp} \quad (4.14)$$

(b) Force $F_{t(1)}$

Having established the relations for the force in a single fiber in the elastic and pull out range, the expressions for the total fiber forces shown in Fig.4.2a can now be deduced. The starting point is to establish the force $F_{t(1)}$. Referring to the stress diagram in Fig.4.2 (a), the total tensile force carried by the fibers during the elastic stage is determined as follows;

$$F_{t(1)} = \int_0^{x_1} dF = \int_0^{x_1} N_f F_{fN}^e \quad (4.15)$$

Where N_f is number of fibers cross the crack and F_{fN}^e is the average force per fiber as established earlier and given by Eq. (4.7). The number of fibers N_f can be derived based on the fraction of fibers V_f crossing a crack of area (bdx) as follows;

$$V_f = \frac{N_f A_f}{A_{sc}} = \frac{N_f A_f}{bdx}$$

$$N_f = \frac{V_f bdx}{A_f} \quad (4.16)$$

Where A_f and A_{sc} are the cross sectional areas of a single fiber and crack surface strip across the beam width (bdx), respectively. Substituting for F_{fN}^e from Eq (4.7) and N_f from Eq.(4.16) above, the relation for $F_{t(1)}$ in Eq.(4.15) can now be obtained as;

$$F_{t(1)} = \frac{2E_f bV_f \psi}{\pi l_f} \int_0^{x_1} x dx$$

$$= \frac{E_f bV_f \psi x_1^2}{\pi l_f} \quad (4.17)$$

When fibers begin to pull out from the concrete (here referred as yielding), $\varepsilon_f = \varepsilon_{fp}$ and from Fig.4.2 (a), $x = x_{l=w}/\psi$, it follows that from Fig.4.4 the following relation is obtained

$$\varepsilon_f = \frac{\Delta l_f}{l_f} \cong \frac{w}{l_f}, \text{ then } w = \Delta l_f = \varepsilon_f l_f, \text{ thus } x_1 = \frac{\varepsilon_{fp} l_f}{\psi} \quad (4.18)$$

Where Δl_f = fiber pull-out displacement corresponding to the crack width (Fig. 4.4) Substituting for x_1 in Eq.(4.17) from Eq.(4.18), the force $F_{t(1)}$ can now be expressed as

$$F_{t(1)} = \frac{E_f V_f b \varepsilon_{fp}^2 l_f}{\pi \psi} \quad (4.19)$$

The above equation can be simplified by substituting the some parameters in Eq. 7.19 with

$$K_1 = \frac{E_f V_f \varepsilon_{fp}}{\pi} \quad (4.20)$$

Resulting in the final version of the force $F_{t(1)}$ given by

$$F_{t(1)} = \frac{K_1 b \varepsilon_{fp} l_f}{\psi} \quad (4.21)$$

(c) Force $F_{t(2)}$

The expression for the total pull out force $F_{t(2)}$ is easily obtained from Fig4.2a Eqs, (4.14) and (4.18) by considering the area $b ((w/\psi)-x_1)$ as follows

$$F_{t(2)} = F_{fN}^p N_f = \frac{2}{\pi} E_f \varepsilon_{fp} V_f b \left(\frac{w}{\psi} - x_1 \right) \quad (4.22)$$

Noting that $K_1 = \frac{E_f V_f \varepsilon_{fp}}{\pi}$ from Eq. (7.20) and $x_1 = \frac{\varepsilon_{fp} l_f}{\psi}$ from Eq.4.18 then

Eq.4.22 can be re written as

$$F_{t(2)} = 2 K_1 b \left(\frac{w}{\psi} - \frac{\varepsilon_{fp} l_f}{\psi} \right) \quad (4.23)$$

4.2.5 Dowel force F_d

The expression for the dowel force F_d has been derived based on dowel load bearing mechanism in concrete road pavements [66]. It is assumed that the relative shear displacement between the crack faces is in tandem with that of the reinforcement bar. Furthermore the deflected reinforcement bar due to dowel action is considered to undergo inflection midway (Fig.4.6). The dowel bars applied in road pavements are not bonded to the concrete, in the contrary, the re-bars in concrete beams are bonded to the concrete. It implies that during deformation there is resistance due to the bond between the concrete and the re bars. This resistance in the form of interfacial bond stress between the concrete and the anchored part of the rebar is considered. It is assumed that this resistance augments the actual dowel action of the re-bars in beam and the total contributions are thus considered as the dowel

contribution to the total shear hesitance of the beam.

To derive a relationship for the total dowel force, the relative displacement of the shear crack faces and re bar are considered. This relative displacement is assumed to be as shown in Fig.4.6. The load acting on a dowel bar is transferred to the supporting concrete across the crack through bearing and the interface bond between concrete and the anchored part of the re-bar. In a research on assessment on dowel bars in concrete road pavements, Porter et al [66] applied the equations proposed by Frigberg [67] in the determination of the bearing stress due to the dowel force. It was assumed that the bearing stress at the face of the joint (Concrete road pavement joints) is directly proportional to the deformation of the concrete at the joint, expressed as

$$\sigma_b = ky_d \quad (4.24)$$

Where σ_b is the bearing stress, y_d is deflection of the dowel bar (mm) and k is the modulus of dowel support (N/mm^2), According to Porter [66], Frigberg suggested that modulus of dowel support would seldom be less than 25% of concrete elastic modulus E_c , and thus a value of 6895MPa was recommended. Porter also reported range of values used by other researchers (Gringer and Witczak) as 2068MPa to 10342MPa. From this assessment, it is evident that definite value of parameter k has not been established. Due to lack of documented experimental values for this parameter applicable to problems as the current one, this research has adopted Frigberg's suggested estimate values as follows;

$$k = 6895 \text{ or } 0.25\sqrt{E_c} \text{ which ever is larger} \quad (4.25)$$

Notes

I is Point of inflection of the bar

$$\delta_v = w \cos \alpha$$

$$\delta_h = w \sin \alpha$$

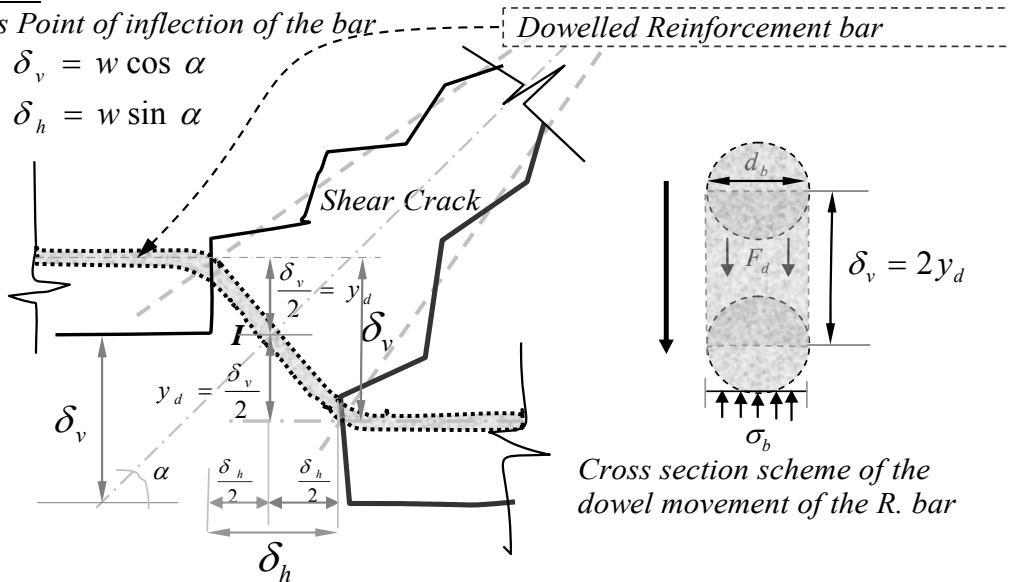


Fig. 4.6 Relative deflections of Reinforcement bar and the crack faces

Referring to Fig.4.6 and applying Eq. (4.24) in the derivation of the actual dowel force F_d as indicated in Fig.4.2a, the following relation is obtained

$$F_d = \sigma_b d_b$$

$$= ky_d d_b \quad (4.26)$$

Re-writing Eq. (4.26) in terms of the area of the reinforcement bar, the relation becomes;

$$F_d = 2ky_d \sqrt{\frac{A_s}{\pi}} \quad (4.27)$$

From Fig 4.1b and Fig 4.6, the relation for the rebar deflection can be estimated by

$$y_d = \frac{\delta_v}{2} = \frac{w \cos \alpha}{2} \quad (4.28)$$

Substituting for y_d the dowel force relation given in Eq. (4.27) becomes;

$$F_d = kw \cos \alpha \sqrt{\frac{A_s}{\pi}} \quad (4.29)$$

However, from the geometry of Fig.4.1a, the shear displacement δ_v in relation to the shear angle γ (equal to shear strain for small angle) is determined as;

$$\delta_v = w \cos \alpha = a \tan \gamma \cong a \gamma \quad (4.30)$$

$$a = c \cos \alpha \quad (\text{From Fig.4.1a}) \quad (4.31)$$

Combination of Eqs (4.30) and (4.31) yields the expression for the shear crack width as

$$w = c \gamma \quad (4.32)$$

Where, c is the general length of the crack path along the shear crack zone.

From the assumed general strain relation given in Fig.4.4, the yield crack width (i.e. maximum crack width which the fibers can control under a pull out force) can be expressed in terms of the fiber pull out strain as follows

$$\varepsilon_{fp} \cong \frac{\Delta l_f}{l_f} \cong \frac{w_y}{l_f} \quad (\text{From Fig 4.4})$$

$$w_y = \varepsilon_{fp} l_f \quad (4.33)$$

However, to determine the crack width due to incremental shear deformations that occur in this case on a beam, while incorporating the fiber pull out effect, the crack width given in Eq. (4.32), can be expressed in terms of the fiber pull out strain, the yield crack width (w_y) and initial yield shear strain γ_y (which is assumed to corresponds to the point when the yield crack width w_y is reached). This is given by;

$$w = c(\Delta \gamma) = c \gamma_y \frac{\Delta \gamma}{\gamma_y} = \varepsilon_{fp} l_f \frac{\Delta \gamma}{\gamma_y} \quad (4.34)$$

Where it is assumed that the initial yield shear crack width occurring in the beam is that controlled by the fibers and is given by

$$c\gamma_y = w_y = \varepsilon_{fp} l_f \quad (7.35)$$

The estimated maximum fiber pull out length is given as $0.25l_f$ [59, 61, 62], however this length is reduced during gradual pull out of the fiber. Thus the expression for the remaining effective length at each shear deformation step after the occurrence of the first crack can be expressed by proportioning the yield crack with controlled by the fibers (Eq.4.33) in terms of the incremental shear strain ratio as follows;

$$l_f^{ef} = \frac{l}{4} l_f - w = \frac{l}{4} l_f - c(\Delta\gamma) = \frac{l}{4} l_f - c\gamma_y \frac{\Delta\gamma}{\gamma_y} \quad (4.36)$$

Substituting the expression given in Eq.4.35 for the yield crack controlled by fibers, then

$$\begin{aligned} l_f^{ef} &= \frac{l}{4} l_f - \varepsilon_{fp} l_f \frac{\Delta\gamma}{\gamma_y} \\ &= \frac{l}{4} l_f \left(1 - 4\varepsilon_{fp} \frac{\Delta\gamma}{\gamma_y} \right) \end{aligned} \quad (4.37)$$

Applying Eq. (4.34) in Eq. (4.29) and re writing the crack width w in terms of equation the general expression for the crack width (Eq.7.34), with use of effective gradual pull out fiber length as given by Eq. (4.37), the expression for the dowel force F_d will be given by

$$F_d = k\varepsilon_{fp} l_f^{ef} \frac{\Delta\gamma}{\gamma_y} \cos \alpha \sqrt{\frac{A_s}{\pi}} \quad (4.38)$$

4.2.6 Re bar tensile force F_s

The tensile force F_s acting on the re-bar can be assessed considering a pull out mechanism in a similar manner as that of the fiber. It is further assumed that 30% of the re-bar length anchored in the overhang from the support will de-bond and gradually pull out to allow further the crack to expand. This length is designated as anchorage l_a and since there is gradual pull out in a similar manner as the fibers, an effective length at each deformation step (due to load increment) is also defined in a similar manner as the fiber. With thee above assumptions, the tensile force acting on the main reinforcement is then derived as follows;

$$\begin{aligned} F_s &= A_s \sigma_s \\ &= A_s E_s \varepsilon_{sp} \end{aligned} \quad (4.39)$$

Where, A_s , E_s and σ_s are the area, elastic modulus and stress acting on the re bar, respectively

The expression for estimating the pull out strain for the rebar can be obtained from Eq. 4.12 with replacement of fiber parameters with those of the bar reinforcement. This is then given by

$$\varepsilon_{sp} = \frac{\tau_b \pi d_b l_a^{ef}}{A_s E_s} \quad (4.40)$$

Where d_b is the re bar diameter and l_a^{ef} is the effective re-bar pull out length, while the other terms remain as previously. Applying Eq.(4.40) in Eq. (4.39) and re writing the re bar diameter in terms of the reinforcement area, the expression for the determination of the rebar pull out force which is considered to augment the actual dowel force will be given by

$$F_s = 2\pi\tau_b l_a^{ef} \sqrt{\frac{A_s}{\pi}} \quad (4.41)$$

$$\text{Where } l_a^{ef} = 0.3l_a - w = 0.3l_a - \varepsilon_{fp} l_f \frac{\Delta y}{\gamma_y} \quad (4.42)$$

4.3 Equilibrium analysis and the shear capacity predictive equations

The expressions for the various internal forces acting to resistant the shear deformations have been established as given in section 4.2. In the section the overall shear strength predictive relation is derived by considering the equilibrium of external and internal forces as depicted in Figs 4.1a and 4.2a.

4.3.1 Equilibrium of forces

Equilibrium of forces given in Fig. 4.2a and as determined in section 4.2 are analyzed here to derive the relation necessary for strength prediction.

(a) Horizontal Equilibrium

Equilibrium of forces (see Fig.4.2a) in the horizontal direction, yield the relation for the interface shear forces (F_{cv}, F_a) and is given by

$$\begin{aligned} (F_{t(1)} + F_{t(2)} - F_c + F_{ct}) \sin \alpha + F_s &= (F_{cv} + F_a) \cos \alpha \\ F_{cv} + F_a &= \left(F_{t(1)} + F_{t(2)} - F_c + F_{ct} \right) \frac{\sin \alpha}{\cos \alpha} + \frac{F_s}{\cos \alpha} \end{aligned} \quad (4.43)$$

(b) Vertical Equilibrium

$$\frac{Q}{2} - (F_{t(1)} + F_{t(2)} - F_c + F_{ct}) \cos \alpha - (F_{cv} + F_a) \sin \alpha - F_d = 0 \quad (4.44)$$

Substituting for $(F_{cv} + F_a)$ from Eq. (4.43), Eq. (4.44) becomes;

$$(F_{t(1)} + F_{t(2)} - F_c + F_{ct}) + F_s \sin \alpha + F_d \cos \alpha = \frac{Q}{2} \cos \alpha \quad (4.45)$$

(c) Moment equilibrium about point O (Fig 7.2a)

By applying moment equilibrium of all the forces about the tip of the advancing shear crack, an expression for the shear capacity prediction can be obtained. It is assumed the crack tip lies at the intersection point between the shear crack path and the neutral axis (see point *O* in Fig. 4.2a).

$$\sum M_o = 0$$

$$\frac{Q}{2} \frac{w}{\psi} \cos \alpha - \frac{1}{2} F_{cc} \left(c - \frac{w}{\psi} \right) - F_{t(2)} \left\{ x_1 + \frac{1}{2} \left(\frac{w}{\psi} - x_1 \right) \right\} - \frac{2}{3} F_{t(1)} x_1 - F_d \frac{w}{\psi} \cos \alpha - F_s \frac{w}{\psi} \sin \alpha - \frac{1}{2} F_{ct} \frac{w}{\psi} = 0 \quad (4.46)$$

Substituting for F_{cc} , F_{ct} , x_1 , $F_{t(1)}$ and $F_{t(2)}$ from Eq. (4.1), (4.2), (4.18), (4.21) and (4.23) respectively, and expanding, Eq. (4.46) above, yields

$$\frac{Q}{2b} \frac{w}{\psi} \cos \alpha - \frac{\sigma_c}{2} \left(c^2 - 2c \frac{w}{\psi} + \left(\frac{w}{\psi} \right)^2 \right) + \frac{1}{3} K_1 \left(\frac{\epsilon_{fp} l_f}{\psi} \right)^2 - K_1 \left(\frac{w}{\psi} \right)^2 - \frac{F_d}{b} \frac{w}{\psi} \cos \alpha - \frac{F_s}{b} \frac{w}{\psi} \sin \alpha - \frac{\sigma_{ct}}{2} \left(\frac{w}{\psi} \right)^2 = 0 \quad (4.47)$$

This can be re-written as

$$\frac{Q}{2b} \frac{w}{\psi} \cos \alpha - \frac{\sigma_c}{2} \left(c^2 - 2c \frac{w}{\psi} + \left(\frac{w}{\psi} \right)^2 \right) + \frac{1}{3} K_1 \left(\frac{\epsilon_{fp} l_f}{w} \right)^2 \left(\frac{w}{\psi} \right)^2 - K_1 \left(\frac{w}{\psi} \right)^2 - \frac{F_d}{b} \frac{w}{\psi} \cos \alpha - \frac{F_s}{b} \frac{w}{\psi} \sin \alpha - \frac{\sigma_{ct}}{2} \left(\frac{w}{\psi} \right)^2 = 0 \quad (4.48)$$

For analysis simplicity, the following relations are applied on Eq. (4.48)

$$Q_1 = \frac{Q}{2b} \cos \alpha, \quad F_1 = \frac{F_d}{b} \cos \alpha, \quad F_2 = \frac{F_s}{b} \sin \alpha \quad (4.49)$$

Equation (4.48) can now be re-written in terms of the relations given in Eq. (4.49) as

$$\left(\frac{w}{\psi} \right)^2 \left\{ -\frac{\sigma_c}{2} + \frac{1}{3} K_1 \left(\frac{\epsilon_{fp} l_f}{w} \right)^2 - K_1 - \frac{\sigma_{ct}}{2} \right\} + \frac{w}{\psi} \{ Q_1 + c \sigma_c - F_1 - F_2 \} = \frac{c^2 \sigma_c}{2} \quad (4.50)$$

4.3.2 Shear strength prediction

Equation (4.50) can be evaluated further such that the resulting expression can be used to predict the shear capacity of SFRC beams. However, an expression for w/ψ must be obtained first.

(a) Determination of w/ψ

The above parameter can easily be obtained from translational equilibrium relations earlier obtained. From Eq. (4.45) the expression for w/ψ is obtained as follows;

$$(F_{t(1)} + F_{t(2)} - F_c + F_{ct}) + F_s \sin \alpha - F_d \cos \alpha = \frac{Q}{2} \cos \alpha$$

Substituting for F_{cc} , F_{ct} , $F_{t(1)}$ and $F_{t(2)}$ from Eqs (4.1), (4.2) (4.21) and (4.23) respectively, as given in section 4.2, the above equation becomes:

$$K_1 b \frac{\varepsilon_{fp} l_f}{\psi} + 2K_1 b \left(\frac{w}{\psi} - \frac{\varepsilon_{fp} l_f}{\psi} \right) - \sigma_c b \left(c - \frac{w}{\psi} \right) + \sigma_{ct} b \frac{w}{\psi} + F_d \cos \alpha + F_s \sin \alpha = \frac{Q}{2} \cos \alpha$$

On applying the relation given in Eq. (4.49), the above equation can be re-written as

$$\begin{aligned} K_1 \frac{\varepsilon_{fp} l_f}{\psi} + 2K_1 \left(\frac{w}{\psi} - \frac{\varepsilon_{fp} l_f}{\psi} \right) - \sigma_c \left(c - \frac{w}{\psi} \right) + \sigma_{ct} \frac{w}{\psi} + F_1 + F_2 &= Q_1 \\ 2K_1 \frac{w}{\psi} - K_1 \frac{\varepsilon_{fp} l_f}{\psi} - c \sigma_c + \sigma_c \frac{w}{\psi} + \sigma_{ct} \frac{w}{\psi} + F_1 + F_2 &= Q_1 \\ \frac{w}{\psi} \left(2K_1 - K_1 \frac{\varepsilon_{fp} l_f}{w} + \sigma_c + \sigma_{ct} \right) &= Q_1 + c \sigma_c - F_1 - F_2 \end{aligned} \quad (4.51)$$

From the equation (4.51) above, the expression for w/ψ is obtained and is as follows

$$\frac{w}{\psi} = \frac{Q_1 + c \sigma_c - F_1 - F_2}{2K_1 - K_1 \frac{\varepsilon_{fp} l_f}{w} + \sigma_c + \sigma_{ct}} \quad (4.52)$$

(b) Shear strength equation

The expression for the shear capacity response is obtained after substituting w/ψ , in Eq. (4.50) with further simplifications as follows; expression for the shear load can be determination as follows;

$$\left(\frac{Q_1 + c \sigma_c - F_1 - F_2}{2K_1 - K_1 \frac{\varepsilon_{fp} l_f}{w} + \sigma_c + \sigma_{ct}} \right)^2 \left\{ -\frac{\sigma_c}{2} + \frac{1}{3} K_1 \left(\frac{\varepsilon_{fp} l_f}{w} \right)^2 - K_1 - \frac{\sigma_{ct}}{2} \right\} + \left(\frac{Q_1 + c \sigma_c - F_1 - F_2}{2K_1 - K_1 \frac{\varepsilon_{fp} l_f}{w} + \sigma_c + \sigma_{ct}} \right) \left\{ Q_1 + c \sigma_c - F_1 - F_2 \right\} = \frac{c^2 \sigma_c}{2}$$

Expanding and simplifying, the above equation reduces to

$$(Q_1 + c \sigma_c - F_1 - F_2)^2 \left\{ \frac{\sigma_c}{2} + \frac{\sigma_{ct}}{2} + K_1 + \frac{1}{3} K_1 \left(\frac{\varepsilon_{fp} l_f}{w} \right)^2 - K_1 \frac{\varepsilon_{fp} l_f}{w} \right\} = \frac{c^2 \sigma_c}{2} \left(2K_1 - K_1 \frac{\varepsilon_{fp} l_f}{w} + \sigma_c + \sigma_{ct} \right)^2$$

$$Q_1 + c \sigma_c - F_1 - F_2 = \sqrt{\frac{c^2 \left(2K_1 - K_1 \frac{\varepsilon_{fp} l_f}{w} + \sigma_c + \sigma_{ct} \right)^2}{1 + \frac{\sigma_{ct}}{\sigma_c} + \frac{2K_1}{\sigma_c} \left[1 + \frac{1}{3} \left(\frac{\varepsilon_{fp} l_f}{w} \right)^2 - \left(\frac{\varepsilon_{fp} l_f}{w} \right) \right]}}$$

$$= c\sigma_c \left(\frac{\frac{K_1 \left(2 - \frac{\varepsilon_{fp} l_f}{w} \right) + 1 + \frac{\sigma_{ct}}{\sigma_c}}{\sqrt{1 + \frac{\sigma_{ct}}{\sigma_c} + \frac{2K_1}{\sigma_c} \left[1 + \frac{1}{3} \left(\frac{\varepsilon_{fp} l_f}{w} \right)^2 - \left(\frac{\varepsilon_{fp} l_f}{w} \right) \right]} - 1}} \right) \quad (4.53)$$

The approximate solution to Eq.(4.53) can be obtained by applying Maclaurins series [68] such that the denominator term in equation (4.53) above is defined as

$$(1+y)^{-\frac{1}{2}} = \frac{1}{\sqrt{1 + \frac{2K_1}{\sigma_c} \left(\frac{\sigma_{ct}}{2K_1} + 1 + \frac{1}{3} \left(\frac{\varepsilon_{fp} l_f}{w} \right)^2 - \left(\frac{\varepsilon_{fp} l_f}{w} \right) \right)}} \quad (4.54)$$

Apply the following Maclaurins relation in the approximate solution of Eq (4.54)

$$(1+y)^n = 1 + ny + \frac{n(n-1)}{2!} y^2 + \dots \text{etc} \quad (4.55)$$

Ignoring higher order terms the approximate solution to Eq. (4.54) will be given by

$$(1+y)^{\frac{1}{2}} = 1 - \frac{K_1}{\sigma_c} \left(\frac{\sigma_{ct}}{2K_1} + 1 + \frac{1}{3} \left(\frac{\varepsilon_{fp} l_f}{w} \right)^2 - \left(\frac{\varepsilon_{fp} l_f}{w} \right) \right) \quad (4.56)$$

Applying Eq. (4.56) in Eq. (4.53) then

$$Q - F_1 - F_2 = c\sigma_c \left(\frac{K_1 \left(2 - \frac{\varepsilon_{fp} l_f}{w} \right) + 1 + \frac{\sigma_{ct}}{\sigma_c}}{\left[1 - \frac{K_1}{\sigma_c} \left(\frac{\sigma_{ct}}{2K_1} + 1 + \frac{1}{3} \left(\frac{\varepsilon_{fp} l_f}{w} \right)^2 - \left(\frac{\varepsilon_{fp} l_f}{w} \right) \right) \right]} - 1 \right) \quad (4.57)$$

Expansion of Eq. (4.57) yields

$$\begin{aligned} Q - F_1 - F_2 = & \\ & c\sigma_c \left\{ \frac{K_1 \left(2 - \frac{\varepsilon_{fp} l_f}{w} \right) + \left(\frac{K_1}{\sigma_c} \right)^2 \left[\left(2 - \frac{\varepsilon_{fp} l_f}{w} \right) \left(\frac{\sigma_{ct}}{2K_1} + 1 + \frac{1}{3} \left(\frac{\varepsilon_{fp} l_f}{w} \right)^2 - \frac{\varepsilon_{fp} l_f}{w} \right) \right]}{\left[1 - \frac{K_1}{\sigma_c} \left(\frac{\sigma_{ct}}{2K_1} + 1 + \frac{1}{3} \left(\frac{\varepsilon_{fp} l_f}{w} \right)^2 - \left(\frac{\varepsilon_{fp} l_f}{w} \right) \right) \right]} + \frac{\sigma_{ct}}{\sigma_c} \frac{\sigma_{ct} K_1 \left[\frac{\sigma_{ct}}{2K_1} + 1 + \frac{1}{3} \left(\frac{\varepsilon_{fp} l_f}{w} \right)^2 - \left(\frac{\varepsilon_{fp} l_f}{w} \right) \right]}{\sigma_c \left[1 - \frac{K_1}{\sigma_c} \left(\frac{\sigma_{ct}}{2K_1} + 1 + \frac{1}{3} \left(\frac{\varepsilon_{fp} l_f}{w} \right)^2 - \left(\frac{\varepsilon_{fp} l_f}{w} \right) \right) \right]} - 1 \right\} \\ & cK_1 \left\{ \left(2 - \frac{\varepsilon_{fp} l_f}{w} \right) - \left(\frac{K_1}{\sigma_c} \right) \left[\left(2 - \frac{\varepsilon_{fp} l_f}{w} \right) \left(\frac{\sigma_{ct}}{2K_1} + 1 + \frac{1}{3} \left(\frac{\varepsilon_{fp} l_f}{w} \right)^2 - \frac{\varepsilon_{fp} l_f}{w} \right) \right] - \left[\frac{\sigma_{ct}}{2K_1} + 1 + \frac{1}{3} \left(\frac{\varepsilon_{fp} l_f}{w} \right)^2 - \left(\frac{\varepsilon_{fp} l_f}{w} \right) \right] + \frac{\sigma_{ct}}{K_1} \frac{\sigma_{ct}}{\sigma_c} \left[\frac{\sigma_{ct}}{2K_1} + 1 + \frac{1}{3} \left(\frac{\varepsilon_{fp} l_f}{w} \right)^2 - \left(\frac{\varepsilon_{fp} l_f}{w} \right) \right] \right\} \\ & cK_1 \left\{ 1 - \frac{1}{3} \left(\frac{\varepsilon_{fp} l_f}{w} \right)^2 + \frac{\sigma_{ct}}{2K_1} - \left(\frac{K_1}{\sigma_c} \right) \left[\left(2 - \frac{\varepsilon_{fp} l_f}{w} \right) \left(\frac{\sigma_{ct}}{2K_1} + 1 + \frac{1}{3} \left(\frac{\varepsilon_{fp} l_f}{w} \right)^2 - \left(\frac{\varepsilon_{fp} l_f}{w} \right) \right) \right] - \frac{\sigma_{ct}}{\sigma_c} \left[\frac{\sigma_{ct}}{2K_1} + 1 + \frac{1}{3} \left(\frac{\varepsilon_{fp} l_f}{w} \right)^2 - \left(\frac{\varepsilon_{fp} l_f}{w} \right) \right] \right\} \\ & \frac{cK_1}{3} \left\{ 3 - \left(\frac{\varepsilon_{fp} l_f}{w} \right)^2 - \left[\frac{K_1}{\sigma_c} \left(2 - \left(\frac{\varepsilon_{fp} l_f}{w} \right) \right) \right] + \frac{\sigma_{ct}}{\sigma_c} \left[\frac{3\sigma_{ct}}{2K_1} + 3 + \left(\frac{\varepsilon_{fp} l_f}{w} \right)^2 - 3 \frac{\varepsilon_{fp} l_f}{w} \right] \right\} + \frac{c\sigma_{ct}}{2} \end{aligned}$$

$$Q_1 = \frac{cK_1}{3} \left\{ 3 - \left(\frac{\varepsilon_{fp} l_f}{w} \right)^2 - \left[\frac{K_1}{\sigma_c} \left(2 - \left(\frac{\varepsilon_{fp} l_f}{w} \right) \right) + \frac{\sigma_{ct}}{\sigma_c} \left[\frac{3\sigma_{ct}}{2K_1} + 3 + \left(\frac{\varepsilon_{fp} l_f}{w} \right)^2 - 3 \frac{\varepsilon_{fp} l_f}{w} \right] \right] \right\} + \frac{c\sigma_{ct}}{2} + F_1 + F_2 \quad (4.58)$$

It can be noted that on substituting the relation for Q_1 from Eq. (4.49) in Eq. (4.58), a relation for the shear capacity per unit width of the beam can be obtained.

Substitute for Q_1 , F_1 , F_2 from Eq. (4.49) in Eq. (4.58) and noting that $c=a/\cos\alpha$ from Fig.4.1a, with the relation for shear span to depth ratio expressed as $a=d/\beta$, then the relation for the shear load is given by

$$\frac{Q}{2} = \frac{db\beta K_1}{3 \cos^2 \alpha} \left\{ 3 - \left(\frac{\varepsilon_{fp} l_f}{w} \right)^2 - \left[\frac{K_1}{\sigma_c} \left(2 - \frac{\varepsilon_{fp} l_f}{w} \right) + \frac{\sigma_{ct}}{\sigma_c} \left[\frac{3\sigma_{ct}}{2K_1} + 3 + \left(\frac{\varepsilon_{fp} l_f}{w} \right)^2 - 3 \frac{\varepsilon_{fp} l_f}{w} \right] \right] \right\} + \frac{db\beta\sigma_{ct}}{2 \cos^2 \alpha} + F_d + F_s \tan\alpha \quad (4.59)$$

Since the shear load is also dependent on shear span, a shear span to depth ratio influence factor can be incorporated by re-writing Eq. (4.59) as follows

$$\frac{Q}{2\beta^2} = \frac{dbK_1}{3\beta \cos^2 \alpha} \left\{ 3 - \left(\frac{\varepsilon_{fp} l_f}{w} \right)^2 - \left[\frac{K_1}{\sigma_c} \left(2 - \frac{\varepsilon_{fp} l_f}{w} \right) + \frac{\sigma_{ct}}{\sigma_c} \left[\frac{3\sigma_{ct}}{2K_1} + 3 + \left(\frac{\varepsilon_{fp} l_f}{w} \right)^2 - 3 \frac{\varepsilon_{fp} l_f}{w} \right] \right] \right\} + \frac{db\sigma_{ct}}{2\beta \cos^2 \alpha} + \frac{1}{\beta^2} (F_d + F_s \tan\alpha) \quad (4.60)$$

The shear span-effective depth influence factor is given by l/β^2 . From equations (4.34), (4.38) and (4.41) the relations for w , F_d , F_s and F_s are obtained. Substitution of this relation in Eq. 4.60 above, with simplification of the dowel contribution part (last term), the shear strength predictive equation is finally obtained and is given by

$$\Delta V = \frac{dbK_1}{3\beta \cos^2 \alpha} \left\{ 3 - \left(\frac{\gamma_y}{\Delta\gamma} \right)^2 - \left[\frac{K_1}{\sigma_c} \left(2 - \frac{\gamma_y}{\Delta\gamma} \right) + \frac{\sigma_{ct}}{\sigma_c} \left[\frac{3\sigma_{ct}}{2K_1} + 3 + \left(\frac{\gamma_y}{\Delta\gamma} \right)^2 - 3 \frac{\gamma_y}{\Delta\gamma} \right] \right] \right\} + \frac{db\sigma_{ct}}{2\beta \cos^2 \alpha} + \frac{1}{\beta^2} \sqrt{\frac{A_c \rho}{\pi}} + \left(k\varepsilon_{fp} l_f \frac{\Delta\gamma}{\gamma_y} \cos\alpha + 2\pi\tau_b l_a^{ef} \tan\alpha \right) \quad (4.61)$$

Where b is the beam width, K_1 is a dimensional term that accounts for the fiber content and characteristic as given in Eq.(4.20), $\gamma_y/\Delta\gamma$ is the incremental shear strain ratio, α is shear crack orientation angle and d is the beam effective depth while the rest of the terms are as previously defined. Equation (4.61) follows the traditionally applied principle of superposition, in which the shear strength contribution constitutes a summation of the individual contributions of the reinforcements and the concrete. This can be simply written as;

$$\Delta V = \Delta V_{fc} + V_c + \Delta V_d \quad (4.62)$$

Whereby the fiber-concrete composite, concrete tensile and dowel action of the main reinforcements contributions are given by

$$\Delta V_{fc} = \frac{dbK_1}{3\beta \cos^2 \alpha} \left\{ 3 - \left(\frac{\gamma_y}{\Delta\gamma} \right)^2 - \left[\frac{K_1}{\sigma_c} \left(2 - \frac{\gamma_y}{\Delta\gamma} \right) + \frac{\sigma_{ct}}{\sigma_c} \left[\frac{3\sigma_{ct}}{2K_1} + 3 + \left(\frac{\gamma_y}{\Delta\gamma} \right)^2 - 3 \frac{\gamma_y}{\Delta\gamma} \right] \right] \right\} \quad (4.63)$$

$$V_c = \frac{db \sigma_{ct}}{2\beta \cos^2 \alpha} \quad (4.64)$$

$$\Delta V_d = \frac{I}{\beta^2} \sqrt{\frac{A_c \rho}{\pi}} \left(k \varepsilon_{\beta}^{ef} \frac{\Delta \gamma}{\gamma_y} \cos \alpha + 2\pi \tau_{b,a}^{ef} \tan \alpha \right) \quad (4.65)$$

Where ΔV_{fc} , V_c and ΔV_d are the fiber-concrete interaction contribution, concrete tension contribution and the re-bar dowel contribution, respectively.

In order for evolution predictions to be made using Eq. (4.62), the shear strain ratio must be applied incrementally.

4.3.3 Shear strain prediction

For shear strength shear strain profiling to be made, an expression for the determination of the shear strain must be established. This is approximated theoretically by applying Gere & Timonshenko [58] shear deformation relations, whereby the yield shear strain is given by

$$\gamma_y = \frac{\xi Q_y}{2GA_c} \quad (4.66)$$

In which the shear modulus G is given by

$$G = \frac{E_c}{2(1 + \mu)} \quad (4.67)$$

Where Q_y is the yield shear load (assumed to occur at shear a strain ratio of 1), ξ is a factor (equal to 1.5 for rectangular beams but reduced in the current study to 1.2), A_c is the cross sectional area of the concrete beam and μ is the Poisson's ratio. By assuming that the yield load (Q_y) occurs at a shear strain ratio of 1, the shear strain values can be generated by applying the shear strain ratio numerically as follows

$$\frac{\gamma_y}{\Delta \gamma} \geq 1 \text{ or } \frac{\Delta \gamma}{\gamma_y} \leq 1, \text{ before yielding}$$

$$\frac{\gamma_y}{\Delta \gamma} < 1 \text{ or } \frac{\Delta \gamma}{\gamma_y} > 1, \text{ after yielding.}$$

Therefore the strain ratio can be generalized by

$$\frac{\Delta \gamma}{\gamma_y} = 0, 1, 2, 3, 4, 6, \dots \text{etc} \quad (4.68)$$

From which the general shear strain γ can be obtained by

$$\gamma = 0 \gamma_y, 1 \gamma_y, 2 \gamma_y, \dots \text{etc} \quad (4.69)$$

4.3.4 Deflection prediction

It is well known that in practice the total deflections of a beam comprise both deflections due to bending and shear. Despite this fact, theoretically deflections due to shear are often ignored. For proper comparisons with experimental deflections, the theoretical study in this research has made an attempt to account for both bending and shear deflections as discussed below.

(a) Bending deflections

Deflections at mid span of the beam are obtained by combination of moment-curvature relations [58] and moment-deflection relations [57]. The curvature ratio relationship in elastic and inelastic bending in beams, is given in Gere & Timonshenko [58] re written here in terms of incremental curvature and moment is given by

$$\frac{\Delta\theta_e^c}{\theta_y^c} = \frac{I}{\sqrt{3 - \frac{2\Delta M}{M_y}}} \quad (4.70)$$

Where, $\Delta\theta_e^c = 1/\Delta\lambda$ and $\theta_y^c = 1/\lambda_y$ are the elastic and inelastic (yield) curvatures, respectively, while, λ , M_y and ΔM are the radius of curvature, yield and general incremental moment, respectively. The general moment M is such that $0 \leq M \leq M_p$, whereby M_p is the plastic moment. In elastic bending, the deflections are given in Mosley [54] as

$$\delta = \xi l_e^2 \Delta\theta_e^c \quad (4.71)$$

Where $\Delta\theta_e^c = \Delta M/EI$, while, E , I , and l_e are elastic modulus, moment of inertia, shear and effective spans, respectively. According to Mosley [57] the factor ξ can also be used to account for the deflection after cracking however a suitable value must be establish for the same. In this study, an expression for the determination for this factor was established and is given by

$$\xi = 0.5 \left(1 - \varphi - \frac{0.0833}{\varphi} \right) \quad (4.72)$$

Where $\varphi = a/l_e$ and a , l_e are the shear and effective beam spans respectively. For continuity, it is assumed that at yield (cracking), $\Delta\theta_e^c \leq \theta_y^c$, therefore the following curvature relations shall also apply

$$\theta_y^c = \frac{M_y}{EI} \quad (4.73)$$

Applying relations in Eqs (4.71), (4.72), and (4.73), in Eq. (4.70), an expression for the approximate determination of the incremental mid span bending deflections will then be given by

$$\Delta\delta_b = \frac{2\xi l^2 l_e^2 \Delta M}{EI \left(3 - \left(\frac{\theta_y^c}{\Delta\theta_e^c} \right)^2 \right)} \quad (\text{Where } 0 \leq M \leq M_p) \quad (4.73)$$

(b) Shear deflections

From Fig.4.1b and Fig.4.6, the general relative shear displacement can be estimated from;

$$\delta_s = \delta_v = a\gamma \quad (4.74)$$

From which an incremental shear strain $\Delta\gamma$ can be obtained in terms of incremental yield shear strain ratio as γ_y ($\Delta\gamma/\gamma_y$) and since the expression for the yield shear strain is given by Eq. (4.66), then the expression for incremental shear deflections can be estimated by

$$\Delta\delta_s = a \frac{1.2Q_y}{2GA_c} \left(\frac{\Delta\gamma}{\gamma_y} \right) \quad (4.75)$$

Where Q_y is the yield shear load (assumed to occur at shear a strain ratio of 1) and the other terms are as defined for Eq. (4.66).

(c) Total deflections

Having established independently the expressions for shear and bending deflections, the total of the same can then be approximated by summation and is given by;

$$\Delta\delta_t = \Delta\delta_s + \Delta\delta_b \quad (4.76)$$

4.4 Parametric analysis and prediction response

Theoretical parametric analysis is applied in this section to evaluate the prediction ability of the derived model. Influence of the steel fibers and the shear span to depth ratio on the shear capacity of SFRC beams is also checked with a view of gauging the model response to the variation of these parameters. Experimental and numerical verification as a means of further verifications are presented and discussed in detail in chapter 7 and 8

4.4.1 Structural and material parameters

In the theoretical prediction analysis, structural and material details shown in Table 4.1 were used. The tensile and compressive strengths used were obtained from concrete cylinder tests [69]; however the bond strength was estimated based on the value proposed by Narayanan R *et al* [32]. For purposes of experimental comparisons, the geometry and main reinforcement of the beams theoretically analyzed in this section are similar to those tested experimentally (Fig. 4.7). The variables applied are the steel fiber content and the shear span to depth ratio.

Table 4.1 Structural and material properties applied in Eq. (4.61)

| Type | | Designation | Value | |
|---------------------------|-----------------------|--|--|-------------|
| Reinforcements | Main Re-bars | Diameter d_s (mm) | 6,13 | |
| | | Elastic modulus E_f (N/mm ²) | 210000 | |
| | | Strength f_{sy} (N/mm ²) | 340 | |
| | | | Maximum de-bonding anchorage length l_a (mm) | 20 |
| | Fibers | | Aspect ratio A_r | 48.4 |
| | | | Diameter d_f (mm) | 0.62 |
| | | | Length l_f (mm) | 30 |
| | | | Elastic modulus E_f (N/mm ²) | 210000 |
| | | | Strength f_{fy} (N/mm ²) | 1000 |
| | | | Fiber content (%) | 0.5,1.0,1.5 |
| Concrete / fiber concrete | | Compressive strength σ_c (N/mm ²) | 38 | |
| | | Plain concrete tensile strength σ_{ct} (N/mm ²) | 3.67 (Ref: [69]) | |
| | | Plain concrete modulus E_c (N/mm ²) | 31108 (Ref [69]) | |
| | | Fiber concrete modulus E_{fc} (N/mm ²): with fiber | Variable, (ref: [69]) | |
| | | Poison ratio ν | 0.195 | |
| | | Bearing strength k (N/mm ²) | 6895 | |
| | | Bond strength τ_b (N/mm ²) | 4.15 ([ref :[8]) | |
| | Structural parameters | | Shear span depth ration β (mm) | Variable |
| | | | Beam effective depth d (mm) | Variable |
| | | | Main reinforcement cover (mm) | 18, 20 |
| | | Beam widths (mm) for small beam Beam widths (mm) for large beam | 100 150 | |

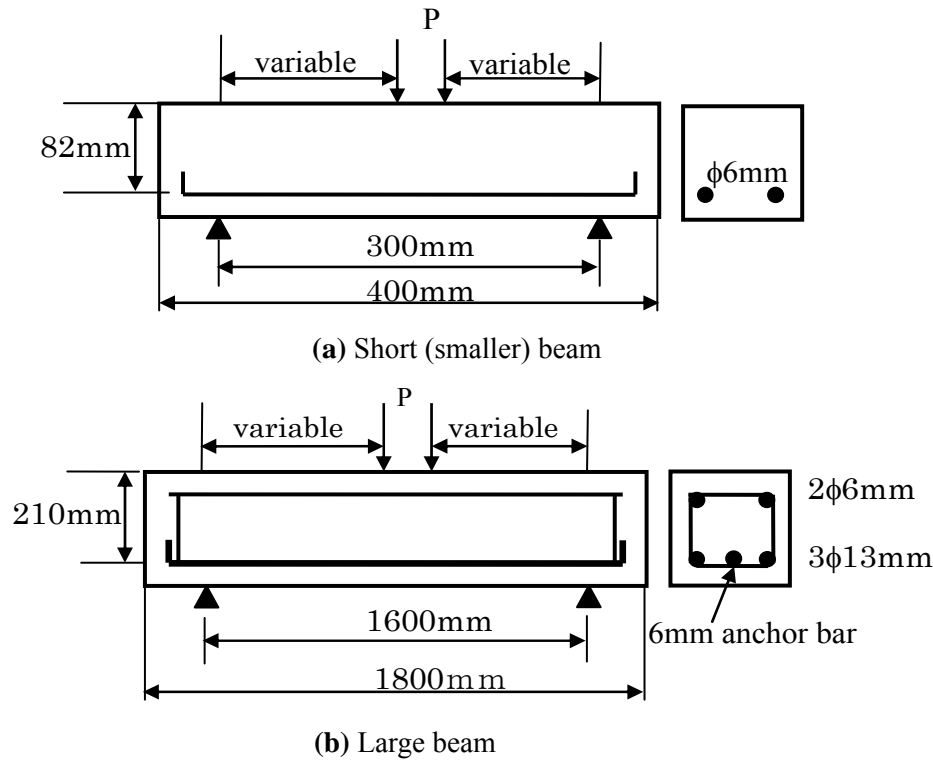


Fig.4.7 Applied Beam details similar to the tests specimens

4.4.2 Influence of fiber content variation

(a) Prediction response for Short (small) SFRC beams

The shear strength and deformation response is obtained by applying the derived equations (Eq.4.61, Eq.4.69 and 4.74). Fig.4.8 shows the theoretical prediction results of the derived model for short beams (Fig. 4.7a). The shear strength-deflection behavior is approximately linear in the initial stages, this is noted to occur until a shear load limit of 10, 15, 20kN in the beams with a shear span to depth ratio of 1, 1.5, 1.82, respectively. Beyond this load range, a non linear behavior is observed with no much variation in the deflections. However, after the above load limits (15, 25, 30kN in $a/d=1, 1.5, 1.82$, respectively), clear deviations occur which is noted to be dependant on the amount of fiber content applied. On the contrary, the stress strain behavior depicts a very stiff initial phase with a sudden deviation at stress levels of 1.5, 2.5, and 3.0MPa in $a/d = 1, 1.5, 1.82$, respectively.

It is evident in these figures that a complete deformation behavior in which increase in the shear strength commensurate with the fiber content is predicted well. The reduction in shear strength and shear strain capacity, with increase in the shear span to depth ratio is also predicted well. This confirms the effectiveness of the shear span to depth ratio influence factor introduced in the predictive model. Although at this stage this can only be considered as a tentative confirmatory behavior, it is shown in subsequent chapters on verification with experiments that in indeed the factor is correct.

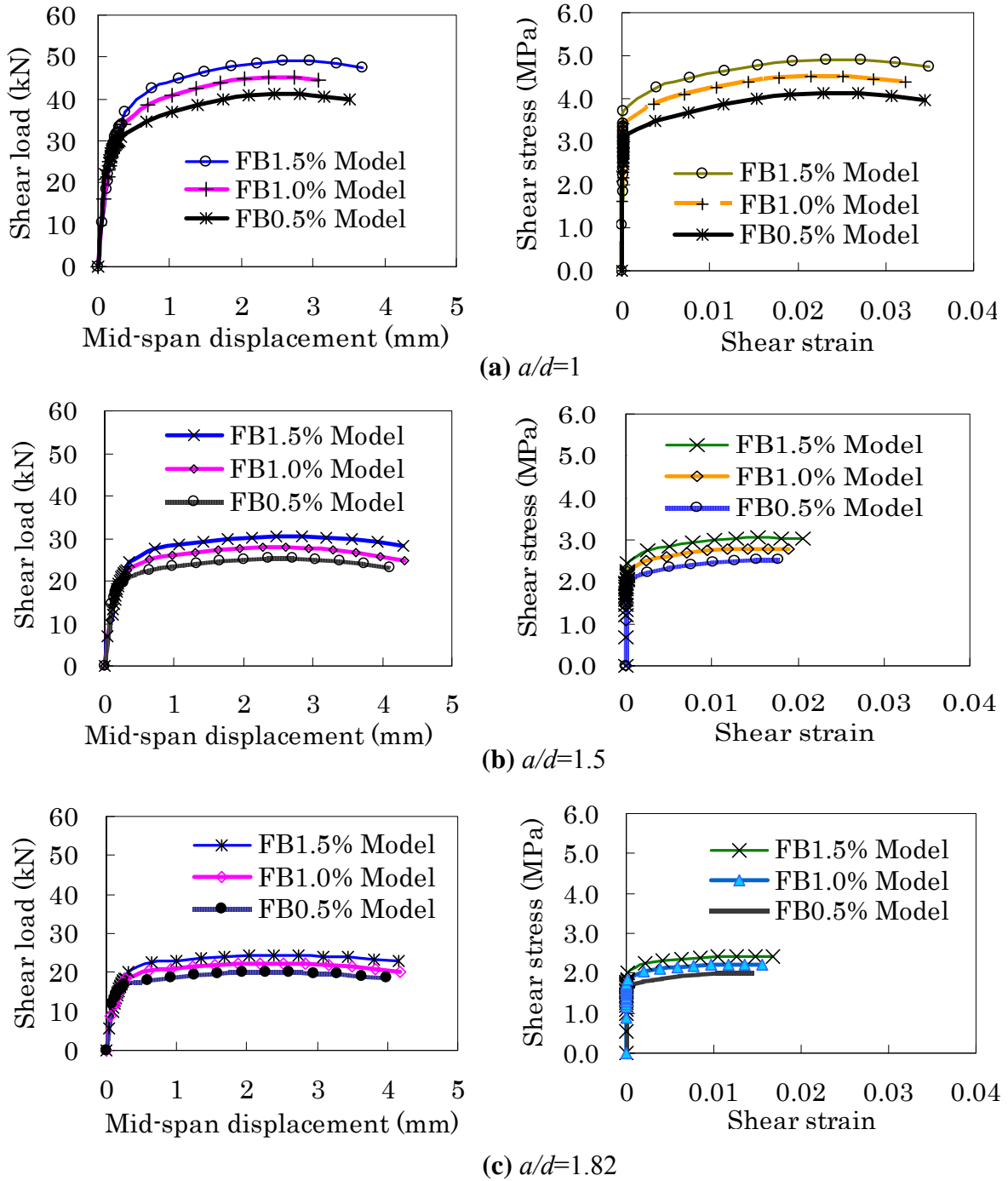


Fig.4.8 Theoretical shear response prediction for small SFRC beams

(b) Prediction response for large beams

Shear behavior is affected by the structural geometry and although this can be partly considered by the variation of the shear span to depth ratio, the over size of the beam also counts. Having established that in beams with small geometrical dimensions, the derived model has good prediction ability as observed in the results shown in Fig.4.8, the response of the model when the overall geometrical and main reinforcement size of the beam are changed (other variables remain same as for small beams) is checked in this section. Fig.4.9 shows the prediction response for beams with larger geometrical

dimensions (Fig. 4.7b), with the other parameters as given in Table 4.1. As expected the shear strength and deflection capacity is higher than that of the small beams due to both geometric and amount/size of reinforcement applied. However, the overall response behavior is similar to that of the small beams whereby there is linear and non linear profile with consistent strength increase with increase in fiber content applied being noted in the non linear stage. Like wise a reduction in strength ductility is noted with increase in shear span to depth ratio.

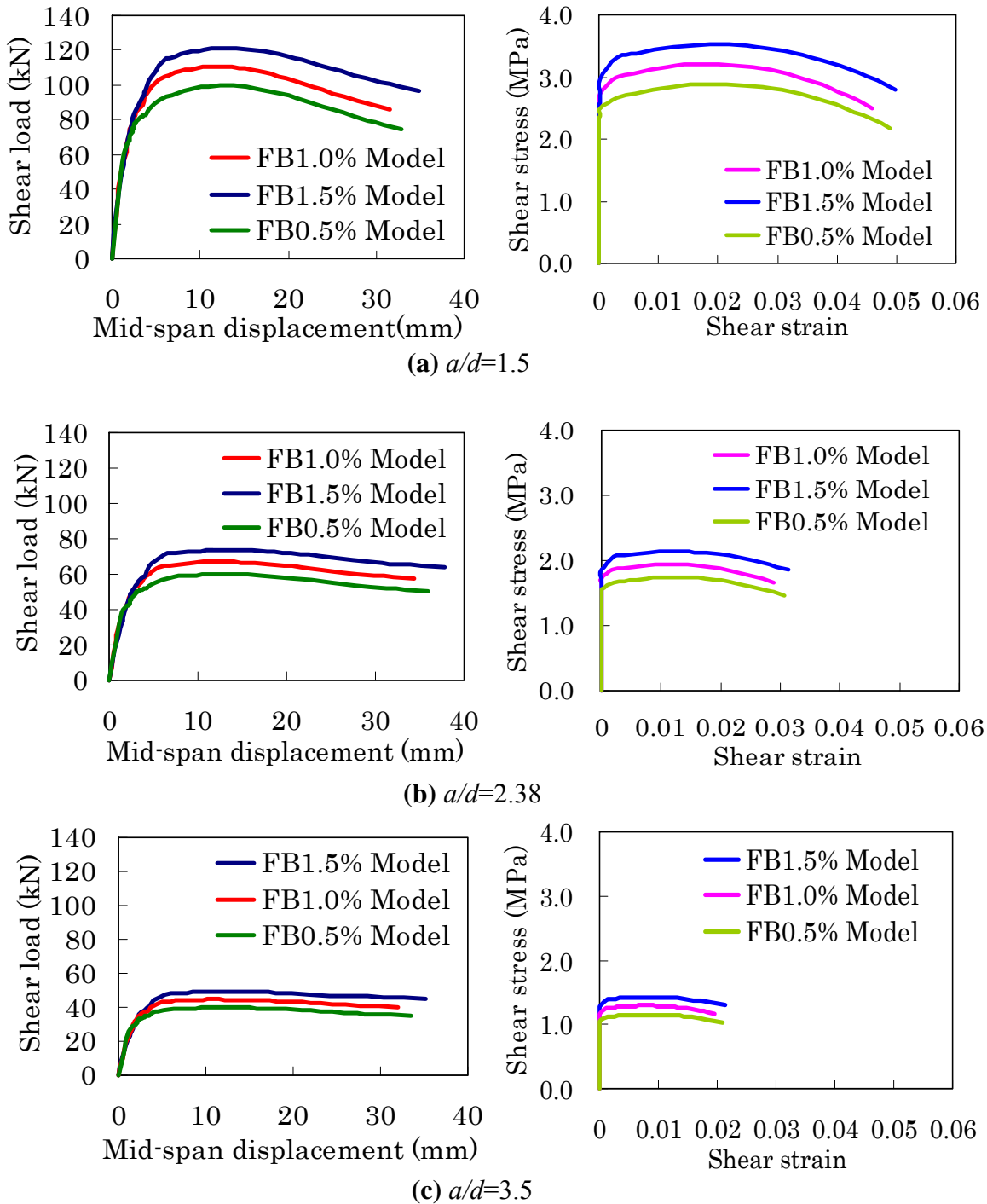


Fig. 4.9 Theoretical shear response prediction for large SFRC beams

4.4.3 Influence of shear span to depth ratio variation

As noted in Figs 4.8 and 4.9, a reduction in shear strength occurs with increase in the shear span (a) to depth ratio (d). To illustrate this trend clearly, an increased shear span to depth ratio (up to $a/d=9.5$) parametric analyses is made while keeping the same fiber content as previously applied. In this case, ultimate shear strength is plotted against a/d . As shown in Fig.4.10, a further reduction in shear strength is noted to occur with the overall response similar to what has been found experimentally to occur. The high shear strength in the initial stages is often attributed to the reserve strength due to compression shear failure, however as the shear span to depth ratio increase, this influence is reduced as the failure mode changes to shear flexure and ultimately flexural mode when a/d becomes large. Increase in strength attributed to the steel fibers can also be observed to be effective in the range $a/d=1$ and 3.5. This is more pronounced in the transition region ($a/d = 1.5$ and 3.0)

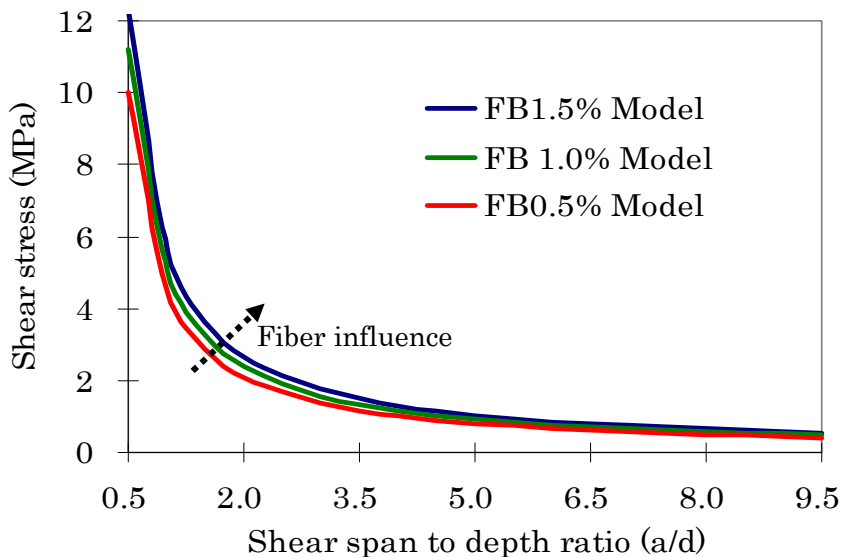


Fig.4 10 Predicted Influence of shear span to depth ratio

4.5 Concluding remarks

A theoretical shear response model has been derived and its preliminary verification made. Its capability of predicting shear strength and deformation response of SFRC beams as confirmed by the theoretical results shown in Figs 4.8 to 4.10 has been illustrated. Variation of the fiber content, shear span to depth ratio and the general size of the beam were made and the results although theoretical appear to predict well the phenomenon commonly observed in practice when beams are subjected to bending shear loads. Moreover, shear strength strain behavior can be predicted which is fundamental given it is often difficult to experimentally measure shear deformations. With the model both shear deflections and strains can be estimated and thus once experimental validity of these deformations is confirmed, then the universal applicability of the model with respect to shear behavior in SFRC beams can be applied.

Chapter 5

Properties of steel fiber reinforced normal concrete

5.1 Introductions

Inclusion of steel fibers in concrete offers a convenient and practical means of achieving improvements in engineering properties of concrete. Plain concrete is brittle while steel fiber reinforced concrete (SFRC) is a homogenous ductile composite product. Steel fibers in concrete are expected to enhance the post cracking tensile strength of the composite and its fracture energy [48, 49]. This could be attributed to the even and random distribution of fibers throughout the volume of concrete at much closer spacing than conventional reinforcements. As a result, enhanced capacity in crack control, fracture toughness, ductility, energy absorption and tensile strengths in SFRC can be realized. Furthermore, limitations in traditional measurement methods hinder the full potential of quantifying and understanding the behavior of the material under deformations. Accurate measurement of surface deformations is much significant in clarifying the governing mechanism of mechanical phenomenon in concrete [50]. Understanding of the aforementioned beneficial material properties and behavior in SFRC therefore requires advanced measurement techniques such as optical methods. Principles and theoretical background of the optical method have been given in details in chapter 3.

In conventional methods, strain measurement is at a point and it depends on stability of the gauges during the deformation of the specimen. Furthermore, definite identification of the actual cracking stage and regions of high deformations is difficult in the conventional approach. The latter approach is only possible after the specimens have physically failed. However, a full-field optical method offers the possibility of capturing these deformations real time

The purpose of this chapter is to clarify the material property characteristics and deformation behavior in steel fiber reinforced concrete (SFRC) as a structural material by optical full field methods. Two dimensional optical full -field ESPI as discussed in chapter 3 was used to measure displacements, strains and capture the deformation patterns in steel fiber concrete beams and cylinders in conjunction with the conventional methods. The tests results pertaining to both fresh and hardened properties of SFRC are presented and discussed. The theoretical work (derived model and the numerical simulation) conducted in this research required certain fundamental material properties. Particular importance to the theoretical analysis is the stress-strain relation from which other parameter such as the elastic modulus, shear modulus, and Poisson ratio were obtained and applied.

5.2 Materials

5.2.1 Fiber Concrete

Normal concrete with an average strength of 41MPa was made from standard ordinary Portland cement and aggregates meeting the JSCE guidelines for Concrete [47]. It was variably (0.5, 1.0 and 1.5%) reinforced with end hooked discrete steel fibers. In order to achieve a workable mix, 0.8% of an AE water reducing admixture (POZOLIS15L) was used to improve the flow without increasing the water content. As discussed in chapter 3, the mix design was carefully designed to ensure that at least the percentage of fines was more than 40% of the total aggregates. Variable mix proportions were used according to the fiber content (see chapter 3 Table 3.2). In effect the steel fibers became part of the mix ingredients and hence substitutes part of the aggregates.

5.2.2 Reinforcements

In addition to the steel fibers, 6mm diameter deformed rebars were used in the beams to reduce the influence of flexural deformations. The steel fibers were 0.62mm in diameter and 30mm in length giving an aspect ratio of 48.4. The properties of these reinforcements are given in Table 5.1

Table 5.1 Characteristics of reinforcements

| Type | Elastic Modulus (kN/mm ²) | Tensile strength (MPa) | Remark |
|---------|--|---------------------------|------------|
| Fibers | 210 | 1000 | End hooked |
| Re bars | 210 | 345 | Deformed |

5.3 Test procedure

The tests specimens consisted of six 400×100×100mm beams and twenty four number cylinders of Ø100mm by 200mm height made from plain and steel fiber reinforced concrete. All the specimens were cured under water for a period of 28 days before to testing. Continuous curing under complete immersion was done in order to maximize the concrete strength gain and improve bonding with the fibers. Tests on the beam and the tensile strength specimens were done using a 300kN capacity universal testing machine. Controlled loading was applied on the specimens while the full-field strains and displacements were monitored and recorded using a set of optical measurements equipment system (ESPI) comprising a desk top computer and CCD camera (2D sensor type). In addition to the universal testing machine, a data logger and laptop for control and recording of loads and conventional strains were used. The complete set up was as shown in Fig.5.1

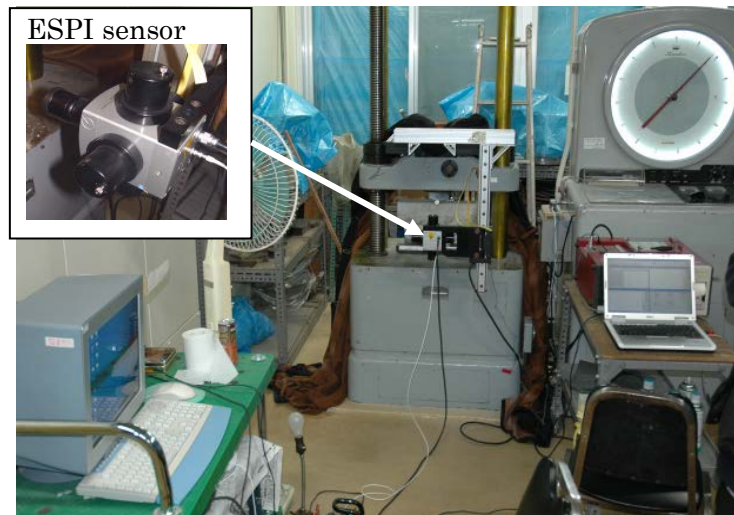
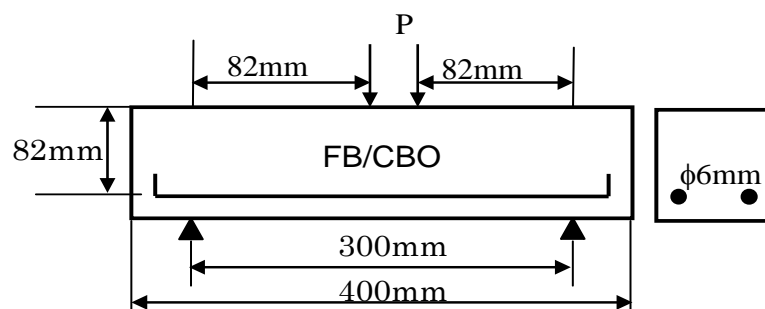
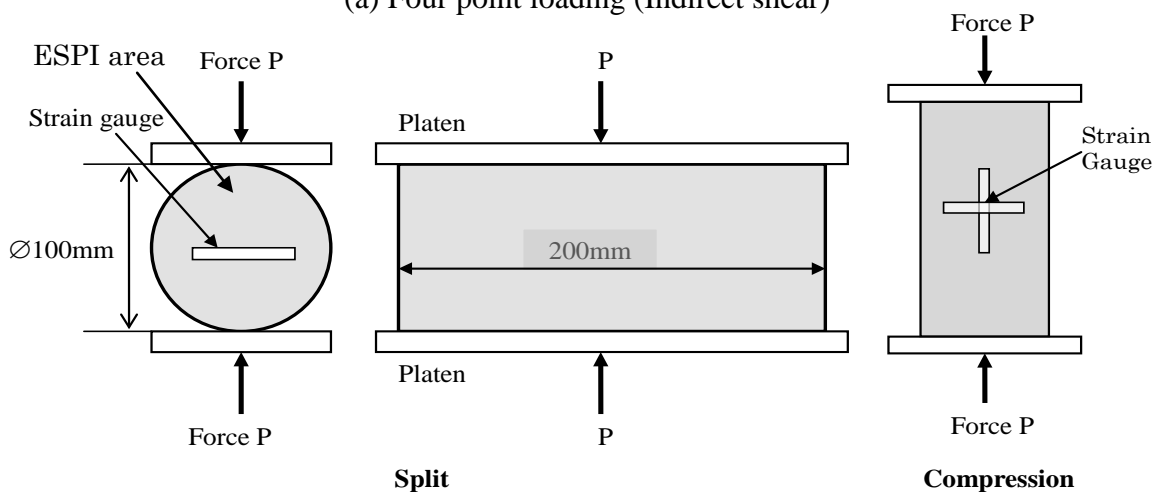


Fig 5.1 Optical and normal test set up

Conventional strains and displacements were measured using normal strain gauges and Linear Variable Differential Transformer (LVDT) displacement probe on the split and flexural test specimens, respectively. Compression test were undertaken using a 600kN universal test machine, while the strains were measured using strain gauges. In order for shear failure to occur, a shear span a of 82mm and depth d of 82mm was adopted (Fig.5.2a). This corresponds to a shear span to depth ratio of 1.



(a) Four point loading (Indirect shear)



(b) Split and Compression

Fig. 5.2 loading arrangement

Selected ESPI strain and displacement data were obtained at along at beam bottom mid section and along the cylinder diameter. Specimens for ESPI measurement had the target surfaces sprayed with special white (UNI Glo) paint to create a reflective surface in order to obtain a better contrast in the captured images during loading. The loading arrangement for the beams and cylinders was as shown in Fig.5.2 (a) and (b).

5.4 Effect of steel fibers on rheology of fresh concrete

The influence of steel fibers of fresh concrete was demonstrated by the difficulty in mixing when the fiber content applied is higher (e.g. in the case when the fiber content was 1.5%). Although workability was improved with the use of an admixture (POZOLIS15LS), mixing of the resulting composite was still noted to be difficulty especially in the higher fiber content. To characterize this influence, slump measurement was undertaken to ascertain the degree of workability of the mixes used. Fig.5.3 illustrates the slump behavior of the SFRC used in the manufacture of test specimens applied in this research.

Increase in fiber content resulted in a drastic loss of workability (slump value) from an average range of 15-20cm in non fibrous mix to 2cm in concrete with 1.5% fiber content. This is because when fiber is added to concrete mix, the composite forms a relatively stable system due to interlocking of fibers that increase the effective cohesion in presence of fibers. As a result free movement of the mix is hampered as observed during mixing.

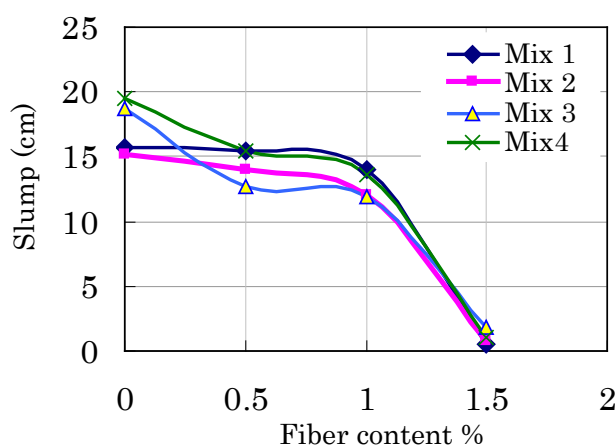


Fig. 5.3 SFRC workability

5.5 Hardened SFRC material properties

5.5.1 Average material properties

Table 5.2 shows the summary of the average material properties obtained from the split and compressive tests respectively. There is an increase in the ultimate tensile strength in the case of 1 and 1.5% fiber reinforced specimens with no improvements in the compressive strengths for all the fiber

reinforced specimens. Generally there is gradual increase in the Elastic modulus but with no significant change on the Poisson ratio.

Table 5.2 Average material properties

| Fiber % | Compressive (N/mm ²) | Tensile (N/mm ²) | Poisson ratio | E N/mm ² |
|---------|----------------------------------|------------------------------|---------------|---------------------|
| 0 | 45.07 | 3.67 | 0.18 | 31108 |
| 0.5 | 37.68 | 3.37 | 0.19 | 46517 |
| 1 | 42.40 | 4.40 | 0.22 | 54504 |
| 1.5 | 37.82 | 4.86 | 0.19 | 54766 |

5.5.2 Compressive strength

Although influence of steel fibers on compressive strength was found to be minimal, there is generally an improvement in stiffness in the initial stages particularly in the fiber reinforced specimens results. As a result the secant Modulus is also observed to have also increased accordingly. Decrease in the ultimate compressive strength was observed to occur in SP0.5 and SP1.5% specimens as depicted in Fig.5.4. Under compressive loads, fibers cause crack-closing forces induced by transverse tension forces resulting in an increase in strength, however existence of porosity due to inclusion of steel fibers in concrete mix have the tendency to cancel the former [26]. The results of the compression test are in agreement with this argument. Because of the cylindrical shape of the specimens, two dimensional ESPI measurements were not undertaken. Three dimensional optical systems could be a best suit this kind of specimen.

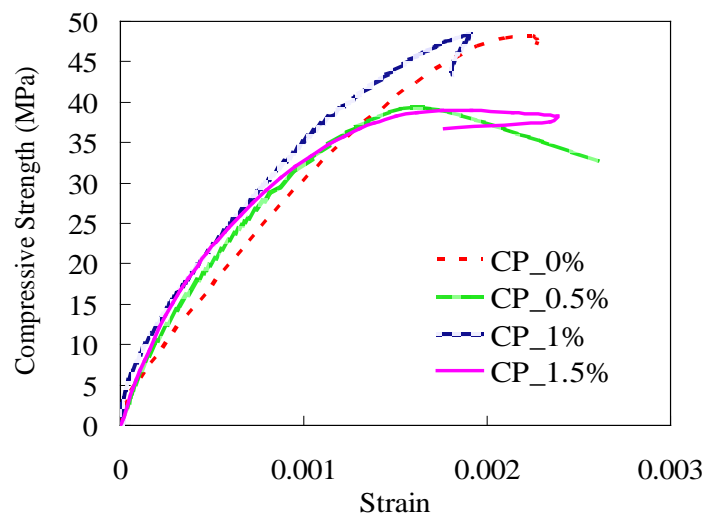


Fig 5.4 Compression strength

5.5.3 Tension strength and deformation

The main parameters that characterized the strength and deformation behavior of the SFRC were the tensile strength and ductility. Fig.5.6 shows the tensile strength results as obtained by Electronic

speckle pattern interferometry (ESPI), while results based on the conventional methods (use of strain gauges) are as shown in Fig.5.5. Generally, the tensile strength and ductility increases in tandem with the increase in steel fiber content present in the concrete. However, clarity in the influence of the steel fibers is more predominant throughout the results in the case of concrete with 1.5% fiber content. An average increase of approximately 32% in ultimate tensile strength is realized in the latter case (Table 5.2). There is generally improvement in both tensile strength and ductility in the case of specimens with 0.5% and 1% fiber content. This superiority is important in fracture control in concrete as fibers tend to reduce cracks and soften the deformation behavior by redistributing the tension stress. Detailed deformation patterns could also be obtained in the case of ESPI measurements as shown in Fig.5.6 (a) and (c). Fig.5.6 (a) 1 and 2 shows ESPI deformation strain pattern images at the ultimate load in SP1.5% and SP0% specimens, while Fig.5.6 (c) shows the ultimate strain behavior across the center face of the split specimen. It is observed in these figures that it is within the mid face of the specimens where cracks occurred and that there exists an increase in deformation as in comparison to other regions. Localized strain behavior as shown in Fig.5.6 (c) can give an indication of the fiber influence and distribution in the concrete. The strains in SP0.5% are higher in comparison to those of SP 1.5% and SP1%. This could be as a result of an optimum distribution of steel fibers in the concrete especially within the cracked region. Generally, it is observed that all the fiber reinforced specimens (SP0.5, SP1 and SP1.5%) had an increased strain capacity at mid face where cracks were observed as compared with specimens without fibers (SP0%). Higher fiber content leads to increased stress redistribution and thus a reducing strain level occurs as observed in SP 1% and SP1.5%. Concrete is a brittle material, and thus as expected, minimal strain is observed in SP0%.

Influence of strain gauge stability after failure can be observed in the conventional measurements results as seen in Fig.5.5. Beside the specimens with 1.5% fiber content, other results showed instability after failure. This is a common phenomenon observed when delaminating or breakage of the strain gauge occurs during measurement.

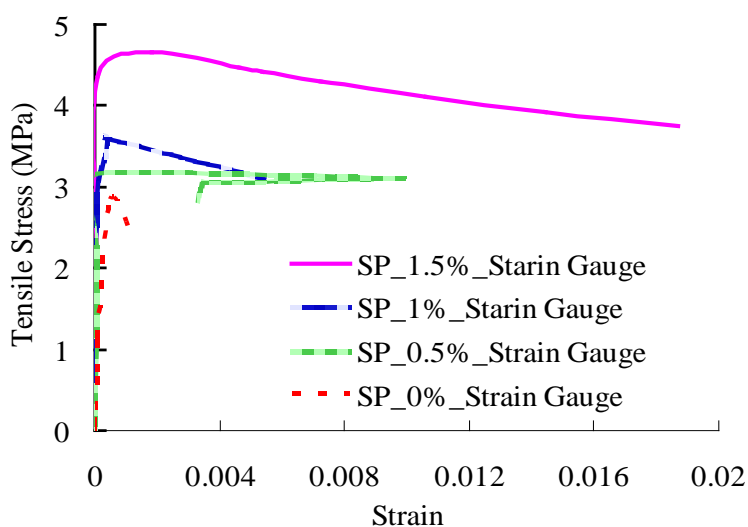


Fig.5.5 Conventional split tensile stress-strain

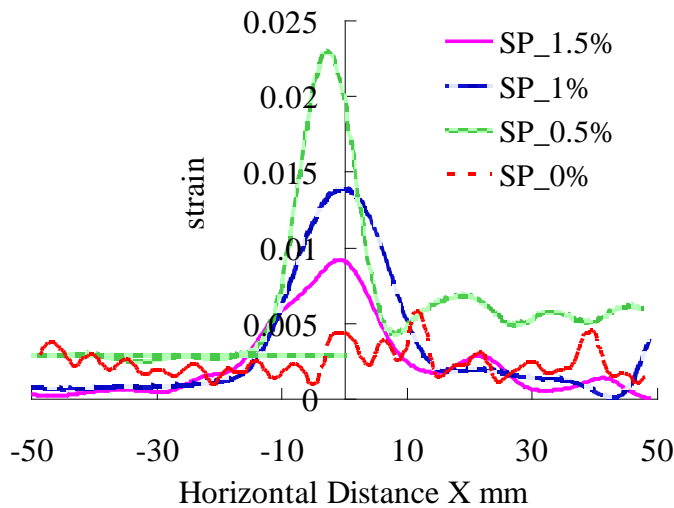
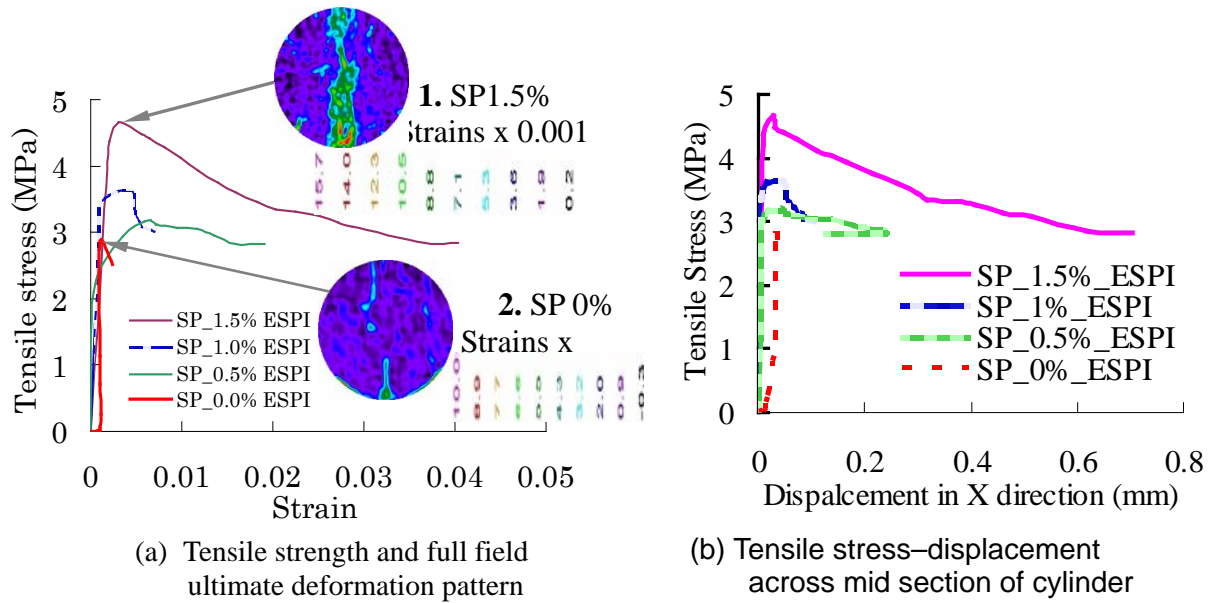


Fig.5.6 ESPI deformation Measurements

5.5.4 Shear deformation and strength

It is normally in reinforced concrete beams and slabs that shear phenomenon is commonly observed and more so considered in design. In this research pure shear test was not used but rather an indirect method of four point testing was adopted based on a parallel on going research on shear as discussed in detail in subsequent chapters. Shear strains and displacement measurements were obtained based on optical ESPI method, however additional displacement measurements were taken using the conventional LVDT probes for comparisons. The results on shear strength where steel fibers were used are thus reported here in brief. Shear failure in concrete is known to be brittle and catastrophic. This problem in part can be reduced with the use of ductile material such as steel fiber reinforced concrete (SFRC). Fig.5.7 and 5.8 indicates that steel fiber concrete has a higher shear capacity compared with plain concrete. All the fiber reinforced specimens showed improved post-yield shear strength as

compared with those without fibers. An approximately 59% increase in ultimate strength is achieved in beam specimens reinforced with 1.5% steel fibers (FB1.5% in Fig.5.7 and 8). Similarly ductile behavior is observed in all the specimens reinforced with steel fibers. Significant ductility is realized in shear when higher fiber content is used, as demonstrated by specimens having a fiber content of 1.5%. Furthermore, crack development and propagation was monitored and recorded with the use of ESPI as seen in the captured images at ultimate stage of shear failure (Fig.5.7), in a similar manner to those captured for the split test (Fig. 5.6 (a) 1 and 2).

All ESPI deformation measurement results showed similar stress-displacement development pattern before yielding. However, on yielding only specimens with higher fiber content (FB1 and FB1.5%) maintained the trend with divergence just before ultimate failure (Fig.5.8a). Pre yielding behavior in the conventional LVDT measurement results showed slight variability in FB0%, FB0.5 and FB1.5% (Fig.5.8b). However, significant difference is noticed throughout, in FB1% results. In both ESPI and LVDT results a slight stress relaxation is observed to occur immediately after yielding in the fiber specimens. This is the consequence of shear softening on occurrence of initial crack. This initial failure is immediately resisted by the steel fibers through crack bridging and stress transfer. As a result a recovery in the strength is achieved thereafter. ESPI ultimate displacement in all the fiber specimens is about 1.2mm. On the other hand LVDT results showed variable ultimate displacement values of 2.3, 3.1 and 1.8mm for FB0.5, FB1 and FB1.5% respectively. In FB1.5% specimens, the maximum displacement value achieved is 3.8 and 5.9mm in ESPI and LVDT respectively. Generally, the conventional displacement results are higher than those from ESPI. Full field (ESPI) displacement measurement were based on the actual specimen point deformation, while LVDT measured data were obtained at an eccentric point from the beam (use of an angle bracket) as necessitated by technical logistics normally encountered in taking such measurements. This explains the differences observed between the ESPI and LVDT measurements results

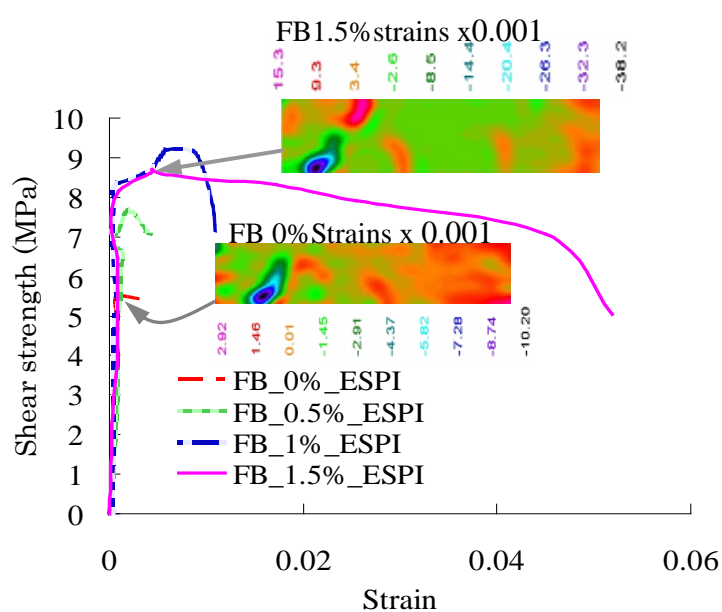


Fig. 5.7 Shear strength-strain relationship and deformation behavior

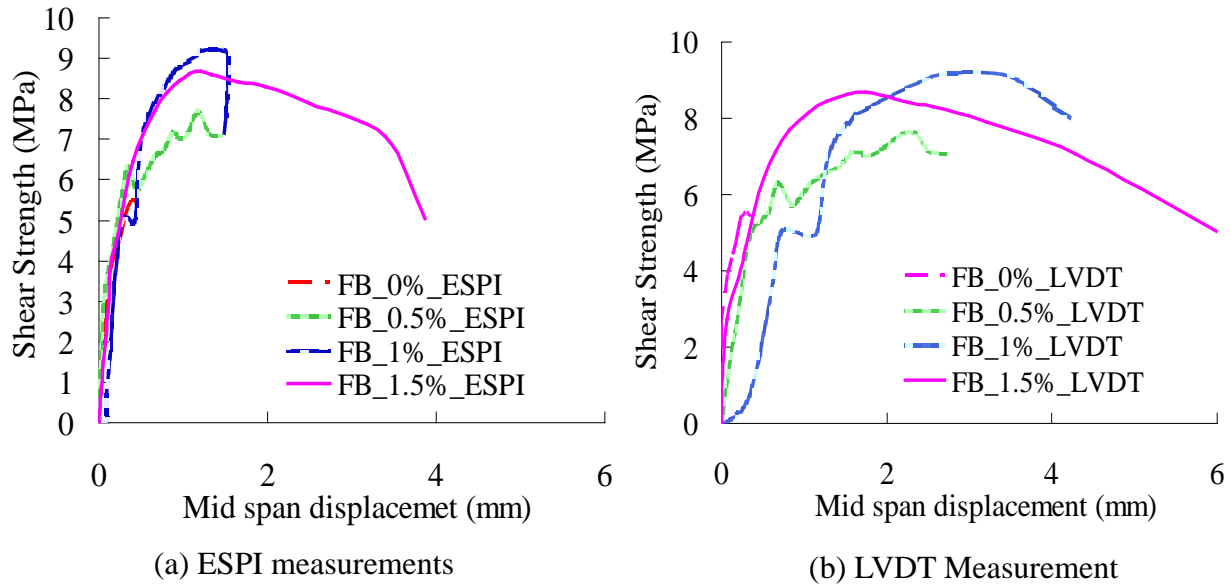


Fig 5.8 Shear strength-mid span Displacement

5.6 Concluding remarks

In this chapter, assessment of the fundamental material properties of SFRC have been presented and discussed. Moreover evaluation of emerging measurements methods such as full field optical ESPI were compared against existing methods. From the study the principal findings are as follows:

- (a) Reduced ultimate compressive strength is observed in steel fiber reinforced concrete.
- (b) Steel fibers improve post yielding (cracking) deformation properties in concrete. Fundamentally, ductility, tensile and shear strengths are also significantly enhanced.
- (c) Deformation and associative parameters can be measured and monitored accurately with ESPI method
- (d) Steel fiber concrete was successfully produced using normal standard materials, with fine aggregate content kept at approximately 43% of the total aggregate content.
- (e) Generally steel fibers were found to reduce the workability of fresh concrete and thus a suitable admixture must be used to control water content.

Chapter 6

Shear strength and deformation characteristics in steel fiber RC beam

6.1 Introductions

It has been proposed that fibers can relieve stirrup reinforcement in congestion areas in structural systems [6, 8, 37, and 39]. More over, the same can be applied as minimum shear reinforcements in load bearing beams. The unknown as stated by Pascal et al [39] is whether steel fibers can replace transverse reinforcements in reinforced concrete beams. The answer is still a research subject, since there is no known application of steel fibers independently as shear reinforcements. However, to clarify the shear strength and deformation merit offered by steel fibers, it is imperative to evaluate these characteristics in detail and compare the performance against an equivalently stirrup reinforced RC beams. In this chapter, experimental results on the shear and deformation capacity in SFRC beams as well as comparative evaluation results with those of equivalently reinforced stirrup beams with similar geometry as the fiber beams are presented. Further the comparative evaluation of the fiber and stirrup RC beams is also applied to establish the validity of the proposed equivalent shear reinforcement content relation given in chapter 3, Eq.(3.8). This equation is fundamental in the proposed equivalent design procedure for SFRC discussed in chapter 8 sections 8.4.

Presence of sufficient fibers in the concrete reduces the brittle shear failure in favor of a ductile failure. The increase in shear capacity attributable to the steel fibers depends not only on fiber volume fraction, but also on the aspect ratio and anchorage conditions [51]. A combined effect of these factors significantly influences the stress redistribution in the cracked concrete and consequently an increased shear and crack control capacity. Shear failure is one major influence on the structural integrity of structural RC members. In this context, using steel fibers can noticeably improve the performance of the RC structure by providing a ductile collapse mechanism through stress redistribution. Because of the way in which steel fibers are incorporated in concrete, clarity of its entire influence on the deformation (cracking, strain, deflection) development characteristics is necessary. However, there is no information on this influence in RC beams under bending shear. This problem is caused by the difficulty in measurements of deformations [52].

6.2 Deformation observation and measurement by ESPI method

Observation of crack development allows for the identification of initial yield states and the subsequent propagation to the ultimate failure. In this study, a two dimensional optical electronic speckle pattern interferometry (ESPI) (see chapter 3, Fig.3.2 and Fig.6.1) gauging technique was used

to measure and monitor the deformation and cracking pattern in the fibrous RC beams under bending-shear. By this method, it was possible to realize the full field and non-contact measurement of strain distribution and the cracking visualization until ultimate failure. ESPI is an optical gauging technique applied in full-field, non-contact deformation measurements. The method utilizes what is termed as “speckle pattern” which is an irregular pattern resulting from mutually irregular phase interference of scattered laser light beamed on a rough surface. Speckle interferometry uses high resolution CCD-camera to take the speckle pattern of the image before and during deformation [53]. The initial speckle pattern is used as the basis for tracking the subsequent deformation changes resulting in what is termed as interference fringes which reveal the displacement of the surface during loading as contour lines of deformation. These qualitative fringe images are of low contrast and noisy due to the presence of the speckles. A procedure called phase shifting is applied on the series of speckle images for each surface state and calculates a quantitative phase map. The phase map contains quantitative and directional information which can directly be transformed into displacement and strain field values. The basic principles of this method is discussed in chapter 2

6.3 Observation of cracking and ductility development in SFRC (0 &1.5%) beams

6.3.1 Specimens and test procedure

The same concrete mix proportions given in Table 3.2 in chapter 2 were used in the manufacture of the specimens. Thus the concrete mix ratios (*Water cement ratio: Cement: Fine: Coarse aggregates*) were in proportions of 0.45:1:1.89:2.48 and 0.45:1:1.84:2.42 for specimens with 0% and 1.5% fibre content, respectively. Due to the limitation of the optical equipment available, scaled down beams of small geometric dimensions were selected. Thus 400×100×100mm short RC beams were made. The beams were reinforced in flexure with 6mm diameter deformed steel bars of 345MPa strength. Ø100mm by 200mm length cylinders specimens (for material property determination and control) were cast concurrently with beam specimens. The cylinders were tested in compression and tension at 28days concurrent with the curing period for all the specimens. All the specimens were cured under complete immersion in water for a period of 28 days before testing.

Bending-shear tests were carried out on simply supported beams as shown in Fig. 6.1 and 6.2. Three (1, 1.5 and 1.83) shear span to depth ratio variations were made. Tests on the specimens were done using a 300kN capacity universal testing machine. Loading was applied on the specimens while the full field deformations were monitored and recorded using a set of optical measurements equipment system (ESPI) comprising a desk top computer (PC) and CCD camera equipped with laser beam sensors ESPI sensor .

ESPI, ISTR program was used to record, control and evaluate the speckle interferograms resulting from the deformation of the specimens. Control and recording of the loads were done using a data logger and laptop PC. Subsequent reductions of the full field raw data was performed using

normal Microsoft excel program. Data for graphical representation of the displacement at various load states were obtained from the full field results at points x (Fig.6.2), while strain distribution profile in these load states were obtained along line 1 as shown in Fig 6.2. This position was chosen as it cross-coincides with the crack paths.

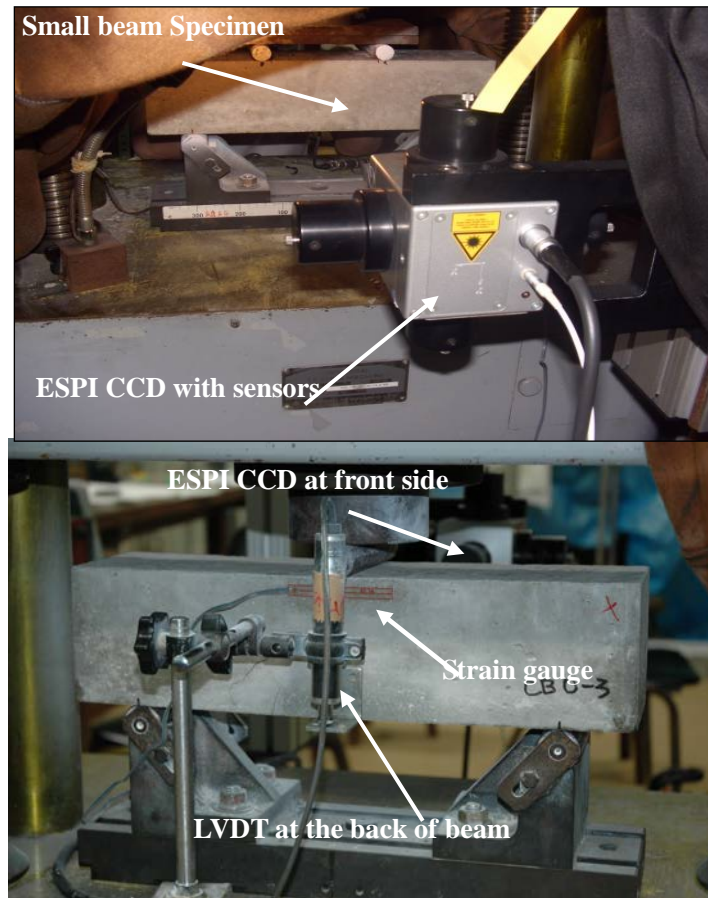


Fig 6.1 Instrumentation and test set up

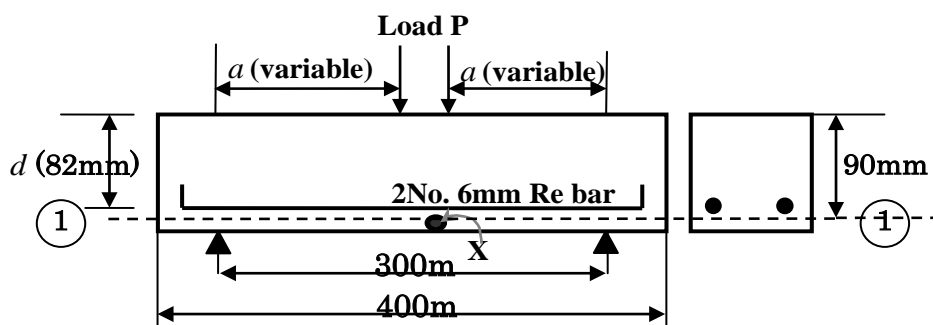


Fig.6.2 loading and deformation measurement locations

6.3.2 Physical failure and load deflection response

The failure mechanisms observed and the ultimate load showed a varied trend which was dependent on the shear span to the depth ratio and fibre content. The fibrous beam with the shear span to the depth ratio of $a/d=1.0$ had a predominant shear crack forming near the support, extending toward the load point (Fig.6.3a). Sudden failure was observed to occur in the control beam in this group (CB0). The trend represents a typical compression failure that occurs as a result of load transfer through

compression struts that form between the support and the load, leading to formation of a splitting shear crack. The Control beam with $a/d=1.5$ failed in flexure however that in $a/d=1.82$ had a flexure-shear failure pattern with formation of diagonal shear cracks. Generally, the failure load in all the control beams was lower than that of the fibrous beams (CB0, FB1.5, see Fig 6.3b). Fibrous beam (FB1.5) in $a/d=1.82$, had a single splitting vertical flexural crack within the mid span a drastic difference with the control beam (CB0) in the same group, where more than three visible diagonal cracks formed (Fig.6.3a). It was observed that the presence of steel fibres lead to improved load capacity (Fig.6.3b) and formation of finer cracks not clearly visible but could be isolated and clarified through strain evaluation at various load stages (see Figs 6.4 to 6.6).

It can be seen from Fig. 6.3b that the highest net increase in ultimate load capacity is in the fibrous beam in the group with $a/d = 1$. Although compression shear failure may have occurred in this group, reserve strength arising out of the arch action can be considered as minimal, given that all the beams had similar geometry and flexural reinforcements, moreover, an improvement is not observed in the CB0 beam. This implies that the fibres are responsible for the observed increase in strength. Improvement in load capacity, albeit small is also observed in the $a/d = 1.5$ and 1.82 group of beams. There is improved ductility in $a/d=1.0$ and 1.5 group of fibrous beams, however FB1.5%, $a/d=1.82$ group showed no much difference in ductility over non fibrous (CB0) beam. This can be attributed to the flexural failure mode, an indication that the influence of the fibres in flexural ductility may be not significant but strength improvement is noted.

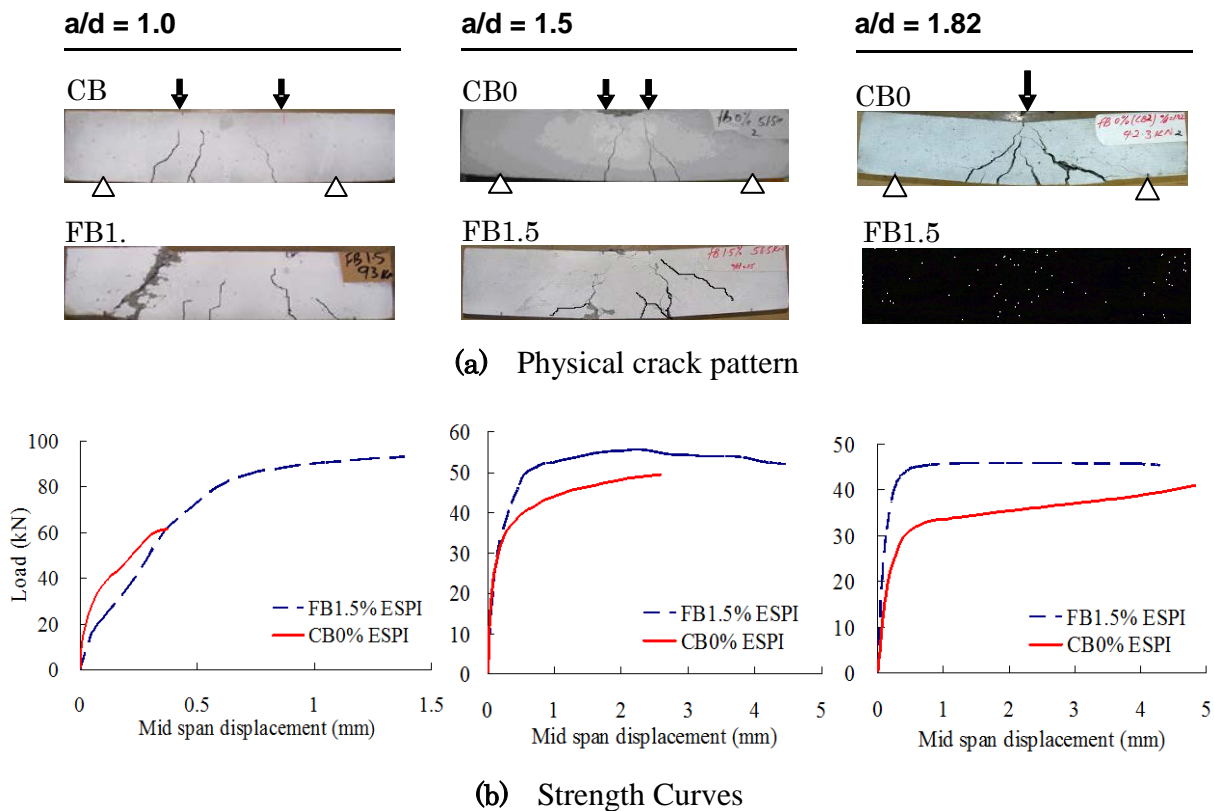


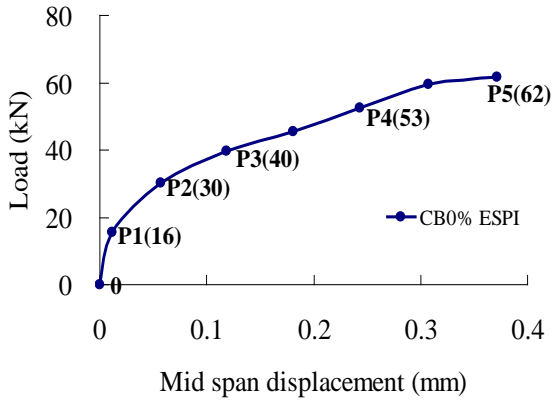
Fig 6.3 Deformation and load deflection capacity behavior

6.3.3 Visualization of cracking development in SFRC beams

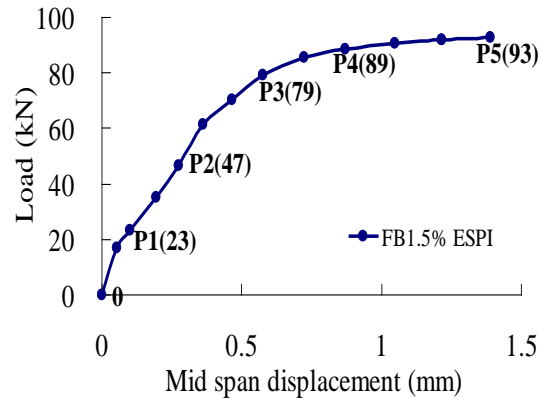
Figs 6.4, 6.5 and 6.6 depict the deformation state of the beams at various load steps. A common feature in all these figures is that initial yielding in CB0% specimens occurred earlier than the fibrous beam (FB1.5%). These are at 16, 15, 10kN for CB0% and 23, 16, 20kN for FB 1.5% beams in the groups $a/d=1$, 1.5 and 1.82, respectively (see P1 in Figs 6.4 (i), 6.5(i) and 6.6(i)). These values are much lower than those noted during testing at onsets of physically observable initial crack which were at 53, 44, 36 for CB0% and 60, 40, 31kN for FB1.5% in the groups $a/d=1$, 1.5 and 1.82, beams, respectively. As shown in these figures, cracking is commensurate with load increase. In the case of CB0% specimens, ultimately a maximum of four cracks occurred. It is observed that soon after initial yielding (P1), crack penetration increased concurrently with the load increase (P2, P3, P4 and P5) without further propagation along the beam span. Strain distribution evaluation (Figs 6.4a, 6.6a, 6.6a (ii) along the beam (crossing the crack paths), confirms this behavior. There are no more points in which peak strains occur (crack strains), however in the specific points where the cracks had occurred, these strains are noted to increase in tandem with the load (P1 to P5). By comparing this trend with the fibrous beams (FB1.5%), it is clear that after initial yielding, increased crack propagation occurred particularly in $a/d=1$, and 1.5 group of beams.

A proportionate increase in the peak value of the strains within areas of crack concentrations is also observed in the subsequent load steps (P2 to P6). Further it can be observed that from P3, some cracks start to fade away while the dominant crack(s) continue to increase in visibility and peak strain value. This may be an indication of crack closing and a shift of the stress to the critical crack(s) responsible for the ultimate failure. Taking for instance Figs 6.4(b)(ii) and 6.5(b)(ii), at load step P3 (79, 29kN), the ESPI visualized cracks which are clearly visible are more however, at ultimate loads (P5, P6) some of these cracks appear to fade and the strain values of the clearly visible cracks are relatively larger resulting in the peak points and values observed. A similar trend is also observed in the fibrous beam in Fig.6.6 (b) (ii). However, this behavior is minimal in the non fibrous beams; this may be an indication of the consequence of absence of steel fibers in the concrete. Shear failure was observed to have occurred (Fig.6.4(a), Fig.6.5(b)(ii) in fibrous beam in $a/d = 1$ group, however, it appears from load step P2, the initial flexural cracks that developed shifted to a combination of shear and flexural type of cracks at load step P3 just at critical stage of failure. It is evident from Fig 6.3a ($a/d=1$) that the flexural cracks are much smaller, and the shear crack is responsible for the failure which seems to have occurred between loads P3 to P4 (Fig.6.4 (b) (i) and (ii)). In the group of beams with $a/d=1.5$, shear failure is observed to have occurred between load P4 and P5 respectively (see Fig.6.5 b i, ii).

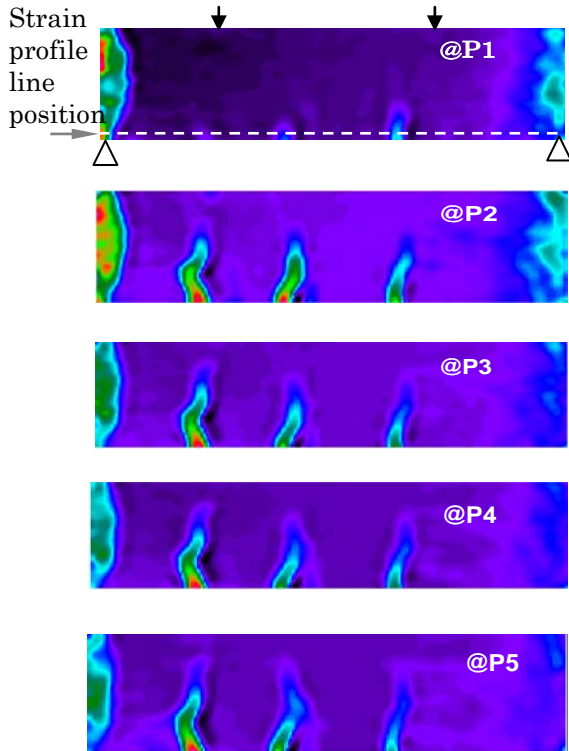
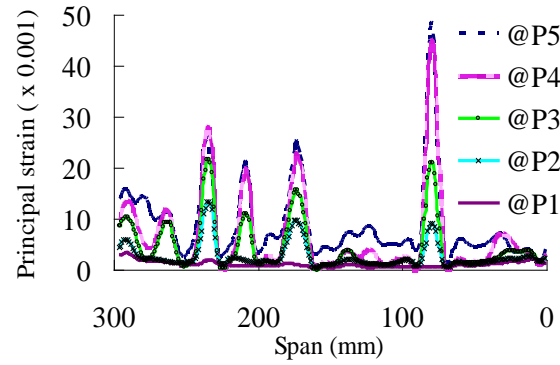
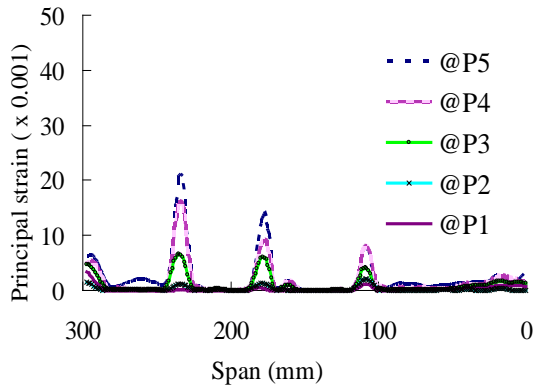
Generally, the ESPI crack pattern reveals more of flexural failure cracks, although from the physical failure mode from Fig.6.3(a), there is indeed a combination of both failure modes, particularly in $a/d=1.0$ and 1.5. This is because the strain analysis is based on the principal strain (tensile), thus shear effects such as cracks are less visible.



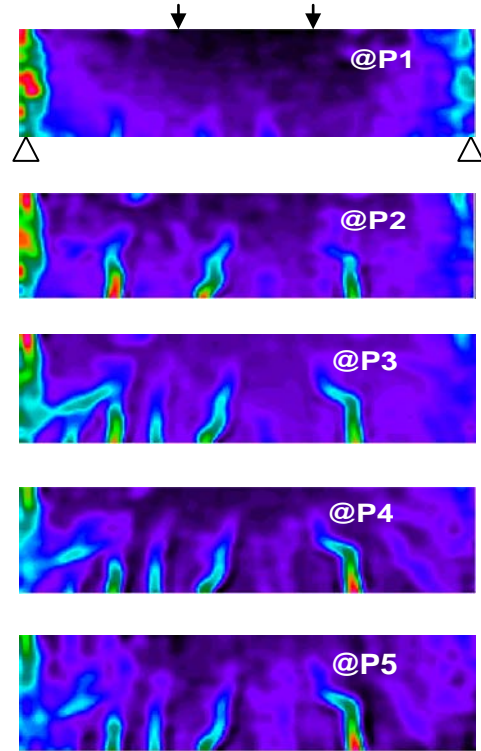
(i) Load deflection curve (fiber 0%)



(i) Load deflection curve (fiber 1.5%)

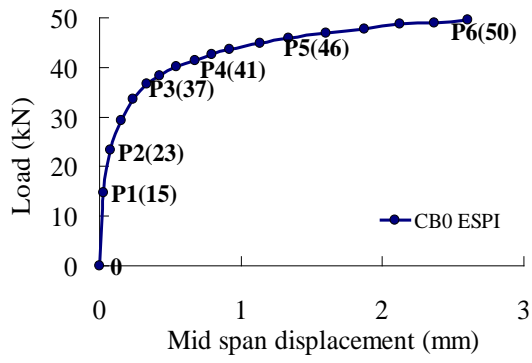


(ii) Strain and crack development
(a) Control beam CBO (0% fiber)

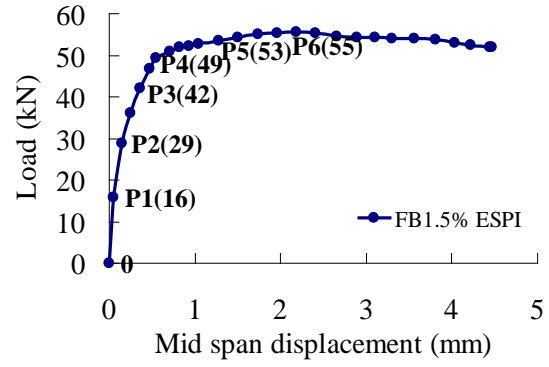


(ii) Strain and crack development
(b) Fiber Beam FB1.5 (1.5% fiber)

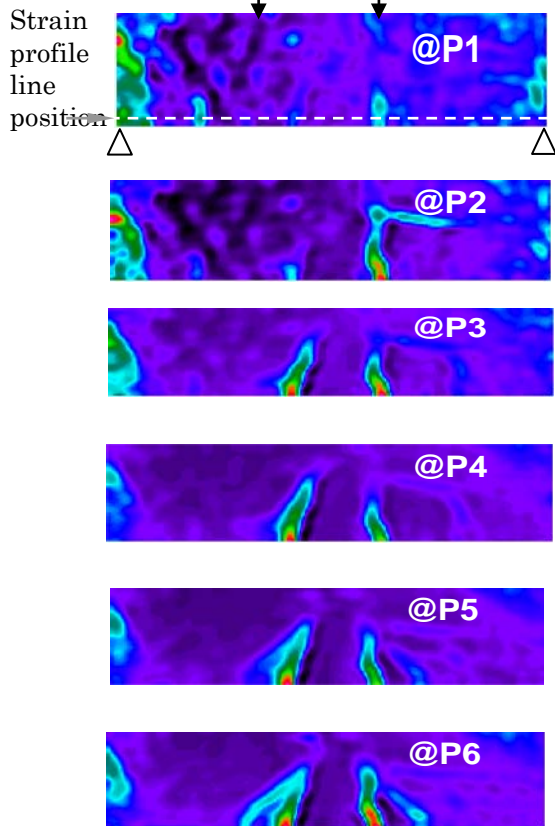
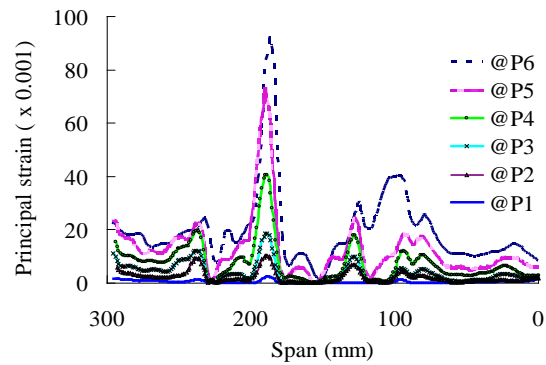
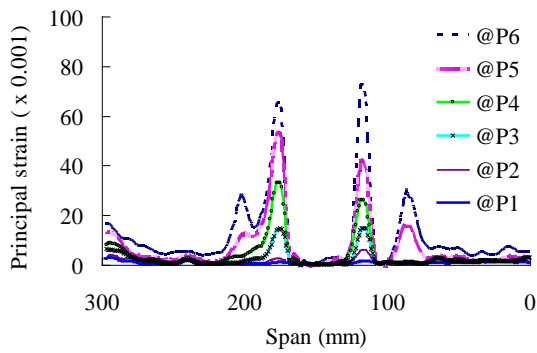
Fig. 6.4 Deformation and cracking behavior for $a/d = 1$ group of beams



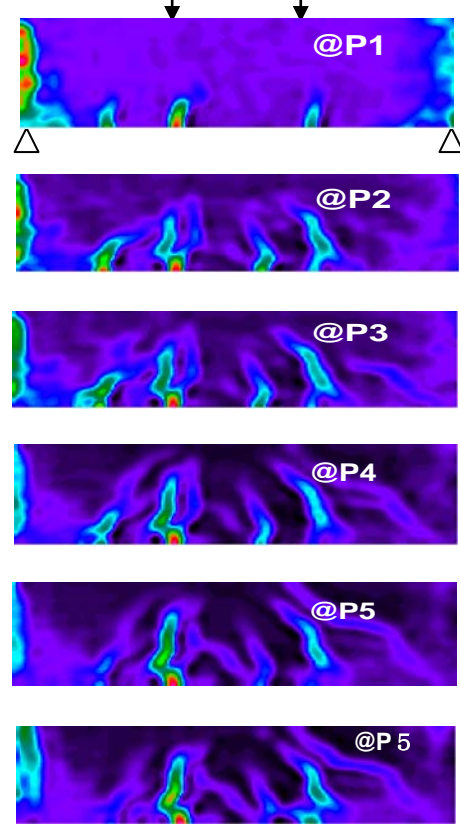
(i) Load deflection curve (fiber 0%)



(i) Load deflection curve (fiber 1.5%)

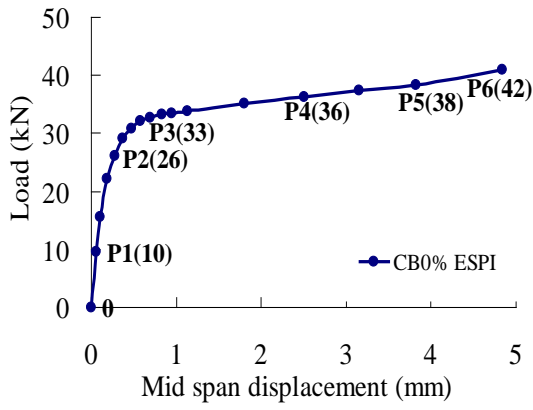


(ii) Strain and cracking development
(a) Control Beam CB0 (0% fiber)

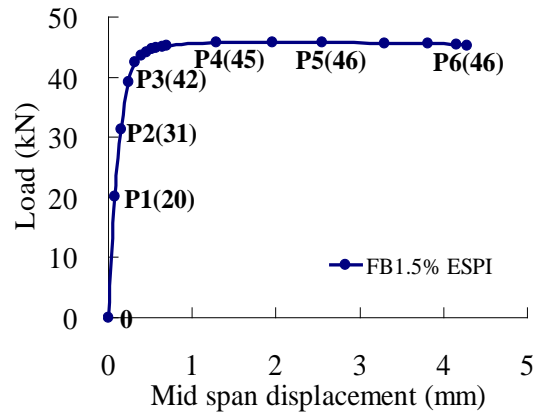


(ii) Strain and cracking development
(b) Fiber Beam FB1.5 (1.5% fiber)

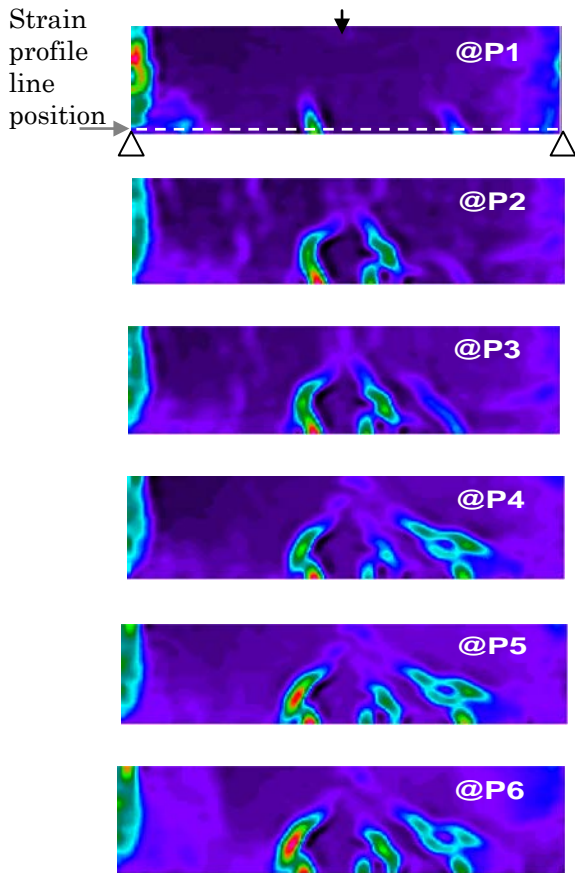
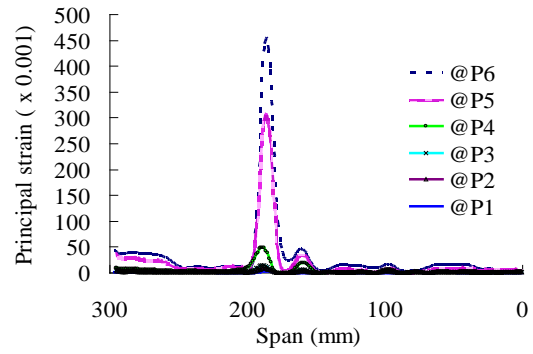
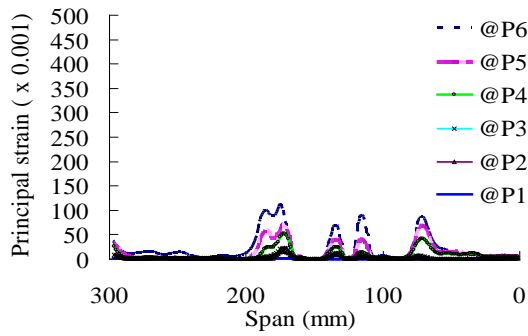
Fig.6.5 Deformation and cracking behavior for $a/d = 1.5$ group of beams



(i) Load deflection curve (fiber 1.5%)

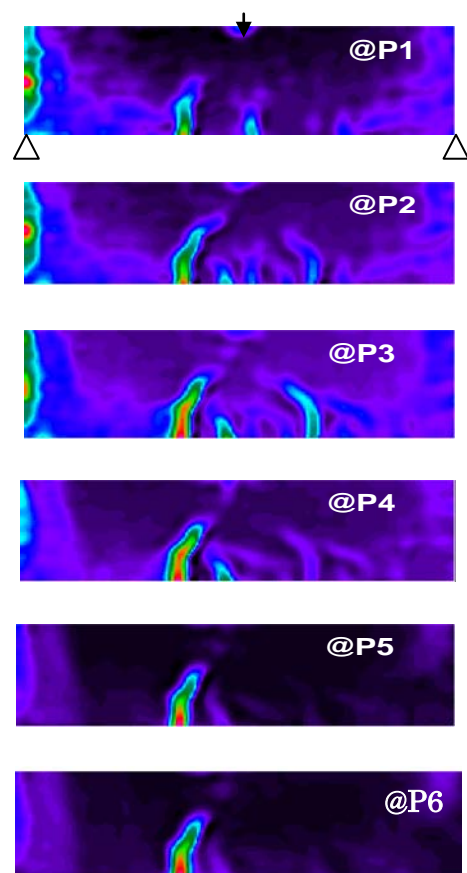


(i) Load deflection curve (fiber 0%)



(ii) Strain and crack development

(a) Fibre Beam CB0 (0% fibre)



(ii) Strain and crack development

(b) Fiber Beam FB1.5 (1.5% fiber)

Fig.6.6 Deformation and cracking behavior for $a/d = 1.82$ group of beams

6.3.4 Ductility and crack strain characteristics

Ductility is a desirable structural property because it allows stress redistribution and provides warning of impending failure. Comparing the load deflection curves and the principal strains at crack points in the fibrous and non fibrous beams, it is evident that fibrous beams could deform more at higher loads. This is the consequence of improved stress redistribution in the fibrous beams. It is found from Fig.6.4, Fig.6.5 (a) (i) and (b) (i) that whereas CB0 beams failed at 62 and 50kN at a displacement of 0.38 and 2.6mm, respectively, the fibrous beams failed at 93 and 55kN with a displacement of 1.39 and 4.4mm, respectively. Correspondingly from the same figures part b (ii), the peak crack strain values were 23, 50 for CB0% in a/d=1 group of beams and 78, 99 for FB1.5% in a/d=1.5 beams, respectively. A difference is noted in the deflection behavior in a/d=1.82 group of beams. The ultimate displacement is almost the same for CB0% (at 4.8mm) and FB1.5% (at 4.2mm) beams, whereas the ultimate load is slightly higher in the fibrous beam, however a drastic deviation is observed in the peak crack strains. In this group, the CB0 beams failed at a much lower crack strain of 145×10^{-3} in comparison to that of the fibrous beam (FB) which is 480×10^{-3} , more than three times that of CB0 beam. It is observed from the visualized crack pattern Fig.6.6(b)(ii) that, the flexural cracks which initially occurred in the fibrous beam at load step P1 congregated probably through stress redistribution into one single crack responsible for the flexural failure as observed in Fig.6.3(a), FB1.5 a/d=1.82. On the other hand, the non fibrous beam (CB0) in the same group, yielded ultimately from a combination of shear-flexural crack. It is generally observed that all the fibrous beams failing in shear showed increased deflections, strain distribution with higher peak crack strains and ultimate loads in comparison with the non fibrous beam (CB0). Furthermore, as noted earlier, the fibrous beam failing in flexure had increased crack strain. This confirms the superiority of the steel fibers in shear resistance and softening the failure mode even in flexure.

6.4 Strength and deformation comparison with stirrup RC beam

6.4.1 Specimens and evaluation procedure

The concrete mix proportions used in the manufacture of the stirrup beam specimens was same as that given in chapter 3, Table 3.2 for control beams (i.e. with no fiber reinforcements). Unlike the fibrous reinforced with steel fibers, the stirrup beams were variably reinforced in shear with stirrups bars determined using the equivalent reinforcement content formula (Eq. 3.8) based on the amount of fiber content applied in the fiber beam which were in the range of 0 to 1.5 % by content. The equivalent shear reinforcement equation was applied in order to equivalently match the fiber content and allow for qualitative test results comparisons and thus establish experimentally the validity of the proposed equation All the beams were reinforced in flexure with 6mm diameter deformed re-bars with yield strength. Bending shear test was conducted in which three shear span (a) to depth (d) ratio variations

($a/d=1, 1.5$ and 1.82) were made. Similar testing procedure and instrumentation as that shown in Fig 6.1 was used and the test set up and deformation measurement points was as shown in Fig.6.7. Full field optical ESPI measurement method was used to obtain the deformation fields; however, ultimate failure images were obtained based on shear strain deformations analysis results. This was done to clearly evaluate the comparative difference in shear deformations (shear strain fields) between the fiber and stirrup beams under bending shear. In the measurement process, data for graphical representation of the shear strain and displacement were obtained from the full field results at points A_1 and A_2 (Fig.6.7a and b) respectively, while strain profiles on the deformed beams were obtained along lines 1 to 6 as shown in Fig.6.1.

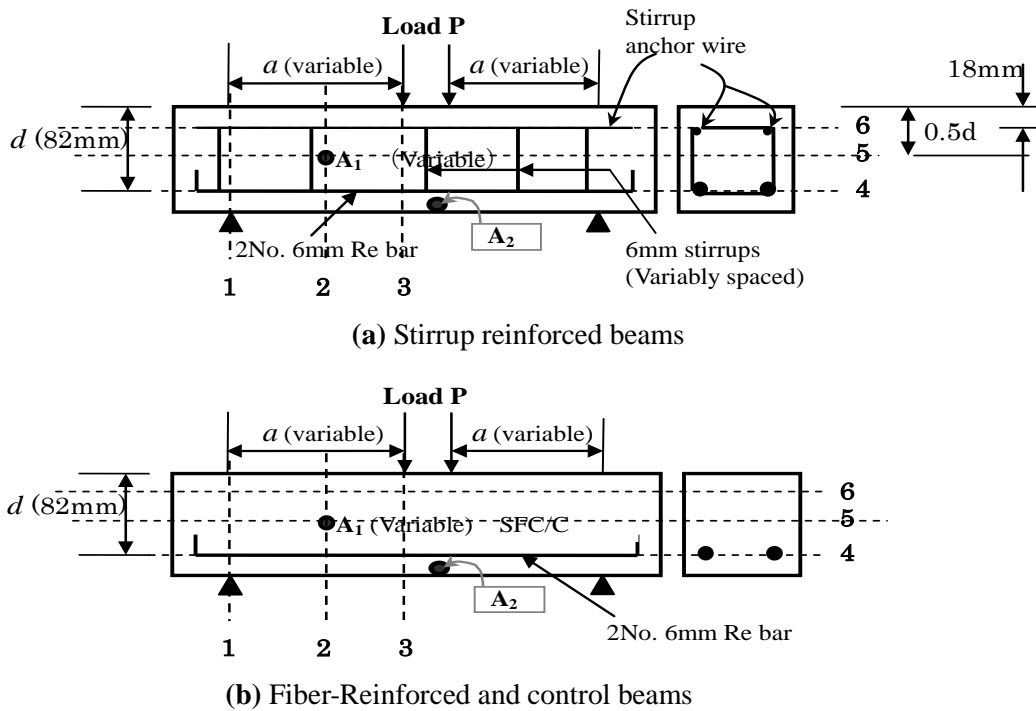


Fig. 6.7 Beam type by reinforcement, test set up and measurement points/lines

6.4.2 Comparative failure modes and ultimate load capacity

For ease of presentation, the designation of the beam specimens as used in subsequent sections is as follows: FB (Number)=Fiber Beam (% fiber content); SB (Number)=Stirrup Beam (% of Stirrup content); CB0 =Control Beam. Fig.6.8 shows the general observed physical failure trend in all the beams. A trend can be seen where fiber and stirrup-reinforced beams showed similar crack patterns but at different ultimate load levels. Control beams CB0, which had no shear reinforcement, failed soon after the formation of the first crack. The appearance of this first crack was almost instantaneous and led rapidly to failure of the beam. On the other hand, beams with fiber and stirrups reinforcement continued to resist higher shear loads, exhibiting considerable ductility particularly at higher reinforcement content. As expected, the mode of failure changed from shear to shear-flexure as the shear span depth ratio increases. In the latter mode, diagonal shear and vertical flexural cracks formed. It can be observed that the failure mode is almost same in each group (here grouping is according to

a/d) of beams for each category with same shear reinforcement content (e.g. FB1 and SB1 in *a/d*=1) with exception of the FB1 and SB1 in *a/d*=1.82.

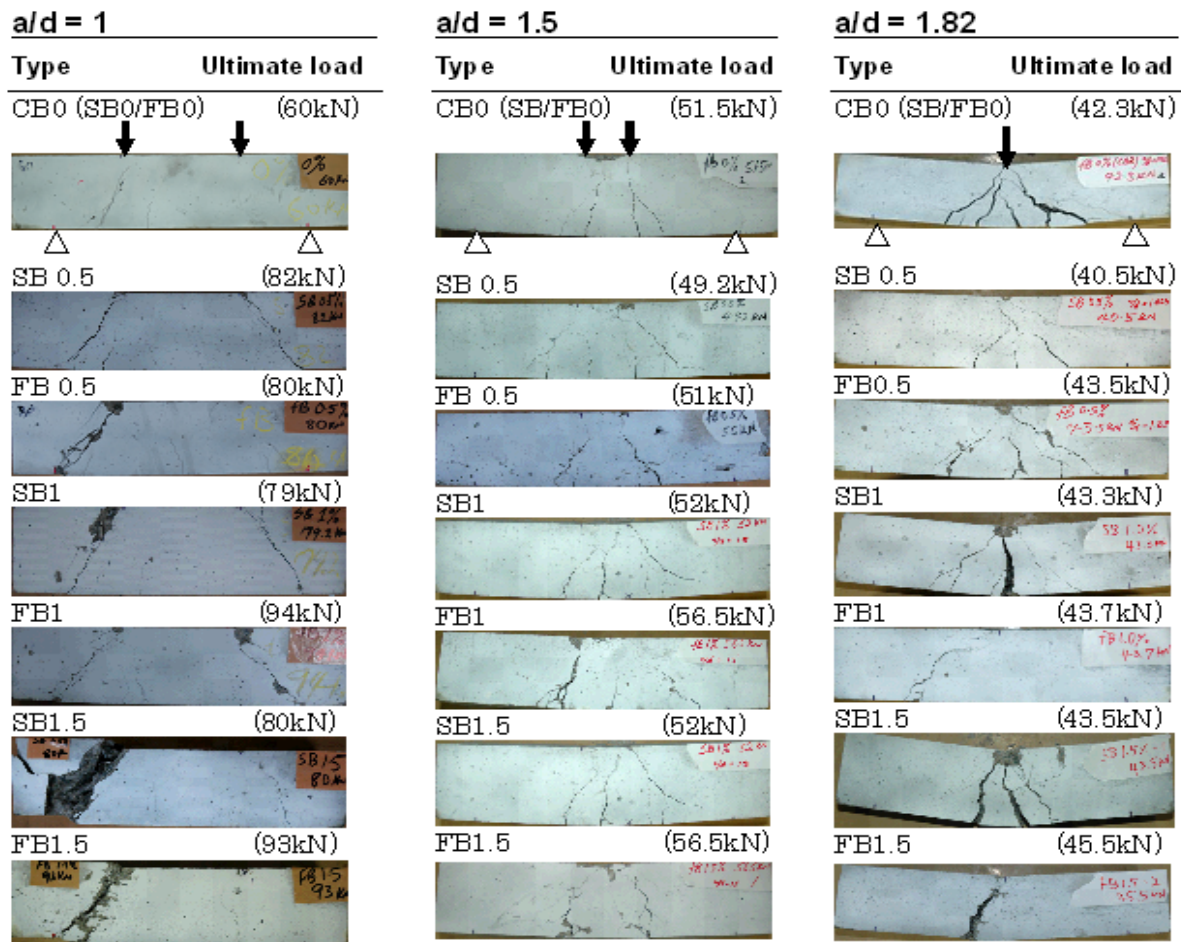


Fig.6.8 Physical failure modes

In comparison to the general physical failure modes shown in Fig.6.8, full-field deformation pattern results from ESPI shear strain image analysis are shown in Fig.6.9. The deformation behavior has been accurately represented with clear identification of the cracked regions. Full-field ESPI results (Fig.6.9) showed that localized strain variations increased in accordance with fiber reinforcement content and the shear span-to-depth ratio. However, there is a reduction in the load capacity when the shear span to depth ratio is increased. This trend can be attributed to the increase in ductility and the failure mode change.

Fig.6.10 summarizes the ultimate load behavior in all the groups investigated across the shear span depth ratio and shear reinforcement content variance. It can be seen that beams that failed mainly in shear (*a/d* =1) showed an increasing ultimate load capacity in line with increasing fiber and stirrup reinforcements because all the beams had similar flexural reinforcements. However, this trend is reduced in the case of beams with shear-flexure failure (*a/d*=1.5 and 1.82). Furthermore, in all cases, fiber-reinforced beams had nearly equal or higher ultimate load capacity in comparison with stirrup-reinforced beams, confirming the beneficial influence of steel fibers in reinforced concrete

beams, particularly in shear resistance.

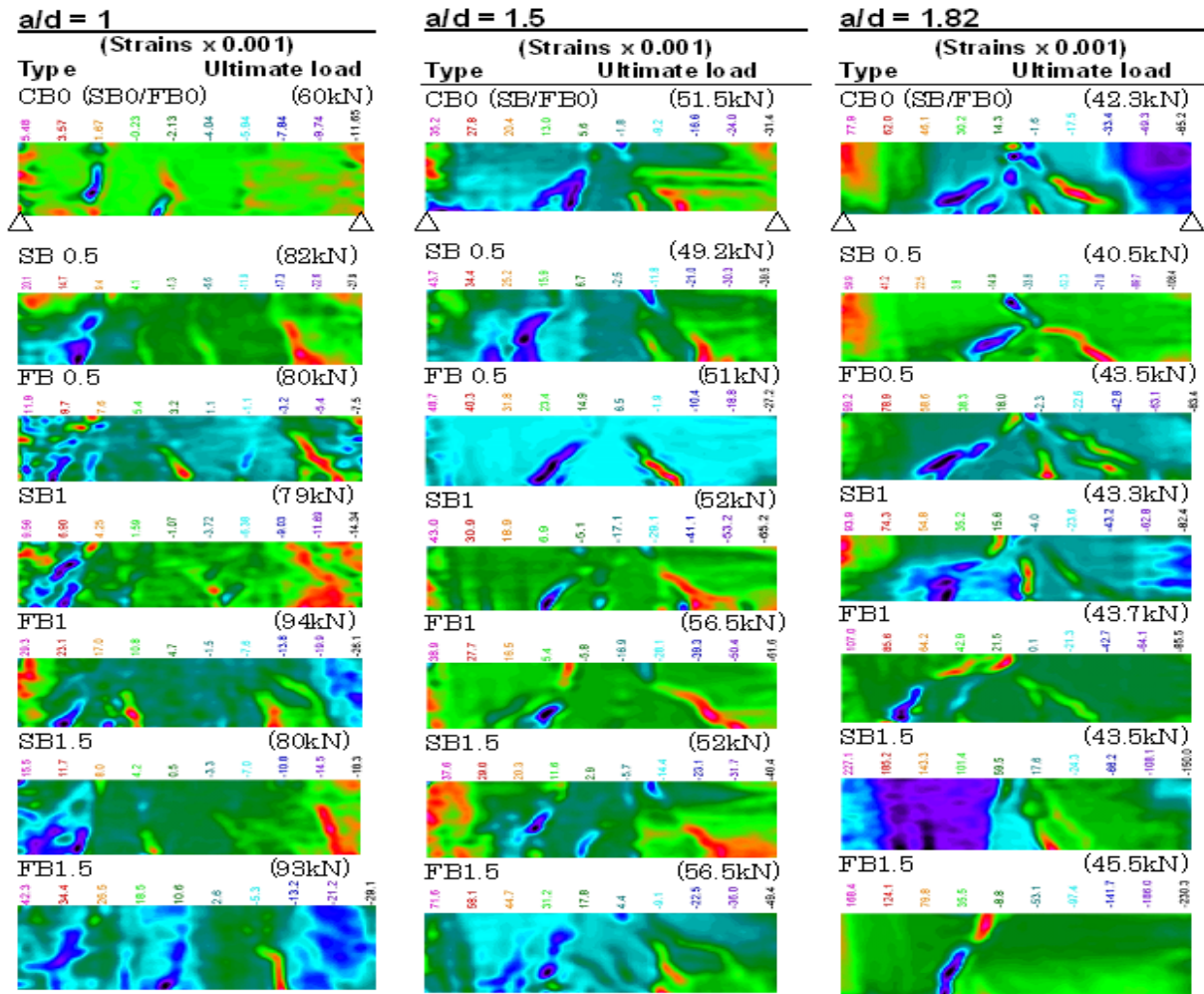


Fig. 6.9 Corresponding ESPI full-field failure characteristics

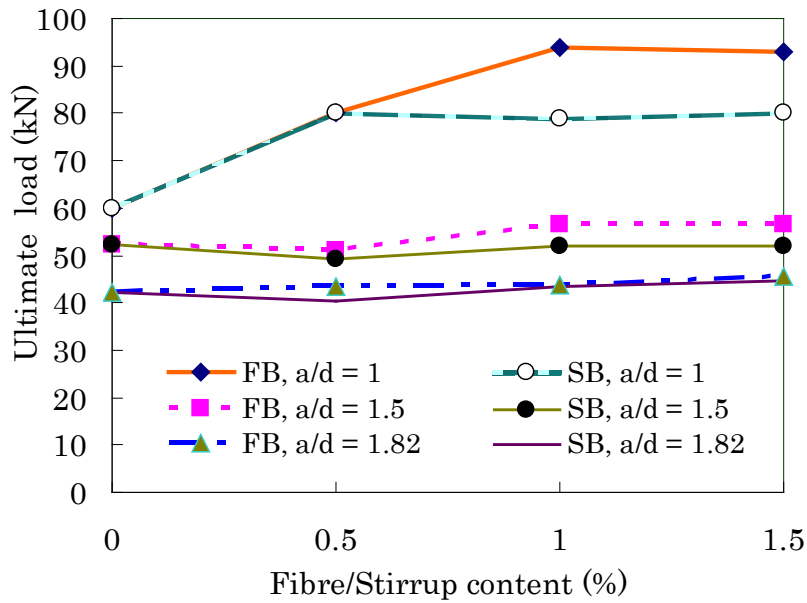
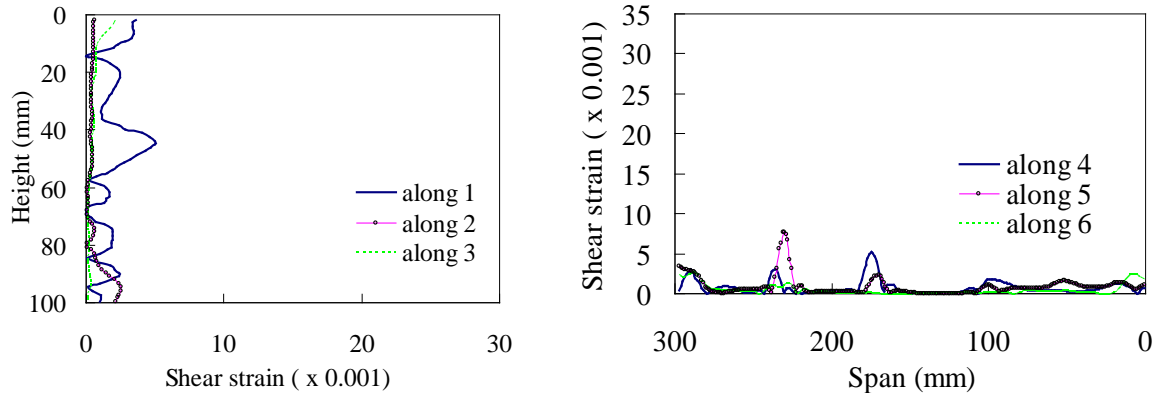


Fig.6.10 Steel fibers and stirrup load carrying capacity

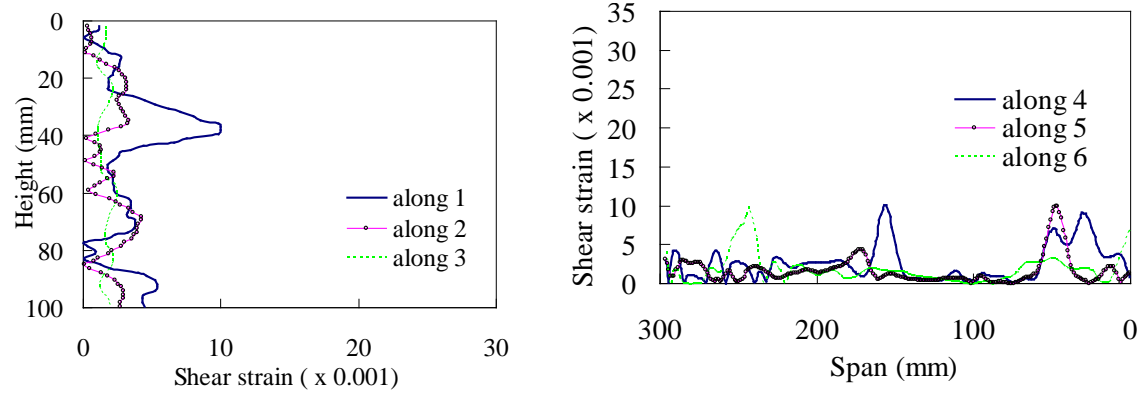
6.4.3 Comparative full-field deformation characteristics

To characterize further the full-field influence of the fibers and stirrups in shear deformation, strain evaluation in the $a/d=1$ group of beams was carried out along lines 1 to 6 as shown in Fig.6.7. Shear strain states at ultimate load levels (see Fig.6.9) were obtained from ESPI shear strain analysis along the beam depth and span at these critical locations (see Fig.6.7). The corresponding shear strain profile results plotted against the beam depths and span along the indicated locations were as shown in Figs.6.11a and 6.12. As depicted in Fig.6.11, shear strains increased both along the span and depth of the beam in tandem with the increase in fiber content. The control beam (CB0) showed minimal straining at failure as expected given that there was no form of shear reinforcement, and it confirmed the sudden failure that was observed during the test. Further, it can be seen that there seems to be a spread of regions with peak strains along the span in these beams (Fig.6.11b, FB1, FB1.5) compared with corresponding stirrup-reinforced beams (Fig.6.12b, SB1,SB1.5). This trend can be attributed to the stress redistribution effectiveness of the steel fibers as they are distributed throughout the volume of the beam.

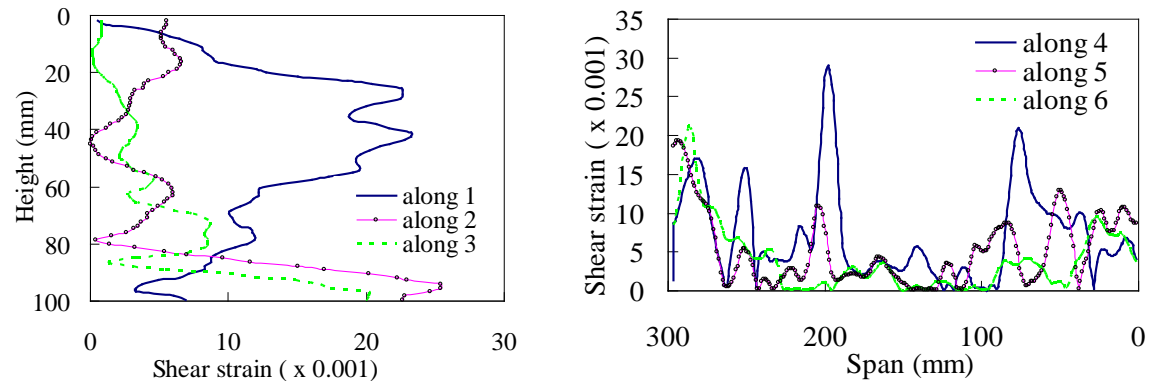
The shear strain behavior along the beam depth (lines 1,2,3) and span (lines 4,5,6 see Fig.6.7) in all the stirrup-reinforced beams is on average within the same range in a specific direction but less than those of corresponding fibrous beams. However, the strain profile is more pronounced in the stirrup beams within the shear regions when viewed longitudinally (Fig.6.12b), a trend different from that observed in the fiber beams (Fig.6.11b) which is fairly well distributed along the beam (Fig.6.11b). Further, a smaller increment in strains is observed in the stirrup beams when compared to the fiber beams in the longitudinal direction, an implication of less stress redistribution. In both types of reinforced beams, the strain profile along lines 1, 2 and 4 (Fig.6.7) is shown to be on average higher than strains at the other locations. Perhaps the measurement lines fall within regions of high shear and flexural stresses. The shear strain profile along the beam depth (i.e. along lines 1, 2, 3) indicates a trend in which the stirrup reinforced beams shows a more evenly distributed strain profile (Fig.6.12a). However as in the case of the fiber beams, the strain profile along the same lines tends to concentrate near the neutral axis (Fig 6.11a). Generally, the longitudinal strains within the mid-span region in SB1 and SB1.5 are less than those of the corresponding fibrous beam. In the beams, all regions in which cracks occurred (see Fig.6.8), correspondingly had localized peak strains (Figs.6.11 and 6.12), a confirmation of accurate visualization (Fig.6.9) of the fracture mechanism by the ESPI method.



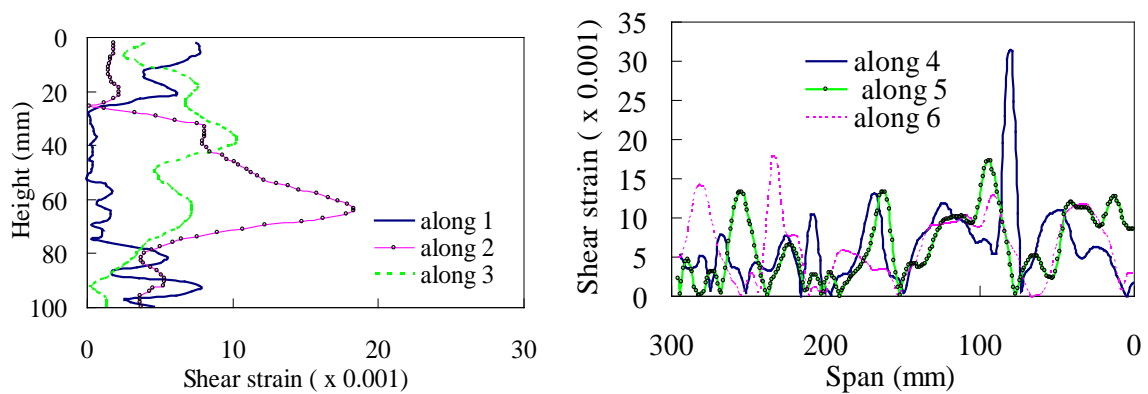
(i) Control beam (CBO)



(ii) Fiber beam (FB0.5)

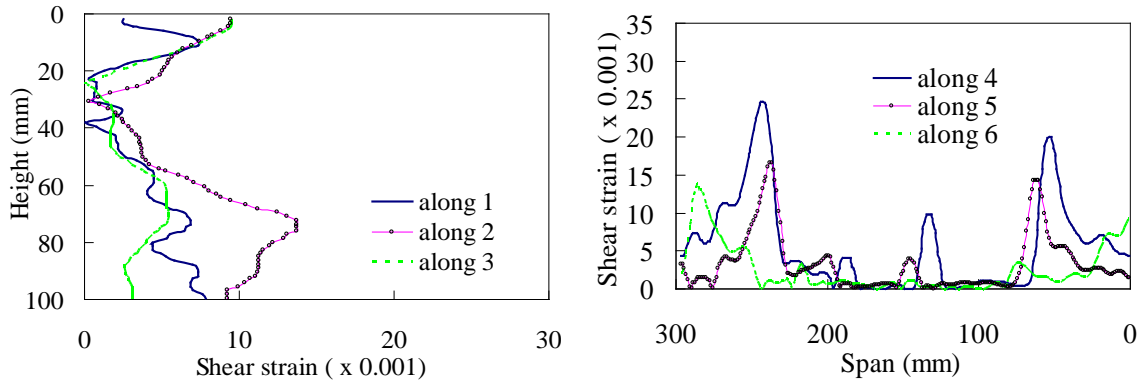


(iii) Fiber beam (FB1.0)

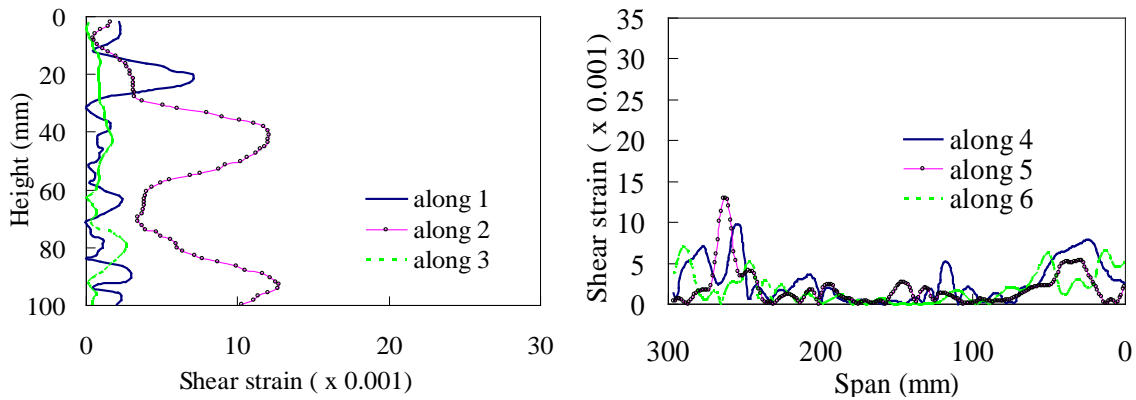


(iv) Fiber beam (FB1.5)

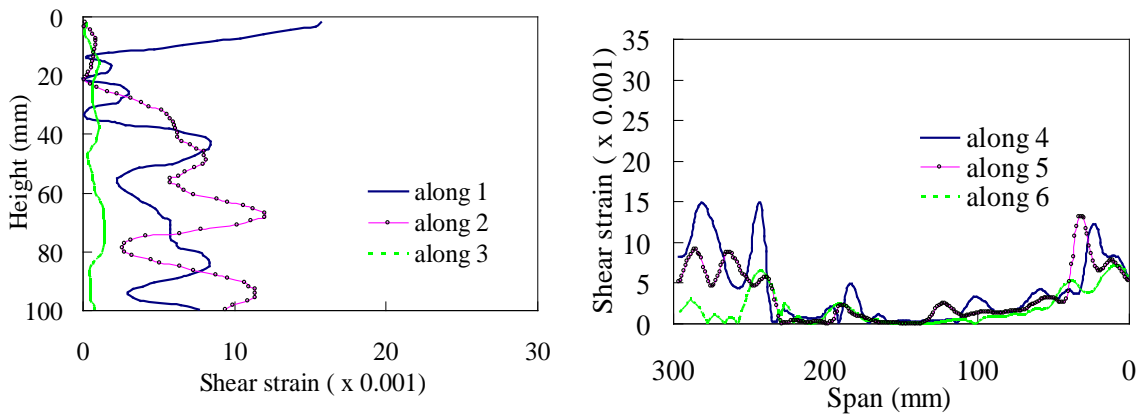
Fig.6.11 ESPI full-field strain profile in control and fiber-reinforced beams (FB, $a/d=1$)



(i) Stirrup beam (SB0.5)



(ii) Stirrup beam (SB1.0)



(iii) Stirrup beam (SB1.5)

Fig. 6.12 ESPI full-field strain profile in stirrup-reinforced beams (SB, $a/d=1$)

6.4.5 Comparative shear stress-deformation responses

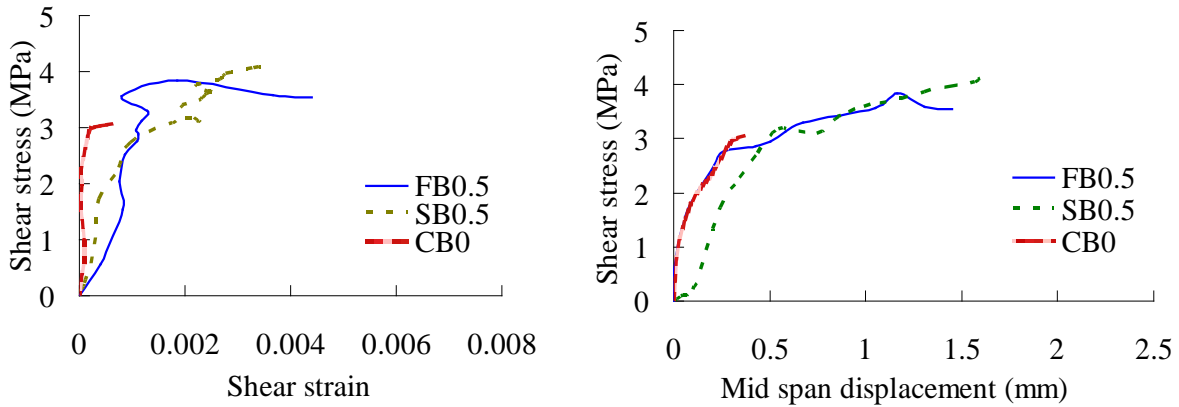
Comparative shear strength deformation response behavior between stirrup and fiber reinforced beams was further evaluated, and average shear stress-strain and mid-span displacement responses were obtained from loading and ESPI strain field analysis. Figs.6.13 to 6.15 shows the results obtained form

this analysis. For graphical representation, shear strain and displacement values through out the loading regime were obtained from locations indicated in Fig.6.7 i.e. at positions A_1 and A_2 , respectively. Generally, all the fiber and stirrup-reinforced beams showed higher ultimate shear strength as compared to control beams. Mid-span deflection in the group of beams with $a/d=1$ (see Fig.6.13) are the least; however, it is almost the same in beams with 0.5% reinforcement content (see Figs.6.13 to 6.15). In the group of beams with $a/d= 1.5$ and 1.82 , higher deflections are achieved. Comparison between FB and SB beams in these figures confirms the positive influence of the steel fibers in the shear strength. As the shear reinforcement content (fibers and stirrups) increases, so does the shear strength and ductility. This is observed more in the beams with higher shear reinforcement content (FB1 and SB1.5). While this observation is evident, also apparent is the ultimate superior performance of the FB beam over the CB and SB beams. Increasing the fiber and stirrup content leads to improvement in the ductility with an upper edge in the fiber beams within the group of beams with $a/d=1$ and 1.5 . However, this trend is reversed in the group with $a/d=1.82$ where it is observed that stirrup reinforced beams performed better in this aspect. This may be attributed to the change in the failure mode coupled with the improved dowel action of main reinforcement bars due to the secondary bearing provided by the stirrups.

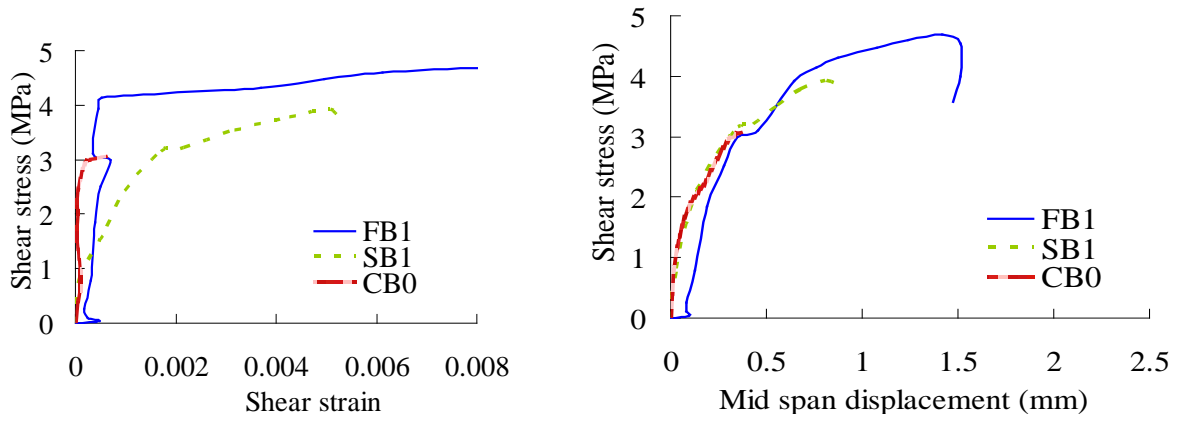
The high shear strength observed in the $a/d=1$ group could partly be a consequence of the reserve strength arising out of beam arch action; however, it can be seen that this group exhibited the highest net increase in shear capacity in accordance with increase in the fiber and stirrup content (Figs.6.10 and 6.13). It is also noted that even with the change in the shear span-to-depth ratio; fibrous beams still exhibited net shear capacity superiority (see Figs.6.13, 6.14 and 6.15). Furthermore, all the beams were of similar dimensions. Thus it can be concluded that the effectiveness of both the fibers and the stirrups was realized in shear rather than in flexure, a confirmation of the ability of both types of reinforcements in resisting shear stress. However, with the fact that conventionally, stirrups are technically the choice for shear reinforcement, the comparable trend from steel fibers is encouraging as this points to a possibility in which stirrup replacement with steel fibers could be undertaken. However, other influences such as size effect can affect the shear behavior in beams, thus there is still a need for further investigation on a larger prototype beam specimen

Although smaller beams were used in the present study due to the limitations and realization of the objective of the study as aforementioned earlier, the results obtained are consistent with what is observed in larger beam specimens. However, unlike the detailed availability design for the flexural capacity requirements in such tests [56] there has been no clear method to determine the required number of stirrups for a particular test situation. This study introduced and adopted a rather new aspect to determine the equivalent shear reinforcement content for comparison purposes with the fibrous beams. Although the method is not a documented standard, it is observed that test results are in agreement with the equivalent reinforcements used. Take for example, the comparative shear strength curves (Figs.6.13, 6.14 and 6.15); it is evident that there is a corresponding increment in the ultimate

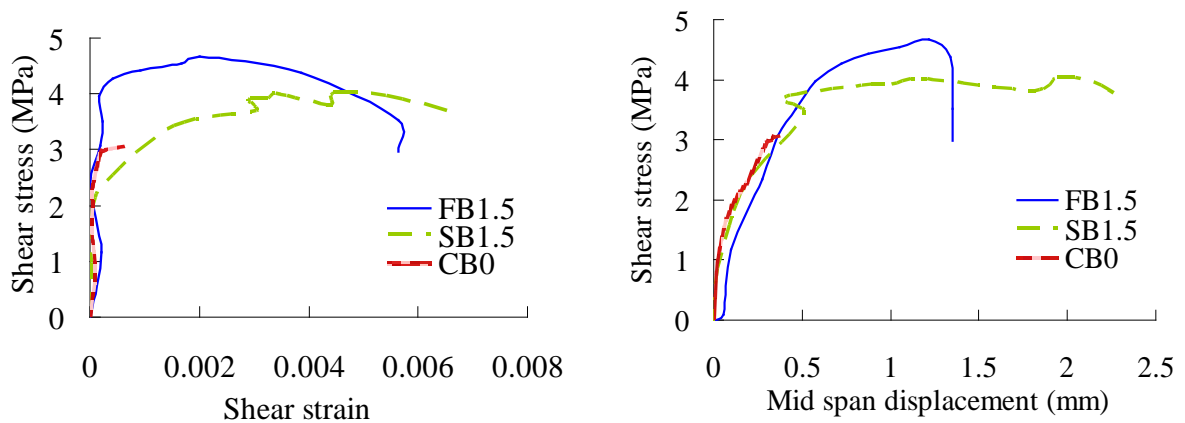
strength with the stirrup content concurrent with that of the fibrous beams. This confirms the effectiveness of the proposed equivalent shear reinforcement content (Eq 3.8) given in chapter 3.



(i) 0.5% fiber and stirrup content

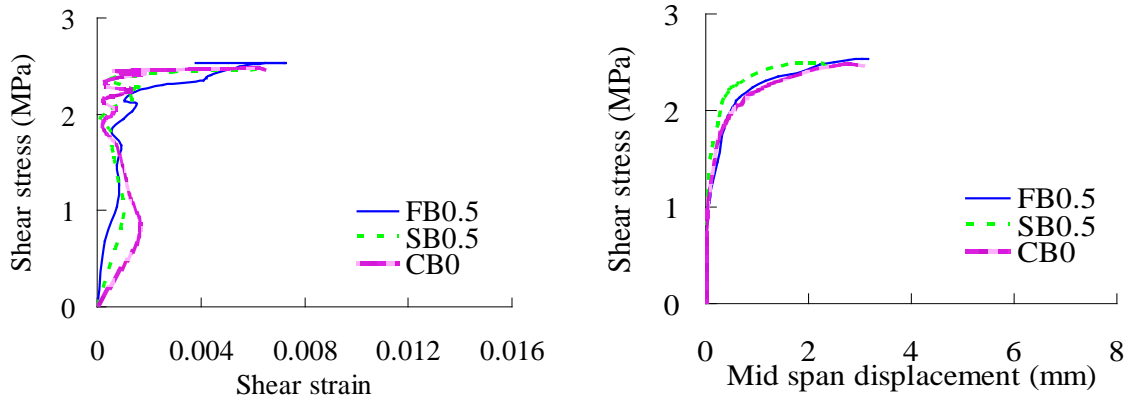


(ii) 1.0% fiber and stirrup content

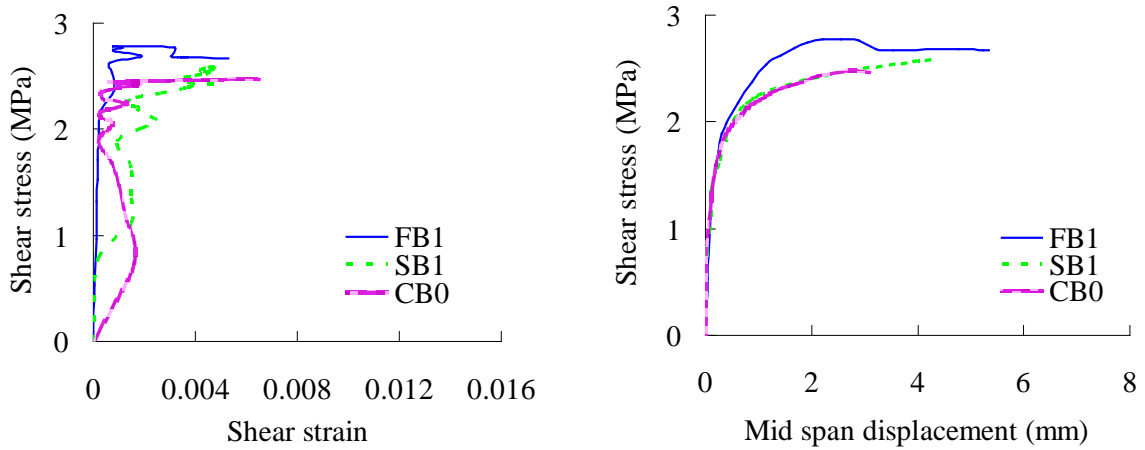


(iii) 1.5% fiber and stirrup content

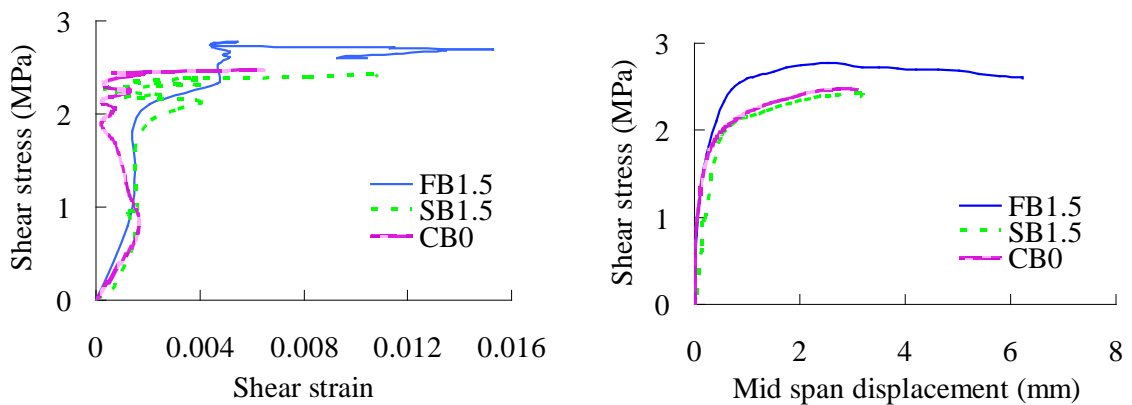
Fig. 6.13 Shear strength curves for $a/d=1$ beams



(i) 0.5% fiber and stirrup content

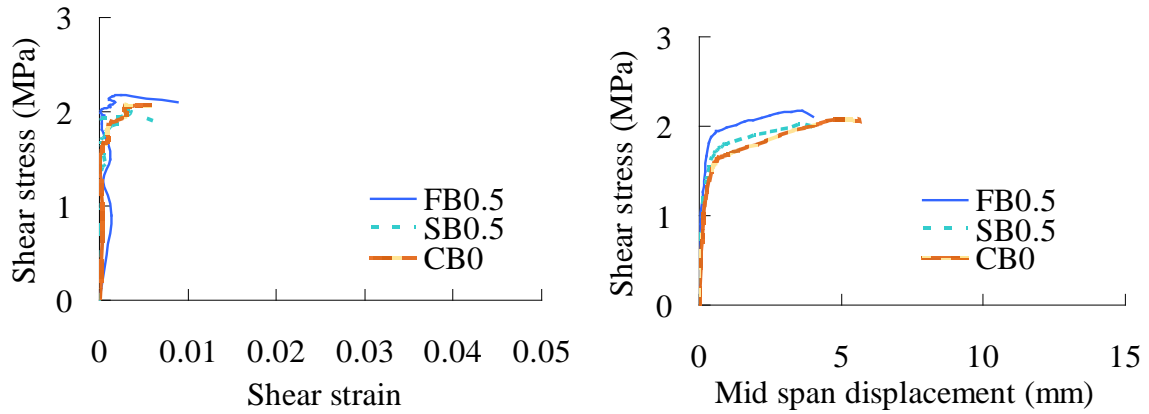


(ii) 1.0% fiber and stirrup content

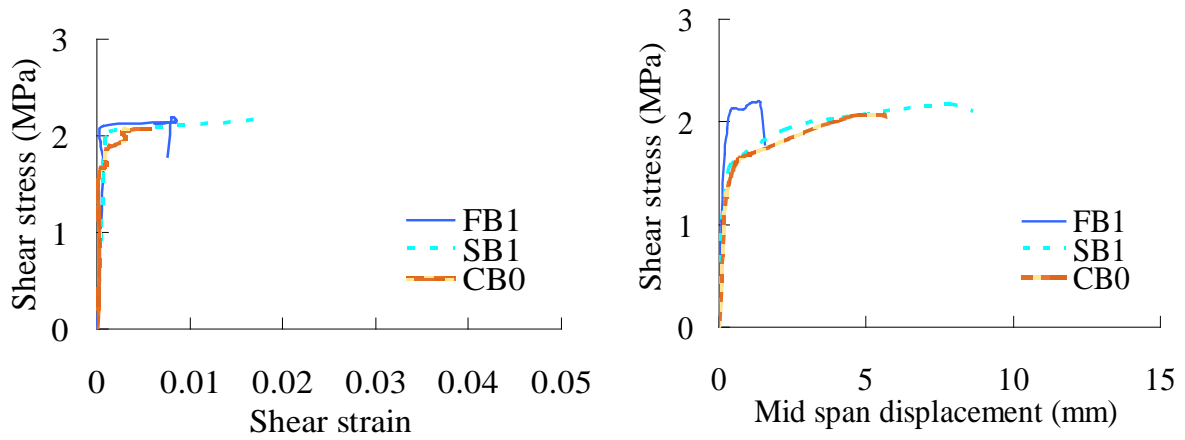


(iii) 1.5% fiber and stirrup content

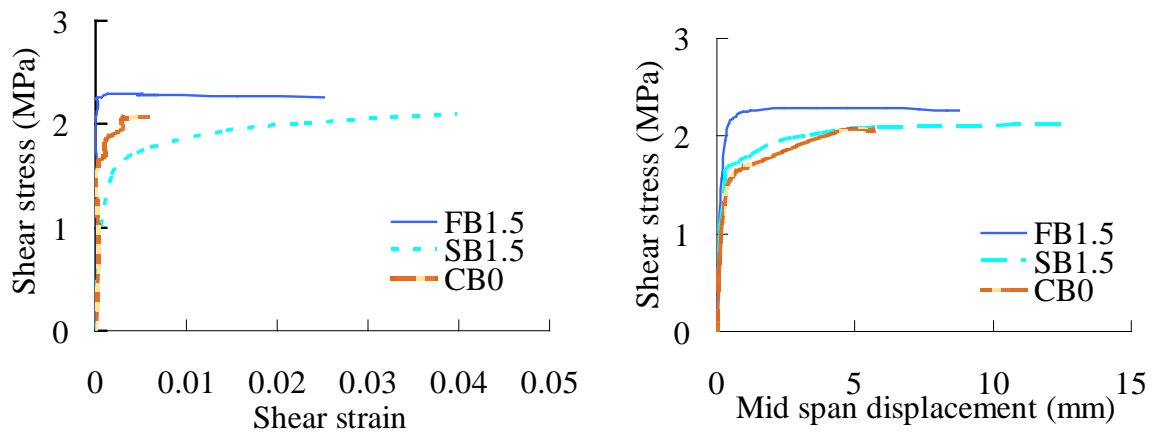
Fig. 6.14 Shear strength curves for $a/d = 1.5$ beams



(i) 0.5% fiber and stirrup content



(ii) 1.0% fiber and stirrup content



(iii) 1.5% fiber and stirrup content

Fig. 6.15 Shear strength curves for $a/d = 1.82$ beams

6.5 Concluding remarks

In this study, the experimental research presented refers to the deformation behavior in SFRC beams and an equivalently reinforced stirrup beams under bending shear. The objective was to evaluate the deformation behavior concurrent with strength development in steel fiber RC beams under bending

shear through progressive crack visualization, strain analysis and load deflection responses. In addition evaluate the validity of an equivalent shear strength determination formula (Eq.3.8) by comparing the shear capacity behavior of the beams reinforced with stirrups determined to match the fiber content selected.

- a) Steel fiber reinforced RC beam has better deformation characteristics in comparison to non fibrous beams; increased yield and ultimate load capacity, ductility and crack propagation. Shear capacity and deflection enhancement was found to be effective in fibrous beams failing in shear. However ultimate crack strain was observed to be much higher in fibrous beams failing in flexure.
- b) The average cracking load in fibrous beams estimated based on ESPI initial crack emergence was found to be approximately 32% of the ultimate load, while that of non fibrous beam was 26%. These values were found to be much lower than those noted during the test, where the first crack load was observed at approximately 68% and 86% on average for fiber and non fibrous beams, respectively. This may be attributed to the fact that ESPI can detect a change in the displacement field and fracture more accurately than the conventional physical measurement.
- c) The influence of the steel fibers was noted to occur after initial yielding whereby increased crack propagation in the beams failing in shear / shear flexure was observed. This behavior was visually noted through ESPI enabled images and strain analysis, to occur until an approximately 90% of the ultimate load where by propagation ceases and a dominant crack or group of cracks persist to ultimately cause the failure.
- d) Comparative evaluation of SFRC and stirrup beams test results established that fibrous beam possesses an analogous and in some cases superior shear capacity performance than that of an equivalently stirrup reinforced beam
- e) The comparable strength test results between fibrous and stirrup beams and the fact that the stirrup content was determined by using eq. (3.8) given in chapter 3, confirms the validity of this equation.
- f) Hitherto difficult measurements such as shear strains and tracking of cracking behavior can be obtained by using of optical ESPI techniques

Chapter 7

FEM simulation of SFRC beams under bending shear and verification

7.1 Introduction

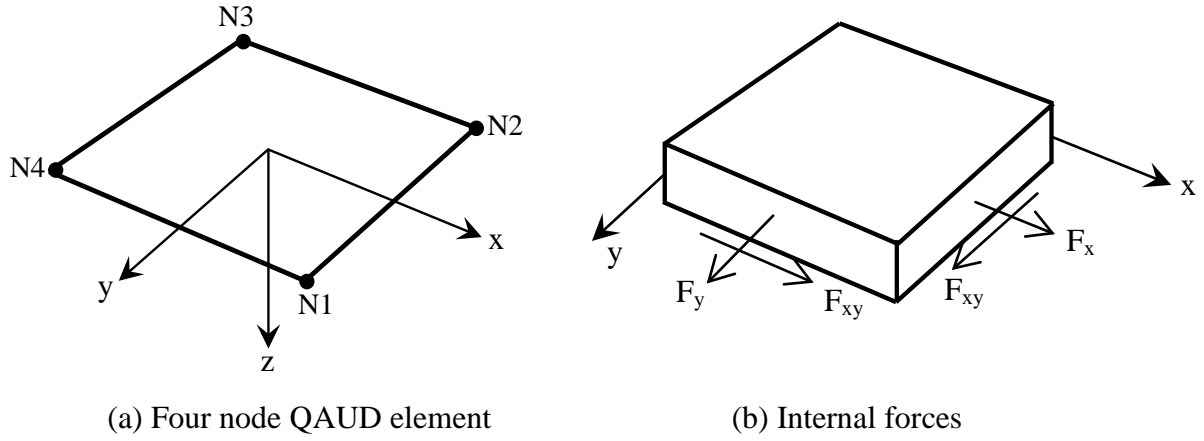
Reinforced concrete structural elements inherently exhibit non linear behavior when subjected to loads leading to failure. Numerical modeling of the nonlinear behavior of reinforced concrete elements generally requires the use of advanced computer codes, which implement material nonlinearities and allow modeling of the structural response. As established in chapter 2, numerical simulation of the structural response of SFRC is seldom investigated [9, 14]. The main hindrance as cited is the lack of appropriate material models for SFRC due to the complexity associated existence of various scales involved in the initiation and propagation of damage leading to failure [9]. Moreover, the discrete and random presence of the steel fibers in concrete technically complicates direct modeling of the fibers individually in a concrete element. In the current study, an attempt is made to apply an experimental SFRC stress strain material model. Strain based models are attractive, since there is no need for abstract sophisticated crack laws, furthermore stress strain relations can be input directly. The terms used and notations in the material behavior are not only recognized in computational mechanics but are familiar with structural engineers dealing with traditional design of concrete structures. In this research, steel fiber-reinforced concrete beams similar to those experimentally tested were analyzed numerically using the finite element code SOFiSTiCK [70] to simulate the deformation behavior in SFRC beams under bending shear. This chapter therefore presents and discusses the basic analysis principles, procedures, formulations, FE analysis of the model beams, verifications and the results obtained. Finite element analysis (FEA) by SOFiSTiCK is shown to fairly simulate the strength and deformation behavior in SFRC beams.

7.2 Basic theoretical principles and analysis procedure

The general basic theoretical and analysis principles applied in finite element analysis are discussed briefly. The FEA of beam specimens in the current research were accomplished by means of plane stress analysis. Thus the FEA principles discussed in this section are based on a plane stress case and with respect to the FE code adopted in the current research (i.e. SOFiSTiCK).

7.2.1 Plane stress element and constitutive formulation

Finite element idealization of reinforced concrete beams in SOFiSTiCK code [70] is accomplished by


Fig 7.1 Element type and internal forces

two dimensional elements which lie in the x - y plane of the beam elevation. Following the assumptions of the Timoshenko beam theory, the resulting stresses are assumed to be constant through the thickness of each element and stresses in the third directions (i.e. σ_z , τ_{xz} and τ_{yz}) are ignored. These assumptions lead to a plane stress field. The displacement field is uniquely described by u and v , displacements in the direction of the Cartesian co-ordinates orthogonal x and y -axes respectively. In SOFiSTiCK FEA, the element formulation of a plane stress state occurs via a classical isoparametric formulation. Fig.7.1 depicts the four node isoparametric quad element and the internal force orientations. The local coordinate system is oriented in such a way that the z axis is given with the normal to the element's plane and the local x axis can be selected freely. The default orientation is parallel to the global XY plane. From the positive direction of the z axis (thus from "above of Fig.7.1), the nodes are numbered counterclockwise (Fig.7.1a). If the element's plane coincides with the global XY plane, the local and the global coordinate systems are then identical. During analysis, the thicknesses as well as the elastic moduli in different directions are taken into consideration and an anisotropic Poisson's ratio is not considered. The simplified orthotropic formulations for the internal forces of a plane stress element (Fig.7.1b) are given as follows

$$F_x = S_x \varepsilon_x - \mu S_{xy} \varepsilon_y \quad (7.1)$$

$$F_y = S_y \varepsilon_y - \mu S_{xy} \varepsilon_x \quad (7.2)$$

$$F_{xy} = G t_{xy} \gamma_{xy} \quad (7.3)$$

With the stiffness given by

$$S_x = \frac{E_x t_x}{1 - \mu^2} \quad S_y = \frac{E_y t_y}{1 - \mu^2} \quad S_{xy} = \frac{E_x t_{xy}}{1 - \mu^2}, \quad G = \frac{E}{2(1 + \mu)} \quad (7.4)$$

In the isotropic case the thickness and elastic modulus is set such that $t_x = t_y = t_{xy} = t$ and $E_x = E_y = E$. Where E is the elastic modulus, μ is the Poisson's ratio, G is the shear modulus, t is the element thickness while ε_x , ε_y and γ_{xy} are the strain components. For a unit cross sectional area (where $t = 1$ with respect to

Eqs (7.1 to 7.4) with element material being homogeneous and isotropic, the stress-strain relation for a plane stress element in a simple form will be given by

$$\begin{Bmatrix} \sigma_x \\ \sigma_y \\ \tau_{xy} \end{Bmatrix} = \frac{E}{1-\mu^2} \begin{bmatrix} 1 & -\mu & 0 \\ -\mu & 1 & 0 \\ 0 & 0 & \frac{1-\mu}{2} \end{bmatrix} \begin{Bmatrix} \varepsilon_x \\ \varepsilon_y \\ \gamma_{xy} \end{Bmatrix} \quad (7.4)$$

In plane stress case the relevant strains of interest are those occurring in the plane and are defined in terms of displacements. The general FE determination of these strain fields is based on the solution of the displacement field u and v at each node of an element and the application of the shape functions (Eq.7.5) for a plane stress problem [71]

$$\begin{Bmatrix} \varepsilon_x \\ \varepsilon_y \\ \gamma_{xy} \end{Bmatrix} = \begin{bmatrix} \frac{\partial N}{\partial x} & 0 \\ 0 & \frac{\partial N}{\partial x} \\ \frac{\partial N}{\partial y} & \frac{\partial N}{\partial x} \end{bmatrix} \begin{Bmatrix} u \\ v \end{Bmatrix} \quad (7.5)$$

Where N is a prescribed function of position commonly referred to as the shape function. In the phase of the solution process the principal strains and stresses are obtained from the strains and stresses in the global coordinate system by applying a transformation [71] as shown in Eq. (7.6) and (7.7)

$$\begin{pmatrix} \sigma_1 \\ \sigma_2 \end{pmatrix} = \begin{bmatrix} \cos^2 \theta & \sin^2 \theta & 2 \sin \theta \cos \theta \\ \sin^2 \theta & \cos^2 \theta & -2 \sin \theta \cos \theta \end{bmatrix} \begin{Bmatrix} \sigma_x \\ \sigma_y \\ \gamma_{xy} \end{Bmatrix} \quad (7.6)$$

$$\begin{pmatrix} \varepsilon_1 \\ \varepsilon_2 \end{pmatrix} = \begin{bmatrix} \cos^2 \theta & \sin^2 \theta & \sin \theta \cos \theta \\ \sin^2 \theta & \cos^2 \theta & -\sin \theta \cos \theta \end{bmatrix} \begin{Bmatrix} \varepsilon_x \\ \varepsilon_y \\ \varepsilon_{xy} \end{Bmatrix} \quad (7.7)$$

Where orientation angle of the principal direction is given by

$$\theta = \text{Tan}^{-1} \left(\frac{\gamma_{xy}}{\varepsilon_x - \varepsilon_y} \right) \quad (7.8)$$

7.2.2 Constitutive laws

(a) Stress strain model

The failure behavior of concrete or SFRC as a concrete composite is characterized by tensile cracking and compressive crushing. This characteristic adds to the nonlinear behavior commonly observed in structural assemblages making use of these materials when under unfavorable loading. This behavior must be considered in analysis and design in structures utilizing these materials. Modern analysis tools

(FEM) implement constitutive material models in the analysis process. Thus the requirements are such that prescriptions of the critical values for a default constitutive model or user defined model are the prerequisite in FE analysis. The default ideal stress strain model implemented in SOFiSTiCK is that of the German Concrete Society's (*Bemessungsgrundlagen für Stahlfaserbeton im Tunnelbau*, see Fig.2.3 chapter 2), however to apply it, a number of material parameters must be determined experimentally by way of flexural tests on notched beams. Alternatively a user defined material model can also be supplied and applied explicitly as in the case in this research.

(b) Failure criterion

Reinforced concrete structures are often subjected to bending moments and they tend to experience biaxial stress combinations (i.e. a combination of tension and compression). These stress states can be modeled by a combination of the yield condition to describe the failure envelopes which is treated as a multi-surface plasticity model. The failure criterion applied in SOFiSTiCK [70] code for concrete is the DRUCKER–PRAGER law for an elasto-plastic material with associated flow rule and the yield function (given here for a two dimensional case) is defined by

$$f = P_2(\sigma_1 + \sigma_2) + \sqrt{J_2} - \frac{P_1}{\sqrt{3}} \leq 0 \tag{7.5}$$

In which the deviatoric stress tensor J_2 is given by

$$J_2 = \frac{1}{2}(S_1^2 + S_2^2) + \tau_{xy} \tag{7.6}$$

$$P_1 = 2 \frac{f_c f_t}{f_c + f_t} \quad \text{and} \quad P_2 = \frac{1}{\sqrt{3}} \frac{f_c - f_t}{f_c + f_t} \tag{7.7}$$

$$S_1 = \frac{2\sigma_1 - \sigma_2}{3} \quad \text{and} \quad S_2 = \frac{2\sigma_2 - \sigma_1}{3} \tag{7.8}$$

Where f_c is the compressive strength, f_t tensile strength, σ_1 and σ_2 are the principal stresses.

7.2.3 Summary of FE analysis method

In the static FE analysis of SOFiSTiCK, the displacement method is used, meaning that the unknowns are deformation values at several selected points, the so-called nodes. Displacements are obtained with an element-wise interpolation of the nodal values. The calculation of the mechanical behavior is based generally on an energy principle (minimization of the deformation work). The result is the stiffness matrix which specifies the reaction forces at the nodes of an element when these nodes are subjected to known displacements. The result is a so-called stiffness matrix. This matrix specifies the reaction forces at the nodes of an element when these nodes are subjected to known displacements. The global force equilibrium is generated then for each node in order to determine the unknowns. A force in the same direction which is a function of this or another displacement corresponds to each displacement.

This leads to a system of equations with n unknowns whereby numerically beneficial banded matrices result, due to the local character of the element-wise interpolation. The complete analysis method is divided into four main parts:

- ✧ Determination of the element stiffness matrices.
- ✧ Assembly of the global stiffness matrix from the element stiffness matrices to obtain the structural stiffness matrix.
- ✧ Application of loads and determination of the corresponding displacements.
- ✧ Determination of the element stresses and support reactions due to the computed displacements.

In nonlinear analysis, the load applied is divided into series of load increments (load steps). At the completion of each incremental solution, the stiffness matrix of the model is adjusted to reflect nonlinear changes in structural stiffness before proceeding to the next load increment. Nonlinear effects are analyzed only with iterations and this is done with a modified Newton method with constant stiffness matrix. The Crisfield method which is implemented for the improvement of the convergence modifies the displacement increments of the current and of the last iteration step with the two factors f and e . For convergence difficulties an improvement of the convergence behavior can be achieved via reduction of the maximum f value, e.g. FMAX 1.5. If the system still not converges, FMAX can be reduced until 0.7. However, many iteration steps are needed then [70].

7.2.4 Implementation procedure

Implementation of numerical simulation with SOFiSTiCK FEM code [70] is generally undertaken based on module programs each defined for a particular task but run mutually and exclusively. In this research, five modules were written in sofistik CADINP language and implemented. These modules are *Aqua*, *Genf*, *Sofiload*, *Bemess* and *Ase*. In the module *Aqua*, the Norm or the design code (e.g EC for Euro code, JIS for Japanese Concrete/Japan Road Association, etc), user defined material model and other relevant parameters can be explicitly defined as appropriate. Definition of design codes is important in the case where a user supplied material model/properties does not exist as well as when reinforcement design is required particularly in a full scale structure analysis and design. The cross section properties for analysis are also determined by the module *Aqua*. Structure modeling, boundary conditions and elements generation is made via *Genf* module based on the input data supplied by means of a text file using the language CADINP. *Sofiload* is used to generate and apply loads on the structure for FE analysis by modules that require it. All the necessary applied loads including self weight are expressly defined in *Sofiload*. Initial reinforcements design is done in the *Bemess* module for linear analysis purposes. However, in non linear analysis, reinforcement design is repeated either with same reinforcement as those applied in the linear analysis or additions are made based on the

design requirements. In the present study, same reinforcements as in *Bemess* (linear analysis) were used in non linear analysis to replicate what was used in the experimental tests without further reinforcement design. The program for Linear and non linear analysis is made and carried out in the module *Ase*. It calculates the static and dynamic effects of general loading on any type of structure. In the present study only static analysis was undertaken on the beams under plane conditions

7.3 FE structural and material models for SFRC beams

The basis of FEA has been discussed albeit in brief in the previous sections. To allow for experimental verification of the FE results, the beams analyzed were structurally designed to be analogous to the experimental beams and experimental material models for SFRC and plain concrete were adopted.

7.3.1 Structural model

Since the structural model was designed to replicate the test specimens, two categories of beams with different geometry and main reinforcements were analyzed. The adopted mesh and geometry of the FE beam analyzed is shown in Fig.7.2. The beams were reinforced with 2 \varnothing 6mm and 3 \varnothing 13mm longitudinal bars for the short beams and large beams respectively. In the analysis, a variable shear span to depth ratio of 1, 1.5 and 2.4 was made for short and large beams respectively. In the meshing process, four-node quadrilateral isoparametric plane stress elements (see Fig 7.1a) were used to model the SFRC/plain concrete elements. In plane elements of SOFISTIK, a general quadrilateral element with four nodes (QUAD) is sufficient, so that the introduction of the six-to nine-noded isoparametric elements is not necessary [70].

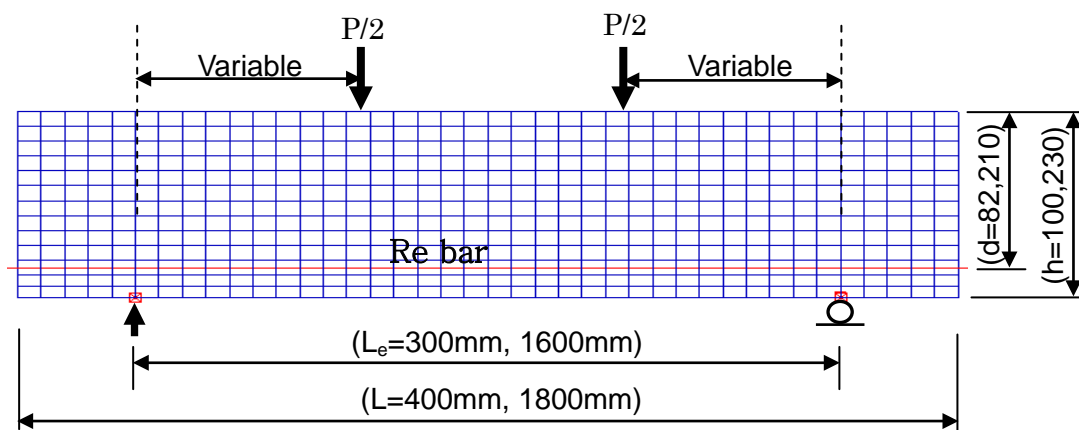


Fig. 7.2 Meshed RC beam model

7.3.2 Material models

According to research findings in this study and elsewhere [3, 26, 38, and 60] it is established that steel fibers do not significantly influence the strength in compression but rather in tension. Based on this finding, a variable non linear stress-strain relation in tension and an average non linear stress-strain relation in compression as shown in Figs 7.3a and b were applied in the in the FE analysis.

The variable material model in tension corresponds to the variable fiber content used (0% to 1.5% content by volume). The variability is occasioned by the different strength-strain capacities attributed to the variable steel fiber content in the concrete. The tension material model as depicted in Fig.7.3a consist of a linear part up to yielding, a non linear part up to ultimate level which is characterized by an increase in strength (in fiber concrete) and a softening part characterized by a reduction in strength and an increasing strain particularly in the case of the higher fiber content (e.g. 1.5%). These material models were assumed to be sufficient for both fiber and non fibrous concrete in the numerical study. Material behavior for the reinforcing bars was defined with a standard elastic-perfect plastic stress strain relation. It is commonly assumed that this behavior is the same for tension and compression as shown in Fig.7.4. The reinforcements were similar to those applied in the tests with a young's modulus of 210kN and yield strength of 345MPa.

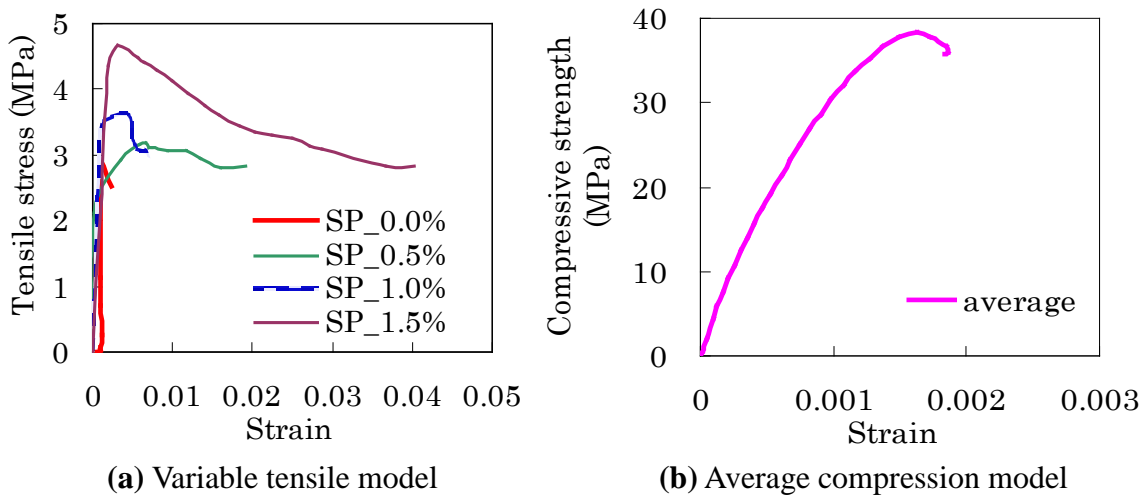


Fig.7.3 Plain/SFRC material models

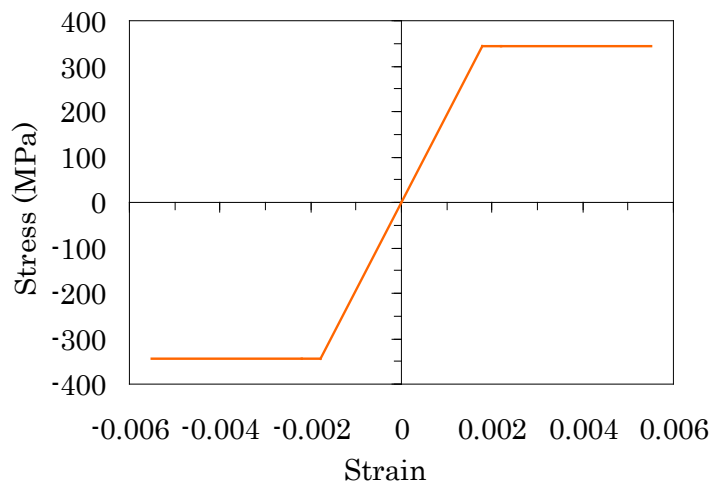


Fig.7.4 Standard steel material model

7.4 FEM analysis results and verifications

The results are presented in form of strength curves, cracking and strain distribution plots. For ease of presentations and discussions, specimens are designated according to the volume percentage of steel fibers used. These designations which are used in the subsequent sections are as follows:

FB0.5 to FB1.5% : *Fiber beams (percentage value represents the fiber content)*

CB0% *Control beam (non fiber)*

7.4.1 FEM shear load deflection response

The variable tensile material model applied in the numerical analysis was used with the expectation that the increased post cracking tensile strength in SFRC material will be reflected in the load carrying capacity of the beams analyzed numerically. This hypothesis was found to be correct as confirmed by the FEM results as shown in Figs 7.5.

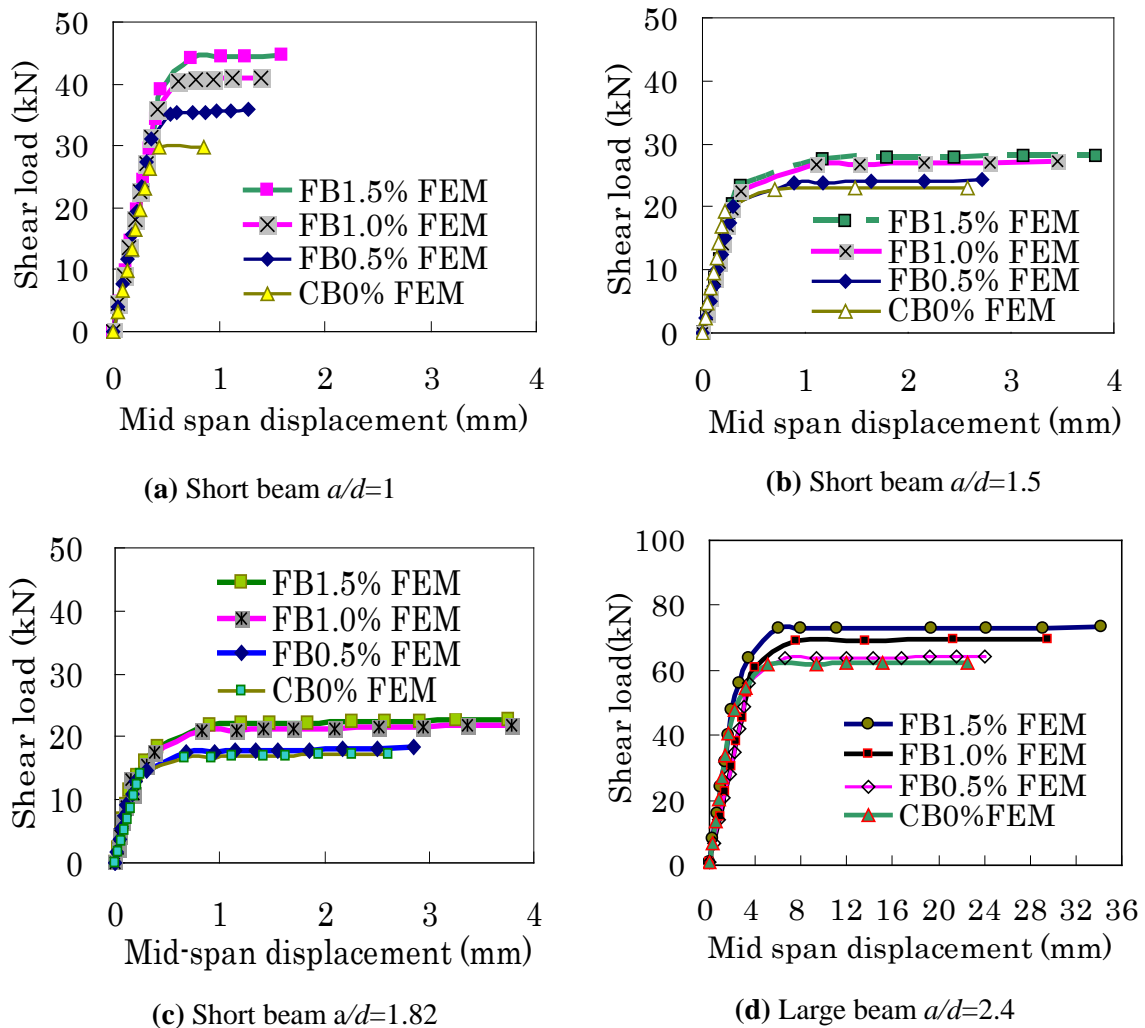


Fig.7.5 FEM shear load deflection response

In the results, all the beams analyzed irrespective of the size showed linear variation until yielding as marked by points of deviation from linearity; approximately at a shear load of 30kN, 20, 15 and 60kN, in Figs 7.10a, b, c and d respectively. The deviations lead to a non linear behavior in which the influence of the strength increase in SFRC is observed. In the case of the short beams where a variable shear span to depth ratio was considered in the analysis (for comparison with experiments) it is noted that the deflection response was smaller in the case of $a/d=1$ (Fig.7.5a) as compared with same result in $a/d=1.5$ and 1.82 (Fig. 7.10b). Perhaps this could be as a result of deep beam effect (compression failure). However, a shear load capacity reduction with increase in the shear span to depth ratio is noted (Fig.7.5a to c). As expected shear load and deflection capacity for the large beams are larger than those of the small beams because of the differences in the structural geometry.

7.4.2 Cracking pattern

Cracking patterns in this section are presented for the control beams CB0%, 1.5% and CB0% FB1% for large and small beams respectively.

(a) Short (small) beams

Figs 7.6, 7.7 and 7.8 depicts the shear-flexural failure modes observed from experiments and the numerical (FEM) analysis obtained from the short beams. It is observed that at ultimate load state, optical ESPI result depicts more cracks that could not be easily observed with the naked eye. This is apparent in the fibrous beams FB1.5%, shown in Fig.7.6c and 7.7c. In the opinion of the author this behavior indicates increased cracking propagation in SFRC beams due to the stress re-distribution efficacy of the steel fibers. This behavior is confirmed further by the increase in crack strain capacity and distribution (Fig.7.17a and b). The FEM cracking pattern compares fairly with the experimental results with evidence of lack of exact match in the rest. The lack of exact match with the experimental pattern can be attributed to the fact that in the numerical analysis, cracking is determined and distributed based on the main reinforcements. The numerical results (Fig.7.5a) shows that in CB0% beam (in $a/d=1$ group), cracks having widths of 0.4mm to 1.4mm were formed, while those in FB1.5% beam range from 0.9 to 3.7mm. In $a/d=1.5$ group (Fig.7.8a), cracks range from 0.7mm to 6.6mm and 0.1 to 1.6mm in the fibrous beam (FB1.5%) and control beam (CB0%), respectively. More flexural cracks are noted in $a/d=1.5$ group of beams which can be expected given that the failure mode also affects the cracking pattern.

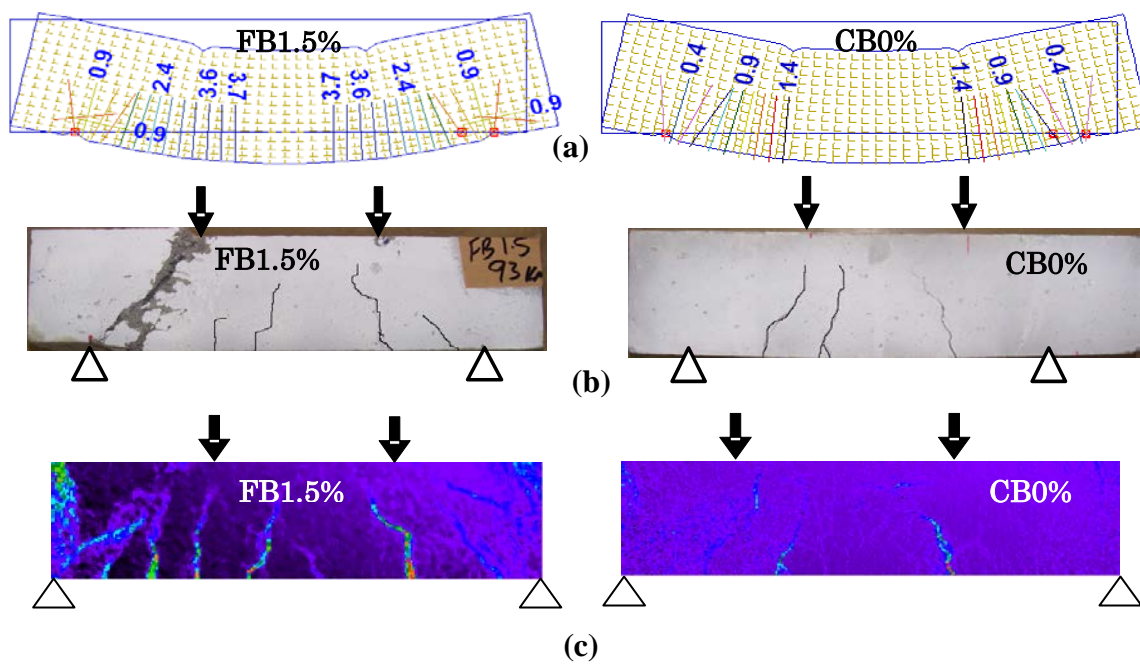


Fig. 7.6 FEM and experimental cracking pattern for $a/d=1$

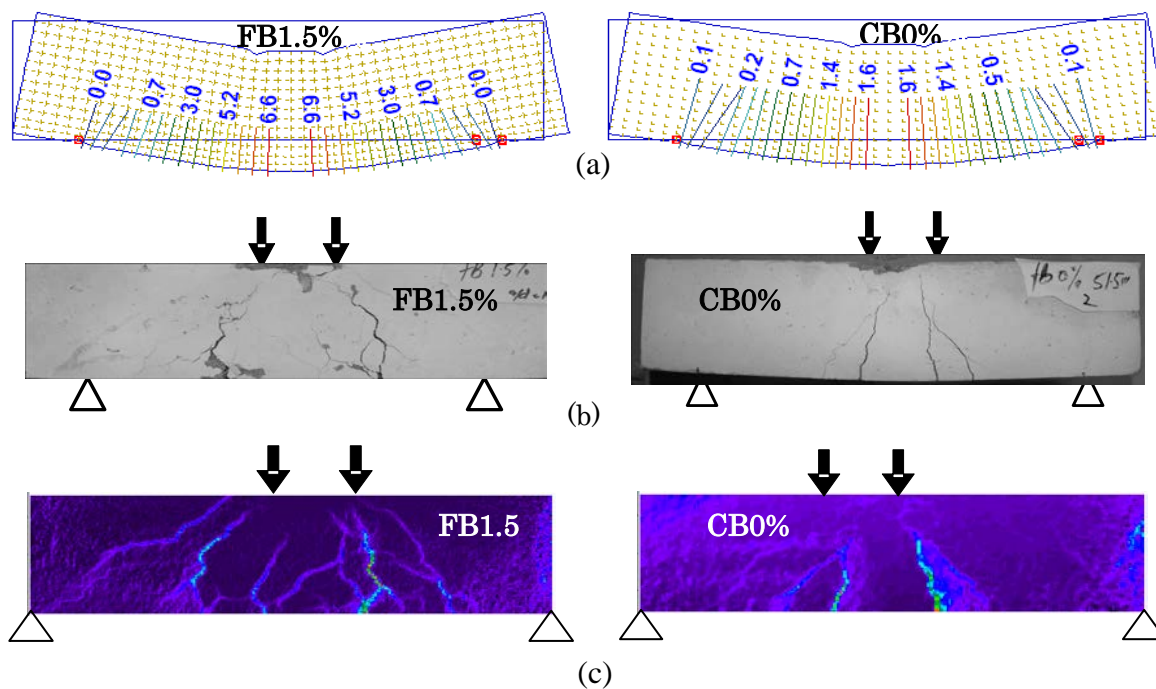


Fig. 7.7 FEM and experimental cracking pattern for $a/d=1.5$

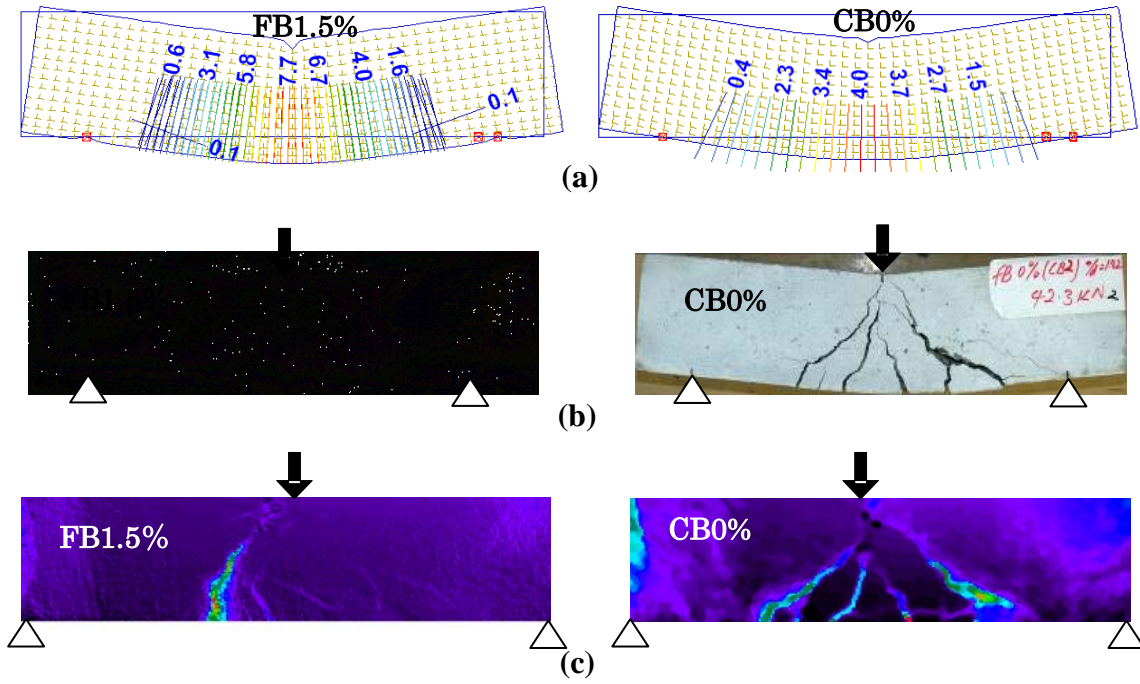


Fig. 7.8 FEM and experimental cracking pattern for $a/d=1.82$

(b) Large beams

The numerical and the experimental cracking pattern in the large beams are as shown in Fig 7.9a and b. As seen in these figures, the large beam numerical result shows similar trend as that of the short (small) beams although with larger flexural crack widths. This largest numerical crack is about 10mm in FB1.5% while that of the control beams (CB0%) is about 6mm. Shear cracks are smaller and in the range of 0.5 to 1.4mm in both cases. The draw back in these numerical results as far as observation of carking pattern is concerned is that the influence of the fibers on cracking can not be deduced. Moreover the exact cracking pattern as observed in the experiments could not be achieved. In addition to the earlier mentioned reason (in part *a* above), another reason for this is that steel fibers were not modeled individually like the main reinforcements as they were applied based on the material strength of the steel fiber concrete material.

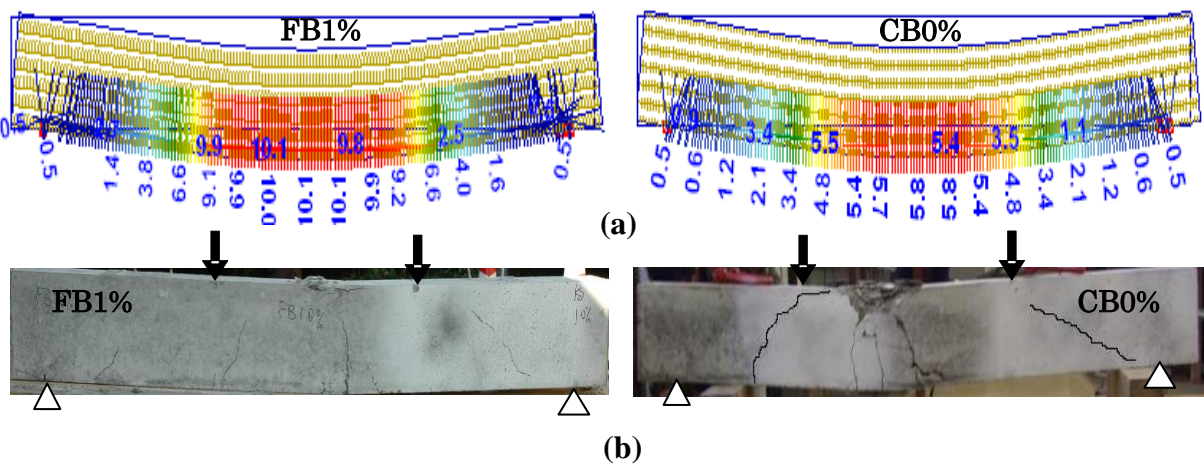


Fig.7.9 FEM and experimental cracking pattern in for $a/d=2.4$

This can be judged by the numerical crack widths which are found to be larger in the case of fibrous beams when compared to the control beam (CB0%). This observation is contrary to the fact that fibers are meant to reduce the crack widths. Perhaps the influence of increased post tensile cracking in SFRC and hence the load carrying capacity in the numerical case is the reason for increased crack widths. The lack of exact prediction of the crack patterns can be attributed to the FEM code used where by the cracking is approximated based on the yielding of the concrete and main reinforcements.

7.4.3 FEM and experimental synchronized load deflection response

To validate the numerical results in detail, matched experimental and numerical comparisons in the beams with equal fiber content were made and the results are as shown in Figs 7.10, 7.11 and 7.12. Short beams have been used in this because all the experimental results which are important for the comparisons are available for all the fiber content range (0.5% to 1.5%). It is evident that in all the cases the numerical (FEM) method predicted well the experiments. Although generally this appears to be true, finer details show a slight variation in the some areas, where minor alternate differences are observed. This minor variation can be observed in and after the transition stage marked by the sharp curvature soon after yielding.

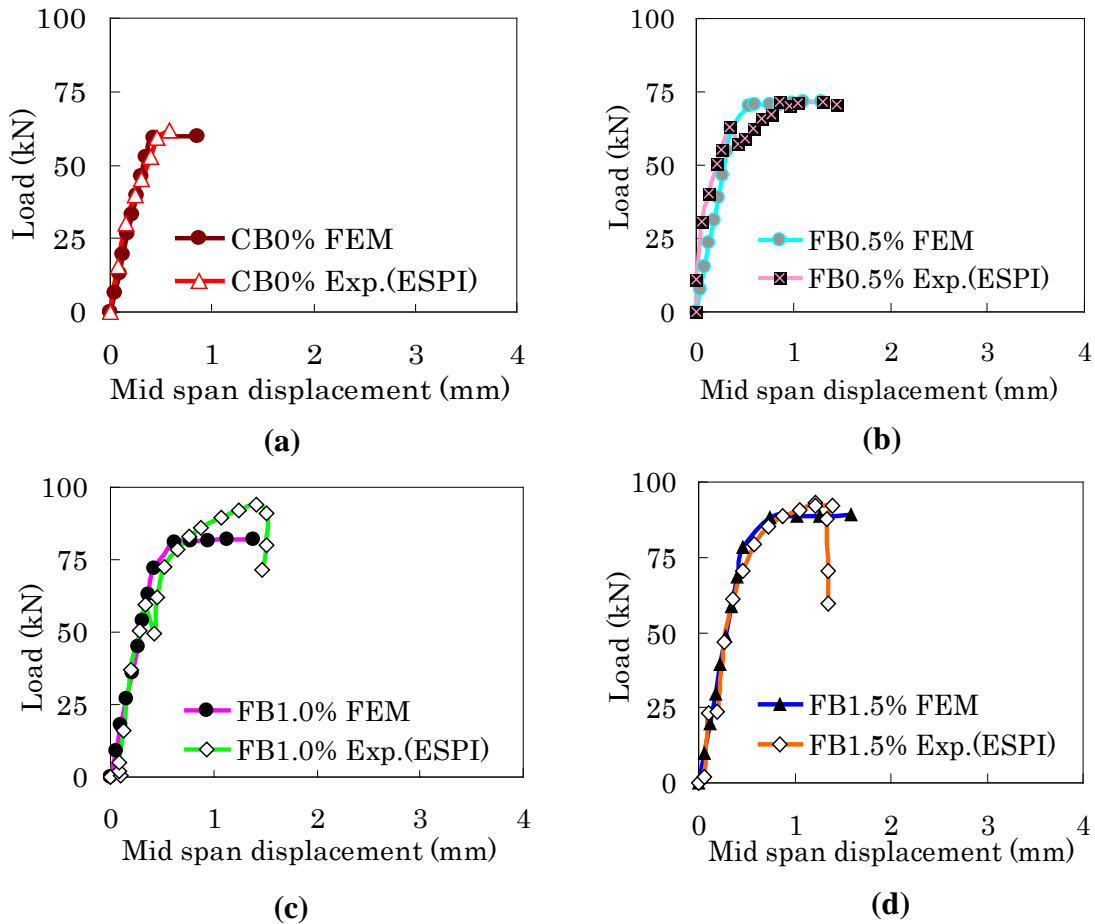


Fig. 7.10 Comparative load deflection response for $a/d=1$

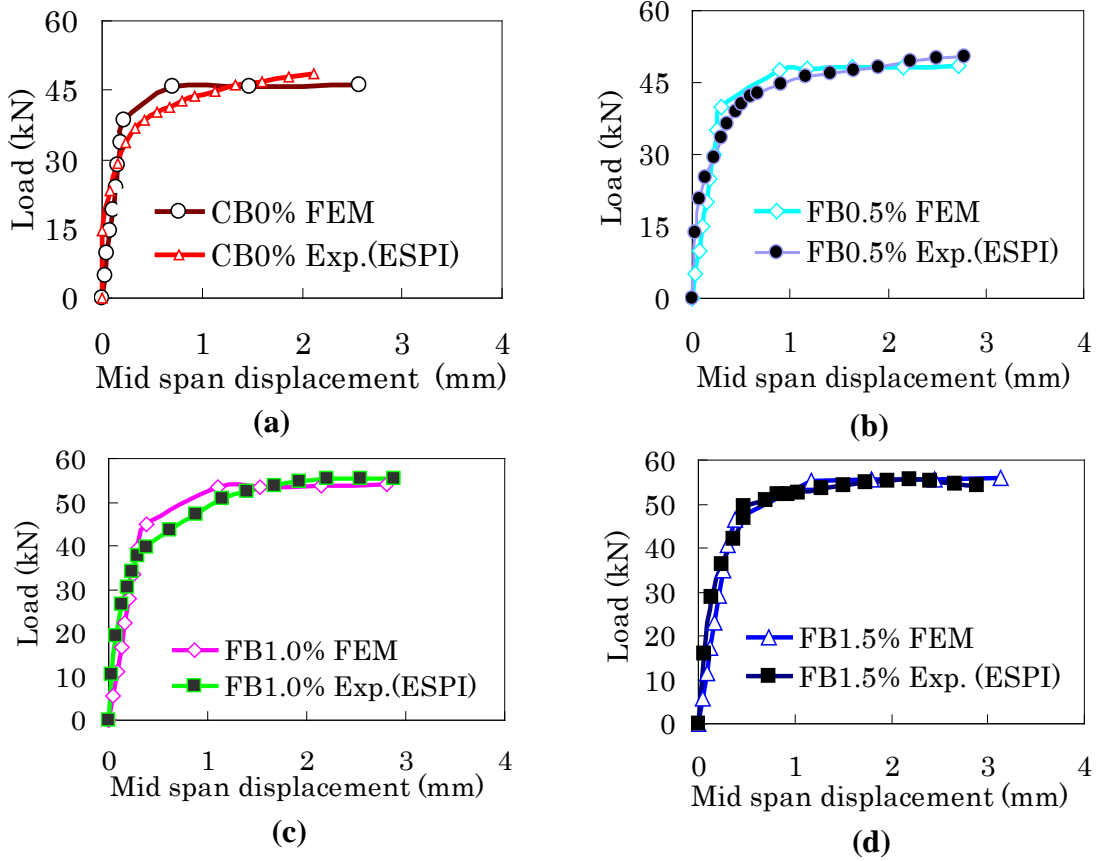


Fig.7.11 Comparative load deflection response for $a/d=1.5$

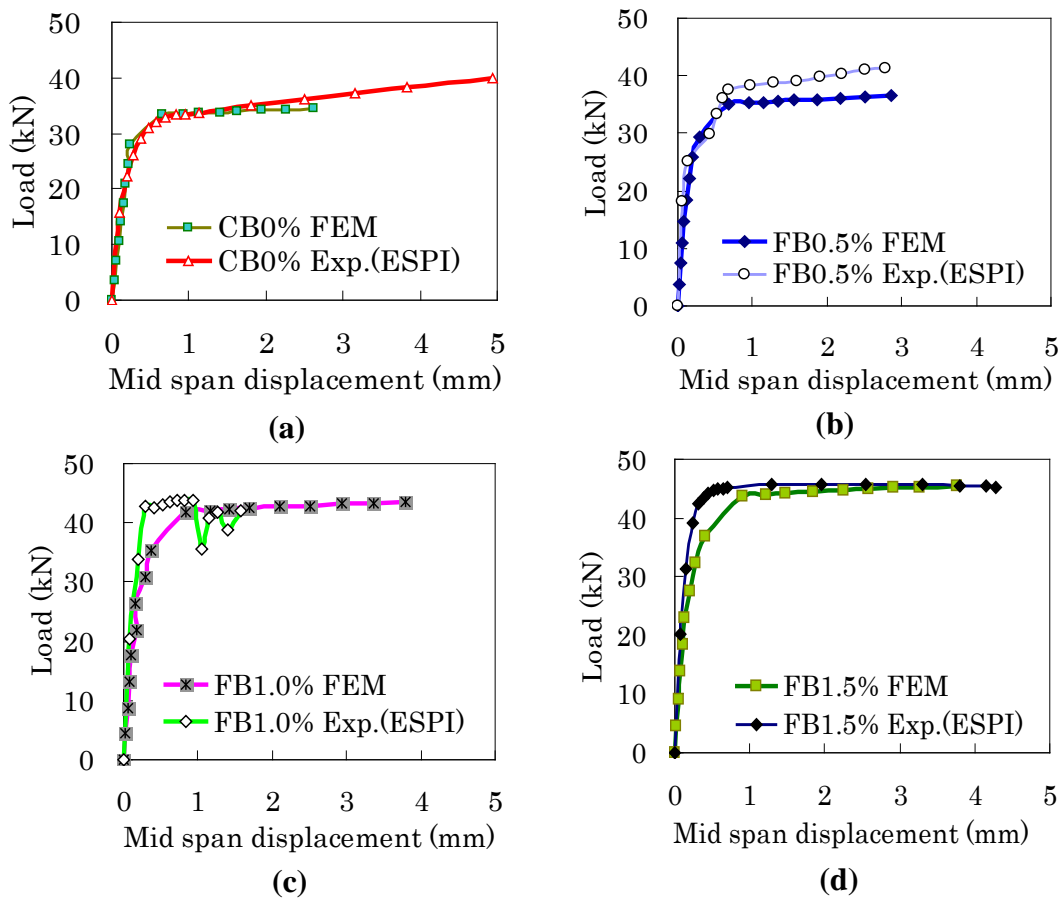


Fig.7.12 Comparative load deflection response for $a/d=1.82$

Generally in $a/d=1$ and 1.5 beams (Figs 7.10 and 7.11) the FEM result is steeper at the transition stage and flattens out soon after, in the plasticization stage whereas the experimental result shows a slightly lower gradient at the transition stage with a increased gradient in the plasticization stage. However the gradient behavior at the transition stage is reduced in the $a/d = 1.82$ beams with fiber content of 0 and 0.5%, but still higher in the case of beam with fiber content of 1.0 and 1.5% (Fig. 7.12). Both the FEM and the experimental result appear to match in the plasticization stage in the case of beams with higher fiber content (Fig.7.12c, d).

7.4.4 FEM and Test ultimate strength comparisons

Summary of the comparative FEM and experimental ultimate strength and its increase in SFRC beams are as given in Table 7.1. In strength increase determination, the base values used are those of the control beam (CB0%). It is evident from the results that fibrous short beams in $a/d=1$ group had higher strength increase. For example in $a/d=1$ group, strength increase of 50% is obtained in both experimental and FEM results for FB1.5% while for the same beam type (FB1.5%) in $a/d=1.5$ and 1.82 group, the increase is 22%, 15% and 28%. In the case of the large beams the increase is in the same range as the short beams in $a/d=1.5$ and 1.82 perhaps because of the shear flexure failure mode. The correlation factors (T/F) shown in Table 7.1 indicates that the FEM ultimate strengths results compare well with the experimental values.

Table 7.1 FEM and test ultimate strength comparisons

| Shear span to depth ratio (a/d) | Beam type | Ultimate load capacity (kN) | | | Strength increase % | |
|------------------------------------|--------------------|-----------------------------|---------|------|---------------------|-----|
| | | Test (T) | FEM (F) | T/F | Test | FEM |
| | | | | | | |
| 1 | Short beams | | | | | |
| | CB0 | 62 | 60 | 1.03 | - | - |
| | FB0.5 | 71 | 72 | 0.99 | 15 | 20 |
| | FB1.0 | 94 | 84 | 1.25 | 52 | 40 |
| | FB1.5 | 93 | 90 | 1.03 | 50 | 50 |
| 1.5 | Short beams | | | | | |
| | CB0 | 49 | 46 | 1.06 | - | - |
| | FB0.5 | 52 | 49 | 1.06 | 6 | 7 |
| | FB1.0 | 55 | 55 | 1.00 | 12 | 20 |
| | FB1.5 | 56 | 56 | 1.00 | 22 | 22 |
| 1.82 | Short beams | | | | | |
| | CB0 | 40 | 36 | 1.11 | - | - |
| | FB0.5 | 41 | 37 | 1.11 | 3 | 3 |
| | FB1.0 | 44 | 44 | 1.00 | 10 | 22 |
| | FB1.5 | 46 | 46 | 1.00 | 15 | 28 |
| 2.4 | Large beams | | | | | |
| | CB0 | 110 | 124 | 0.90 | - | - |
| | FB1 | 133 | 139 | 0.96 | 21 | 12 |

Although the higher increase in the short beams whose failure mode was predominantly shear, could be partly due to the additional reserve strength arising out of the shear compression failure, all the beams in each category (short/large) had the same flexural reinforcement, geometry (cross sectional and longitudinal) and were tested under the similar set up conditions, it can be concluded that the strength increase in fibrous beams was due to the fibers influence, rather than compression reserve strength, otherwise the ultimate strength results should have been the same for all the beams (with or without fiber). The steel fibers are effective in stress transfer across the cracks there by enhancing the strength capacity.

7.4.5 Stress strain distributions

In this section beams in $a/d=1$ and $a/d=1.5$ groups have been selected to illustrate the comparison between numerical and the experimental stress strain distributions. Fig.7.13 depicts the general numerical deformation stress distribution behavior of the analyzed beams. In this section beams in $a/d=1$ and 1.5 group have been selected to illustrate the comparison between numerical and the experimental stress strain distributions. Legend FEM plot results are compared with graphically plotted experimental result. Figs.7.14a,b and 7.15a,b shows the FEM shear stress and strain distribution behavior, while, Figs.7.17a and b depicts the experimental shear stress strain curves, respectively. Figs.7.17a and b shows the strain distribution behavior in these beams along the indicated location (A-A). From Fig.7.14 and 7.16, the numerical ultimate shear stress in fibrous (FB1.5%) is approximately 1.5 and 1.33 times that of the control beam (CB0%), respectively. These values are 4.7MPa, 3.1MPa and 2.4MPa, 16MPa in FB1.5% and CB0%, respectively. It is noted that these values are in agreement with the ultimate experimental shear stress values shown in Fig.7.15a and b. The predominant effect of steel fibers on the strain behavior after cracking is evident in Fig.7.18a and b where cracking is marked by points with peak strain concentrations. It can be seen that higher peak crack and increased strains distribution occurs in the fibrous beams (FB1.5%) in comparison with Control beam (CB0%). The maximum strains achieved in the vicinity of a crack in FB1.5% is 0.04 and 0.073 while in the control beams (CB0%) the result is 0.016 and 0.056 in $a/d=1$ and 1.5 group of beams, respectively (see Figs.7.18a and b). These points with maximum crack strains also indicate the positions of the largest crack that occurred in each beam (see Figs 7.6b and 7.7b). The average experimental principal strain values (mean of all strain values along line A-A in each beam type) are found to be 0.002 and 0.004 for CB0% and FB1.5%, respectively in $a/d=1$ while in $a/d=1.5$ the results are 0.008 and 0.010 for CB0% and FB1.5% respectively. These values compare fairly well with the corresponding average FEM principal strain values (mean of all the values in the tension region as given by the positive values shown in the key title of Fig.7.14 and 7.15 b), and are found to be 0.006 and 0.002 in $a/d=1$ and 0.013 and 0.004 for FB1.5% and CB0%, respectively. Generally fibrous beams showed superior deformation behavior which can be attributed to increased post cracking strength occasioned by the SFRC improved tensile strength as opposed to normal concrete.

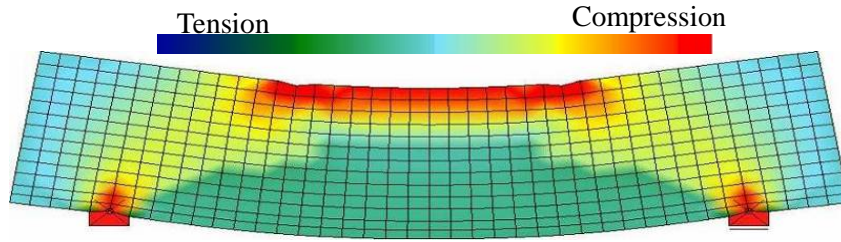


Fig.7.13 FEM beam deformation pattern

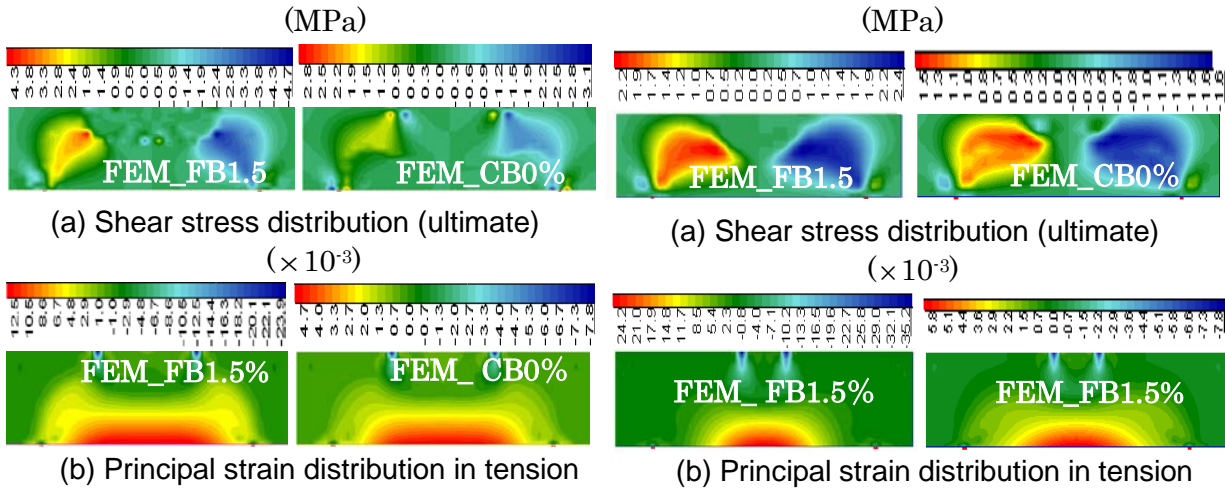
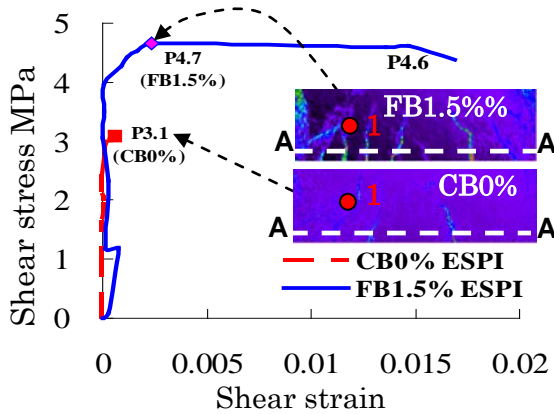
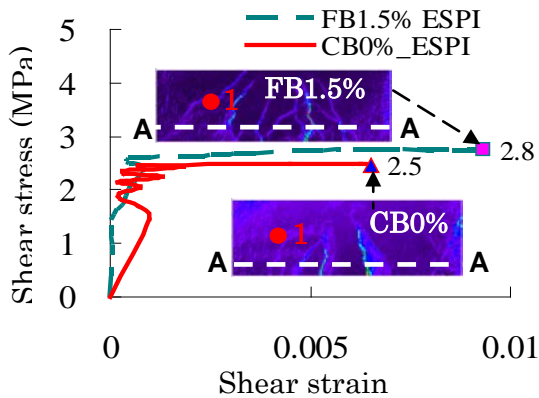


Fig.7.14 FEM Shear stress and principal strain distribution for $a/d=1$ beams

Fig.7.15 FEM Shear stress and principal strain distribution for $a/d=1.5$ beams

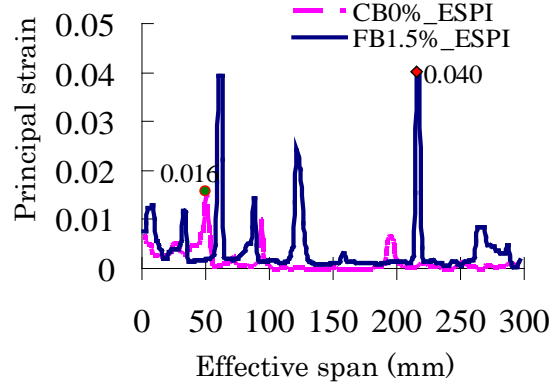


(a) $a/d = 1$

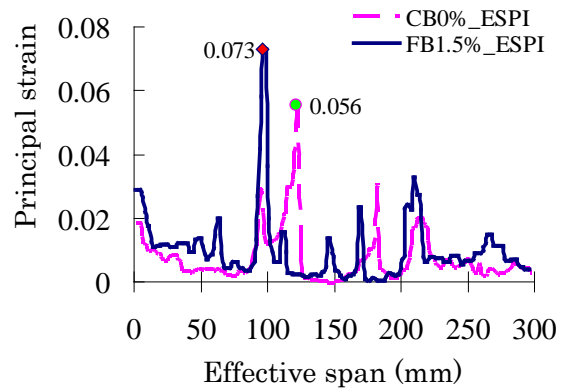


(b) $a/d=1.5$

Fig.7.16 Shear stress-strain curve and strain profile locations for $a/d=1.5$ beams



(a) $a/d = 1$



(b) $a/d=1$

Fig.7.17 Strain distribution along A-A for $a/d=1.5$ group of beams

7.5 Concluding remarks

In this chapter, numerical (FEM) investigation on shear strength and deformation behavior in SFRC beams, subjected to monotonic loading in bending shear were undertaken. The influence of the steel fibers and the effectiveness of the numerical method were examined. Verification was made by comparing the FEM results against the experimental results. From the study, the following principal findings and conclusions are made: (a) FEM results for the fibrous RC beams (FB0.5% to FB1.5%) showed improved strength and deformation (deflection and strain) characteristics in comparison with the non fibrous beams (CB0%). However, exact cracking pattern as observed in the test specimens could not be achieved. This lack of match could be attributed to the deficiency in the numerical tool used which is mainly for general analysis and design and does not consider special modeling of cracking behavior at a micro level. Moreover, steel fibers were not modeled individually due to technical limitations earlier discussed in section 7.1 of this chapter. (b) FEM results reproduced fairly well the experimental load deflection response until failure. The reduction in strength with increase in shear span to depth ratio as observed in these results is attributed to the change in the failure mode from shear to flexural-shear type. (c) Use of an experimentally derived SFRC stress strain material model was found to be effective in the numerical simulation of the load deflection response of SFRC beams.

Chapter 8

Theoretical model verification and design application

8.1 Introduction

In chapter 4, derivation of the shear strength and deformation response model as well as preliminary predictive ability was undertaken. The model was shown to theoretically predict the shear strength-deformation response behavior until failure. However, theoretical predictions alone do not lend credibility unless the results are subjected to practical verification process. Moreover, the applicability of any theoretical model depends on its accuracy and the ability to simulate the real response of the structural system or its assemblage. In this chapter, verification of the model is made by comparing the theoretical results with experiments undertaken in this research as well as experimental data obtained elsewhere in the literature [8]. In the latter case parameter values (e.g. compressive strength, fiber content, fiber aspect ratio, re-bar ratio) from the literature sources were used as the base data in the current model and the prediction results compared with the experimental results given in the source reference. The experimental data from the literature are those applied in the experiential investigations which were used in the development of the empirical ultimate based models discussed in chapter 2 and thus the experimental results given are basically ultimate strength values. It is for this reason that the verification process in the latter case entailed evaluation of the ultimate strength predictive capacity and the sensitivity of the model to variable input parameters as used in these experimental investigations. As an additional verification process, results obtained by means of numerical analysis are also evaluated against the model results.

The purpose of analytical models is to apply in evaluations and design of structural systems. It was noted earlier in the literature review that currently there is no design guideline or method for structural application of SFRC. An effort is made in this thesis to address this by introducing a possible design method in which the current model or any other empirical model can be applied in design. Therefore a design method is proposed in this chapter and a load bearing structural system is chosen to illustrate the applicability of the proposed method.

8.2 Model prediction comparisons with experimental results

8.2.1 Synchronized load deformation response

In order to evaluate closely the comparisons between experiential and theoretical results, matched verification of the results is made. Each figure compares results from the model and the experiment for individual fiber content used. Two sets of results (i.e. load deflection and stress strain relations) have

been compared to illustrate the versatility of the derived model. Test results from the short beams in which the full fiber content range (0.5% to 1.5%) and variation of the shear span to depth ration was made are used. Results from the large beam which was reinforced with 1.0% fiber content are also compared with the theoretical results.

(a) Short beams (re-bar ratio 0.6%)

Verification with results from beams associated with $a/d=1$

Matched theoretical and experimental strength-deformation curves for each fiber content applied in $a/d=1$ are shown in Fig.8.1. The model results reproduces well load deflection response until failure after which deviation occurs whereby the model predicts a further continuity of the deflections. On the other hand, the stress strain response shows good agreement in the initial phases and on yielding there is a more distinct deviation where by the model over predicts on strains and strength in some case (e.g. FB 1.5% and FB0.5%). The experimental deflection and strain values do not show much ductility as compared to the theoretical results. This can be attributed to the disadvantage of excessive damage at

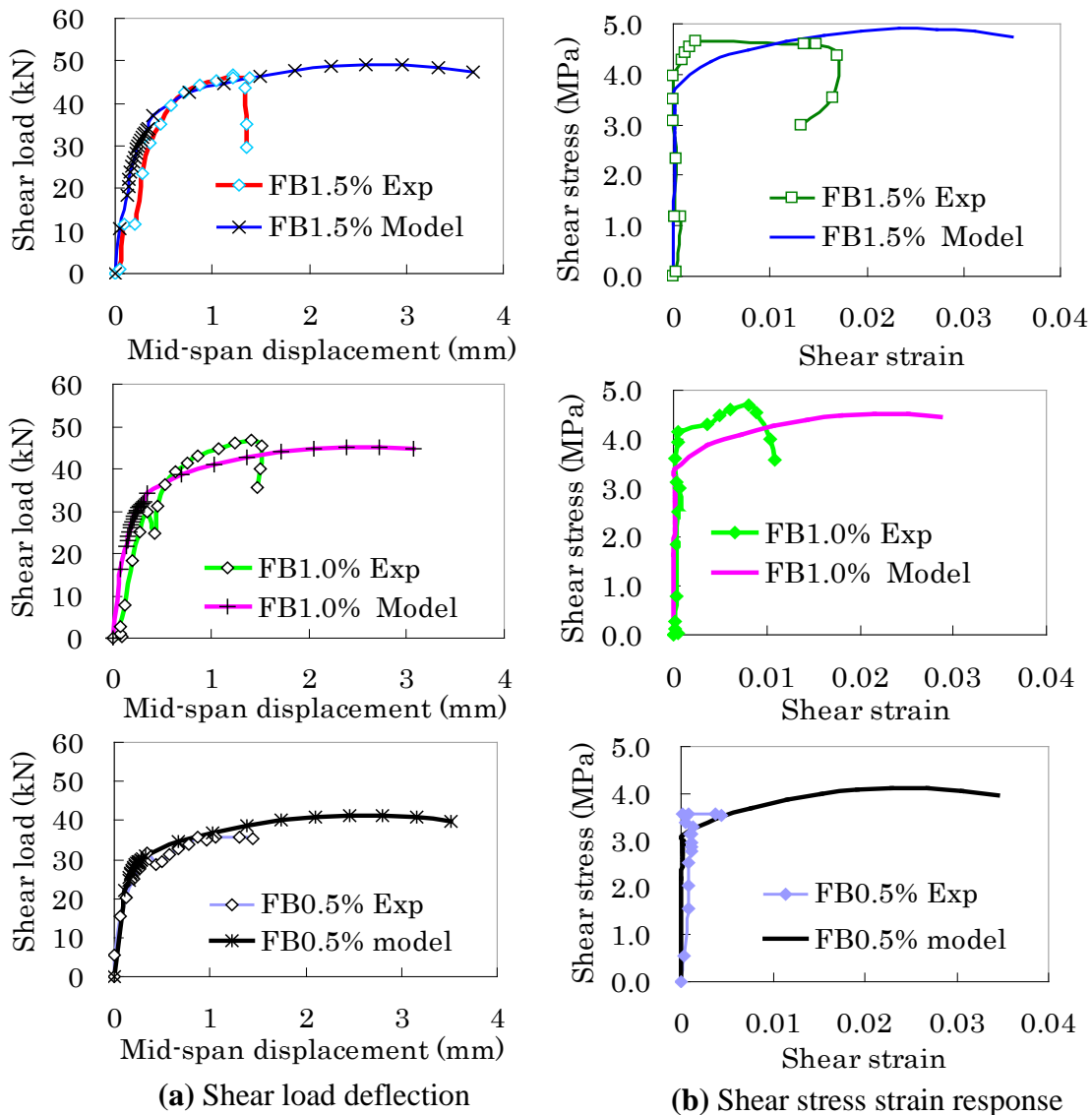


Fig.8.1 Predicted and test results comparisons for beams associated with $a/d=1$

the measurement point.

Verification with results from beams associated with $a/d=1.5$

In the case of $a/d=1.5$, the comparative response was as shown in Fig.8.2. It can also be observed that comparative response (Fig.8.2a), between the model and the experimental results are in good agreement in the initial elastic stages until yielding after which a slight variation occurs in the non linear range particularly in the case of FB1.5% where there is a minor over estimation by the model. As compared to the previous results in $a/d=1$, deflection results are in good accord even in the non linear phase. It can be noted that both experimental and model deflection values extent equally in the non linear phase. However, this is not the case for the stress strain curves, whereby the strain values at failure lags the model values. As previously mentioned, the disadvantage of strain determination by optical methods when excessive deformations (e.g. cracking) occur may be the cause.

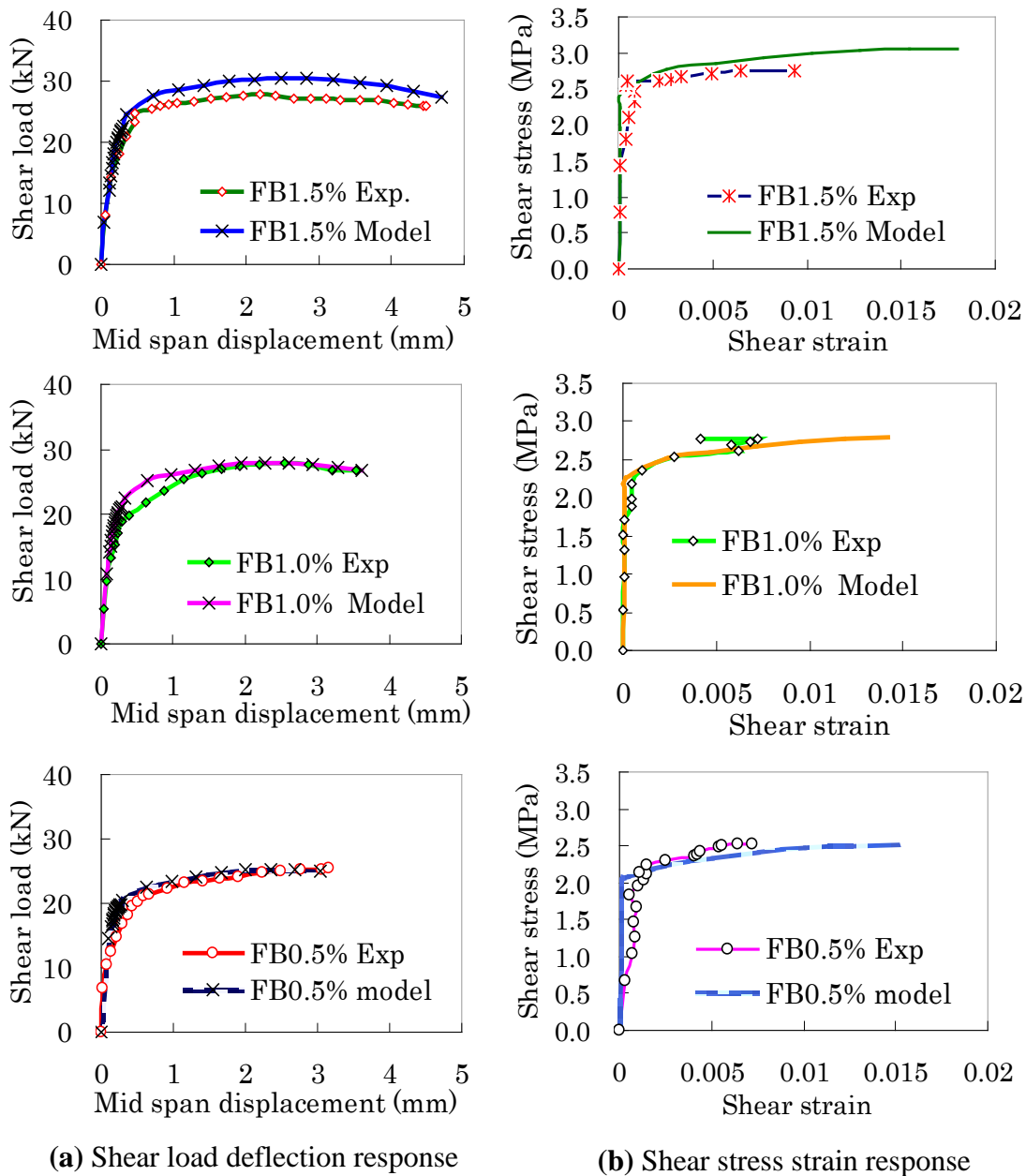
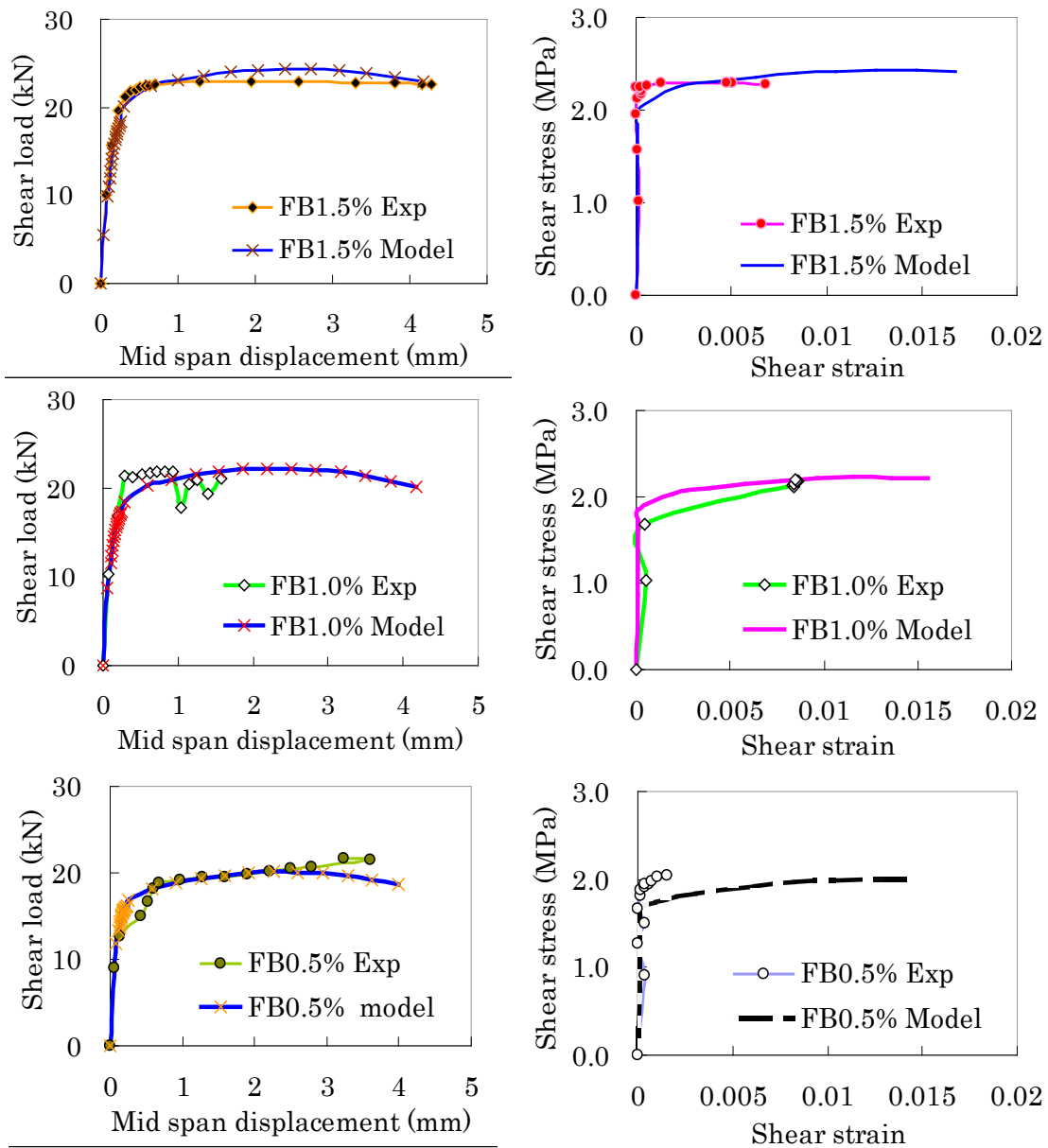


Fig.8.2 Predicted and test results comparisons for beams associated with $a/d=1.5$

Verification with results from beams associated with $a/d=1.82$

Fig.8.3 depicts the comparative trend for the results obtained from analysis and tests on beams associated with a shear span to depth ratio. It can be seen that there is a similar predictive trend as that of the previous beams in the overall replication of the experimental results. Load deflection response closely reproducing the experiments until failure. However as earlier noted the model deformation results particularly the strain values are higher than those of the experiment only after failure. Further it can be observed that the model has predicted well the reduction in strength as associated with change in the shear span to depth ratio (see Figs 8.1 to 8.3).



(a) Shear load deflection

(b) Shear stress strain

Fig.8.3 Predicted and test results comparisons for beams associated with $a/d=1.82$

(b) Verification with large beams $a/d = 2.4$ **Large beam with 1% fiber content and bar ratio of 1.2%**

In the process of evaluating a design method for SFRC (discussed further in subsequent sections), two large beams were designed. A fiber content of 1% was applied in one and the other reinforced with stirrups for comparative evaluations. The test results are used here to evaluate the predictability of the model to gauge the response of the model in the case where the overall geometry and size of the main reinforcements are changed. As depicted in Fig.8.4 the model results agree very well in both load deflection and stress strain response. Shear strains are generally smaller as compared to those of the short beams previously discussed. Perhaps this could be because of the bending shear failure mode that occurred with a bias to bending failure. In the large beam, deformation measurements were obtained by Digital image correlation method (DICM). Although it is an optical measurement method similar to the ESPI (applied in the short beams), there are differences in the analysis and processing of the data which could lead to minor differences in final deformation outputs. It was noted that majority of beams tested and analyzed (large and short beams) shear stress strain response in both theoretical and experiments is characterized by a very stiff initial response and a near flattened non linear range as depicted in the near vertical profile (see Figs 8.1 to 8.4b). The stiff characteristic in the initial stages and the sudden change at the onset of the non linear stage illustrates the abrupt shear failure commonly associated with it. Noting that in the determination of the theoretical model, deformation in the shear region was considered and the fact the experimental shear strain measurements were determined in the shear regions confirms further the validity of the derived model.

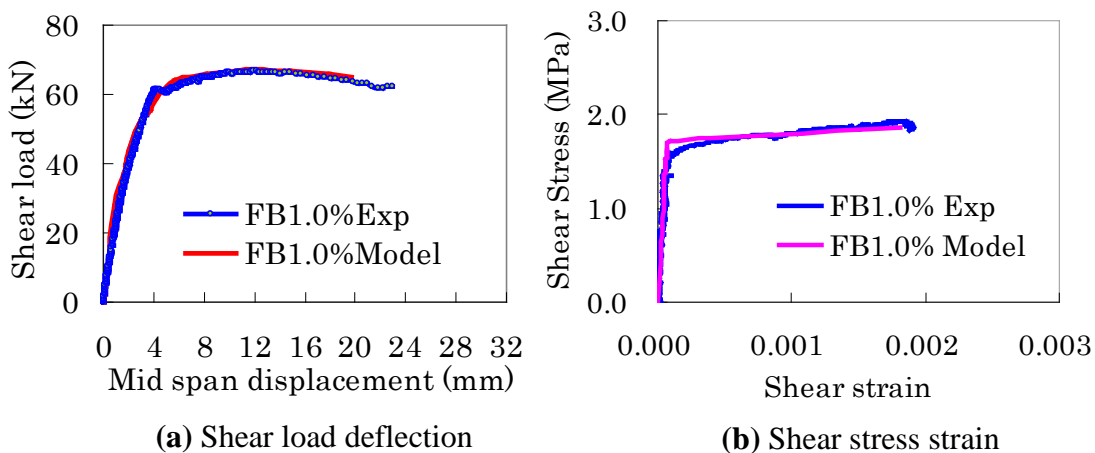


Fig.8.4 Predicted and test comparisons for large beam group with rebar ratio of 1.2

8.2.2 Ultimate strength comparison with experimental result found in the literature.

In the previous sections shear strength–deformation evolution predictability of the model has been demonstrated. As mentioned earlier in the literature review (chapter 2), past studies relating to shear in SFRC beams mainly target the ultimate strength. In this section, the verification process of the ultimate shear strength prediction of the model is further evaluated. Base data (e.g. beam geometry,

shear span depth ratio compressive strength, fiber content, fiber aspect ratio, re-bar ratio) as used in different experiential investigation by nine other researchers [8] have been applied in the current model and the result compared with the experimental results from these sources. In the analysis of the previous results as given in Figs 8.1 to 8.4, it was consistently established that the ultimate load occurs at a shear strain ratio ($\gamma_y/\Delta\gamma$) of 0.00833. To determine the theoretical ultimate strength values using the derived model, this ultimate strain ratio value was applied in Eq.(4.61) together with various geometric, materials and structural parameters of the beams tests undertaken by nine other researches Comparisons of predicted ultimate shear strength using the proposed analytical equation (Eq.4.61) and experimental data from the nine different investigators as documented by Madhusudan K, et al [8] was made and the results were as shown in Fig 8.5 and Table 8.1.

Fig.8.5 depicts the graphical relation between theoretically predicted and experimental (from the nine different investigators) ultimate strengths. Table 8.1 documents all the parameters and experimental results as sourced from ref [8] including the type of the steel fiber used as well as correlation between predicted and experimental results. The results indicate a slight under prediction of the experimental result with exception of the tests result of Adebar (Table 8.1, and Fig.8.5). Five out of the nine researcher’s experimental results were predicted well with the average ratio between the experimental and predicted values being 0.75 and a standard deviation of 0.17. However for all the 9 cases, these values are 0.60 with standard deviation of 0.09 (see Table 8.1). The best predicted experimental ultimate strength values are those of Mansur, Lim, Narayanan, Adebar and Murty with correlation factors of 0.83, 0.73, 0.70, and 1.2 respectively. This result is encouraging given the variability of the fiber type, material and geometric properties of the test data applied in the consulted sources. Moreover, a number of assumptions were applied in the derivation of the theoretical model. From Fig.8.5 it is seen that the overall relationship between ultimate analytical and experimental results is linear. Generally the ultimate analytical predictions are slightly lower than the experimental. Noting that generally in design, a slightly lower bound results is more suitable as it underpins safety incase of unforeseen errors in the design calculations.

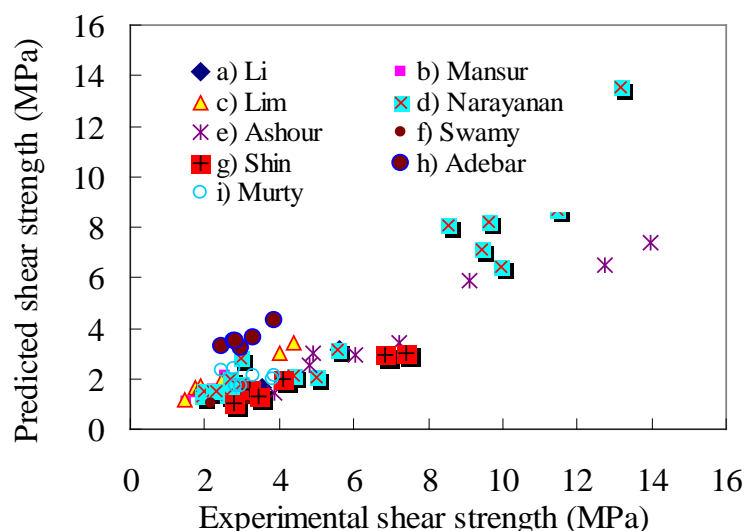


Fig.8.5 Predicted and experimental ultimate shear strength relationship (see Table 8.1)

Table 8.1 Comparison of experimental (Source [8]) and predicted ultimate shear strength

| <i>(a) Li wardandHamza (Crimped and hooked steel fibers used)</i> | | | | | | | | |
|--|-----------------------|-----------------------|-------------------|-------------------------------|-------------------------------------|-------------------------------|------------------------------------|-------------|
| Fiber content $V_f\%$ | Aspect ratio A_r | Rebar ratio ρ | Beam depth d | Comp. strength f_c (MPa) | Shear span to depth ratio (a/d) | Exp. (E) shear strength (MPa) | Predicted (P) shear strength (MPa) | P/E |
| 1 | 60 | 2.2 | 102 | 22.7 | 3.0 | 3.16 | 1.505 | 0.5 |
| 1 | 60 | 1.1 | 102 | 22.7 | 3.0 | 2.43 | 1.459 | 0.6 |
| 1 | 60 | 1.1 | 102 | 22.7 | 1.5 | 5.64 | 3.140 | 0.6 |
| 1 | 100 | 2.2 | 102 | 26.0 | 3.0 | 3.55 | 1.636 | 0.5 |
| 1 | 60 | 2.2 | 204 | 22.7 | 3.0 | 3.05 | 1.464 | 0.5 |
| 1 | 100 | 2.2 | 204 | 26.0 | 3.0 | 3.05 | 1.626 | 0.5 |
| | | | | | 2.75 | | Mean | 0.52 |
| | | | | | | | S.D | 0.05 |
| <i>(b) Mansur,Ong and Paramasivam(hooked steel fibers used)</i> | | | | | | | | |
| 0.50 | 60 | 1.3 | 197 | 29.1 | 2.0 | 2.54 | 2.097 | 0.8 |
| 0.50 | 60 | 1.3 | 197 | 29.1 | 2.8 | 1.78 | 1.455 | 0.8 |
| 0.50 | 60 | 1.3 | 197 | 29.1 | 3.6 | 1.52 | 1.114 | 0.7 |
| 0.75 | 60 | 2.0 | 197 | 29.9 | 2.8 | 2.20 | 1.583 | 0.7 |
| 0.75 | 60 | 2.0 | 197 | 20.6 | 2.8 | 2.03 | 1.456 | 0.7 |
| 0.75 | 60 | 2.0 | 197 | 33.4 | 2.8 | 2.91 | 1.613 | 0.6 |
| | | | | | 2.80 | | Mean | 0.73 |
| | | | | | | | S.D | 0.10 |
| <i>(c) Lim,Paramasivam and Lee (hooked steel fibers used)</i> | | | | | | | | |
| 0.5 | 60 | 1.1 | 221 | 34 | 2.5 | 1.73 | 1.67 | 1.0 |
| 0.5 | 60 | 2.2 | 221 | 34 | 1.5 | 4.02 | 3.03 | 0.8 |
| 0.5 | 60 | 2.2 | 221 | 34 | 2.5 | 1.90 | 1.71 | 0.9 |
| 0.5 | 60 | 2.2 | 221 | 34 | 3.5 | 1.47 | 1.19 | 0.8 |
| 1.0 | 60 | 2.2 | 221 | 34 | 1.5 | 4.39 | 3.41 | 0.8 |
| 1.0 | 60 | 2.2 | 221 | 34 | 2.5 | 2.46 | 1.94 | 0.8 |
| | | | | | 2.33 | | Mean | 0.83 |
| | | | | | | | S.D | 0.08 |
| <i>(d) Narayanan and Darwish (Crimped steel fibers used)</i> | | | | | | | | |
| 0.25 | 100 | 2.0 | 130 | 61.0 | 2.0 | 2.96 | 2.80 | 0.9 |
| 0.25 | 100 | 2.0 | 130 | 61.0 | 3.0 | 2.77 | 1.38 | 0.5 |
| 0.25 | 100 | 2.0 | 130 | 39.2 | 2.0 | 2.71 | 2.00 | 0.7 |
| 0.25 | 100 | 2.0 | 130 | 39.2 | 3.0 | 1.94 | 1.32 | 0.7 |
| 0.50 | 133 | 2.0 | 130 | 36.0 | 3.0 | 1.97 | 1.54 | 0.8 |
| 1.00 | 100 | 2.0 | 130 | 36.0 | 3.0 | 2.97 | 1.77 | 0.6 |
| 0.50 | 133 | 2.0 | 130 | 49.0 | 3.5 | 2.61 | 1.38 | 0.5 |
| 1.00 | 133 | 2.0 | 130 | 57.4 | 2.0 | 5.57 | 3.14 | 0.6 |
| 0.50 | 133 | 3.7 | 130 | 36.0 | 3.0 | 2.24 | 1.54 | 0.7 |
| 0.50 | 133 | 5.7 | 130 | 36.0 | 3.1 | 2.33 | 1.49 | 0.6 |
| 1.00 | 133 | 3.7 | 130 | 57.4 | 3.0 | 4.37 | 2.10 | 0.5 |
| 0.50 | 100 | 3.6 | 350 | 60.0 | 0.7 | 9.42 | 7.08 | 0.8 |
| 1.00 | 100 | 3.6 | 350 | 60.0 | 0.5 | 13.16 | 13.54 | 1.0 |
| 1.00 | 100 | 3.6 | 350 | 60.0 | 0.9 | 9.97 | 6.46 | 0.6 |
| 1.00 | 100 | 3.6 | 350 | 67.0 | 0.7 | 11.48 | 8.71 | 0.8 |
| 1.00 | 100 | 3.6 | 350 | 38.0 | 0.7 | 8.52 | 8.07 | 0.9 |
| 1.00 | 100 | 3.6 | 350 | 42.0 | 0.7 | 9.65 | 8.21 | 0.9 |
| 1.25 | 100 | 3.6 | 350 | 68.0 | 0.7 | 11.39 | 9.18 | 0.8 |
| | | | | | 2.03 | | Mean | 0.70 |
| | | | | | | | S.D | 0.2 |

Continuation of Table 8.1

| <i>(e) Ashour, Hasanain and Wafa (Hooked steel fibres)used</i> | | | | | | | | |
|---|-----------------------|-----------------------|-------------------|-------------------------------|-------------------------------------|-------------------------------|------------------------------------|-------------|
| Fiber content $V_f\%$ | Aspect ratio A_r | Rebar ratio ρ | Beam depth d | Comp. strength f_c (MPa) | Shear span to depth ratio (a/d) | Exp. (E) shear strength (MPa) | Predicted (P) shear strength (MPa) | P/E |
| 0.50 | 75 | 2.8 | 215 | 99 | 1.0 | 9.09 | 5.87 | 0.6 |
| 0.50 | 75 | 2.8 | 215 | 99 | 2.0 | 4.82 | 2.52 | 0.5 |
| 1.00 | 75 | 2.8 | 215 | 95 | 1.0 | 12.74 | 6.50 | 0.5 |
| 1.00 | 75 | 2.8 | 215 | 95 | 2.0 | 6.06 | 2.95 | 0.5 |
| 1.50 | 75 | 2.8 | 215 | 96 | 1.0 | 13.95 | 7.36 | 0.5 |
| 1.50 | 75 | 2.8 | 215 | 96 | 2.0 | 7.21 | 3.39 | 0.5 |
| 1.00 | 75 | 4.6 | 215 | 94 | 2.0 | 4.89 | 3.03 | 0.6 |
| 1.00 | 75 | 4.6 | 215 | 94 | 4.0 | 3.88 | 1.42 | 0.4 |
| | | | | | 1.88 | | Mean | 0.5 |
| | | | | | | | S.D | 0.1 |
| <i>(f) Swamy and Bahia (Crimped steel fibres used)</i> | | | | | | | | |
| 0.4 | 100 | 4.0 | 210 | 44.4 | 4.5 | 2.16 | 1.00 | 0.5 |
| 0.8 | 100 | 4.0 | 210 | 46.8 | 4.5 | 3.10 | 1.19 | 0.4 |
| 0.8 | 100 | 3.1 | 210 | 47.7 | 4.5 | 3.22 | 1.19 | 0.4 |
| 1.2 | 100 | 4.0 | 210 | 49.8 | 4.5 | 3.13 | 1.38 | 0.4 |
| | | | | | 4.50 | | Mean | 0.4 |
| | | | | | | | S.D | 0.0 |
| <i>(g) Shin, Oh and Ghosh (Plain steel fibres used)</i> | | | | | | | | |
| 0.50 | 100 | 3.6 | 175 | 80 | 2.0 | 6.84 | 2.93 | 0.4 |
| 0.50 | 100 | 3.6 | 175 | 80 | 3.0 | 3.19 | 1.60 | 0.5 |
| 0.50 | 100 | 3.6 | 175 | 80 | 4.5 | 2.78 | 1.06 | 0.4 |
| 1.00 | 100 | 3.6 | 175 | 80 | 2.0 | 7.40 | 3.00 | 0.4 |
| 1.00 | 100 | 3.6 | 175 | 80 | 3.0 | 4.10 | 1.98 | 0.5 |
| 1.00 | 100 | 3.6 | 175 | 80 | 4.5 | 3.44 | 1.31 | 0.4 |
| | | | | | 3.17 | | Mean | 0.4 |
| | | | | | | | S.D | 0.1 |
| <i>(h) Adebar, Mindess, St pierre and Olund (Hooked steel fibres used)</i> | | | | | | | | |
| 0.75 | 60 | 2.2 | 557 | 54 | 1.35 | 3.30 | 3.63 | 1.1 |
| 1.50 | 60 | 2.2 | 557 | 50 | 1.35 | 3.87 | 4.29 | 1.1 |
| 0.40 | 60 | 2.2 | 557 | 55 | 1.35 | 2.44 | 3.29 | 1.3 |
| 0.60 | 60 | 2.2 | 557 | 56 | 1.35 | 2.77 | 3.49 | 1.3 |
| 0.40 | 100 | 2.2 | 557 | 47 | 1.35 | 2.95 | 3.24 | 1.1 |
| 0.60 | 100 | 2.2 | 557 | 41 | 1.35 | 2.83 | 3.49 | 1.2 |
| | | | | | 1.35 | | Mean | 1.2 |
| | | | | | | | S.D | 0.1 |
| <i>(i) Murty and Venkatacharyulu (Plain steel fibres used)</i> | | | | | | | | |
| 0.50 | 60 | 1.2 | 186 | 28.7 | 2.0 | 3.3 | 2.09 | 0.6 |
| 0.50 | 60 | 1.2 | 186 | 32.2 | 2.0 | 3.87 | 2.13 | 0.5 |
| 1.00 | 60 | 1.2 | 186 | 29.0 | 2.0 | 2.44 | 2.36 | 1.0 |
| 1.00 | 60 | 1.2 | 186 | 32.6 | 2.0 | 2.77 | 2.41 | 0.9 |
| 1.00 | 100 | 1.2 | 186 | 32.1 | 3.0 | 2.95 | 1.72 | 0.6 |
| 1.00 | 100 | 1.2 | 186 | 32.3 | 3.0 | 2.83 | 1.72 | 0.6 |
| 1.50 | 100 | 1.2 | 186 | 32.8 | 3.0 | 3.83 | 1.98 | 0.5 |
| | | | | | 2.43 | | Mean | 0.7 |
| | | | | | | | S.D | 0.17 |
| | | | | | | | Over all mean | 0.70 |
| | | | | | | | Over all standard deviation (S.D) | 0.10 |

8.3 Model prediction comparisons with FEM results

Preceding experimental verification sections have confirmed the predictability of the theoretical model. However, in this section further evaluation is made to gauge the response of the derived model when compared with numerical (FEA) results. The details of the numerical analysis of the beams are discussed in chapter 7. In the comparative evaluation, short beams in the group $a/d = 1$ and 1.5 and large beam with a shear span to depth ratio of 2.4 are used for the comparative evaluation.

Figs 8.6 and 8.7 show the synchronized load deflection relations between the FEM and the model. In the case of large beams, (Fig.8.6), predicted results are in close agreement with the numerical results until ultimate level whereby a reduction in strength with increase in deflection is noted while the numerical result shows increased deflection with minimal change in the shear load capacity. In Fig.8.7, there is fair agreement in the case of $a/d=1$, but in the case of $a/d=1.5$, an improvement is noted. The model results shows over prediction of both strength and deflection in the non linear phase in the former case. Comparing the magnitudes of both strength and deflection result; it is can be seen that these values are much smaller for the short beams in comparison with those of the large beam. This is expected outcome for a correct model, as it should be able to recognize the differences in the structural geometry and material parameters applied.

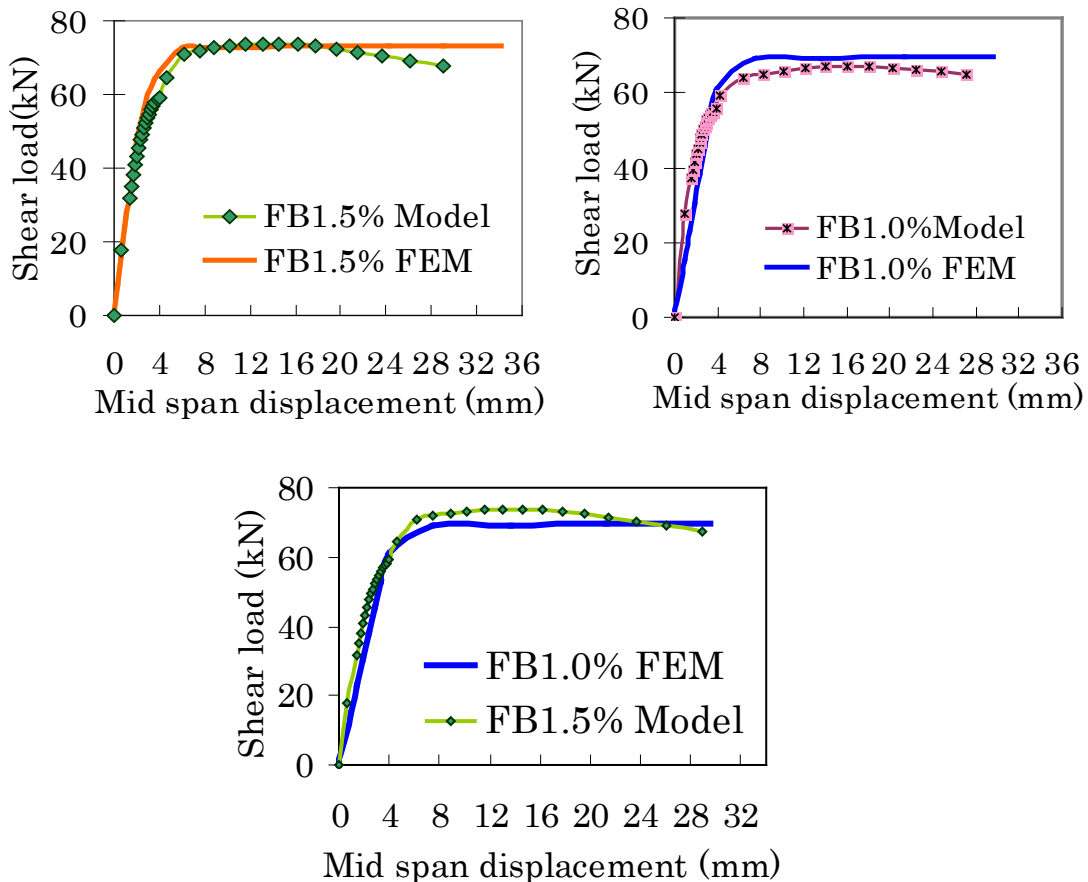


Fig.8.6 Model and FEM response comparisons for large beam associated with $a/d=2.4$

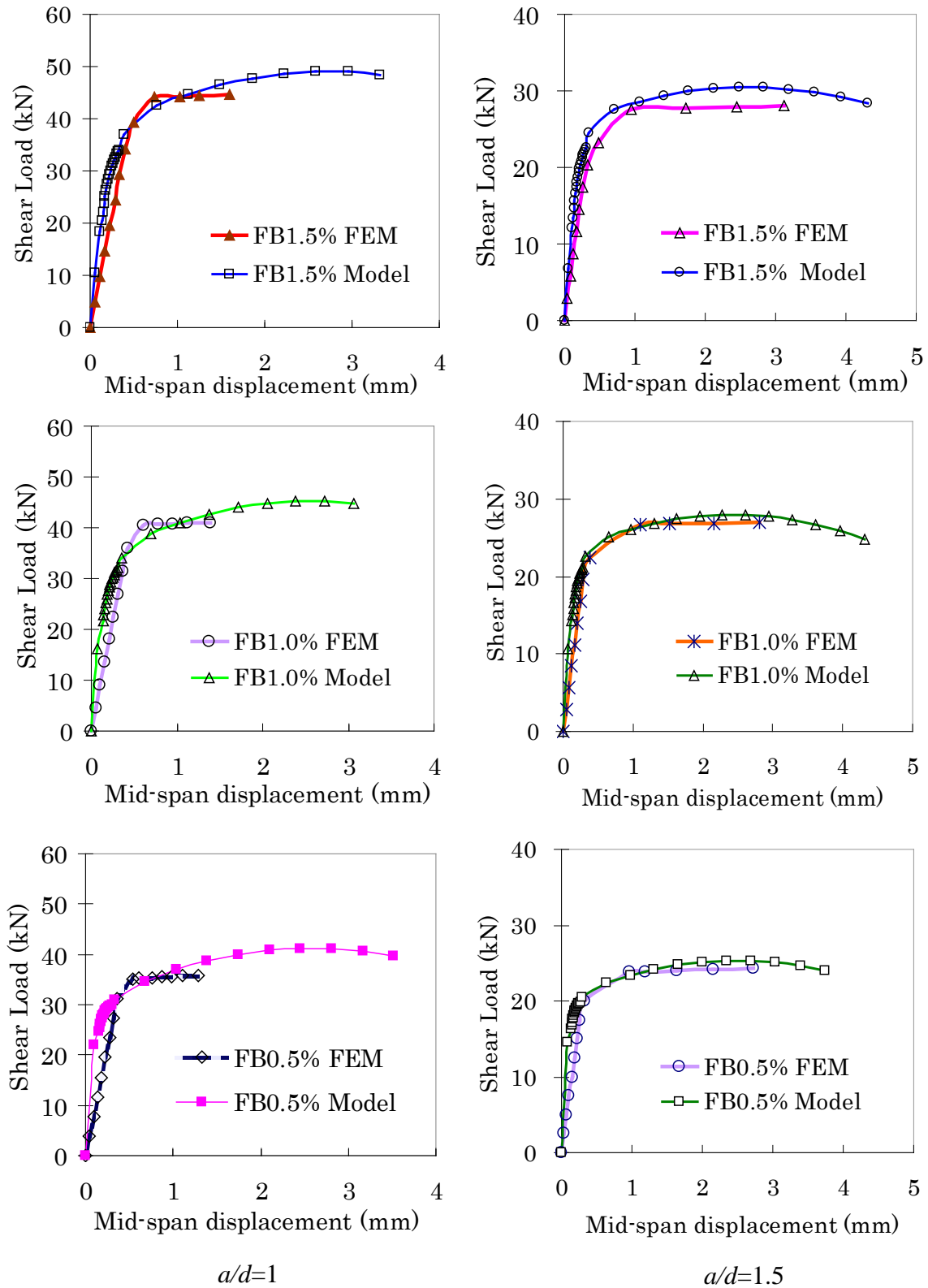


Fig.8.7 Model and FEM response comparisons for short beams

8.4 Shear design application and performance evaluation

As previously stated in chapter 2, the technical merit in the current application of steel fibers is mainly for crack control, ductility and resistance to abrasion and fatigue. The potential application which has been identified is shear strengthening in RC beams either as partial or complete replacement of conventional stirrups. Although complete replacement of stirrups in RC structures exposed to heavy shear loads may not be possible, strengthening by partial supplement is possible noting that even in stirrup beams shear failure is often brittle and catastrophic. This brittle failure can be reduced with incorporation of steel fibers. In the case of load bearing structures (Fig.8.9 see also Fig. 2.2a chapter 2), the magnitude of the shear loads are small given that a major component of the structure load is directly carried by the structural walls. From economic and structural point of view, the beam elements in these structures which act as ties and supports over openings (Fig.8.9) can be designed with use of steel fibers as replacement of the minimum shear reinforcement requirements. The fact that steel fiber reinforced concrete (SFRC) is a ready to use material implies that fabrication of stirrups and manual labor required for fixing is reduced or avoided. These merits result in robust and faster structure construction in which cost savings can be made leading to adequate and affordable supply of shelter. However, it has been noted that practical application of SFRC in RC beams is hampered by lack of design guidelines [7]. This problem is attributed to the limited understanding of SFRC material [2, 7] and lack of transparency in the existing information on SFRC [2]. To contribute to a design solution for application of steel fibers in shear reinforcing, a simple shear design method (applying the derived shear strength predictive relations among others) is proposed and tested. For ease of understanding the method has been code named Equivalent Shear Design method (ESDM) as discussed in subsequent sections.

8.4.1 Proposed Equivalent Design method (EDM)

Despite the reported shear strengthen efficacy of steel fibers there is no method for a design application. Moreover, limited amount of experimental information is available in the case where coupled use of fibers and stirrups is applied [17, 28]. Unlike the availability of detailed design methods for the flexural capacity requirements applicable in beams tests [4] there has been no clear method to determine the required number of shear reinforcements for a particular test situation such as in the case where comparative performance evaluation is required between fiber and stirrup reinforced beams. Equivalent shear design method (ESDM) as proposed here in is based on the shear design for conventionally reinforced stirrup RC beams and the proposed design equations for SFRC beams (Eqs 8.1, 8.3). Design for shear is carried with the guide of an appropriate or desired conventional design code (e.g. BS8110 [69]). Then the desired amount of fiber content is determined based on the designed required number of stirrups by applying Eq.(8.1). The design strength check for SFRC is then

evaluated based on a proposed shear strength equation (Eq.8.3 derived from 7.61 in its ultimate form) developed by the authors whose details are given and discussed in detail in chapter 4. As a counter check on the results of the theoretical formula (Eq.4.61), an empirical formula recommended by committee 544 [12] for SFRC was also applied. Summary of the design procedure to be followed is given in the schematic design flow chart shown in Fig 8.8. Complete design calculations applied in the ideal case evaluated in this research is given in appendix IV in this dissertation.

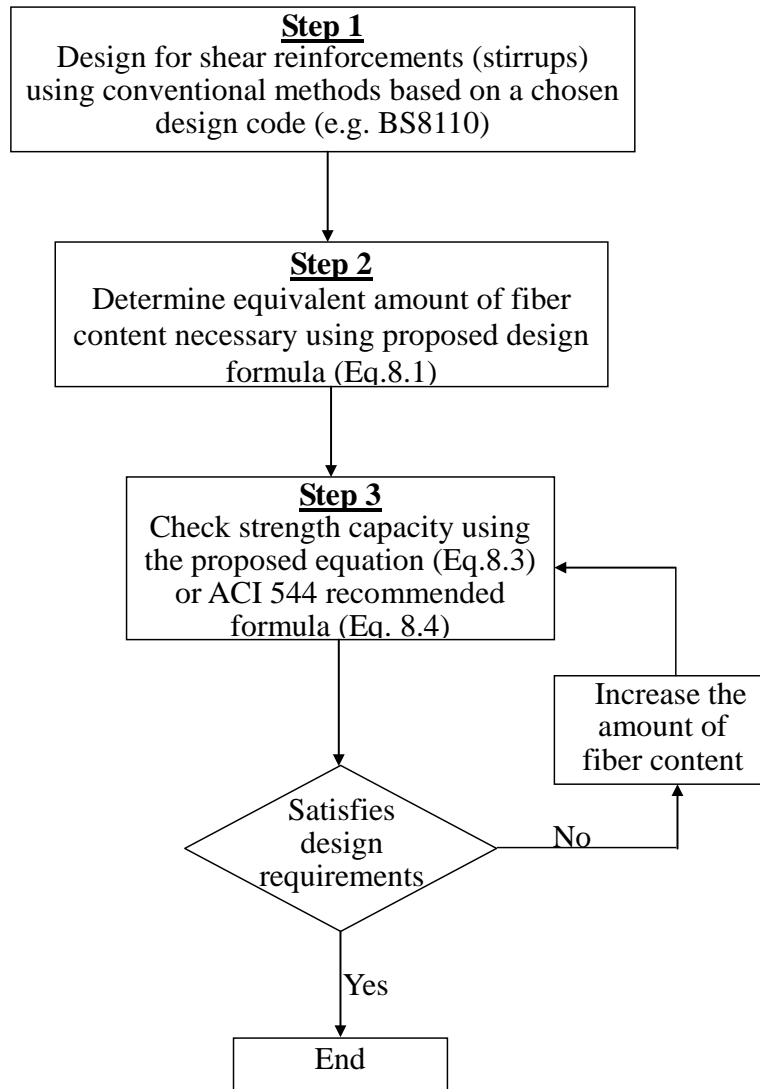


Fig 8.8 ESDM Design procedure flow chart

(a) Determination of equivalent fiber content from the number of stirrup

In order to apply the equivalent shear design method (ESDM), a simple relation for determination of the equivalent fiber content, was derived and tested (see chapter 3 Eq.3.8 and chapter 6 for test results) and is reproduced in this section with the fiber content as the subject of the formula (Eq.8.1) for design application purposes. If the amount of fiber content is adopted by rule of thumb as is the practice by

most researchers, then conversely an equivalent number of stirrups (N_s) can be determined (Eq.3.8 chapter 3). The two equations (Eqs 3.8 and 8.1) are mutually inclusive and hence are applicable in the case where investigation comparative performance between fiber and stirrup reinforced beams is undertaken. This is the case in the current research where the performance between designed stirrup and fiber beams was necessary in order to qualify the proposed design method (EDM). In this regard Eq.8.1 is used to estimate the amount of fiber content required in the fibrous beams so that its shear capacity would be at least equivalent or higher than that of the stirrup reinforcements.

$$v_f = \frac{N_s a_s l_s}{l_b A_b} \quad (8.1)$$

Where, v_f is the equivalent fiber fraction, N_s is the number of stirrups required and it corresponding to an equivalent fiber content, l_b is the beam length, b is the beam width, A_b is cross sectional area of the beam, a_s and l_s are the stirrup cross-sectional area and lab length, respectively.

(d) Basis for application of equation 8.1 in design

Prior to applying Eq. (8.1), a preliminary design and comparative shear capacity performance evaluation was first under taken experimentally on short (400×100×00mm) beams reinforced with, 0, 0.5, 1.0, 1.5% fiber content and another series of similar beams reinforced with an equivalent number (0, 2, 4, and 6) of stirrup (N_s) determined from Eq.(3.8) (see chapter 3) to match the fiber content. The test results of these comparative performance evaluations in terms of strength and deformation behavior are presented and discussed in detail in chapter 6. Comparative evaluation test specimens with stirrup content determined from Eq. (3.8) was made to gauge its validity and hence that of Eq. (8.1) before applying it in a design case study as will show in the subsequent sections. In chapter 6 it is shown that the comparative ultimate strength behavior as well as the overall load deflection response is in favor of the fiber beams for all the fiber content range considered. Although a slightly higher strength was noted in the fiber beams as compared with the stirrup beams (see chapter 6), this gives an advantage as any design application of the Eq. (8.1) for shear strengthening in SFRC beams will guarantee a higher strength which is critical for safety reasons.

8.4.2 Typical design case for shear in SFRC beams by EDM

In the typical design case by ESDM and its performance evaluation, a tie beam spanning over a typical window (1600mm) opening of a load bearing structure (Fig.8.9) was structurally designed and three replica beams (control, stirrup and fiber reinforced beams) were made and tested. The stirrup beam was first conventionally designed for shear with reference to BS8110 [62] where the required number of stirrup reinforcement was determined. Eq.(8.1) was then applied to determine the equivalent amounts of steel fibers needed to reinforce the fiber beam (see design details in the appendix IV). In

the case of SFRC beams, shear strength was determined using Eq. (8.3) and also checked with Eq.(8.4) which has been recommended by ACI committee number 544 [12]. The summary of the design results are given in Table 8.2, however, the full design calculation are given in appendix1. The authors shear strength predictive formula for SFRC beams Eq.8.2 (see also chapter 7) is given here in terms of average shear stress, while ignoring the dowel contribution term for purpose of comparing with the ACI committee 544 recommended formula (Eq.8.4), which does not consider the dowel contribution from the flexural reinforcements. In any case consideration of the dowel action would lead to a higher strength which is even better for safety reasons. However, since the worst case scenario (lower strength basis) is the best option in design calculations, then the design strength bench mark (to be compared with the applied load) should be lowered, thus ignoring the dowel action in this case is advantageous. Eq. (8.3) is a simplified ultimate version of Eq.(8.2) where by the ultimate strain ratio value ($\gamma_y/\Delta\gamma = 0.00833$) as discussed in section 8.2.2 section and shear crack angle $\alpha = 45^\circ$ has been applied.

$$\Delta\tau_{fc} = \frac{K_1}{3\beta \cos^2 \alpha} \left\{ 3 - \left(\frac{\gamma_y}{\Delta\gamma} \right)^2 - \left[\frac{K_1}{\sigma_c} \left(2 - \frac{\gamma_y}{\Delta\gamma} \right) + \frac{\sigma_{ct}}{\sigma_c} \right] \left[\frac{3\sigma_{ct}}{2K_1} + 3 + \left(\frac{\gamma_y}{\Delta\gamma} \right)^2 - 3 \frac{\gamma_y}{\Delta\gamma} \right] \right\} + \frac{\sigma_{ct}}{2\beta \cos^2 \alpha} \quad (8.2)$$

Where $K_1(0.639) = (E_f v_f \epsilon_{fp})/\pi$, E_f is the elastic modulus, v_f is the fiber content, $\epsilon_{fp} = (\tau_b A_r)/E_f$ is the fiber pull out strain, τ_b is the bond strength (4.15MPa), A_r is the fiber aspect ratio(48.3), σ_{ct} is the tensile strength of plain concrete (3.67MPa for the concrete in this study), σ_c is the average compressive strength (38MPa this study), β is a shear span to depth ratio factor ($a/d = 2.38$ for this study), α is the angle of shear crack inclination (45 degrees) and $\gamma_y/\Delta\gamma$ is shear strain ratio which was established from shear strength evolution analysis on SFRC beams to be approximately 0.00833 at ultimate level. Therefore Eq. (8.2) can be re written and simplified as:

$$\tau_{fc}^u = \frac{2}{3} K_1 \frac{d}{a} \left\{ 2.99 - \left[\frac{\sigma_{ct}}{\sigma_c} + \frac{1.99 K_1}{\sigma_c} \right] \left[\frac{3\sigma_{ct}}{2K_1} + 2.98 \right] \right\} + \sigma_{ct} \frac{d}{a} \quad (\text{Author's formula}) \quad (8.3)$$

$$\tau_{fc}^u \frac{2}{3} \sigma_{ct} \left(\frac{d}{a} \right)^{0.25} \quad (\text{ACI committee 544 recommended formula}) \quad (8.4)$$

Eq.8.3 above constitutes shear strength contribution from the fiber concrete in which the last term is the contribution from the plain concrete. A summary of the design results for the large beam based on the loading from the typical load bearing structure (see Fig.8.9) are given in Table 8.2. The designation of the beam specimens as used in subsequent Table 8.2 and subsequent sections implies that FB1 =Fiber Beam (1% fiber content), SB1 =Stirrup Beam (1% equivalent stirrup content) and CB0=Control Beam (No fiber).

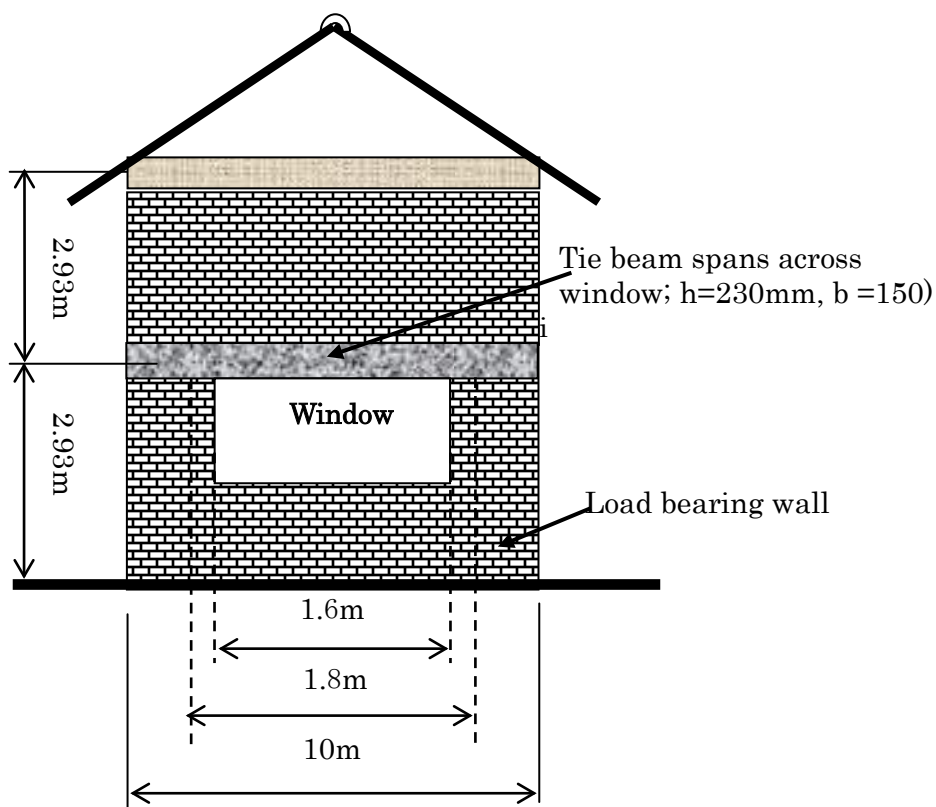


Fig 8.9 Idealized geometry showing target designed tie beam (floor span 4m)

Table 8.2: Shear design summary results for the large beam (group1) (Tie beam Fig 8.8)

| Beam type | Shear reinforcement requirements (design) | | | | |
|------------|---|--|---------------------------------------|---|---|
| | applied shear stress | Design according to BS8110 clause 3.4.4.4, Table 3.7 and 3.9 | | Design according to EDM Eq.(1), Eq.(3) and Eq (4) | |
| | N/mm ² | Design stress N/mm ² | Stirrups requirement (minimum amount) | Fiber requirements (equivalent amount) | Check SFRC shear strength N/mm ² |
| CB0 | 1.2 | 0.66 | Control beam | Control beam | - (No fiber) |
| FB1 | 1.2 | 0.66 | - | 0.6% (approx. 1%) | 1.83(Eq.3)ok |
| SB1 | 1.2 | 0.66 | 18No.R6@100mm | - | 2.22 (Eq.4) |

8.4.3 Performance evaluation of the beams designed by ESDM

(a) Performance test programme

The experimental programme for the short beams has been discussed in detail in chapter 6, as for the large beams, which was specifically tested to evaluate the performance of the design made; bending shear tests (Figs 8.10 and 8.11) was conducted.

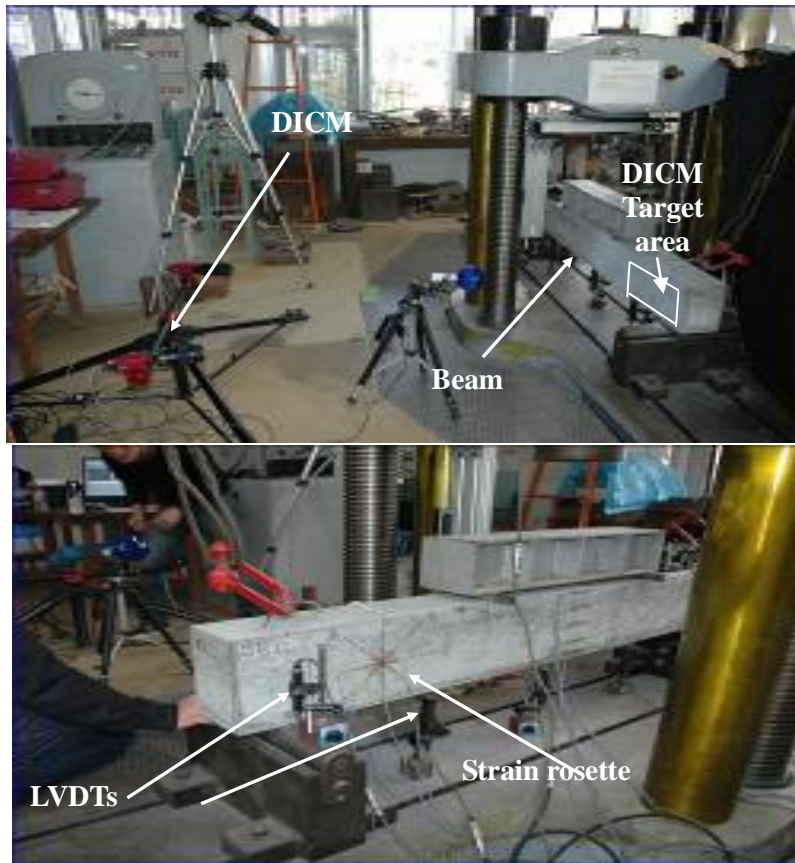
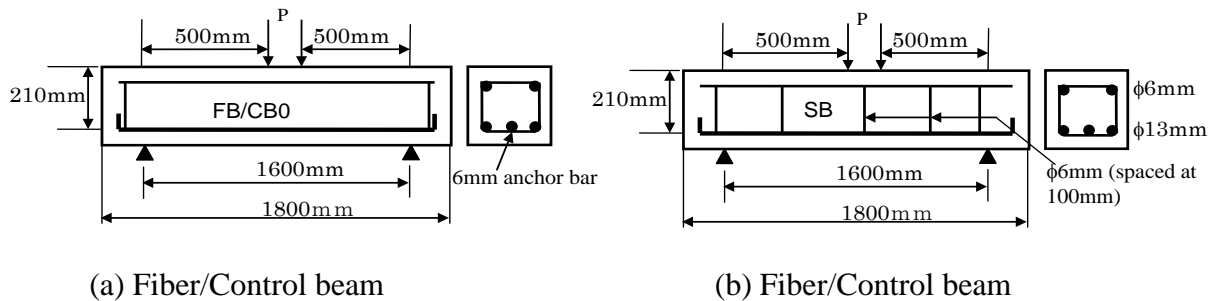


Fig.8.10 Beam testing set up



(a) Fiber/Control beam

(b) Fiber/Control beam

Fig.8.11 Large beam details

As discussed in section 8.4.2 the shear reinforcement requirements were determined by ESDM method. Deformations were measured by conventional methods and Digital image correlation method (DICM) in which the target was the shear region. Same fiber type with similar properties as discussed in chapter 3 was used in the large beam. However, the flexural rebars were larger as determined in the design (see Fig.8.11a, b). These flexural reinforcement were first designed conventionally, thereafter increased appropriately to ensure a diagonal shear failure mode incase the beams were to fail in shear. This was done based on the relative flexural capacity analysis by Russo and Puleri [53]. All the specimens were cured for a period of 28 days before testing.

(b) Failure modes of the designed large beams

General physical failure modes and the cracking behavior in the shear region as captured by DCIM method were as shown in Fig.8.12 (a), (b) and (c). As depicted in these figures, a trend is noted whereby the fiber and stirrup-reinforced beams ultimately failed at different load levels. It appears that a combination of diagonal tension failure, flexural cracking near the mid span and concrete crushing in the compression region were responsible for the ultimate failure of the beams. This was more pronounced in the control beam which had no any form of shear reinforcements. The failure load for the fiber reinforced beams (FB1) was higher than that of the stirrup beam (SB1). Indeed both fiber and stirrup reinforced beams failed at higher loads than the control beam (CB0). By means of optical digital correlation image method, the shear cracks which could not be clearly seen by the naked eye were monitored and captured as depicted in Fig.8.12.

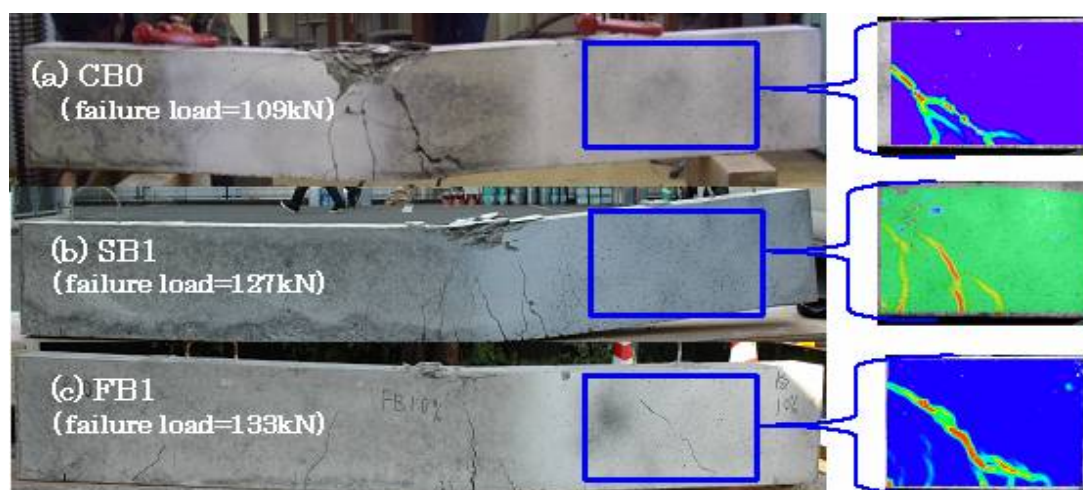


Fig.8.12 Failure pattern/shear cracking visualization

(c) Load deflection response comparisons between fiber/stirrup and control beams

Fig.8.13 shows the performance response in terms of load deflection curves for the large beams reinforced with 1% shear reinforcements (FB1 and SB1) and the control beam (CB0). From these figures, it is apparent that the beams reinforced in shear with the use of steel fibers and stirrups showed higher strength capacity when compared with the control beams. This was expected given the strengthening effect of the fibers and stirrups reinforcements in shear. As earlier indicated in Fig.8.12, the failure loads were 109kN, 127kN and 133kN for CB0, SB1 and FB1, respectively. There seem to be minimal difference in ductility between the control and the reinforced beams (FB1 and SB1). In Fig.8.13 the strength increase in the fiber / stirrup beams is noted to start at yielding (load deviation point between fiber/stirrup beams and Control beam). This load point is considered the stage at which concrete cracks and is noted to occur at approximately 40kN.

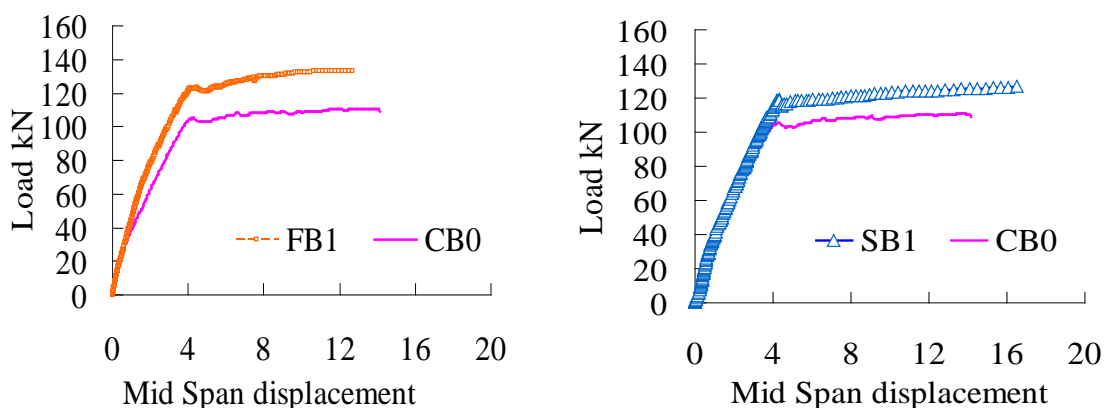


Fig.8.13 Fiber/stirrup design beam performance over control beam (until ultimate)

(d) Load deflection response comparisons between fiber and stirrup reinforced beams

The design method adopted for the beams reinforced in shear with steel fibers was meant to evaluate the validity of the method experimentally. Already from the results discussed earlier, it is evident that there is commensurate strength increase in the designed fiber and stirrup beams. However, since the design was based on determination of equivalent fiber volume that can give equal or higher strengths than that of a conventionally designed stirrup reinforced beam, it is worthwhile to compare the performance between fiber reinforced and stirrup reinforced beam directly. For this reason, synchronized comparative strength and deformation performance between designed stirrup and fiber beams was made as shown Fig.8.14. It is apparent from this figure that the fiber/stirrup beams has a higher strength and deformation capacity than the stirrup beam. Given that at the design stage the fiber content obtained by means of the ESDM method was about 1% (round figure of what was determined: 0.6% in the case of the large beams), the comparative trend observed confirms the validity of the equivalent design method (ESDM). The observed difference in strength between stirrup and fiber reinforced beams can be explained from two different perspectives; one being that the extra amount of fiber over and above the 0.6% figure determined may have contributed to the extra strength capacity seen in Fig.8.14. The other can be explained based on the results of the small beams (see comparative results in chapter 6) whose stirrup reinforcements were conversely determined (see Eq. (3.8) in chapter 6) to be equal to a fiber content of 1%. As seen for example in Fig.6.12 in chapter 6, the fiber beams have a slightly higher load capacity than SB1. Thus the extra strength increase could also be attributed to the extra loading capacity provided by the fibers through stress transfer across emerging cracks in the concrete. This stress capacity transfer is higher than that provided by the stirrup reinforcements because of the dispersed and random presence of the steel fibers through out the concrete volume of the beam. Moreover, the fibers are more closely spaced than the stirrups reinforcements. The extra strength increase with use of an equivalently determined amount of steel fibers over that provide by an equivalently amount of stirrups in the beam (Fig.8.13) is found to be approximately equal to 5% in the large beams.

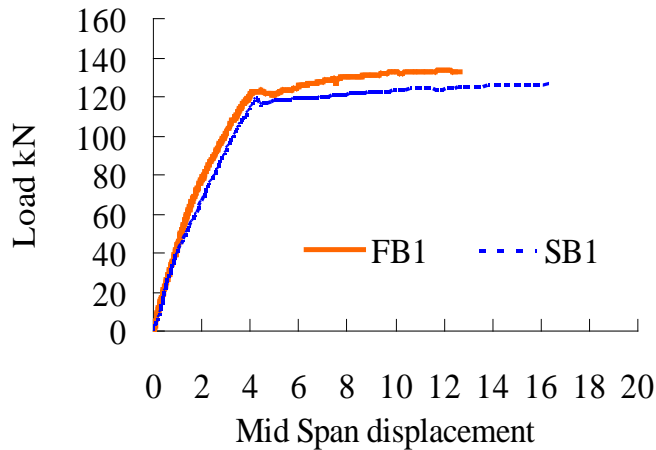


Fig.8.14 Fiber /stirrup reinforced beams comparative design performance (until ultimate)

(e) Shear stress-strain performance

Fig.8.15 shows the comparative relationship between average shear stress and shear strains in the designed beams. As depicted in this figure, two sets of stress strain curves were made to also compare the strain measurements by the optical full field method and those obtained by strain gauge rosette. In the experimental case the average shear stress is given by

$$\tau_{xy} = \frac{P}{2bh} \tag{8.5}$$

Where, P is the applied load while b and h are width and depth of the beam, respectively. Shear strains refer to the strains obtained from analysis of the strains measured by the strain rosette and those from the DICM measurement. As for the strain rosette the shear strains are determined by

$$\gamma_{xy} = 2\varepsilon_d - (\varepsilon_x + \varepsilon_y) \tag{8.6}$$

Where γ_{xy} is the shear strain, ε_d is the diagonal strain values (measured along a 45° orientation) while ε_x and ε_y are the strain measurements along the Cartesian coordinates x and y respectively of the strain rosette.

DICM shear strains were obtained by averaging the DICM shear strain values within an area approximately equal to that covered by the strain rosette and within the geometric locations as the strain rosette.

Since the shear stresses are derived from the load response as previously discussed, a similar performance is noted in the fiber and stirrup beams over the controls beam in terms of strength. Ultimately the fiber concrete performed better both in terms of shear strength and strain ductility. The influence of the steel fibers in the shear region is clearly illustrated by the high strength-strain capacity in FB1%. Comparison of the strain measurements by DICM and strain rosette shows a close agreement, however as for the stirrup beam (SB1%), it appears the measurement point coincided with

a point of excessive shear deformations at failure which affected the results particularly after ultimate load.

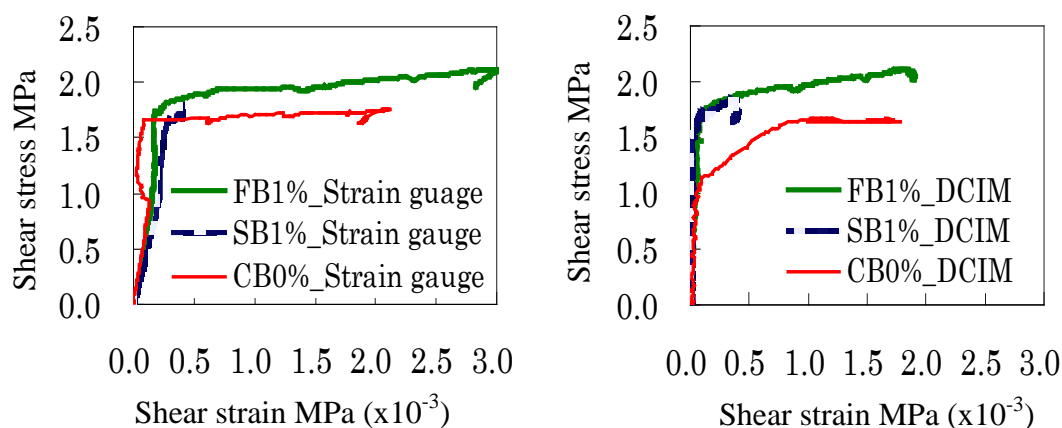


Fig.8.15 Comparative shear stress strain behavior

8.5 Concluding remarks

A theoretical model has been derived and validated against experimental and finite element analysis results. Verification of the proposed model showed fairly consistent agreement in most of the cases considered. Shear load deflection response in which, increase in the strength and ductility with increase in the fiber content has been predicted well. Influence of the shear span to depth ratio is also in accordance with the verification results. The validity of the key assumptions made and the method adopted in the derivations has been confirmed. Predictive models such as the one proposed in chapter 4 and as verified in chapter 8, are fundamental in quantifying structural performance which are a necessity in design guidelines development and applications. The proposed model is aimed at quantifying theoretically the structural capacity of steel fibers in RC beams with a view to contributing to the development of design guidelines for potential structural application of SFRC in RC structures as envisaged in this chapter. In this regard, a general design method making use of the proposed model among other equations was proposed and tested. The comparable performance in the designed stirrup and fiber beams as illustrated this chapter and supported by the previous results from the short beams as discussed in chapter 6 confirms at tentatively the applicability of the proposed ESDM method.

Chapter 9

Overall discussions, conclusions and recommendations

9.1 Overall discussion

The research conducted and presented in this dissertation has provided insights into the characteristics of SFRC as a structural material and in shear strengthening in RC beams. The mechanisms that exist in SFRC in resisting cracking and enhancing post cracking tensile strength which indeed is responsible for the observed shear strengthening in RC beams is fundamental in its structural applications. As established from the literature review, there has been neither a method of evaluating the deformation behavior in detail in SFRC beams nor a method for the evolution predictions of the shear capacity response to failure. In the latter case it was found that ultimate shear strength has been the predominant target in the analytical models that have so far been developed for SFRC beams. The efficacy of steel fibers in structural strengthening in concrete obviously begins at yielding (concrete cracking). In the evaluation of the deformation characteristics, conventional measurement methods may not be able for example to identify the actual point of initial yielding (cracking) since initiation of cracking is difficult to identify with the naked eye. It is for this reason that optical methods can be applied in addressing this problem as proven in this research.

In the case of shear capacity, ultimate based models will not account for the yield strength as well as the contribution of the fibers throughout the post cracking regime. As discussed in chapter 2, literature review showed that the methods employed in development of these models are mainly empirical and in some cases adopted from relations obtained from non fibrous beams. Realistically, empirical models can only yield results that are only valid if the input parameters fit the actual test parameters. In any case, majority of the ultimate based empirical models describe the contribution of the steel fibers based on compressive strengths. It is noted that a description of the shear phenomena is not realistic by using cube compressive strength criterions because unlike the shear capacity, the cube strength does not increase when steel fibers are added to the concrete [15, 69]. As a result, these existing empirical relations become non versatile especially when prediction is desired in the case where variable fiber made. The experimental assessment of the fundamental structural properties of SFRC and SFRC beams in which, full field optical measurements methods were employed, yielded unique results giving insights on strength and deformation characteristics of SFRC and SFRC beams, details of which are discussed in chapters 5 and 6 of this dissertation. Moreover, derivation and verification of a unique theoretical relation for the complete evolution prediction of the shear capacity in SFRC beams under bending shear as given in chapters 4 and 8 respectively, is adequate in addressing the shortcomings inherent in the existing ultimate based empirical models.

As discussed in chapter 2, there is indeed a lack of numerical research on SFRC structural members. As stated by Pascal [39], simple empirical relations may be applied in conventional analysis, but finite elements analysis method is best for the study of the damage to structures for which the use of SFRC is advantageous. This indeed applies to all cases of structural damage including shear failure. However, due to the technical limitations such as material models for SFRC, FE simulations for SFRC have not attracted much attention in research. An attempt was made in the current study, in which a simple experimental material model was applied for SFRC in which fair strength capacity results were obtained. However, it was noted that the prediction of cracking in SFRC could not be simulated. In the opinion of the author, this may indeed require tailor made modules or complete FE code that addresses cracking and fiber interaction with it at micro level in the SFRC composite.

9.2 Conclusions

Material and structural characteristics are important in understanding the inherent structural merit as well as impediment present when steel fibers are incorporated in normal concrete. In the experimental investigations conducted on SFRC as a structural material, it was established that steel fibers do not significantly affect compressive strength and the trend observed was such that there is a slight reduction in it with increase in fiber content. However, presence of steel fibers in concrete (SFRC) was found to significantly improve post cracking tensile strength and deformation characteristics in concrete. Generally in fresh concrete, the fibers were found to reduce the workability and thus a suitable admixture must be used to control water content.

The observed post cracking strength and deformation in SFRC was reflected in the experimental results obtained from SFRC beams tested under bending shear. Through full field optical experimental methods, SFRC beams were noted to have better deformation characteristics particularly in regions where cracking occurs when compared to non fibrous beams, mainly; increased yield and ultimate load capacity, strain ductility and cracking propagation. Of significant was the shear capacity enhancement in fibrous beams failing in shear. In the short beams, it was noted that ultimate crack strain was much higher in fibrous beams failing in flexure. The influence of the steel fibers was noted to occur after initial yielding whereby increased crack propagation in the beams failing in shear and shear flexure was observed. This behavior was visually noted through ESPI enabled images and strain analysis, to occur until an approximately 90% of the ultimate load where by propagation ceases and a dominant crack or group of cracks persist to ultimately cause the failure.

In this research, it was found imperative to also evaluate the shear strength merit offered by steel fibers in an RC beam by comparing with reinforced stirrup beams. A stirrup and or fiber content determination relation was proposed, applied and tested in the process of this comparative evaluation. Principally, it was established that fibrous beams had a closely analogous shear capacity performance as that of an equivalently reinforced stirrup beam. This was true in the most of the beams tested.

However, this is a tentative confirmatory of the possibility of applying steel fibers in shear strengthening. The comparable strength test results between fibrous and stirrup beams and the fact that the stirrup content in the short beams was determined by using the proposed equivalent formula (Eq.3.8 chapter 3), confirmed the validity of the proposed relation. Application of the proposed equivalent content determination formula (Eq.3.8) in a design method called equivalent shear design method (ESDM) as referred in this dissertation further showed consisted performance in the test results of both fibrous and stirrup beams in the large beams tested. Generally, the results showed that the pre-crack behavior is practically unaffected by the presence of shear reinforcement (fibers or stirrups). At this stage, strength and deformation regime is dominated by the matrix properties and stiffness provided by the main reinforcements. On yielding, the fibers (through crack bridging and stress transfer), stirrups and the main reinforcements (through dowel support) contribute to the post cracking shear capacity. It was noted that low volumes of shear reinforcements (fibers or stirrups e.g. 0.5% content) do not enhance much the shear capacity in RC beams.

An attempt was made in this research to derive a predictive theoretical model for shear capacity evolution and theoretical evaluation made by applying a variation of fiber content, shear span to depth ratio and the beam geometry. The theoretical results obtained as discussed in chapter 7 appear to predict well the phenomenon commonly observed in practice when beams are subjected to bending shear. Moreover, shear strength strain behavior could be predicted which is fundamental, given that it is often difficult to experimentally measure shear deformations. Validation of the theoretical results was made against the experimental results obtained from this research and finite element analysis results. A further validation of the ultimate strength prediction of the theoretical model was made by applying experimental parameters from other researchers which constituted variable geometric and material parameters, and it was established that about 70% of the experimental ultimate values could be realized (see Table 8.1). Verification of the proposed model showed good agreement in most of the experimental cases considered; however, fair agreement was achieved in FE results. Shear load deformation response in which, increase in the strength and ductility with increase in the fiber were found to be in accord with the test result. Influence of the shear span to depth ratio was also noted to be in accordance with the verification results. The validity of the key assumptions made and the method adopted in the derivations were therefore confirmed. Predictive models such as the one proposed in this dissertation (chapter 4 and 8) are fundamental in quantifying structural performance which is a necessity in design guidelines development and applications. The proposed model is aimed at quantifying theoretically the structural capacity of steel fibers in RC beams with a view to contributing to the development of design guidelines for potential structural application of SFRC such as in shear strengthening in RC structures as envisaged in this dissertation. It is for this reasons that a general design method making use of the proposed model among other equations was proposed as discussed in chapter 8. The comparable performance in the designed stirrup and fiber beams as illustrated in this chapter confirms tentatively the applicability of the proposed design method.

Finite Elements analysis conducted on the SFRC beams under bending shear and the subsequent verification with tests results showed a fairly similar trend as the test results. The variable material model for SFRC applied in the FE analysis to simulate the variable strengths and deformation capacity simulated fairly well the variable shear capacity which was obtained in the test results. There was indeed improved strength and deformation in the characteristics in the analyzed SFRC model beams when comparison with the non fibrous model beams. However, exact cracking pattern as observed in the test specimens could not be achieved. In the opinion of the author this lack of match could be attributed to the deficiency in the numerical tool used which is mainly for general analysis and design and does not consider special modeling of cracking behavior at a micro level. However, it can be concluded tentatively that use of an experimentally derived SFRC stress strain material model is effective in the numerical simulation of the load deflection response of SFRC beams.

9.3 Recommendation for future work

Although this research has made an attempt to shade light into the theoretical and experimental structural aspects of SFRC as applied in beams, there is still a number of areas that would need further research in order to have a better understanding and wider application of the material in structures. The future prospects that would be of interest in SFRC structural characterization and application, include but not limited to the following;

- (a) Further investigations on larger sample of prototype SFRC and stirrup beams should be conducted to arrive at a conclusive strength merit comparisons between the two types of reinforced in shear strengthen. This perhaps would also consider the influence of steel fibers on the size effect in SFRC beams.
- (b) The role in which steel fibers play in flexural capacity in RC beams should also be investigations with the possibility of developing an analytical model for prediction of the flexural capacity in SFRC beams.
- (c) Strength and deformation characteristics with use of variable fiber type should be investigated.
- (d) Further studies on finite elements analysts (FEA) on SFRC should be conducted and although difficult, development of a constitutive material model for SFRC should be considered.
- (e) The efficacy of steel fibers in crack control and strength enhancement has been confirmed, however, steel fibers are susceptible to corrode, and its use in concrete structures exposed to aggressive environments should be investigated.

References

- [1] Sidney, M. and Arnon B. “Fiber Reinforced cementations composites”, New York: *Elsevier science publishers Ltd*, 1990.
- [2] Dupont D and Vandewalle L. Bending capacity of steel fiber reinforced concrete (SFRC) beams. *Proc. of the International congress on challenges of concrete construction, Dundee*, pp. 81–90, 2002.
- [3] Balendran RV, Zhou,FP, Nadeem A and Leung A Y T. influence of steel fibers on strength and ductility of normal and lightweight high strength concrete. *Building and environment* ,No.37: pp.1362-1367, 2004
- [4] Rossi, P., “Steel fiber reinforced concrete; an example of French Research”, *Materials Journal, ACI, Vol.91*, pp 273-279, 1994.
- [5] Altum, F. et al, Effects of steel fiber addition on mechanical properties of concrete and RC beams, *Construction and building materials No.21*, pp. 654-661, 2007.
- [6] Choi, K *et al*: Shear strength of steel fiber reinforced concrete beams without web reinforcements, *ACI Structural Journal, V.104, No.1*, pp.12-21, 2007.
- [7] Brandt, MA.: Fibre reinforced cement based (FRC) composites after over 40years of development in building and civil engineering, *Composite structures, No.86* pp. 3-9, 2008.
- [8] Khuntia, M., Stojadinovic, B., and Goel, S.: Shear strength of normal and high strength fiber reinforced concrete beams without stirrups, *ACI Structural Journal* , V.96, No. 2, pp 282-290, 1999.
- [9] Feheling, E. and Bullo, T. Ultimate load capacity of reinforced steel fiber concrete deep beams subjected to shear, *Proc. of Finite elements in civil engineering applications, hendriks & Rots (eds) Swets & Zeitlinger, lassie*, pp 209-218. 2002.
- [10] Katzer, J. Steel fibers and steel fiber reinforced concrete in Civil engineering, *Pacific Journal of science and technology, Vol.7, No. 1*, pp. 53-58, 2006.
- [11] Aztec Building Products, solutions for concrete construction
http://www.aztecbuildingproducts.ie/pages/fibres_advantages.html
- [12] ACI committee No. 544. Design considerations for steel fiber reinforced concrete, *ACI Structural Journal*, pp. 563-580, 1988.
- [13] Rao, G.D.T. and Seshu, R.D., “Analytical model for torsional response of steel fiber reinforced concrete members under pure torsion,” *Cement and concrete composites No.27*, pp. 493-501, 2005.
- [14] Minelli, F. and Vicchio, J.F.“Compression field modeling of fiber-reinforced concrete members under shear loading,” *ACI structural journal, Vol. 103, No. 2* , , pp. 244-252, 2006.
- [15] Lars Kützing¹, Martin Meister², Some aspects of the shear capacity of steel fiber reinforced concrete (SFRC) beams, *LACER* , No. 3, pp 153-164, 1998.
- [16] Greenough, T and Monecef, N.: Shear behavior of fiber-reinforced self consolidating concrete slender beams, *ACI material journal, V.105, No. 5*, pp 282-290, 2008.

- [17] Gucchiara, C. *et al.*, “Effectiveness of stirrups and steel fibers as shear reinforcements, *Cement and concrete composites*, No.26, pp.777-786, 2004.
- [18] Altum, F. *et al.* Effects of steel fiber addition on mechanical properties of concrete and RC beams, *Construction and building materials* No.21, pp. 654-661, 2007.
- [19] Kooiman, G.A. Modeling steel fiber reinforced concrete for structural design, *PhD thesis Technical Delft of University of Technology, Netherlands*, 2000.
- [20] Subramanian, N. shear behavior of steel fiber reinforced concrete beams with low shear span to depth ratio, the *Indian journal*, pp. 48-50, 2007.
- [21] Shitote, S.M. Prediction of the response of fiber reinforced concrete beams in combined shear and flexure using the compression field theory, *Research paper, Department of Structural Mechanics, Delft University of Technology, Netherlands*, 2000.
- [22] Niwa, J. Structurally concrete guide (in Japanese), Suurikougakusha press, Tokyo, 1999
- [23] ACI committee 318. Building code requirements for structural concrete and commentary (318R-99) *ACI Farmington Hills, mich.*1999, 391pp.
- [24] Comite Europeen de normalization (CEN), Euro-code 2-Design of concrete structures part 1-1: General rules and rules for buildings, ENV1992-1-1, 1992, 100pp.
- [25] Kwak Y.K,*et al.* Shear strength of steel fiber reinforced concrete beams without stirrups. *ACI Structural Journal*, V.99, No. 4, pp.530-538, 2002.
- [26] Kutzing L. and Konig G., “Design principals for steel fiber reinforced concrete; a fracture mechanics approach,” *Lacer* No.4, pp.176-183. 1999.
- [27] Choi, K *et al.* A unified shear strength model for reinforced concrete beams-Part11: verification and simplified method, *ACI Structural Journal*, V.104, No. 2, pp.153-161, 2007.
- [28] Sharma, A K. Shear strength of steel fiber reinforced concrete beams, *ACI Journal*, pp. 624-628, 1986.
- [29] Choi, K *et al.* Effects of steel fibers on short beams loaded in shear, *ACI Structural Journal*, V.104, No. 2, pp.765-774, 2003.
- [30] Vandewalle, L *et al.* Cracking behavior of concrete beams reinforced with a combination of ordinary reinforcement and steel fibers, *ACI Structural Journal*, V.104, No. 2, pp.765-774, 2003.
- [31] Ahour A S. *et al.* Shear behavior of high strength fiber reinforced concrete beams, *ACI Structural Journal*, V.89, No. 2, pp.176-184, 1992.
- [32] Narayanan, R. and Darwish, IYS. Use of steel fibers as shear reinforcements, *ACI Structural Journal*, pp. 224-227, 1987.
- [33] Zsutty, T. Shear strength prediction for separate categories of simple beam tests, *ACI Journal*, pp.138-143, 1971.
- [34] Imam, M *et al.* Shear domain of fiber reinforced high strength concrete beams, *Engineering structures*, pp.738-747, 1997.

- [35] Swamy, R.N et al. The mechanics of fiber reinforcement of cement matrices, *SP 44-1, ACSE*, pp.1-28, 1974.
- [36] Bazant, Z.P and Sun H.H. Size effect in diagonal shear failure: influence of aggregate size and stirrups, *ACI materials Journal*, pp.259-272, 1986.
- [37] Lim, D.H. and Oh B.H., “Experimental and theoretical strength investigation on shear of steel fiber reinforced concrete beams,” *Engineering Structures, No.21*, pp. 937-944. 1999
- [38] Nyomboi, T. *et al.*, Stress Strain Relations for Steel Fiber Reinforced Concrete Beams in Shear, *Proc. of International Conference on Applied Mechanics, Durban, S. Africa*, pp. 355-368, 2000.
- [39] Pascal, C., Pierre, R. Isabelle, S. Can steel fibers replace transverse reinforcements in reinforced concrete beams? *ACI materials Journal, Vol. 94 , No. 5*, pp. 341-353, 1997.
- [40] Yasuhiko S., *et al.*: Diagonal tensile failure mechanism of reinforced concrete beams, *Journal of advanced concrete technology Vol. 2, No 3*, pp. 327-341, 2004.
- [41] Matsuda, H. *et al.* Non contact and Whole field measurement of the cracking generation and development process of the RC beam by the Speckle interference method, *JSCE, Journal of structural Engineering, Vol.52. No.1*, pp. 11-18, 2006. (In Japanese).
- [42] Tyson, J., *et al.* Advanced Photogrammetry for robust deformations and strain measurement, *SEM 2002 Annual conference, Milwaukee, WI*, June, pp 1-2, 2002
- [43] Ettmeyer, A. non contact and whole filed strain analysis with a laser optical strain sensor, *VIII international congress on Experimental mechanics, Nashville, Tennessee*, 10-13, 1996,.
- [44] Ettmeyer A.G, *ESPI sensor, operational manual V1.5*, pp. 7-9, 2001
- [45] Alan P. *et al*, Measurement of Whole-Field Surface displacements and strain using a Genetic Algorithm Based Intelligent Image Correlation Method. *Journal of Dynamic Systems, Measurement, and Control, No.126*, pp 479-488, 2004.
- [46] Tay C.J, *et al.* Digital image correlation for whole field out-of-plane displacement measurement using a single camera, *optics communication, No 251*, pp. 23-36, 2005
- [47] Japan Society of Civil Engineers. Standard specification for concrete structures–2002 (Materials and Construction), *JSCE Guidelines for Concrete. No.6*. pp. 76-77, 345.
- [48] Holschemacher, K., *et al.*, “Application of steel fiber Reinforced concrete for Timber – Concrete Composite Constructions”, *Lacer No. 7*, pp 161-170, 2002.
- [49] Shitote, S.M., Shah S.P., “A fracture Mechanics formulation for shear analysis of short steel fiber reinforced concrete beams”, *3rd Asia Pacific specialty Conference on Fiber Reinforced Materials*, Shangai Hunan China, pp 209-220,2003.
- [50] Pallewatta, M.T., et al., “Measurement of surface Displacement Field of Concrete by Laser Speckle method”, *JCI Proc*, pp 835, 1990.
- [51] Yoon keun K., *et al.*, “Shear strength of fiber reinforced concrete beams without stirrups”, *ACI structural Journal*, Vol. 99, No.4, pp. 530-538, 2002.

- [52] Shah R H., Mishra S.V., Crack and deformation characteristics of SFRC deep beams”, *IE (I) Journal-CV*, 2003, pp. 44-48.
- [53] Pierre J, Mauro F., “Interferometric imaging using holographic and speckle techniques; fundamentals and characteristics, *Proceedings of the second international on Conference Imaging Technologies and Applications in Civil engineering. ASCE*, , pp. 217-234, 1997.
- [54] Dieter D., *et al.*, “Improved evaluation of electronic speckle pattern interferograms by photogrammetric image analysis, *Optics and Lasers in Engineering Journal*, 2006, 44, pp. 443–454
- [55] Yul, Y. J., Wang L. and Zhang Z. J., “Design of phase-shifting ESPI system for 3D deformation measurement.” *Journal of Physics, Conference Series 48*, pp 911–915, 2006.
- [56] Russo G. and Puleri G., 1997 “Stirrup effectiveness in reinforced concrete beams under flexure and shear.” *ACI Structural Journal, No.3, Vol. 94*, pp.227-238.
- [57] Mosley, W. H. and Bungey J.H.: Reinforced concrete design, fourth edition, Macmillan Ltd, pp. 119-127, 1990.
- [58] Gere, J.M., and Timoshenko, S.P. Mechanics of Materials. Second Edition, pp. 407 – 409, Boston, PWS Engineering, 1989.
- [59] Voo, Y.L., *et al.*: Shear strength of fiber reactive powder concrete pre-stressed girders without stirrups, *Journal of advanced concrete technology, Vol.4, No.1*, p 123-132, 2006.
- [60] Li V.C, Micromechanics of crack bridging in fiber-reinforced concrete *Materials and structures No.26*, pp.486-494, 1993.
- [61] Stroeven, P and Hu, J. Effectiveness near boundaries of fiber reinforcement in concrete, *Materials and structures, No.39* pp. 1001-1013, 2006
- [62] Hannant, D.J., Additional data on fiber corrosion in cracked beams and theoretical treatment of the effect of fiber corrosion on beam load capacity. In Adam Neville, fiber reinforced cement and concrete, *Proc. Symp., colloque Rilem.1975, Vol 2*: pp.533-538, construction press Ltd, Lancaster, 1976.
- [63] Yang, E.H. *et al.*.Fiber-bridging constitutive law of engineering cementations composites, *Journal of advanced concrete technology, Vol.6 No.1*, 181-193, 2008.
- [64] Lim D.H. and Oh B.H., Experimental and theoretical investigation on the shear of steel fiber reinforced concrete beams, *Engineering structures*,; No.21 pp. 937-944,1999
- [65] Kutzing L, Gert K. Design Principals for fiber reinforced concrete. A fracture mechanics approach. *LACER No. 4*. pp. 176-183, 1999.
- [66] Max LP *et al.* Assessment of Dowel bar research. Iowa DOT Project HR-1080 CTRE project 00-93, Iowa State University. pp. 52 -58, 2002.
- [67] Friberg BF. Design of Dowels in Transverse Joints of Concrete Pavements. Transactions, *ASCE; Vol. 105, No. 2081*. 1940.
- [68] Stroud K.A *et al.* Engineering mathematics. Fifth edition, Palgrave Macmillan, pp. 784-785, 2001

- [69] Nyomboi, T. Matsuda, H. et al.. Strength and deformation behavior in normal steel fiber reinforced concrete by optical (ESPI) methods, *JCI, Vol.30, No. 3*, pp. 1489-1494, 2008
- [70] SOFiSTiK FEM Software. Analysis programmes, versions 23, 14.30, 14.16, 13.08, 12.73, 11.16, 11.15. SOFiSTiK AG, berschleissheim, CD ROM, 2006
- [71] Zienkiwicz O.C. The finite element method, third edition, Tata McGraw-Hill, New Dheli, 1990.
- [72] British Standard 8110 (BS 8110), Structural use of concrete, Part 1.*Code of practice for design and Construction*, BSI, 1997.
- [73] Construction materials mix design and test methods, Japan materials institute, pp261, 2005 8 in Japanese).

Appendix**(I) Notations used**

| | |
|---------------------------------|--|
| E_f | Fibre elastic modulus (MPa) |
| E_c | Concrete elastic modulus (MPa) |
| σ_{ft} | Fibre tensile stress (MPa) |
| σ_c | Concrete compressive stress (MPa) |
| σ_{ct} | Concrete tensile strength |
| σ_{fy} | Fibre yield stress (MPa) |
| σ_{fc} | Fibre compression stress |
| σ_b | Bearing stress (MPa per unit width of beam) |
| τ_b | Interface bond shear strength (MPa) |
| ε_{fp} | Fibre pull out strain |
| ε_{sp} | Steel bar pull out Strain |
| ε_f | Fibre strain |
| l_a | Reinforcement bar anchorage length |
| A_f | Cross sectional area of fibre (mm ²) |
| A_r | Fibre aspect ratio |
| A_s | Cross sectional area of main steel reinforcements (mm ²) |
| A_c | Beam cross sectional area (mm ²) |
| ρ | Main steel reinforcement ratio |
| ψ | Crack rotation angle |
| k | Modulus of dowel support (MPa) |
| v_d | Dowel shear resistance (MPa) |
| d_b | Main reinforcement bar diameter (mm) |
| d_f | Fibre diameter (mm) |
| l_f | Fibre length (mm) |
| V_f | Fibre content (Volume fraction) |
| N_f | Number of fibres |
| α | Shear crack inclination angle |
| θ | Fibre orientation angle |
| θ_e^c | Beam elastic curvature |
| θ_y^c | Beam yield curvature |
| w | Crack width (mm) |
| v_c | Concrete shear resistance (MPa) |
| v_{fc} | Fibre concrete shear resistance (MPa) |
| γ_y | Yield shear strain |
| γ | Shear strain |
| $\frac{\Delta\gamma}{\gamma_y}$ | Incremental shear strain ratio |

| | |
|-------------------|---|
| μ | Poisson ratio |
| F_d | Dowel force acting on main steel re bars (N) |
| F_s | Tensile Force in the main steel rebars (N) |
| F_a | Crack Slip / aggregate interlocking shear force (N) |
| $F_{f(1,2)}$ | Fibres tensile force (N) |
| F_c | Concrete compressive force (N) |
| F_v | Shear force in compression (N) |
| Q | Applied load (N) |
| Q_y | Yield load (N) |
| V | Shear load (N) |
| ΔV | Predicted incremental shear strength (N) |
| ΔV_{fc} | Predicted incremental shear strength contribution from fiber concrete (N) |
| ΔV_c | Predicted incremental shear strength contribution from plain concrete (N) |
| ΔV_d | Predicted incremental shear strength contribution from dowel action of rebars (N) |
| $\Delta \delta_b$ | Predicted incremental bending deflections (mm) |
| $\Delta \delta_s$ | Predicted incremental shear deflections (mm) |
| M | Moment (kNm) |
| M_p | Plastic moment (kNm) |
| M_y | Yield moment |
| l | Length of the beam |
| h | Beam depth (mm) |
| d | Effective beam depth |
| a | Shear span (mm) |
| c | Shear crack path length (mm) |
| δ_v | Vertical displacement of the shear crack at origin |
| δ_h | Horizontal displacement of the shear crack at the its origin |
| SFRC | Steel fiber reinforced concrete |
| DICM | Digital Image correlation method |
| ESPI | Electronic speckle pattern interferometry |
| EDM | Equivalent design method |
| JSCE | Japan society of civil engineers |
| ACI | American concrete institute |
| JCI | Japan concrete institute |

| (II) List of figures | Page |
|--|-------------|
| Fig.1.1 Schematic summary of the dissertation chapters and content | vii |
| Fig.2.1 Various types of structures in which steel fibers are applied | 5 |
| Fig.2.2 Load bearing and frame structures | 6 |
| Fig.2.3 Shear resistive mechanism in RC beam without shear reinforcement | 8 |
| Fig.2.4 Shear resistive mechanism in stirrup RC beam and the truss model | 8 |
| Fig.2.5 Shear resistive mechanism in SFRC beams | 11 |
| Fig.2.6 Strength contributions in SFRC beam | 14 |
| Fig.2.7 Stress strain diagram according to DBV, Markblatt, 1992 | 16 |
| Fig.2.8 Stress strain diagram according to RELIM TC 162-TFD, 2000 | 17 |
| Fig.3.1 Forms of bending-shear tests | 20 |
| Fig.3.2 In plane ESPI measurement system1 | 22 |
| Fig.3.3 Phase distribution | 23 |
| Fig.3.4 Schematic representation of DCIM equipment in front of a specimen | 24 |
| Fig.3.5 Idealized schematic deformation process | 24 |
| Fig.3.6 Beams main reinforcement | 27 |
| Fig.3.7 Collated end hooked steel fiber | 28 |
| Fig.3.8 SFRC manufacture and specimen casting | 29 |
| Fig.3.9 casting of specimens | 29 |
| Fig.4.1 Conceptual model beam and shear deformation details | 33 |
| Fig.4.2 Tensile and compressive forces, strain and crack opening, diagrams | 33 |
| Fig.4.3 Idealized stages in the shear response behavior | 34 |
| Fig.4.4 Fiber orientation across a shear crack and strain deduction | 35 |
| Fig.4.5 Fiber pull-out equilibrium mechanism | 36 |
| Fig.4.6 Relative deflections of Reinforcement bar and the crack faces | 40 |
| Fig.4.7 Applied Beam details similar to the tests specimens | 52 |
| Fig.4.8 Theoretical shear response prediction for small SFRC beams | 53 |
| Fig.4.9 Theoretical shear response prediction for large SFRC beams | 54 |
| Fig.4.10 Predicted Influence of shear span to depth ratio | 55 |
| Fig.5.1 Optical and Normal test set up | 58 |
| Fig.5.2 loading arrangement | 58 |
| Fig.5.3 SFRC workability | 59 |
| Fig.5.4 Compression strength | 60 |
| Fig.5.5 Conventional split tensile stress-strain measurements | 61 |
| Fig.5.6 ESPI deformation Measurements | 62 |
| Fig.5.7 Shear strength-strain relationship and deformation | 63 |
| Fig.5.8 Shear strength-mid span Displacement | 64 |
| Fig.6.1 Instrumentation and test set up | 67 |
| Fig.6.2 Loading and deformation measurement locations | 67 |
| Fig.6.3 Deformation and load deflection capacity behavior | 68 |
| Fig.6.4 Deformation and cracking behavior for $a/d=1$ group of beams | 70 |
| Fig.6.5 Deformation and cracking behavior for $a/d=1.5$ group of beams | 71 |
| Fig.6.6 Deformation and cracking behavior for $a/d=1.82$ group of beams | 72 |
| Fig.6.7 Beam type by reinforcement, test set up and measurement points/lines | 74 |

| | | |
|----------|---|-----|
| Fig.6.8 | Physical failure modes | 75 |
| Fig.6.9 | Corresponding ESPI full-field failure characteristics | 76 |
| Fig.6.10 | Steel fibers and stirrup load carrying capacity | 76 |
| Fig.6.11 | ESPI full-field strain profile in control and fiber-reinforced beams (FB, $a/d=1$) | 78 |
| Fig.6.12 | ESPI full-field strain profile in stirrup-reinforced beams (SB, $a/d=1$) | 79 |
| Fig.6.13 | Shear strength curves for $a/d = 1$ beams | 81 |
| Fig.6.14 | Shear strength curves for $a/d = 1.5$ beams | 82 |
| Fig.6.15 | Shear strength curves for $a/d = 1.82$ beams | 83 |
| Fig.7.1 | Element type and internal forces | 86 |
| Fig.7.2 | Meshed RC beam model | 90 |
| Fig.7.3 | Plain/SFRC material models | 91 |
| Fig.7.4 | Steel material model | 91 |
| Fig.7.5 | FEM shear load deflection response | 95 |
| Fig.7.6 | FEM and experimental cracking pattern for $a/d=1$ | 94 |
| Fig.7.7 | FEM and experimental cracking pattern for $a/d=1.5$ | 94 |
| Fig.7.8 | FEM and experimental cracking pattern for $a/d=1.82$ | 95 |
| Fig.7.9 | FEM and experimental cracking pattern in for $a/d=2.4$ | 95 |
| Fig.7.10 | Comparative load deflection response for $a/d=1$ | 96 |
| Fig.7.11 | Comparative load deflection response for $a/d=1.5$ | 97 |
| Fig.7.12 | Comparative load deflection response for $a/d=1.82$ | 97 |
| Fig.7.13 | FEM beam deformation pattern | 100 |
| Fig.7.14 | FEM Shear stress and principal strain distribution for $a/d=1$ beams | 100 |
| Fig.7.15 | FEM Shear stress and principal strain distribution for $a/d=1.5$ | 100 |
| Fig.7.16 | Shear stress-strain curve and strain profile locations for $a/d=1.5$ | 100 |
| Fig.7.17 | Strain distribution along A-A (Fig.1) for $a/d=1.5$ group of beams | 100 |
| Fig.8.1 | Predicted and test results comparisons for beams associated with $a/d=1$ | 103 |
| Fig.8.2 | Predicted and test results comparisons for beams associated with $a/d=1.5$ | 104 |
| Fig.8.3 | Predicted and test results comparisons for beams associated with $a/d=1.82$ | 105 |
| Fig.8.4 | Predicted and test results comparisons for large beam associated with $a/d=2.4$ | 106 |
| Fig.8.5 | Predicted and exp. ultimate shear strength relationship (see Table 8.1) | 107 |
| Fig.8.6 | Model and FEM response comparisons for large beam associated with $a/d=2.4$ | 110 |
| Fig.8.7 | Model and FEM response comparisons for short beams | 111 |
| Fig 8.8 | ESDM design procedure flow chart | 113 |
| Fig 8.9 | Idealized geometry showing target designed tie beam (floor span 4m) | 116 |
| Fig.8.10 | Beam testing set up | 117 |
| Fig.8.11 | Large beam details | 117 |
| Fig.8.12 | Failure pattern/shear cracking visualization | 118 |
| Fig.8.13 | Fiber/stirrup design beam performance over control beam | 119 |
| Fig.8.14 | Fiber and stirrup reinforced beams comparative design performance | 120 |
| Fig.8.15 | Comparative shear stress strain behavior | 121 |
| Fig.A.1 | Design load bearing wall structure (appendix) | 139 |
| Fig.A.2 | Aggregates grading curves (appendix) | 139 |

| (III) List of Tables | Page |
|---|-------------|
| Table 3.1 Specimens matrix series | 26 |
| Table 3.2 Mix design proportions | 28 |
| Table 4.1 Structural and material properties applied | 51 |
| Table 5.1 Characteristics of reinforcements | 59 |
| Table 5.2 Average material properties | 60 |
| Table 7.1 FEM and test ultimate strength comparisons | 98 |
| Table 8.1 Experimental (Source [8]) and predicted ultimate shear strength | 108 |
| Table 8.2 Shear design summary results for the large beam | 116 |
| Table A1 Sieve analysis for coarse Aggregates (Appendix) | 139 |
| Table A2 Sieve analysis for fine Aggregates (Appendix) | 139 |
| Table A3 Aggregates water absorption and densities (Appendix) | 140 |
| Table A4 Initial standard sump values | 140 |
| Table A5 Initial standard aggregates, water and air content proportions | 140 |
| Table A6 Revision factors for measured values | 141 |
| Table A7 Trial mix design proportions without steel fibers | 141 |
| Table A8 Revision of trial mix proportions using adjustment factors (from Table A6) | 141 |
| Table A9 Revised mix proportions to include steel fibres (Example analysis) | 142 |

(IV) Equivalent shear design procedure

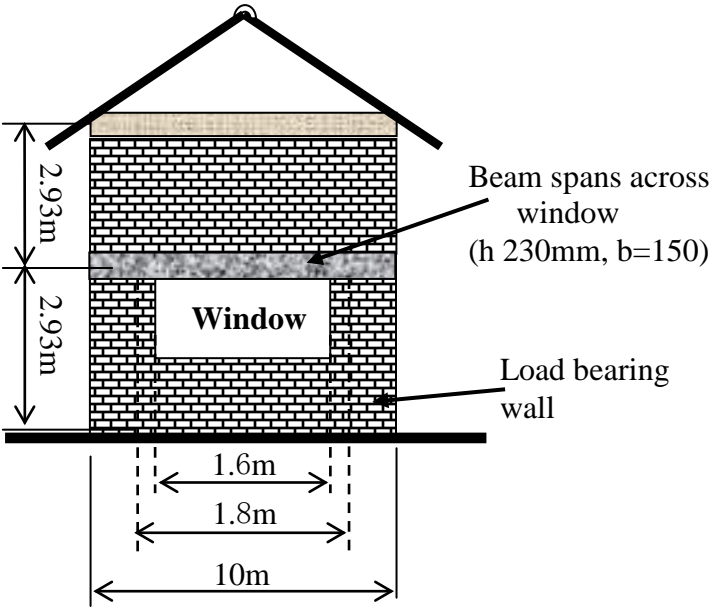
| DESIGN STEP | RESULT | REF |
|---|--|--|
| <p>1. STRUCTURE LAYOUT AND LOADING</p> <p>(a) Layout</p> <ul style="list-style-type: none"> ✧ Application target structure: load bearing buildings  <p>(b) Loading</p> <p>Contribution from the Slab:</p> <ul style="list-style-type: none"> - Area = 40m^2 (one way design approach) - Slab depth $4000/20=200\text{mm}$ +cover +1/2 reinf'ts - Slab depth 4000/20=200mm +cover +1/2 reinf'ts - Self weight = $24 * 0.220 * 1 = 5.28$ - Finishes = $\underline{1.0}$ - Dead load G_k = 6.28 - Live load Q_k = $3.0 < 5$ - Factored load = $1.4G_k + 1.6Q_k$ <li style="padding-left: 20px;">$= 1.4 * 6.28 + 1.6 * 3$ - load transferred to the ring beam per meter width of the slab = $13.59 * 4/2 * 1$ (one way) <p>Loads on the Beam</p> <ul style="list-style-type: none"> - beam size 230mm by 150mm (assumed) - effective length 1800 - Self weight = $0.230 * 0.150 * 24 = 0.828\text{kN/m}$ - Upper floor wall = $0.150 * 2.93 * 22.5 = 9.89\text{kN/m}$ - Finishes + roof loading (assumed) = $\underline{2\text{kN/m}}$ - G_k = 12.718 - Factored load = $1.4G_k = 1.4 * 12.72$ - Total load acting on the ring / lintel beam = 17.80 - Per meter length = $27.18 + 17.80 = 44.98$ | <p>220mm</p> <p>6.28kN/m^2</p> <p>3.00kN/m^2</p> <p>13.59kN/m^2</p> <p>27.18kN/m</p> <p>$h = 230\text{mm}$ $d = 200\text{mm}$ $L = 2000\text{mm}$</p> <p>12.72kN/m</p> <p>17.80kN/m</p> <p>44.98kN/m</p> | <p>BRITISH Standards (BS8110) [69], ACI 544 [12] and this research</p> <p>BS8110 [69] Cls 3.5.2.3 Cls 3.4.6.3</p> <p>Cls 3.5.2.3</p> <p>Table 2.1 cls 3.5.3</p> <p>cls 3.4.1.2</p> |

Fig. A.1 Design load bearing wall structure

- ✧ Upper floor concrete dimensions = 10m x 4m (span)
- ✧ Beam effective length L_e across window = 1.8m

(b) Loading**Contribution from the Slab:**Area = 40m^2 (one way design approach)

- Slab depth $4000/20=200\text{mm}$ +cover +1/2 reinf'ts
- Slab depth 4000/20=200mm +cover +1/2 reinf'ts
- Self weight = $24 * 0.220 * 1 = 5.28$
- Finishes = $\underline{1.0}$
- Dead load G_k = 6.28
- Live load Q_k = $3.0 < 5$
- Factored load = $1.4G_k + 1.6Q_k$
- $= 1.4 * 6.28 + 1.6 * 3$

- load transferred to the ring beam per meter width of the slab = $13.59 * 4/2 * 1$ (one way)

Loads on the Beam

- beam size 230mm by 150mm (assumed)
- effective length 1800
- Self weight = $0.230 * 0.150 * 24 = 0.828\text{kN/m}$
- Upper floor wall = $0.150 * 2.93 * 22.5 = 9.89\text{kN/m}$
- Finishes + roof loading (assumed) = $\underline{2\text{kN/m}}$
- G_k = 12.718
- Factored load = $1.4G_k = 1.4 * 12.72$
- Total load acting on the ring / lintel beam = 17.80
- Per meter length = $27.18 + 17.80 = 44.98$

| DESIGN STEP | RESULT | REF |
|--|---|---|
| <p>2. DESIGN FOR BEAM REINFORCEMENTS</p> <p>(a) Flexural reinforcements</p> <p>◇ $K = \frac{M}{bd^2 f_{cu}} = \frac{44.98 * 1.6^2 * 10^9}{8 * 0.150 * 0.2 * 0.2 * 35} = 0.069$</p> <p>◇ $A_s = \frac{M}{0.87 f_y Z} = \frac{44.98 * 10^3 * 1.6^2 * 10^3}{8 * 460 * 0.95 * 182} = 181 \text{mm}^2$</p> <p>(b) Shear reinforcements</p> <p>(i) Using stirrups</p> <p>- Shear stress $\tau = V/bd$</p> $= \frac{44.98 * 10^3 * 1.6}{2 * 150 * 200} = 1.2 \text{N/mm}^2$ <p>- $\tau < 0.8 \sqrt{f_{cu}} = 4.93$ ($f_{cu} = 38 \text{N/mm}^2$)</p> <p>- $\frac{100 A_s}{bd} = 0.66$</p> <p>Thus design concrete shear stress = 0.665</p> <p>$0.5 \tau_c < \tau < (\tau + 0.4)$ beam requires minimum links for the whole length</p> <p>- $A_{sv} = \frac{0.4 * b_v s_v}{0.95 f_{yv}}$</p> <p>Try spacing of 120mm; area of stirrup will be</p> <p>- $A_{sv} = \frac{0.4 * 150 * 100 *}{0.95 * 275} = 23 \text{mm}^2$ (R6=28.3mm²)</p> <p>(ii) Using Steel fibers reinforcements</p> <p>- Determine actual amount of equivalent fiber content</p> $v_f = \frac{N_s a_s l_b}{l_b A_b}$ $v_f = \frac{18 * 28.3 * 2(150 + 230)}{1800 * 34500} * 100\% = 0.6\% \approx 1\%$ <p>- Check shear strength contribution SFRC with use of 1% content steel fiber (ignore dowel action)</p> $\Delta \tau_{fc} = \frac{K_1}{3\beta \cos^2 \alpha} \left\{ 3 - \left(\frac{\gamma_y}{\Delta \gamma} \right)^2 - \left[\frac{k_1}{\sigma_c} \left(2 - \frac{\gamma_y}{\Delta \gamma} \right) + \frac{\sigma_{ct}}{\sigma_c} \right] \right\} \left\{ \left[\frac{3\sigma_{ct}}{2k_1} + 3 + \left(\frac{\gamma_y}{\Delta \gamma} \right)^2 \right] - 3 \frac{\gamma_y}{\Delta \gamma} \right\}$ $+ \frac{\sigma_{ct}}{2\beta \cos^2 \alpha}$ <p>$\gamma_y/\Delta \gamma$ is shear strain ratio which was found from analysis of shear strength evolution for SFRC beams to be equal to 0.00833 at ultimate level. Therefore, in its ultimate form equation 8.1 is</p> | <p>No compression. Re bars. required</p> <p>Try 2Y13 ($A_s = 266 \text{mm}^2$) O.K. (For tests adopt 3No.)</p> <p>1.2N/mm²</p> <p>O.K.</p> <p>0.66N/mm²</p> <p>Requires R 6 @ 100mm (total = No.18)</p> <p>approx 1%</p> | <p>BS8110 [69]</p> <p>Cls 3.4.4.4</p> <p>”</p> <p>Cls 3.4.5.2</p> <p>Cls 3.4.4.4</p> <p>Table 3.8</p> <p>Table 3.7</p> <p>Proposed formula Chapter 8 Eq. 8.1</p> <p>Proposed formula Chapters 4,8 Eqs 4.61, 8.2</p> |

| | | |
|--|---|---|
| <p>given by</p> $\tau_{fc} = \frac{2K_1}{3\beta} \left\{ 2.99 - \left[\frac{\sigma_{ct}}{\sigma_c} + \frac{1.99K_1}{\sigma_c} \right] \left[\frac{3\sigma_{ct}}{2k_1} + 2.98 \right] \right\} + \frac{\sigma_{ct}}{\beta}$ <p> $\diamond K_1 = \frac{E_f V_f \varepsilon_{fp}}{\pi} = K_1 = \frac{210000 * 0.01 * 0.000956}{\pi} = 0.639$ </p> <p> $\diamond \varepsilon_{fp} = \frac{\tau_b A_r}{E_f} = \varepsilon_{fp} = \frac{4.15 * 48.4}{210000} = 0.000956$ </p> <p> $\diamond \beta = a/d = \frac{d}{1/4L_e} = 2.25 \quad (2.4)$ </p> <p> $\diamond \sigma_c = 35, \sigma_{ct} = 4.14 \quad (\text{for 1\% from split test})$ </p> <p> $\diamond \alpha = 45^\circ$ </p> <p>Therefore sfrc shear strength contribution for 1% will be;</p> <p> $\diamond \tau_{fc} = 1.97$ </p> <p>Actual shear stress = 1.2N/mm² < 1.97</p> <p>- Check shear strength contribution SFRC with use of 1% according to Sharma's formula and as recommended by ACI committee 544</p> <p> $\diamond \tau_{frc} = \frac{2}{3} \sigma_{ct} \left(\frac{d}{a} \right)^{0.25}$ $= 2/3 * 4.14 * (1/2.38)^{0.25} = 2.22 \text{N/mm}^2$ σ_{ct} taken as tensile strength for 1% (split test) </p> <p>Actual shear stress = 1.2N/mm² < 2.22</p> | <p>1.97N/mm² OK</p> <p>2.22 OK</p> | <p>Proposed formula Chapter 8 Eq. 8.3</p> <p>ACI 544 [12]</p> |
|--|---|---|

(V) Mix design**(a) Sieve analysis and grading curves****Table A1** Sieve analysis for coarse Aggregates (CA)

| Coarse Aggregates (Sokotsuzai) | | | | | | | | | |
|---------------------------------------|------------------------|------------|-------------------------------|--|------------------------|------------|--------------------------|--------------------|-------|
| Type | Crushed | | | average Passing (CA1 & CA2) % | Crushed | | | Standard (JSCE) | |
| Sieve mm | CA1 | | Passing <i>Ochiru</i> % | | CA2 | | Passing <i>Ochiru</i> | | |
| | Cumulative retained | | | | Cumulative retained | Limit | | Limit | |
| | g | % | | g | % | g | | % | Limit |
| 30 | 0 | 0 | 100 | 100 | 0 | 0 | 100 | | |
| 25 | 0 | 0 | 100 | 100 | 0 | 0 | 100 | 100 | 100 |
| 20 | 118 | 6 | 94 | 94 | 112 | 6 | 94 | 90 | 100 |
| 15.7 | 318 | 16 | 84 | 82 | 256 | 13 | 80 | 60 | 83 |
| 10 | 1330 | 66 | 34 | 36 | 1216 | 61 | 39 | 20 | 55 |
| 5 | 1984 | 99 | 1 | 1 | 1982 | 99 | 1 | 0 | 10 |
| 2.5 | 2000 | 100 | 0 | 0 | 2000 | 100 | 0 | 0 | 5 |
| 1.2 | 2000 | 100 | 0 | 0 | 2000 | 100 | 0 | | |
| 0.6 | 2000 | 100 | 0 | 0 | 2000 | 100 | 0 | | |
| 0.3 | 2000 | 100 | 0 | 0 | 2000 | 100 | 0 | | |
| 0.15 | 2000 | 100 | 0 | 0 | 2000 | 100 | 0 | | |
| Total | | 688 | | | | 678 | | | |
| Aver. | F.M | 6.7 | | 6.7 | F.M | 6.7 | | | |

Table A2 Sieve analysis for fine Aggregates (FA)

| Coarse Aggregates (Saikotsuzai) | | | | | | | | | |
|--|------------------------|------------|-------------------------------|--|------------------------|--------------|--------------------------|--------------------|------------|
| Type | Sea sand | | | average Passing (FA1 & FA2) % | Sea sand | | | Standard (JSCE) | |
| Sieve mm | FA1 | | Passing <i>Ochiru</i> % | | FA2 | | Passing <i>Ochiru</i> | | |
| | Cumulative retained | | | | Cumulative retained | Limit | | Limit | |
| | g | % | | g | % | g | | % | Limit |
| 10 | 0 | 0 | 100 | 100 | 0 | 0 | 100 | 100 | 100 |
| 5 | 1.3 | 0 | 100 | 100 | 1.5 | 0 | 100 | 90 | 100 |
| 2.5 | 19.5 | 4 | 96 | 96 | 19.5 | 4 | 96 | 80 | 100 |
| 1.2 | 75.7 | 15 | 85 | 85 | 76.6 | 15 | 85 | 50 | 90 |
| 0.6 | 193.4 | 39 | 61 | 61 | 197.8 | 40 | 60 | 25 | 65 |
| 0.3 | 346.7 | 69 | 31 | 30 | 349.5 | 70 | 30 | 10 | 35 |
| 0.2 | 486.7 | 97 | 3 | 3 | 488.1 | 98 | 2 | 2 | 10 |
| Pan | 500 | 100 | 0 | 0 | 500 | 100 | 0 | | |
| Total | | 325 | | | | 226.6 | | | |
| | F.M | 2.2 | | 2.3 | F.M | 2.266 | | | F.M |

F.M = Fineness modulus (standard **2.83**) JSCE = Japan Society of Civil Engineers

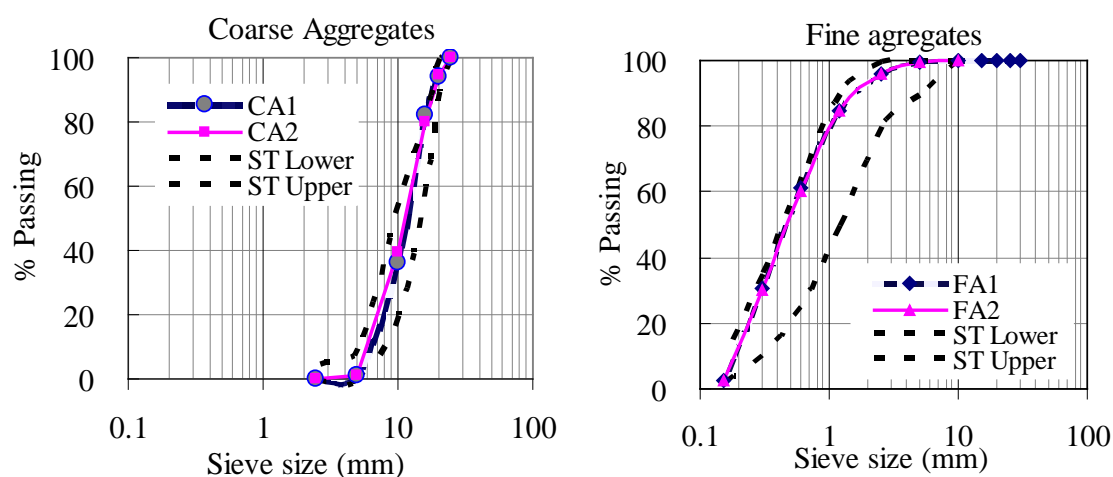


Fig A.2 Aggregates grading curves

(b) Design parameter Tables

Table A3 Aggregates water absorption and densities

| Aggregate densities and water absorption | | |
|--|------------------|---------|
| Type | water absorption | density |
| Fines (Sea sand) | 0.6 | 2.57 |
| Coarse Aggregates (crushed stone) | 1.2 | 2.56 |

Table A4 Initial standard slump values [73]

| Description | | Slump | |
|-----------------------|---------------|-----------------|-------------|
| | | Normal concrete | AE concrete |
| Reinforced concrete | Normal volume | 5~12 | 12~18 |
| | Large volume | 3~10 | 8~15 |
| Unreinforced concrete | Normal volume | 5~12 | - |
| | Large volume | 3~8 | - |

Table A5 Initial standard aggregates, water and air content proportions [73]

| Aggregate Nominal size (mm) | Total Aggregate Content (a) (%) | Air Content | AE Concrete | | | |
|-----------------------------|---------------------------------|-------------|-------------------------------------|------------|---|------------|
| | | | Proportions for Air Entraining only | | Proportion for Air entering with reduction in water content | |
| | | | s/a (%) | Water (Kg) | s/a (%) | Water (Kg) |
| 15 | 58 | 7.0 | 47 | 180 | 48 | 170 |
| 20 | 62 | 6.0 | 44 | 175 | 43 | 165 |
| 25 | 67 | 5.0 | 42 | 170 | 43 | 160 |
| 40 | 72 | 4.5 | 39 | 165 | 40 | 155 |

a = total aggregate content, s = sand (fine aggregates)

Table A6 Revision factors for measured values [73]

| Description | | Revision Factors | |
|-------------|---|-------------------------|-----------|
| | | S/a | Water (W) |
| Type | Amount of deviation of measured from standard value | (Increase or reduce by) | |
| W/C | ±0.05 | ±1% | 0 |
| FM | ±0.1 | ±0.05% | 0 |
| Slump | ±1cm | 0 | ±1.2% |
| Air content | ±1% | ±(0.5~1)% | ±3% |
| s/a | ±% 1 | — | ±1.5Kg |

(c) Mix design calculations and proportion adjustments [73]

✧ Target mean strength $f_c = 35MPa$

$$\diamond \frac{C}{W} = \frac{f_c + 12.1}{21.7} = 2.171 \quad (\text{Eq.A1})$$

✧ $\frac{W}{C} = 0.46$ for W=165, C =358.23kg per m³ (trial values)

For Normal concrete with 20mm normal size aggregate with desired use of AE for W/C control (see Table A5) the trial mix quantities are determined as given in Table A7 below:

Table A7 Trial mix design proportions without steel fibers

| Norm (mm) | Average std Slump (cm) | W/C | Std normal Air (%) | s/a (%) | Total Aggregate Content (%) | Quaintly per 1m ³ | | | | |
|-----------|------------------------|------|--------------------|---------|-----------------------------|--|-------|--------|-------------|--------|
| | | | | | | Std normal Air (Ar)+ Entrained air =C*1% | W | C | a (0.65986) | |
| | | | | | | | | | FA (s) | CA |
| 20 | 8.5 | 0.46 | 6 | 45 | 62 | 0.06114 | 0.165 | 0.114 | 0.2969 | 0.3629 |
| | | | | | | Quaintly per kg/m ³ | | | | |
| | | | | | | | 165 | 358.23 | 742.30 | 979.83 |

Density of cement 3150Kg/m³, Coarse aggregates 2700 Kg/m³, Fine aggregates 2500 Kg/m³,
AE type Pozzolith 15SL: for 0.55W/C ratio, s/a = 46.5 provide C*1% AE (trial value)

Table A8 Revision of trial mix proportions using adjustment factors (from Table A6)

| Determined or measured parameter | Adjustment of s/a (%) | Adjustment of water W |
|--|--|---|
| FM (std =2.8, measured=2.3) | (2.8-2.3)/0.1*0.5 = -2.5 | No adjustment |
| W/C (determined=0.46, for type used AE =0.55) | (0.55-0.46)/0.05*1= 1.8 | No adjustment |
| Slump (aver. std= 8.5, trial 8) | No adjustment | (9-8)*1.2=1.2% |
| Air content (std=6, measured 4.5) | (6-4.5)*0.75=1.125 | (6-4.5)*3=4.5% |
| s/a (value of adjusted =0.43%, deviation limit 1%) | (sub total adjusted) (-2.5+1.125-1.8)= 0.43 | (1.5*(0.43/1))=-0.645kg |
| Total adjustments | s/a=43-0.43=42.57 | 165*(0.012+0.045)-0.65=8.76Kg W= 165+8.76=173.76 |

Table A9 Revised mix proportions to include steel fibres (Sample analysis for 1.5% fiber content)

| Summary of mix ratios for 1.5% fiber content for inclusion of 1.5% steel fiber content | | | | | | |
|---|-------------|------------------|------------------------|-----------------------------|---|---------|
| Description | Cement (Kg) | Sand (Kg) | Coarse aggregates (kg) | Water (kg) | Fibers (Kg) | AE (Kg) |
| Quantity per 1m ³ | 377.67 | 694.556 | 915.62 | 170.85 | 117.750 | 3.02 |
| Ratios | 1.00 | 1.84 | 2.42 | 0.45 | 1.50% | 1% |
| Analysis | | | | | | |
| Aggregate Norm size 20mm fiber content 1.5% | | | | | | |
| Description | Wt Kg | Content % | Volume m ³ | Densities Kg/m ³ | Remark | |
| Cement | 377.08 | 6 | 0.119894668 | 3150 | Adjusted (Eq A1) | |
| Normal air content | | | 0.06 | 100 | - | |
| Water | 173.76 | | 0.174 | 1000 | Table A7 | |
| AE admixture | 3.017 | 0.8 | 0.008 | | Reduced slightly from trail value of 1% x <i>Cement</i> | |
| Fibers | 117.750 | 1.5 | 0.015 | 7850 | Addition | |
| Total aggregates (a) | | Sub total | 0.376894668 | | | |
| s/a | | 42.6 | 0.623105332 | | adjusted | |
| Sand F.A (s) | 683.088 | | 0.265442872 | 2570 | | |
| C.A | 915.887 | | 0.357662461 | 2560 | | |

Note

For summary of final mix proportions for all the fibre contents used please refer to Table 3.2 chapter 3

(VI) CADINP Language analysis Program (Sample for 1.5% RC BEAM)**+Prog aqua urs: 1 Define reference standards and material parameters**

Head Fiber RC beam (1.5% a/d =1)

Echo full yes

NORM JS (JRA) (default standard =Japanese standard: Japan railway association)

Echo mat full

conc 1 EC 46724 QC 0.195 GAM 24.5 FEQT -2.753

ssla eps sig type=SPL Material model (from split and compression tests)

-1.63 -38.39;-1.49 -37.80;-1.27 -35.29;-0.98 -30.39;-0.67 -23.22;

-0.46 -17.42; 0 0; 1.01 2.12; 2.02 4.37; 3.11 4.66; 5.58 4.48; 8.04 4.29;

11.85 3.93; 15.90 3.60; 20.21 3.34; 25.06 3.25; 28.79 3.09; 40.33 2.83

STEE 2 SJS 345 tmax 0 ! Rebar material model

SSLA EPS SIG TYPE=POL

-5.5 -344.6; -2.2 -344.6; -1.7855 -344.6; 0 0 ; 1.7855 344.6 ; 2.2 344.6 ; 5.5 344.6

End

+Prog genf urs: 3 Generate geometry and mesh

SYST Spac

\$ GDIR zz GDIV 10000 (Global coordinates)

Node no x y fix

(1 41 1) (0 0.01) 0 \$ increase horizontal by no of Elements and vertically by no. of nodes

(42 82 1) (0 0.01) -0.006

(83 123 1) (0 0.01) -0.012

(124 164 1) (0 0.01) -0.02

(165 205 1) (0 0.01) -0.028

(206 246 1) (0 0.01) -0.036

(247 287 1) (0 0.01) -0.044

(288 328 1) (0 0.01) -0.052

(329 369 1) (0 0.01) -0.060

(370 410 1) (0 0.01) -0.068

(411 451 1) (0 0.01) -0.076

(452 492 1) (0 0.01) -0.084

(493 533 1) (0 0.01) -0.092

(534 574 1) (0 0.01) -0.100

Node x y ! Support conditions

6 0.05 0 zmpypxpz ! Pined

36 0.35 0 zmpypz ! Simple support

Meshing and numbering by looping

grp 0 ! Grouping elements with unique materail and or geometric Properties

let#a1 1

quad (#a1 #a1+39 1) (#a1 1) (#a1+1 1) (#a1+42 1) (#a1+41 1) t 0.1

grp 0

let#a1 #a1+40 1

quad (#a1 #a1+39 1) (#a1+1 1) (#a1+2 1) (#a1+43 1) (#a1+42 1) t 0.1

let#a1 #a1+41 1

grp 1

quad (#a1 #a1+39 1) (#a1+1 1) (#a1+2 1) (#a1+43 1) (#a1+42 1) t 0.1

let#a1 #a1+41 1

grp 2

loop 10

quad (#a1 #a1+39 1) (#a1+1 1) (#a1+2 1) (#a1+43 1) (#a1+42 1) t 0.1

let#a1 #a1+41 1

End loop

End

+Prog sofiload urs: 6 Define loading conditions and application

lc 1 fact 1 dlx 0 dly 1 dlz 0, lc 2 fact 0.1 titl 'Applied load', node 547,561 type py p1 49
 lc 3 fact 0.2 titl 'Applied load' , node 547,561 type py p1 49, lc 4 fact 0.3 titl 'Applied load'
 node 547,561 type py p1 49, lc 5 fact 0.4 titl 'Applied load', node 547,561 type py p1 49
 lc 6 fact 0.5 titl 'Applied load', node 547,561 type py p1 49, lc 7 fact 0.6 titl 'Applied load'
 node 547,561 type py p1 49, lc 8 fact 0.7 titl 'Applied load', node 547,561 type py p1 49
 lc 9 fact 0.8 titl 'Applied load', node 547,561 type py p1 49

End

+Prog Bemess urs: 10.1 Define reinforcement proprties

Para nog 1 (group number) du 6 (*Max diam upper layer*) du2 1(*Min dia upper layer*)
 dl 6 (max dia lower) dl2 1 ssu 345 (*strength*) ssu2 1 ssl 345 ssl2 1 bsu 0.283 bsl 0.283 asu 0.283 asl
 0.283 (*areas*)

End

+Prog Ase urs: 7.1 Linear Analysis

HEAD Calculation of forces and moments
 ECHO OPT FULL VAL YES \$ Default of all options
 SYST PROB line
 GRP (0,1,2) facs 1/4 !factor for group stiffness
 LC 1,2,3,4,5,6,7,8,9 ! load case
 END

+Prog sofiload urs: 19.1 Load case Combination Manager

Echo FULL VAL FULL \$ Default of all other options
 ECHO OPT ACT VAL FULL \$ Actions
 ECHO OPT LOAD VAL EXTR \$ Loading
 LC 10 fact 0.9 type (D) TITL 'Non linear'
 copy 1 1 type all \$ 1: G Load case 1
 copy 9 0.9 type all \$ 2: G Load case 9
 End

+Prog Ase urs:5 Non linear analysis

ECHO full val extr \$ extensive output of text lists
 Echo opt crack
 Ctrl warn val 197
 Ctrl warn val 350
 Ctrl warn val 351
 Ctrl warn val 352
 Ctrl warn val 353
 Ctrl warn 354
 Ctrl opt solv val 1 v2 1
 Ctrl opt afix val 4 v2 6 Control of movable degrees of freedom
 Ctrl OPT MFIX VAL 1 Fastened rotational degrees of freedom
 Ctrl opt iter val 1 v2 0 Iteration control
 Ctrl opt nlay val 50 Control of analysis layers
 Ctrl CONC val=0 Concrete in cracked condition in which tensile failure energy applied based
 on the length of the softening stress strain curve in the tension (use of
 material model)
 SYST PROB NONL ITER 100 TOL 1.4 nMAT YES fmax 0.7 emax 500 emin -500
 Ulti step 30 fak1 1 dfak 0.003 pro 1 DL yes prim yes
 GRP (0, 1, 2)
 REI2 NOG 1 top 0 0 ht 0.018 0.0 hb 0.018 0.0 ! Location of Reinf
 AST 0.283 asb 0.283 at 0.006 att 0.00 ab 0.006 abt 0.00 ! Cross sect areas of reinf
 BST 0.283 BSB 0.283
 REIQ LCRS 99
 Ksb tso control of tension stiffening
 GRP (0,1,2) FACS 1/3 ! Factor for group stiffness (non linear analysis)
 LC 10
 End
 END

(VII) List of research output publications

1. Timothy NYOMBOI, Hiroshi MATSUDA, Akira DEMIZU and Kohei MAKINO : Experimental and Analytical Study on Shear Capacity in Steel Fiber and Stirrup RC Beam, *JSCE Journal of Structural Engineering*, Vol.56A , 2010. (accepted paper; in press) (chapters 3,4, 7)
2. Timothy NYOMBOI and Hiroshi MATSUDA : Shear strength and deformation prediction in steel fiber RC beams, *Proc. of the fifth International Structural Engineering and Construction Conference (ISEC-5), Challenges, Opportunities and solutions in structural engineering and construction*, Francis and Taylor CRC press, ISBN 978-0-415-56809-8, pp.119-126, 2009 (Chapters 3, 4, 7).
3. Timothy NYOMBOI, Hiroshi MATSUDA and Yukihiro ITO : Effects of steel fibers on shear strength and deformation behavior in short SFRC beams without stirrups by full field optical ESPI and FEM methods, *コンクリート工学年次論文集 (Proc. of Japan Concrete Institute)*, Vol.31-No.2 pp.1303-1308, 2009 (Chapters 3,7)
4. Timothy NYOMBOI and Hiroshi MATSUDA : Shear design performance of beams reinforced with steel fibers and stirrups, *Proc. of International Association for Bridge and Structural Engineering (IABSE)*, Vol.96 (print of extended abstract) pp.242-243, CD-ROM (full paper), 2009, (Chapter 3and 8).
5. Timothy NYOMBOI and Hiroshi MATSUDA : Observation of cracking development in steel fiber RC beams under bending and shear by optical full-field measurement method, *Pro. of Eleventh East Asia-Pacific Conference on Structural Engineering & Construction (EASEC-11), Building a Sustainable Environment*, CD-ROM, 2008, Chapter 3, 6).
6. Timothy NYOMBOI, Hiroshi MATSUDA, Tsutomu YAMASHITA and Tomohiro OHARA : Strength and deformation behavior in steel fiber reinforced normal concrete by optical (ESPI) methods, *コンクリート工学年次論文集 (Proc of Japan Concrete Institute)*, Vol.30-No.3, pp.1489-1494, 2008, Chapters 3, 5).
7. Timothy NYOMBOI, Hiroshi MATSUDA, Ryu HIRAYAMA and Hiroshi NISHIDA : Theoretical prediction of shear strength evolution in steel fiber reinforced concrete beams without stirrups, *Reports of Faculty of Engineering, Nagasaki University*, Vol.38-No.71, pp.20-27, 2008.10 (Chapter 3, 4and 8)

END